



Norwegian University of Life Sciences  
Faculty of Environmental Sciences  
and Natural Resource Management

Philosophiae Doctor (PhD)  
Thesis 2024:25

# Modelling infiltration dynamics in the frozen unsaturated zone: Implications for flood hazard

Modellering av infiltrasjonsdynamikk i frossen  
umettet sone: Implikasjoner for flomfare

Joris Cornelis Stuurop



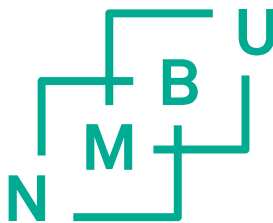
# Modelling infiltration dynamics in the frozen unsaturated zone: Implications for flood hazard

## Modellering av infiltrasjonsdynamikk i frossen umettet sone: Implikasjoner for flomfare

Philosophiae Doctor (PhD) Thesis  
Joris Cornelis Stuurop

Norwegian University of Life Sciences  
The PhD programme in Environmental Sciences  
at the  
Faculty of Environmental Sciences and Natural Resource Management

Ås 2024



Thesis number 2024:25  
ISSN 1894-6402  
ISBN 978-82-575-2104-2





Paintings by Gertie Offermans.

# Supervisor and Evaluation Committee

## PhD Supervisors

Helen K. French  
Norwegian University of Life Sciences  
Høgskoleveien 12, 1433 Ås, Norway

Sjoerd E.A.T.M. van der Zee  
Wageningen University & Research  
Droevendaalsesteeg 4, 6708 PB Wageningen, The Netherlands

Clifford I. Voss  
United States Geological Survey  
345 Middlefield Road, Menlo Park, CA 94025, United States

## Evaluation committee

Attila Nemes  
Norwegian University of Life Sciences  
Høgskoleveien 12, 1433 Ås, Norway

Thomas Pabst  
Norwegian Geotechnical Institute (NGI)  
Sandakerveien 140, 0484 Oslo, Norway

Per-Erik Jansson  
KTH Royal Institute of Technology  
Brinellvägen 8, 114 28 Stockholm, Sweden

*Gratitude to Sjoerd van der Zee (1955-2022) for his supportive guidance and kind spirit during my PhD. I am grateful he was my supervisor. We shared warm conversations and discussions throughout. He was considerate yet sharp and constructive with feedback, and my visits to Wageningen and his and Gemma's home in Utrecht are pleasant memories. I am deeply saddened by his passing.*

## Acknowledgements

I would like to thank my supervisor, Helen French, for all her support throughout the years and for the kindness with which she has allowed me to explore my own path within the broad topic of my PhD project. Thanks also to Clifford Voss for visiting me in Norway to aid me in the modelling process and to help shape my research aims. I would also like to thank my mother Gertie Offermans, especially for the paintings, but of course also for providing me with a moment of time in our universe.

Thanks also to Perrine Fernandez, Ellen Kayendeke, and Bart Immerzeel, you were great colleagues and friends to start the PhD with, but a shame you all left so quickly. Many thanks to Mariya Kelova, Marina Bakhtina, Nikolay Kelova, Hannah Wenng, Emil Jarosz, Jan Vermaat, Andries van der Wijk, and Mikhail Fominykh for their friendship during the years and company at boardgame evenings. Thank you to Mari Haugene for *gezellige* gatherings, dinners, and cheerful support from the beginning until the end. Thanks to Bilal Tariq for the good times in office. Dank and grazie to Simon Schowanek and Stefano Ninfole. The latter part of the PhD would have been terrible without you.

Furthermore, thanks to Fabiana Engelsbel, Alexandra Stuurop, Rafaela Stuurop and Elias Stuurop for being a kind and loving family. And naturally, the old, tried and tested, friends from Amsterdam and surroundings: Fabian van Amerongen, Jeroen Bosschaert, Michelle Hu, Elena Fonseca Neves, Chani Currie, Joost Lurvink, and Ewoud Luiten. For Jeroen and Michelle: I hope you will beat the island invaders for good, with whatever spirit power it will take.

Thanks also to my brother Lucas Stuurop for stirring up the ether. Special gratitude to Claire Devos for letting me win at Hive every so often, for listening to me talk about frozen things, and for melting the snow in Ås. And last but not least, dear thanks to my cat Miyu, who gave the best advice during my entire PhD by telling me to just lie down and not care.

# Contents

Supervisor and Evaluation Committee .....	4
Acknowledgements.....	5
Symbols and Constants .....	9
List of Papers .....	12
Abstract .....	13
Norwegian Summary / Norsk Sammendrag .....	14
1. Introduction to the thesis .....	16
1.1 Motivation for the research .....	16
1.2 Main research question .....	18
1.3 Assumptions.....	22
1.4 Relevant processes included in the scope of the thesis.....	23
1.5 Research aims per subtopic .....	26
1.6 Methods .....	29
1.7 Outline of the thesis.....	31
2. A multi-decadal literature review of theory related to the freezing of soils, from detailed physics to catchment-scale implications .....	33
2.1 Introduction .....	33
2.2 Frozen soil: freezing point depression .....	34
2.3 Frozen soil: cryosuction.....	45
2.4 Frozen soil: permeability reduction .....	56
2.5 Frozen soil: catchment hydrology .....	60
2.6 Conclusion.....	62
3. Numerical modelling of frozen soil: different approaches.....	64
3.1 Introduction .....	64
3.2 Methods.....	66
3.3 Results.....	73



3.4 Discussion.....	78
3.5 Conclusion.....	85
3.6 Acknowledgements.....	87
4. Infiltration into frozen soil: controlling factors.....	88
4.1 Introduction .....	88
4.2 Methods.....	90
4.3 Results & Discussion .....	96
4.4 Conclusion.....	119
5. The role of microtopography and macropores .....	121
5.1 Introduction .....	121
5.2 Methods.....	123
5.3 Results.....	130
5.4 Discussion.....	143
5.5 Conclusion.....	146
6. Cryosuction and water migration within frozen soil .....	149
6.1 Introduction .....	149
6.2 Methods.....	149
6.3 Results.....	150
6.4 Discussion.....	154
7. Snowmelt erosion and flooding in a small agricultural catchment.....	156
7.1 Introduction .....	156
7.2 Methods.....	159
7.3 Results.....	166
7.4 Discussion.....	184
7.5 Conclusion.....	188
8. Discussion & Conclusion .....	190
9. Conclusion diagram.....	205

10. Epilogue.....	206
11. References.....	207
12. Appendices.....	247
Appendix A. Chapter 3 .....	247
Appendix B. Chapter 4 .....	251
Appendix C. Chapter 7 .....	256
Appendix D. CryoFlow-1D manual .....	258

## Symbols and Constants

Abbreviation/symbol	Parameter/variable	Units
$K_s$	Saturated hydraulic conductivity	$\text{ms}^{-1}$
$K_f$	Hydraulic conductivity (including ice effect)	$\text{ms}^{-1}$
$K_u$	Hydraulic conductivity (liquid water content)	$\text{ms}^{-1}$
$K_m$	Hydraulic conductivity (adjusted)	$\text{ms}^{-1}$
$k_s$	Saturated permeability	$\text{m}^2$
$k$	Relative permeability	-
$\alpha$	Soil water retention parameter	$\text{m}^{-1}$
$n$	Soil water retention parameter	-
$\theta_r$	Residual volumetric water content	$\text{m}^3\text{m}^{-3}$
$\theta_s$	Saturated volumetric water content	$\text{m}^3\text{m}^{-3}$
$\theta_t$	Total volumetric water content	$\text{m}^3\text{m}^{-3}$
$\theta_u$	Volumetric liquid water content	$\text{m}^3\text{m}^{-3}$
$\theta_i$	Volumetric ice content	$\text{m}^3\text{m}^{-3}$
$\theta_a$	Volumetric air content	$\text{m}^3\text{m}^{-3}$
$\varepsilon$	Porosity	$\text{m}^3\text{m}^{-3}$
$\psi_f$	Matric potential including ice effect	m
$\psi_w$	Matric potential based on total water content	m
$w$	Empirical soil freezing curve parameter	-
$z$	Elevation	m
$t$	Time	s
$P_w$	Pressure of liquid water	Pa
$P_i$	Pressure of ice	Pa
$P$	Pressure	Pa
$v_w$	Specific volume of liquid water	$\text{m}^3\text{kg}^{-1}$
$v_i$	Specific volume of ice	$\text{m}^3\text{kg}^{-1}$
$T$	Temperature	K
$T_f$	Standard freezing point of water	K
$T^*$	Capillary freezing point of water (Eq. 19)	K

$\rho_w$	Density of water	$\text{kgm}^{-3}$
$\rho_s$	Density of soil particles	$\text{kgm}^{-3}$
$\rho_i$	Density of ice	$\text{kgm}^{-3}$
$\rho_a$	Density of air	$\text{kgm}^{-3}$
$H_w$	Specific heat of water	$\text{Jkg}^{-1}\text{K}^{-1}$
$H_a$	Specific heat of air	$\text{Jkg}^{-1}\text{K}^{-1}$
$H_s$	Specific heat of soil particles	$\text{Jkg}^{-1}\text{K}^{-1}$
$H_i$	Specific heat of ice	$\text{Jkg}^{-1}\text{K}^{-1}$
$H_t$	Total heat capacity of the soil	$\text{Jkg}^{-1}\text{K}^{-1}$
$\bar{c}$	Average soil thermal conductivity	$\text{Wm}^{-1}\text{K}^{-1}$
$c_w$	Liquid water thermal conductivity	$\text{Wm}^{-1}\text{K}^{-1}$
$c_i$	Ice thermal conductivity	$\text{Wm}^{-1}\text{K}^{-1}$
$c_a$	Air thermal conductivity	$\text{Wm}^{-1}\text{K}^{-1}$
$c_s$	Soil particle thermal conductivity	$\text{Wm}^{-1}\text{K}^{-1}$
$L_f$	Latent heat of fusion of water	$\text{Jkg}^{-1}$
$\gamma_{sa}$	Interfacial tension at the solid-air interface	$\text{mJm}^{-2}$
$\gamma_{sl}$	Interfacial tension at the solid-liquid interface	$\text{mJm}^{-2}$
$\gamma_{la}$	Interfacial tension at the liquid-air interface	$\text{mJm}^{-2}$
$\gamma_{wi}$	Interfacial tension at the water-ice interface	$\text{mJm}^{-2}$
$r$	Radius	m
$\sigma$	Contact angle	°
$p_c$	Capillary pressure	Pa
$\rho_d$	Dry density of bulk soil	$\text{kgm}^{-3}$
$\alpha_2$	Empirical parameter (impedance equation)	-
$\beta$	Empirical parameter (impedance equation)	-
$S_e$	Effective saturation	-
$C_h$	Bulk transfer coefficient for sensible heat	$\text{Wm}^{-2}\text{K}^{-1}$
$Q_a$	Energy exchange between atmosphere and soil	J
$u_a$	Windspeed at height $z_a$	$\text{ms}^{-1}$

$T_a$	Air temperature at height $z_a$	$^{\circ}\text{C}$
$T_s$	Soil surface temperature	$^{\circ}\text{C}$
$z_a$	Measurement height of atmospheric variables	m
$C_{hn}$	$C_h$ during stable atmosphere	$\text{Wm}^{-2}\text{K}^{-1}$
$k$	von Karmin's constant	-
$z_0$	Aerodynamic roughness of soil surface	m
$n_2$	Manning coefficient	$\text{sm}^{-1}$
$h$	Height (surface water level, or capillary rise level)	m
$s$	Slope	$\text{mm}^{-1}$
$v$	Flow velocity	$\text{ms}^{-1}$
$g$	Gravitational acceleration	$\text{ms}^{-2}$
$\Phi_i$	Empirical parameter for the effect of ice on matric potential (cryosuction)	-
$\Omega_i$	Empirical parameter for permeability reduction due to ice (impedance factor)	-
Constant	Value	Units
$\Phi_i$	1.8	-
$c_w$	0.6	$\text{Wm}^{-1}\text{K}^{-1}$
$c_i$	2.14	$\text{Wm}^{-1}\text{K}^{-1}$
$c_a$	0.024	$\text{Wm}^{-1}\text{K}^{-1}$
$H_w$	4182	$\text{Jkg}^{-1}\text{K}^{-1}$
$H_a$	2108	$\text{Jkg}^{-1}\text{K}^{-1}$
$H_s$	840	$\text{Jkg}^{-1}\text{K}^{-1}$
$H_i$	1003	$\text{Jkg}^{-1}\text{K}^{-1}$
$L_f$	334000	$\text{Jkg}^{-1}$
$\rho_w$	1000	$\text{kgm}^{-3}$
$\rho_s$	916	$\text{kgm}^{-3}$
$\rho_i$	2648	$\text{kgm}^{-3}$
$\rho_a$	1.2754	$\text{kgm}^{-3}$
$g$	9.81	$\text{ms}^{-2}$

## List of Papers

**Paper 1 (published) (Chapter 3):** Simulating water and heat transport with freezing and cryosuction in unsaturated soil: Comparing an empirical, semi-empirical and physically-based approach. By *J.C. Stuurop, S.E.A.T.M. van der Zee, C.I. Voss, H.K. French* in Advances in Water Resources Year 2021, Volume 149.

**Paper 2 (published) (Chapter 4):** The influence of soil texture and environmental conditions on frozen soil infiltration: A numerical investigation. By *J.C. Stuurop, S.E.A.T.M. van der Zee, H.K. French* in Cold Regions Science and Technology Year 2022, Volume 194.

**Paper 3 (draft) (Chapter 5):** The effect of microtopography and macropores on frozen soil infiltration dynamics. By *J.C. Stuurop, S.E.A.T.M. van der Zee, H.K. French*.

**Paper 4 (published) (Chapter 7):** Groundwater seepage causes surface runoff and erosion during snowmelt in a tile-drained agricultural catchment: Field observations and modelling analysis. By *J.C. Stuurop, S.E.A.T.M. van der Zee, T.K. Thiis, H.K. French* in CATENA Year 2023, Volume 220A.

**Paper 5 (draft) (Chapter 1):** A multi-decadal literature review of theory related to the freezing of unsaturated soils, from detailed physics to catchment-scale implications. By *J.C. Stuurop, H.K. French*.

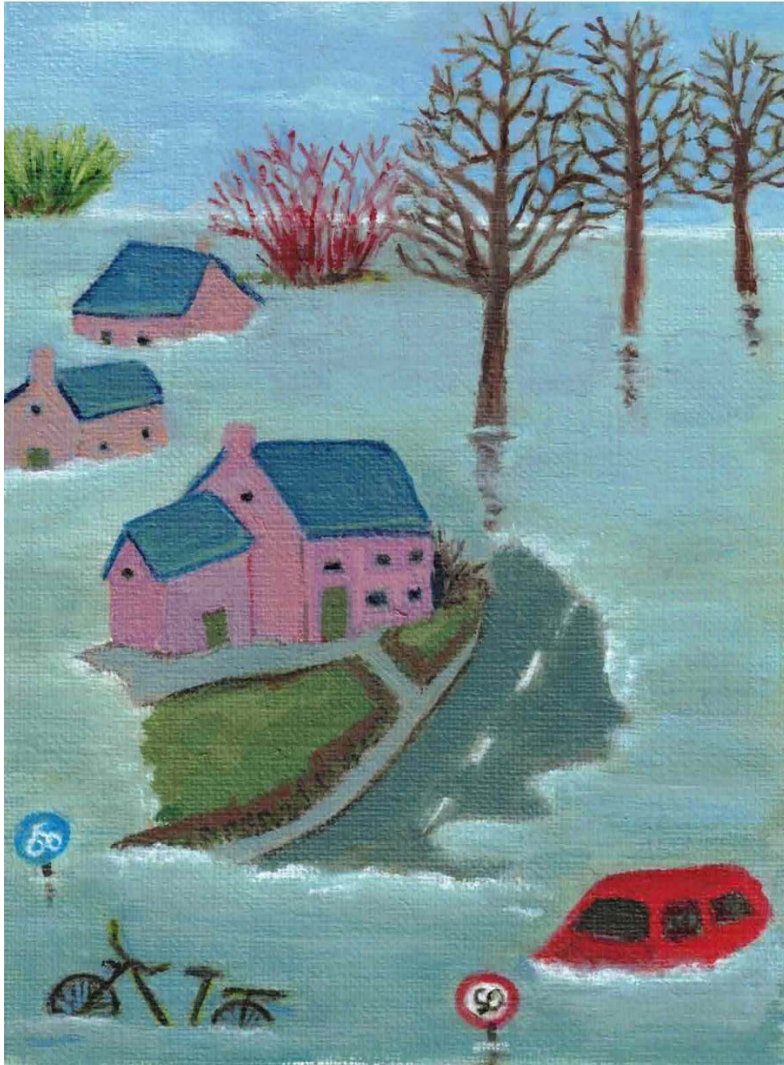
## Abstract

This PhD research investigated numerical modelling of frozen soil, implications of soil freezing on infiltration, snowmelt flooding in an agricultural landscape, and literature on soil freezing physics. The main goal was to better understand frozen soil conditions that lead to infiltration capacity decrease and thus increased flood hazard. The work resulted in five manuscripts of which three are published at the time of writing, and two are drafts. First, a numerical model called CryoFlow was developed to simulate water and heat transport in soil with phase change. Three different approaches were tested against experimental data: a physically-based, semi-empirical and empirical approach. These entailed different functions for freezing point depression and for matric potential change due to freezing (cryosuction). It was found that all variants predicted experimental results well. The semi-empirical version was however preferred because it required the least amount of empirical parameters and was therefore used for the remainder of the research. Secondly, numerical simulation of a large number of scenarios revealed the influence of soil water content, boundary temperature conditions, water input rate, soil type, microtopography, and macropores on frozen soil infiltration capacity. Specific combinations of variables and conditions were associated with various amounts of infiltration reduction (and thus increased flood hazard). Thirdly, fieldwork was carried out in a small agricultural catchment to better understand flooding and erosion due to snowmelt. Groundwater seepage was found to initiate substantial surface runoff and erosion, while in a prior winter the cause was found to be frozen soil. Finally, an overview was written of current theory and knowledge gaps concerning various aspects of frozen soil physics, such as matric potential increase with phase change, and the permeability decrease because of decreasing liquid water content.

## Norwegian Summary / Norsk Sammendrag

I dette doktorgradsarbeidet er konsekvensene av jordfrysing for infiltrasjon under snøsmelting og mulig bidrag til flom undersøkt ved hjelp av numerisk modellering av frossen jord med ulike fysiske egenskaper. Den numeriske modellen er basert på tidligere dokumentasjon om fryse og tineprosesser i litteraturen.. Hovedmålet var å bedre forståelsen av forhold som fører til redusert infiltrasjonskapasitet i frossen jord, og dermed økt flomrisiko. Arbeidet har resultert i fem manuskripter, hvorav tre er publisert og to er utkast, på tidspunktet for innlevering av avhandlingen. . Først ble den numeriske modellen, kalt CryoFlow, utviklet for å simulere vann- og varmetransport i jord med faseforandring. Tre forskjellige tilnærminger ble testet mot eksperimentelle data: en fysisk-basert, semi-empirisk og empirisk tilnærming. Disse innebar forskjellige funksjoner for å beskrive frysepunktreduksjon og endring av matrikspotensial på grunn av frysing (frostindusert matrikspotensial). Alle de testede funksjonene predikerte eksperimentelle resultater godt. Den semi-empiriske versjonen ble imidlertid foretrukket for det videre arbeidet fordi den krever færrest empiriske parametere. Videre viste de numerisk simuleringene av et stort antall scenarioer , med forskjellig kombinasjoner av initialbetingelser av vanninnhold, temperatur (jord og ved overflaten)infiltrasjonsrater, jordtyper, mikrotopografi og makroporer, effekten på infiltrasjonskapasiteten til frossen jord. Spesifikke kombinasjoner av variabler og fysiske forhold ga forskjellig reduksjon av infiltrasjonsmengde (og dermed flomrisiko). For det tredje ble det utført feltarbeid i et lite landbruksdominert nedbørfelt for å bedre forståelsen av flom og erosjon på grunn av snøsmelting. Grunnvannsutstrømning observert her viste seg å initiere betydelig overflateavrenning og erosjon, mens frost var dominerende årsak tidligere vintere. Til slutt ble det skrevet en oversikt over gjeldende teori og kunnskapshull om fysiske prosesser i frossen jord, slik som matrikspotensialøkning med faseforandring, og reduksjon i vannledningsevne på grunn av redusert flytende vanninnhold.





# 1. Introduction to the thesis

## 1.1 Motivation for the research

### *Motivation*

Water in liquid form is one of the defining characteristics of Earth. While most of Earth's natural cycles proceed at timespans far beyond that of a human life, the water cycle is prevalent at small timescales. It moves at various speeds between reservoirs, such as the atmosphere, oceans, rivers, and soil (Skinner and Porter, 1995). While the liquid form of water is essential to life on Earth, it also seasonally or interannually occurs in solid form in various cold regions. The water cycle in cold climates is different compared to warmer regions because it includes the seasonal or interannual phase change of water to ice of a substantial amount of water in the form of snow, surface ice, and soil frost. The fact that soils in cold regions seasonally or interannually contain ice has consequences for the soil's hydrological behaviour.

The most important effect of the freezing of soil from a flood hazard perspective is the reduction of the soil's permeability, and thereby its infiltration capacity (Burt & Williams, 1976a). Freezing of soil also affects the distribution of moisture in the soil by a process known as cryosuction, which entails that liquid water is drawn towards the frozen zone, resulting in less storage space for infiltrating water (Miller, 1980). The zone in which ice grows has an increased capillary suction compared to the unfrozen state, which explains the moisture migration. The cryosuction process can also cause frost heave, meaning that ice lenses grow in the soil which deform the soil's structure (Miller, 1980). This poses geotechnical problems for constructions such as roads and buildings in cryosphere regions. With specific cases, infiltration capacity might be increased after the frost thaws due to an altered soil structure. Specific to frozen soil is also the decrease in the freezing point of water due to a soil's capillary forces. More elaborate detail on the physics of frozen unsaturated soil is provided in Chapter 2.

A part of the seasonal snowfall in cold regions is intercepted by the canopy of trees, other vegetation, and manmade structures, but most of the

snowfall will result in snowpacks on the ground surface (Lundberg & Halldin, 2001). Once deposited, snow can be redistributed by wind, leading to a spatial heterogeneity in snow cover depth (Hartman et al., 1999). Snowpacks store a certain quantity of water, and over subsequent snowfall episodes, this quantity can become high. The snowpacks stay in a (mostly) frozen state until positive air temperatures are reached, which is usually in spring, though midwinter melt events also occur. The snowmelt event is associated with swelling of streams, over-saturation of soils, flood hazard, and erosion (Graybeal & Leathers, 2006; Hayhoe et al., 1995).

Water that cannot infiltrate into frozen soil will pond or flow over the land. Especially in combination with the large water flux during snowmelt, the hazard of flooding can therefore be seriously increased due to frozen soil conditions (Shanley & Chalmers, 1999). Overland flow will also increase the risk of erosion (Starkloff et al., 2017). This is of particular concern in agricultural areas. Fertile soil could be lost while contaminants and nutrients quickly reach streams, thereby degrading the water quality (Starkloff et al., 2017). Also affected by freezing of soil is contaminant transport (French et al., 2002) and groundwater recharge (Mohammed et al., 2019), but those topics are not addressed in this thesis.

In the scientific literature, it remains unclear to what extent frozen soil is connected to a catchment-scale response to rainfall or snowmelt. In a meta-analysis of frozen soil catchment studies, Ala-Aho et al. (2021) reviewed cases with a strong, weak or no hydrological response of a catchment to freezing. It shed little light on the responsible variables, i.e., it is unclear why frozen soil sometimes has an effect, and sometimes not, on streamflow or surface runoff. In a catchment, the effect of single variables is easily obscured, whereas the effect of frozen soil is in principle a question of the effect of decreased infiltration capacity, as we will see later. More detail on the knowledge gap concerning frozen soil and a catchment-scale response can be found in Chapter 2, Section 5.

The lack of knowledge concerning the extent and conditions under which freezing of soil potentially increases flood hazard (overland flow and/or streamflow) because of altered infiltration dynamics motivates this PhD

research. A better understanding of frozen soil in this regard will benefit flood hazard forecasting and mitigation.

The relevance of frozen soil conditions for future flood hazards could be affected by climate change, such as the increase in frost depth due to reductions in snow cover (Zhu et al., 2019), and more frequent high intensity rainfall on frozen ground events (Zaqout et al., 2023). Ultimately, more accurate flood hazard forecasting and mitigation during frozen conditions will benefit protection of land, property, and life in both current and future climates.

## 1.2 Main research question

This thesis does not study flooding itself but the potential increase of flood hazard due to seasonal soil freezing (permafrost will be excluded). The focus of the performed research therefore lies with the dynamics of the seasonally frozen unsaturated zone, instead of the dynamics of flooding, because an answer to the question of flood hazard relates to the dynamics of the frozen unsaturated zone instead of the scale-dependent and interrelated complexities of flooding in a catchment with innumerable process parameters. However, a short introduction to flooding is necessary to arrive at the main research question that relates flood hazard to soil freezing, which can be found at the end of this subsection.

In this thesis, the following definition will be used regarding the concept of soil freezing: the process that causes phase change from liquid water to ice in the soil; therefore, a soil at subzero temperature (Celsius scale) but without ice is not considered to be frozen. Idem, soil thawing only occurs if there is phase change from ice to water. If the soil is at such a subzero temperature that infiltrated water freezes in-situ, the soil is also considered to be frozen despite the initial absence of ice.

In any catchment, a too large amount of water added will always cause a flooding, e.g., 1 billion mm of water added within 1 hour will always cause flooding in a catchment on planet Earth (even if this quantity is absolute fiction). Following this logic, there is always a threshold for any catchment at which a certain water addition rate combined with the total volume of water

added (primary variable) will cause flooding, and there will be different thresholds for different intensities of flooding and different types of flooding. In its broadest definition (the term has no clear universally accepted definition) flooding is any form of water standing or flowing on normally dry land – this will be the definition used in this thesis. The main freshwater types of flooding could be river flooding, pluvial flooding, lake flooding, or groundwater flooding (many alternative categorizations exist) (Chen et al., 2010; Leal et al., 2017).

The thresholds for different types of flood hazard are not static through time, because some of the variables that determine these thresholds could vary on even small timescales (e.g., in an hour some of the variables could already change significantly) (Chang & Franczyk, 2008). A question then with regards to the central motivation of the thesis is the following: which of the flood-related variables are affected by soil freezing, and to which extent are they affected? Let us therefore have a look at the major secondary variables that affect flood hazard.

The following secondary variables are recognized in the scientific literature to be major factors in determining flood hazard (Chang & Franczyk, 2008; Li et al., 2019; Hernández Atencia et al., 2023; Apel et al., 2008; Cobby et al., 2009; Pourali et al., 2016):

- Soil infiltration capacity
- Storage space for infiltrating water (which in turn depends on porosity, antecedent moisture content, ice content, and groundwater level)
- Topography
- Vegetation cover (mainly through interception; affects other variables)
- Surface roughness
- Storage capacity of the stream network
- Subsurface flow velocity and discharge

From these variables, we will consider topography, surface roughness, vegetation cover, and storage capacity of the stream network to not be affected by soil freezing – at least not on the relevant time scales involved with flood hazard (e.g., a single season). In the literature, no mention could be found of such an impact of freezing on these variables to affect the short-time hydrology of a catchment (e.g., a single season).

Subsurface flow velocity and discharge affect flooding because it determines the rate at which the soil's storage space is maintained during infiltration, as well as the rate at which streams receive water from a precipitation or snowmelt event. Rapid subsurface flow could increase peak discharge in streams (Li et al., 2020). Slow subsurface flow could increase the risk of oversaturation of the soil (the groundwater table rises and reduces the soil's storage space). Nevertheless, the effects of soil freezing on subsurface flow velocity and discharge will not be considered for two reasons: 1) the effect will likely be dependent on complex and highly specific spatially-varying variable combinations from which it is hard to generalize, 2) overland flow is recognized to be a significantly more important factor for flood hazard as opposed to subsurface flow because the velocity of overland flow is usually much greater (extremely rapid subsurface flow due to manmade drainpipes or natural cavities not considered) (Hernández Atencia et al., 2023; Li et al., 2020).

For many cases, water that infiltrated into the soil would no longer be considered to contribute toward flooding (Hernández Atencia et al., 2023) – i.e., the water is stored in the subsurface, partly evaporates, and flows slowly. Furthermore, overland flow can already be considered a type of pluvial flooding by itself. Therefore, only potential changes to overland flow due to soil freezing will be considered regarding flood hazard.

There remain only two flood-hazard related variables to be affected by soil freezing: infiltration capacity, and the storage space for infiltrating water. When the infiltration capacity reduces, the water addition rate at which overland flow occurs will decrease (Ferreira et al., 2015). If the storage space for infiltrating water is reduced, the soil will saturate more quickly; in other words, over-saturation induced overland flow will occur at a lower threshold,

i.e., at a lower volume of water infiltrated into the soil. In short, soil freezing affects overland flow by lowering the threshold when overland flow occurs, as well as by increasing the amount of overland flow when it occurs (up to a certain maximum at which oversaturation of the soil would have also occurred during unfrozen conditions – the point at which infiltration capacity is practically 0).

Overland flow is considered to increase flood hazard because of in-situ inundation of the land, and because of quicker routing of water to streams in a topographical setting compared to subsurface flow (Hernández Atencia et al., 2023; Li et al, 2020; Ferreira et al., 2015). Also, the failed infiltration implies that the water could not be stored in the subsurface, meaning that the water must be stored in the other reservoirs of a catchment (on the surface directly, or in streams). Based on the connection between overland flow and flood hazard, we can now formulate the following primary research question of the thesis:

**Under which conditions, and to what extent, could freezing of unsaturated soil reduce infiltration and storage capacity, subsequently cause, or enhance, overland flow, and thus increase flood hazard?**

The question will be examined for various soil types, initial conditions, and boundary conditions through a newly developed numerical model (CryoFlow). Through testing of different frozen soil numerical modelling approaches, review of frozen soil theory, numerical simulation of test cases, and a case study of a minor snowmelt flooding event in a small catchment, it is attempted to contribute toward part of an answer on the main research question. These different subprojects are further described in the other sections of this Chapter. The cases examined will mostly entail highly simplified 1D or 2D scenarios to be able to isolate the effect of frozen soil on infiltration dynamics regarding different variable combinations (soil type, initial moisture content, freezing temperature, etc.).

A flood hazard increase because of an increase in overland flow as implied in this research, would also equate to an increase in stream discharge, if the frozen-soil-induced overland flow is connected to the stream network,

irrespective of whether the stream would overflow its banks. In other words, the research results, through the study of reduced infiltration capacity, could help predict the hydrograph response to soil freezing in a catchment. Many catchment-scale hydrological models incorporate infiltration capacity as an important variable (Ferreira et al., 2015), and the changes in infiltration capacity due to freezing (if incorporated) would likely affect the simulated stream hydrograph.

Finally, it should be noted that the research in this thesis does not quantify actual flood hazard, but only relates decreased infiltration capacity to a proportional but inestimable effect on flood hazard – an actual flood hazard can only be predicted and quantified for specific real-world cases.

### 1.3 Assumptions

The following core assumptions underpin the research in this thesis:

- Freezing of soil reduces infiltration capacity and storage space for infiltrating water to varying degrees dependent on a set of variables.
- Water that flows overland increases flood hazard (and can in itself already be considered a type of pluvial flooding according to the broadest definition of flooding).
- If all variables in comparable hypothetical cases (e.g., frozen vs unfrozen) are equal (topography, soil type, initial moisture content, etc.), the case with freezing of soil will have increased flood hazard due to the decrease in infiltration, with varying degrees of infiltration decrease dependent on the magnitude of freezing, initial moisture content, soil type, and other factors (McCauley et al., 2002; Hayashi, 2013).
- The soil in question has non-negligible infiltration during rainfall or snowmelt in unfrozen conditions (e.g., it is not on a 90° slope, is not part of the saturated zone, is not underlying a paved surface, etc.).
- A flood hazard increase does not equate to an actual flood hazard occurrence, the latter being dependent on a multitude of variables (e.g., spatially and temporally varying water input, catchment-specific properties, initial conditions in the catchment, etc.).



- The part of the landscape with frozen soil receives water (from precipitation or snowmelt), and this water is part of the flood hazard in question – otherwise, the reduced infiltration capacity does not contribute to that flood hazard.
- The soil structure remains intact upon freezing and thawing, and other factors such as vegetation cover and topography are not significantly affected by freezing as to lead to changes in flood hazard in a landscape.

In cases where these assumptions are violated or not applicable, certain results and interpretations in this thesis are (partly) invalid with regards to flood hazard. For example, cases in which the infiltration capacity increases after thawing due to frost heave.

#### 1.4 Relevant processes included in the scope of the thesis

This thesis focuses on seasonally frozen unsaturated soil, in other words, soil that contains ice only in winter. Permafrost is a different area of interest, although part of the results in this thesis are also relevant to permafrost dynamics. The physical processes relevant to this PhD research project can be divided into two over-arching categories, namely freezing/thawing of soil, and meltwater flux into the unsaturated zone. Regarding frozen soil, the following processes or factors are of importance and need to be accounted for in numerical models:

- Heat transport through conduction. The thermal conductivities of soil constituents need to be considered (liquid water, air, soil particles, and ice). These influence the soil water temperature.
- Heat capacity of soil constituents. (liquid water, air, soil particles, and ice). These determine the amount of energy required for a certain change in temperature.
- Latent heat flux and phase change. When freezing or melting temperature of the soil water is reached, phase change occurs, resulting in an increase/decrease in ice/liquid water content. Latent heat is released or absorbed during the processes.

- Matric potential. Unsaturated soil exerts a suction force on water because the soil pores act as capillaries, quantified as the soil's matric potential.
- Relative permeability. Hydraulic conductivity of soil reduces with decreasing water content, because flow occurs through progressively smaller pores upon desaturation.
- Soil water transport. Important for calculations on infiltration, permeability and water availability for freezing and cryosuction.
- Advection of heat. In soil, part of the heat is transported via the mass flux of soil water.
- Soil hydraulic properties. The required set of parameters to simulate water transport includes porosity, water retention parameters (soil water retention characteristic curve), residual water content and saturated hydraulic conductivity.
- Reduction of permeability with freezing. When ice forms in soil pores, flow paths become restricted, and permeability is reduced.
- Cryosuction. Ice growth in soil pores results in water flow towards the frozen zone because of a matric potential increase.
- Freezing point depression. Due to capillary pressure, the freezing point of water is reduced in soil pores compared to water at standard atmospheric pressure.

Processes that are ignored in this thesis, even though they are part of frozen soil dynamics are the following:

- Vapor flux. The transport of water in the gas phase is usually found to be minor (Ippisch, 2001), although in some studies it was up to 10% of total water transport in a freezing soil (Zhang et al., 2016).
- Osmotic effects. The effect of solutes in water on total potential and water freezing point is ignored. In real soil, an osmotic effect in freezing soil is expected but its magnitude is generally unknown, although Drotz et al. (2009) reported an osmotic potential contribution to total water potential ranging between 10 to 69%. Although an osmotic effect is not directly taken into account in this thesis, calibration and empirical formulations would implicitly

include an osmotic effect since solute concentrations affected the data for which calibration and empirical constants are formulated.

- Frost heave. It is well known that freezing of soil can result in uplift and destruction of soil structures. A body of research exists that deals with this problem specifically, usually from a geotechnical perspective (O'Neill, 1983). A prerequisite of frost heave is known to be cryosuction because it provides the moisture needed for ice lens growth (Sarsembayeva & Collins, 2017). The exclusion of frost heave in this thesis is a drawback, because if it occurs, it likely has effect on soil hydraulic properties. There is however too little information in the scientific literature to formulate relations between frost heave and hydraulic properties, especially since it is hard to predict how soil structure recovers after thawing of ice lenses. The effect of cryosuction, in creating ice rich impermeable zones, is however incorporated in this thesis. Perhaps the discrepancy by not including frost heave might not be too large. Especially if net soil structural change after a complete freeze-thaw cycle is small. Yet, there is no means to quantify the discrepancy, and all experimental results to which the model in this thesis was compared with entailed non-frost heaving soils. In effect, caution should be employed when applying the results of this research to soils undergoing frost heave.

The following processes or factors are most relevant to the topic of meltwater flux in a landscape:

- Atmospheric precipitation of water, both in the form of liquid water and solid (snow, hail, etc.).
- Solar radiation, as it influences the thermal state of snow.
- Air humidity, as it influences condensation, sublimation and vaporisation of water at the snow-air interface.
- Windspeed and direction, as it controls the redistribution of snow cover in a landscape, as well as its thermodynamic state.
- Snowpack properties, such as water content, density, snow crystal shape and albedo. These properties influence the thermodynamics and water flux in a snowpack.

- Topography of the landscape, because it influences the distribution of snowcover as well as the radiative energy flux received by the snowpack from the sun.
- Forest cover, because it influences the longwave and shortwave radiation a snowpack receives. Shading for example reduces snowmelt by reducing solar irradiation, while tree trunks heated up by the sun radiate in the longwave spectrum, thereby stimulating snowmelt.
- Land cover, because vegetation and the roughness of the soil surface influence the pathways of meltwater flow and strength of erosion of soil material. Such factors could also directly or indirectly influence the thermal state of the snowpack.
- Groundwater, because shallow flow and seepage provide heat for snowmelt, and seepage would further increase erosion hazard because also subsurface water fluxes are often large during snowmelt.

### 1.5 Research aims per subtopic

As mentioned before, the major research aim of this thesis is to understand when frozen soil conditions could potentially increase flood hazard. This entails looking at the conditions during which infiltration into the unsaturated zone is impeded. To be able to contribute toward an answer to the main research question, the research was subdivided into smaller research aims, each resulting in different scientific papers that form the basis of the chapters. In short, these subdivisions were: 1) creating and testing a numerical model for water and heat transport in the unsaturated zone with phase change, 2) testing of various 1-dimensional infiltration scenarios with frozen soil conditions, 3) testing of 2-dimensional infiltration scenarios (microtopography and macropores) with frozen conditions, 4) a case-study of snowmelt overland flow and erosion in an agricultural catchment, and 5) providing an overview of theory relating to frozen soils, from detailed physics to catchment-scale effects.

A more comprehensive overview of the specific aims for each of the research papers / thesis Chapters / subtopics is formulated below, listed chronologically in roughly the order in which the research was carried out.

**Paper 1 (Chapter 3):** The goal of the first research project in the PhD project was threefold: 1) to construct a functional soil water and heat transport model that could simulate freezing and thawing of unsaturated soil, 2) to test the model predictability through comparison with data from experiments, 3) to compare three different approaches toward unsaturated frozen soil simulation as found in the literature, ranging from empirical, semi-empirical to physically-based (an explanation of these terms will follow later in the concerning Chapter). Experimental data for testing of the model came from three published sources: Mizoguchi (1990), Watanabe et al. (2012) and Zhou et al. (2014). The latter two studies performed measurements of ice content, liquid water content and soil temperature, which allowed for testing of all relevant output variables of the model; in Mizoguchi (1990), only total water content was measured.

This first research project was intended to result in a functioning soil water and heat transport model that could be employed to simulate frozen soil infiltration dynamics, and thus help explore the relationship between soil freezing and flood hazard. By testing different approaches, an informed choice could be made in selecting the variant of the model to further study those dynamics with.

**Paper 2 (Chapter 4):** This paper focused on the process of infiltration into frozen soil. The goal of this project was twofold: 1) to test the created soil water and heat transport model with phase change against an experiment that included infiltration into frozen soil; 2) to simulate a large number of synthetic scenarios to uncover controlling factors on infiltration capacity of frozen soil and subsequent overland flow generation. The aim was to provide a link between the reduction of infiltration capacity and frozen conditions for different soil types, initial conditions and boundary condition (e.g., water input rate, and temperature). The results of this study form a major part of the answer to the main research question.

**Paper 3 (Chapter 5):** In the third study, the effect of microtopography and macropores on the infiltration of melt- and rainwater on a frozen slope with slight inclination was studied. In the literature, it can be found that microtopography could affect meltwater infiltration into frozen soil (only two studies; H. French & Binley, 2004 and Hayashi et al., 2003). Macropores are understood to sustain preferential flow paths despite subzero temperatures (Celsius scale) (Mohammed et al., 2018). In the third paper, the aim was therefore 1) to understand water and heat transport dynamics during freezing, thawing and infiltration into frozen soil with microtopographic or macro-porous features, and 2) to assess the effect of microtopography and macropores on overall frozen soil infiltration for a range of boundary and initial conditions. Again, several synthetic scenarios were developed and simulated with the constructed model from Paper 1 (modified to include 2 dimensions and atmospheric energy fluxes). The results of this study shed light on the occurrence of spatially varying infiltration and storage capacity reduction due to freezing, and help to better understand the effect of soil freezing on infiltration and overland flow from the perspective of a highly simplified landscape.

**Paper 4 (Chapter 6):** This study brought the topic of frozen soil dynamics at the soil column / field plot level to snowmelt and frozen soil at the landscape level. With the help of UAV-imaging, frequent hydrological observations were made during a snowmelt period in a small agricultural catchment. Coincidentally, during the melt season a surge of groundwater seepage in response to snowmelt occurred, which caused substantial overland flow and erosion. Comparisons were made with prior study winters (older studies). The eventual goals of this study were to 1) identify the possible role of frozen soil during snowmelt in a landscape, and 2) to characterize and understand sudden groundwater seepage in response to snowmelt. The results of this study provide a case example of frozen soil impact on overland flow, and shed light on another mechanism through which flood and erosion hazard might be increased during the snowmelt flux.

**Paper 5 (Chapter 2):** In this paper, the aim was to provide an overview of theories encountered in the literature on frozen soil physical behaviour,

especially relating to freezing point depression, cryosuction, and permeability. Such theoretical considerations help to better understand why frozen soil decreases infiltration and storage capacity in the first place, and which mechanisms influence it. Most of the earlier frozen soil theory was formulated in the second half of the 20th century. The inconclusiveness of studies performed in that time period, and the open-ended discussions that were ongoing, seemed to have been 'forgotten' in more recent decades. Therefore, the aim of this chapter is also to re-open the debate on theory relating to the freezing of unsaturated soil, which will ultimately help improve frozen soil models and thus flood hazard assessment. New theoretical reflections are added, but without further testing or development because the focus of the thesis does not lie with the theoretical physics of frozen soil dynamics but with the consequences of soil freezing for infiltration and storage capacity. A better understanding of frozen soil theory could lead to better numerical models that simulate the process, which will ultimately aid frozen soil flood hazard assessment. Also included in this paper was the current state of knowledge on the effect of frozen soil on catchment hydrology, and thereby provides a more in-depth overview of the major knowledge gap this thesis addresses; see Chapter 2, Section 5. *Because a theoretical background of soil freezing could be informative to the reader before being presented the results of the other studies, this paper has been brought forward in the thesis to form Chapter 2.*

## 1.6 Methods

The main methods of this study entailed numerical modelling of synthetic scenarios with a newly developed water and heat transport model with phase change (called CryoFlow for easy reference), comparison of model results to previously published experimental results, and field work in a small agricultural catchment. The mathematical details of the model can be found in Chapter 3, in which the model is introduced. In Chapters 4 and 5, modifications to the model are described. A full overview of the functionality, code, equations, and optional modules of CryoFlow, are given in the manual for the model, provided in the Appendix of this thesis. The model is available online as freeware at <https://sites.google.com/view/cryoflow>. The model is constructed with Visual Basic Application

code in macro-enabled Excel software using the Forward Euler method with small time steps for numerical calculation.

Various previously published experimental results are used for testing of the model (Table 1). Each chapter describes the datasets used in that specific modelling study in detail, but an overview will be given here. Data from three studies was used to assess accuracy of the model to simulate freezing of an unsaturated soil column. Other results from a freeze-thaw study were used to further assess accuracy of thermodynamic simulation of multi-day diurnal freeze-thaw cycles. Finally, results from an infiltration into frozen soil experiment were used to assess the ability of the model to simulate infiltration dynamics during frozen conditions. The model was also tested against Hydrus1D and SUTRA-ICE for general assessment of proper numerical solution of simple water and heat flux cases without and with freezing (unsaturated conditions excluded, because SUTRA-ICE did not include matric potential changes upon freezing).

Fieldwork was carried out in a small agricultural catchment in southern Norway (details in Chapter 6). A combination of UAV-photographs, photogrammetry, in-situ snow depth and density measurements, a drainage pipe discharge and surface channel discharge monitoring station, and field observations were used to assess snowmelt processes in the catchment. Groundwater modelling (MODFLOW) was undertaken to simulate the observed groundwater seepage. Study site characteristics are described in Chapter 6, as well as further details on the field and modelling methods. Data from previous winters was used as well (Starkloff et al., 2017) and used as input for the groundwater model, as well as for the CryoFlow model, to assess the role of snowmelt and frozen soil in causing overland flow and erosion during the various study winters.



Table 1. Datasets used in this PhD research.

Dataset from prior study	Measurements used for comparison with model results	Number of different experimental setups tested	Chapters in which the data was used
Mizoguchi (1990)	Total water content	1 (3 different time points)	Chapter 3
Watanabe et al. (2012)	Total water content, liquid water content	3 (initial saturation varied)	Chapter 3
Zhou et al. (2014)	Total water content, liquid water content, ice content, temperature	2 (initial saturation varied; 2 different time points)	Chapter 3
Wang et al. (2017)	Temperature	1 (3 different depths, continuous measurement)	Chapter 4
Pittman et al. (2020)	Liquid water content, temperature, cumulative infiltration	2 (initial saturation varied; 3 different time points)	Chapter 4

## 1.7 Outline of the thesis

This section partly repeats the information of section 1.3 but presents it in the order by which the topics are introduced in the thesis. Firstly, a very detailed literature overview of frozen soil theory is provided (**Chapter 2**) including pore-scale physics and landscape-scale hydrological implications. The questions postulated in this chapter do not serve as questions to be answered in this thesis, but as open-ended questions to stimulate scientific curiosity and revival of certain debates. Section 5 of this Chapter will be most relevant regarding the direct implications of soil freezing for flood hazard.

**Chapter 3** provides the results of the study on different modelling approaches towards soil freezing. It also introduces the CryoFlow model

created in this PhD project. It furthermore includes some of the test cases of the model against previously published experimental data.

In **Chapter 4**, the study on frozen soil infiltration dynamics via numerical modelling is described. It includes the results of a large number of synthetic test cases, and also a test of the model against previously published experimental infiltration data.

**Chapter 5** contains the study on microtopography and macropores, in which the 2D version of the CryoFlow model is applied. Insights are given on the interplay during freezing and thawing between microtopography and macropores on the one hand, and boundary, soil and initial conditions on the other hand. The short **Chapter 6** describes the magnitude of cryosuction for various soil types and model conditions. It is not a full manuscript, but it provides useful background to the process of cryosuction, which is a central aspect of frozen soils. In **Chapter 7**, the results of a small catchment case-study are described in which groundwater seepage in response to snowmelt played a major role. The chapter includes UAV images of snowmelt in the landscape, overland flow, and erosion marks. The contributions of each chapter with regards to the main research question and overall research topic will be discussed in **Chapter 8**, which will also provide a conclusion, limitations of the performed research, and an outlook for further research.

## 2. A multi-decadal literature review of theory related to the freezing of soils, from detailed physics to catchment-scale implications

*This chapter is based on the upcoming manuscript “A multi-decadal literature review of theory related to the freezing of unsaturated soils, from detailed physics to catchment-scale implications.” by J.C. Stuurop and H.K. French.*

### 2.1 Introduction

The freezing of unsaturated soil has been researched for decades and for various reasons. Freezing of unsaturated soil has implications for geotechnical engineering, contaminant transport, flood hazard, and groundwater recharge. Several models have been developed to simulate water and heat transport with phase change in unsaturated soil. Such models are often based on equations derived from earlier theory. Most of the earlier theory was formulated in the second half of the 20th century (Williams & Smith, 1989). There seems to be the tendency of recent studies to ignore the inconclusiveness of studies performed in that time period, and the open-ended discussions that were ongoing (e.g., Miller, 1980; Jumikis, 1957). Recent models are formulated based on specific theoretical principles from that time period (for an overview, see for example, Kurylyk & Watanabe, 2013) despite the myriad of non-falsified theories. It is therefore important to revisit the fundamental principles of frozen soil theory, and to revive the debate. Better understanding of frozen soil theory will ultimately benefit model development, and subsequently flood hazard prediction due to frozen soil conditions.

There are four core principles of frozen soil that will be discussed: freezing point depression, matric potential change, permeability reduction, and implications for catchment-scale hydrology. While significant progress has been made on each of those phenomena, such progress can only be maintained through the acknowledgement of the existing knowledge gaps and unresolved issues. This Chapter will investigate the different theories that were postulated regarding the four core principles, and pinpoint unresolved issues and non-falsified hypotheses. Open-ended reflections are

added to the literature review to encourage a revival of the debate. These questions are not intended to be answered within this thesis, and do not serve as research questions for the PhD project. Instead, the theory discussed in this Chapter mostly serves as detailed background explanation to the processes and equations incorporated in the performed numerical modelling, whereas Section 5 relates soil freezing directly to observed catchment responses (and thus flood hazard).

## 2.2 Frozen soil: freezing point depression

Liquid water is still present in soil even if the temperature drops well below the standard freezing point of water (Ayers & Campbell, 1951). Soil ice content progressively increases with decreasing temperature. Currently, the predominant explanation in the literature is that the lower freezing point of water in soil is the result of capillary pressure (Kurylyk & Watanabe, 2013). In this section, the underlying physical mechanisms of freezing point depression will be discussed.

### What is capillary pressure?

First, we must fully understand capillary action in soils, because in the literature one could sometimes find incorrect interpretations of capillary action and negative pressure. Capillary action is the result of two types of forces, namely adhesion of water molecules to a solid material, and cohesive forces between water molecules at the water-gas, water-vacuum, water-liquid, or water-solid interface, which create surface tension (Morrow & Szabo, 1970). If a capillary tube with adhesive properties, e.g., a glass tube, is partially immersed in water, the water molecules are attracted to the wall and flow upward against gravity (Morrow & Szabo, 1970). Water molecules further away from the capillary wall are flowing upward as well because of the cohesion forces between water molecules. Consequently, we observe a rise of the water level in the tube (Figure 1).

By considering the water in the tube to be at lower pressure than atmospheric, the physics of the capillary system can be described and calculated (Hassanizadeh & Gray, 1993). If the water in the capillary was not at a lower pressure than the atmospheric pressure weighing down on the

water surface outside of the capillary, the water could not be elevated within the tube, as there would be no pressure differential. The smaller the radius of the capillary tube, the higher the rise of the water in the tube, therefore the lower the capillary pressure. This happens because with smaller radius, there is less weight of water to be pulled upward, resulting in less gravitational force downward, hence the water can rise higher until the point at which capillary pressure equals the water column pressure due to gravity. Also in absolute terms, the capillary pressure will be lower in a smaller capillary, because the surface area at the water-air interface at which capillary forces are enacted is smaller (pressure = force / area). The capillary pressure is recorded as a negative pressure compared to atmospheric pressure but would also be recorded as such in a vacuum.

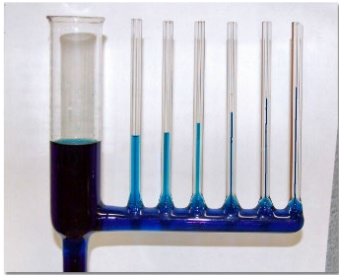


Figure 1. Capillary rise in tubes of different radius. The smaller the radius, the higher the rise in the tube. Image source: United States Geological Survey, Dr. Keith Hayward.

But what are the forces that result in the negative capillary pressure exactly, and is it truly a negative pressure? At the interface where adhesion occurs (water-solid), these are the intermolecular forces between water molecules and molecules of the capillary wall (such as electrostatic forces). If cohesive forces within a liquid would be stronger than the adhesive forces to the capillary wall, the liquid would be repelled by the capillary and capillary pressure becomes positive (water level in the capillary tube drops compared to the surrounding water level; see Figure 2). If adhesive forces are stronger, capillary pressure is negative (water rises in the capillary). The net force resulting from the balance of adhesive versus cohesive forces is represented

by the contact angle measurement: the angle a droplet of liquid forms with a horizontal surface upon contact (Good, 1992).

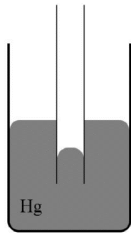


Figure 2. Positive capillary pressure exists when a narrow glass tube is immersed in mercury, because mercury does not adhere to glass. Image source: Onyshchenko (2018), PhD thesis: 'Atmospheric pressure plasma jet for multipurpose plasma activation of polymeric substrates'.

The Young equation relates intermolecular forces at the liquid-solid interface and cohesive forces within the liquid to the contact angle (Young 1805):

$$\cos\sigma = \frac{\gamma_{sa}-\gamma_{sl}}{\gamma_{la}} \quad [0]$$

Where  $\sigma$  is the contact angle,  $\gamma_{sa}$  is the interfacial tension at the solid-air interface,  $\gamma_{sl}$  is the interfacial tension at the solid-liquid interface (at which adhesive forces play a role), and  $\gamma_{la}$  is the interfacial tension at the liquid-air interface (what is commonly meant with surface tension). Notice that when the solid-liquid interfacial tension decreases, the contact angle becomes smaller (more hydrophilic conditions); hence, adhesion reduces the water's surface tension because the water molecules bond with the solid material.

The other force responsible for capillary pressure is the cohesive force within a liquid, which in water results from bipolar electrostatic bonds (positively charged Hydrogen atoms to negatively charged Oxygen atoms). At the surface of the liquid, these forces have an inward direction resulting in a surface tension, which can be quantified. It is measured as the force required to increase the surface area of a liquid. The surface tension is maximum at the liquid-gas or liquid-vacuum interface (gas usually contains so few molecules that in effect it is like a vacuum). The surface tension is altered when in contact with a solid or another liquid because the outer water molecules (at the interface) might be attracted to the solid or other liquid.

The Young-Laplace equation (Young, 1805; Laplace, 1805) calculates the capillary pressure resulting from both adhesion (quantified as the contact angle) and cohesion (quantified as the surface tension):

$$p_c = \frac{2\gamma_{la}\cos\sigma}{r} \quad [1]$$

Where  $p_c$  is the capillary pressure (Pa) and  $r$  is the radius of the capillary.

If the contact angle is greater than  $90^\circ$ , capillary pressure will be negative, whereas if it is lower than  $90^\circ$ , it is positive. The number 2 results from  $2\pi r$ , thus the surface tension acts along the inner circumference of the tube ( $\text{Nm}^{-1}$ ). Only the ' $r$ ' remains in the denominator, but without simplification of the formula it would be  $2\pi r^2$ , which gives the circular surface area of the capillary tube. The cohesive force along the inner circumference of the tube is divided by the surface area of the tube, resulting in capillary pressure ( $\text{Nm}^{-2}$ ). The smaller the area of the tube, the greater the pressure because the tension force remains at constant value while the surface area changes.

To calculate the height of the capillary rise in a tube, we then only need to divide the capillary pressure by the gravitational pressure on the liquid (known as Jurin's Law; Jurin, 1718):

$$h = \frac{2\gamma_{la}\cos\sigma}{\rho_l g r} \quad [2]$$

Where  $h$  is the capillary rise (m),  $\rho_l$  is the liquid density ( $\text{kgm}^{-3}$ ) and  $g$  is the gravitational acceleration ( $\text{ms}^{-2}$ ).

The capillary pressure thus equals the hydrostatic pressure of the water column that rose (or dropped) in the capillary. Out of convenience, capillary pressure is therefore often expressed as a negative water column height (or positive in case of repelling capillary walls). In an adhesive capillary (contact angle  $< 90^\circ$ ), it is a negative pressure compared to atmospheric pressure because the force is outward from the perspective of the liquid (the liquid is being 'pulled' on and being stretched). The negative pressure can drop far below 0 Pascals absolute pressure (vacuum) if the capillary radius is small enough (Vera et al., 2016). At such low pressures, water cavitates and boils away. But in the absence of nucleation sites, water can stay in a metastable

liquid phase, akin to a superheated state (Or & Tuller, 2002). In lack of a better word, the water is “superstretched”.

However, there is an error in this common physical description of the capillary system because negative absolute pressure is impossible (it would otherwise imply absolute negative energy density). In the same vein, an absolute negative magnitude of force cannot exist. It must therefore be concluded that capillary pressure is a convenient way to describe flow due to ‘imagined’ pressure differentials in a capillary system, but it is physically incorrect. In reality, the liquid in a capillary is not under absolute negative pressure, instead it is under tensile stress due to adhesive and cohesive forces. The negative sign in front of a capillary pressure reading is simply an arbitrary denotation meaning “opposite in the direction of positive”; thus, it has directional meaning, but not physical.

In other words, a liquid can stretch like an elastic due to surface tension; the smaller the capillary, the greater the tensile stress. Calculating fluid behaviour with capillary pressure works because the magnitude of combined adhesive and cohesive forces is correctly represented, as it is the outward force pulling water in any direction along the entire area of the water surface in the capillary (force / area). In case of positive capillary pressure (liquid level dropping in a capillary), there is a ‘pushing’ instead of a pulling force. The cause of water flow in the capillary is a difference in energy level at the molecular interface between water and solid, and water and air, which result in capillary forces to attain the lowest possible energy configuration. These forces are thus quantifiable as ‘negative pressure’ simply because of the inverted direction of pressure. These considerations of the water not attaining absolute negative pressure but tensile stress and overstretched states in capillaries, are relevant in the context of freezing point depression.

Despite their complex shape, soil pores are commonly considered to behave like capillary tubes, although even the concept of a soil as a bundle of capillaries could be questioned (Hunt et al., 2013). The conceptual model of soil physics underlying the numerical model in this thesis is based upon capillary bundle theory, however. A discussion of capillary bundle theory is outside the scope of this research project.



### Causes of freezing point depression

In a soil, the lower-than-atmospheric pressure in the capillaries is expressed as the soil's tension, matric potential, suction pressure, or matric potential, among other terms – in this thesis, it will consistently be referred to as matric potential (keeping in mind that it is actually an inverted pressure measurement representing tensile stress). Given the fundamental relationship between pressure and phase change for any substance, the notion that the freezing point of water in a soil is changed due to capillary pressure seems logical. In the literature, this notion leads to implementation of the Clausius-Clapeyron equation (Hayashi, 2013), which relates phase change to both temperature and pressure (sometimes simply called Clapeyron equation). It calculates the slope of the tangent along the coexistence curve of two phases within a phase diagram:

$$\frac{dT}{dP} = \frac{(v_w - v_i)T_f}{L_f} \quad [3]$$

Where T is the temperature (K), P is the pressure (Pa),  $v_w$  is the specific volume of water ( $\text{m}^3\text{kg}^{-1}$ ),  $v_i$  is the specific volume of ice ( $\text{m}^3\text{kg}^{-1}$ ),  $T_f$  is the freezing point of water at standard atmospheric pressure (273.15 K), and  $L_f$  is the latent heat of fusion ( $\text{Jkg}^{-1}$ ).

An apparent problem emerges when applying this notion to capillary water, however. The freezing point of water increases with a decrease in pressure (because ice has a higher specific volume than liquid water), while the opposite occurs in capillaries with negative pressure: the freezing point is lowered. However, a common phase change diagram assumes equal pressure distribution for both phases along the coexistence curve, while in frozen soil, ice is under atmospheric (and possibly overburden) pressure, while water is under capillary pressure. Consequently, the freezing point of water is lowered with decreasing pressure, as the Clapeyron relationship collapses to Eq. 4 wherein the ice pressure times ice density is omitted (because its value is 0 in case of no overburden pressure, with 0 being referenced to the atmospheric pressure):

$$dT = \frac{T_f P_w}{L_f \rho_w} \quad [4]$$

Where  $P_w$  is the pressure of liquid water (Pa) and  $T$  is the temperature (K). The pressure of liquid water in the soil is assumed to be equal to the capillary pressure, or the soil's matric potential. In this equation,  $dT$  gives the magnitude of the freezing point depression.

But if negative pressure is actually tensile stress, how could negative pressure affect phase change? Water in capillaries should potentially cavitate with very low 'negative pressure', and this has been observed (Or & Tuller, 2002). The freezing point depression also correlates well with the predictions of the Clapeyron relationship in Eq. 4 (Williams & Smith, 1989). Therefore, tensile stress can be considered a negative pressure with regard to the physics of phase change. Yet how could negative pressure (tensile stress) both cause cavitation and lower the freezing point of water at the same time? This would require too much detail on thermodynamics to be answered here. It suffices to mention that the process of nucleation and the phase diagram of water are highly complex with various coexistence curves of different phases and over 17 forms of ice phase, including pseudo-ice clathrates (Huang, 2016).

In any case, we are able to calculate the freezing point of water in a capillary based on capillary pressure and capillary radius satisfactorily (Koopmans & Miller, 1966). It is furthermore known that the freezing point depression is not the result of supercooling (absence of nucleation sites), as it has been found that actual freezing point depression takes place, even if supercooling can play an additional role as well (Jumikis, 1957; Miller, 1980; Williams, 1967). An interesting question in this discussion would be: how is the freezing point of a liquid altered in a capillary tube with non-adhesive properties, such as mercury in a glass capillary? The answer could not be found in current literature.

The graph below (Figure 3) demonstrates the freezing point depression with decreasing pressure according to Eq. 4. It can be observed that there is no significant freezing point depression until approximately a pF of 3.5, whereas the freezing point drops rapidly above a pF value of 4. Above a pF of 5.5 or 6 approximately, the freezing point depression becomes extreme. At such

negative pressures however, the physics of water phase change becomes more complex, and the simple Clapeyron relationship is unlikely to hold, as the existence of clathrates becomes a possibility, and the cavitation limit of surface tension is exceeded (Huang et al., 2016).

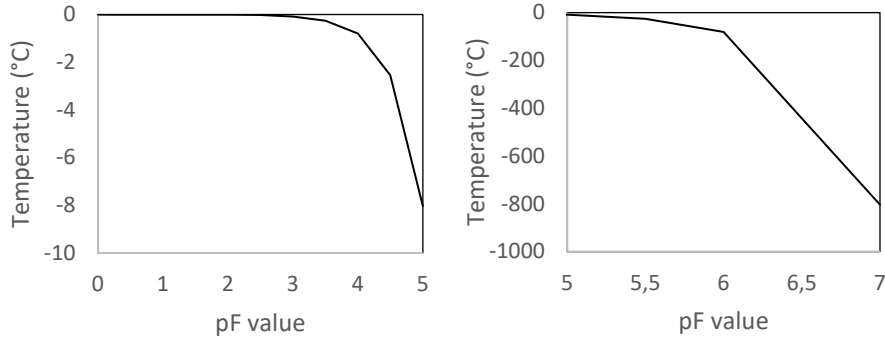


Figure 3. Freezing point depression related to capillary pressure (expressed as pF value) based on Eq. 4.

When the ice phase pressure is not equal to zero (atmospheric pressure) because of overburden pressure, the ice pressure has to be taken into account as well. The following variant of the Clapeyron equation includes both the ice pressure and liquid water pressure (Williams & Smith, 1989):

$$T - T_f = \frac{(P_w v_w - P_i v_i) T}{L_f} \quad [5]$$

Where  $P_i$  is the ice pressure. The  $T$  in this case is the temperature at which freezing initiates.

Experiments with capillary tubes have shown the freezing point depression to indeed depend on capillary radius (Blachere & Young, 1972; Hosler & Hosler, 1955; Sorby, 1859). This principle is the basis of the Kelvin equation (Liu et al., 2003). The following variant of the Kelvin equation gives the freezing point of water in relation to capillary radius and interfacial energies (Mazur, 1977):

$$T^* = \frac{2v_w \gamma_{wi} T_0 \cos \sigma}{L_f r} \quad [6]$$

Where  $v_w$  is the specific volume of liquid water ( $\text{m}^3\text{kg}^{-1}$ ),  $\sigma$  is the interfacial excess energy per unit area of ice-water interface ( $\text{Jm}^{-2}$ ),  $T_0$  is the freezing point of water at standard atmospheric pressure (273.15 K),  $\gamma$  is the contact angle between the solid-liquid interface and the capillary wall,  $L_f$  is the latent heat of fusion of water,  $r$  is the radius of the capillary, and  $T^*$  is the new freezing point of water (K).

The Kelvin equation circumvents the concept of capillary pressure, but it is in effect equivalent since capillary pressure is equal to  $\frac{2\gamma_{wi}\cos\sigma}{r}$ . Therefore, the Clapeyron relationship and the Kelvin equation have equal solutions.

Another cause of freezing point depression of water in soil is the presence of solutes (Spaans & Baker, 1996). Once water turns to ice, solutes are expelled, resulting in higher concentrations of solutes in the liquid water. Since solutes interfere with ice crystallization, the higher the osmotic potential, the lower the freezing point of the water (Jones & Getman, 1903). This effect adds to the freezing point depression due to capillarity. The relative magnitude of matric and osmotic potential is unknown, but the study by Drotz et al. (2009) mentions a range between 10% to 69% for the contribution of osmotic potential to total water potential.

*From here and further on in the text, the notion that negative matric potential (tensile stress) correlates to a lower freezing point of water according to the Clapeyron relationship (Eq. 4), will be considered as correct for the physical behaviour of water in freezing soil.*

#### Equations to calculate freezing point depression in soil

The Clapeyron relationship enables us to relate matric potential in the soil to the proportion of soil water that remains unfrozen based on the soil's temperature. This gives rise to the Soil Freezing Curve (SFC), which describes the relationship between liquid water content and temperature in the soil (Koopmans & Miller, 1966; Spaans & Baker, 1996). Researchers have found through experimentation that the liquid water content – temperature relationship is independent of initial total water content (Anderson & Tice, 1973; Fisher, 2002; P. J. Williams, 2015). When initial water content did have

an effect (Suzuki & Suzuki, 2011; Yong, 1964), measurement error was suggested by other authors (Kruse et al., 2017; Watanabe & Wake, 2009).

To obtain the SFC, some authors have incorporated the Clapeyron equation into common expressions for the Soil Water Retention Curve (SWRC), e.g., the Brooks-Corey, Van Genuchten, and Fredlund and Xing equations (Kurylyk & Watanabe, 2013; Ren et al., 2017). An example is given here from Zhang et al. (2016) who combined the Clapeyron equation with the van Genuchten equation:

$$\theta_u = \theta_r + (\theta_s - \theta_r) \left[ 1 + \left( \alpha \frac{L_f T}{g T_0} \right)^n \right]^{1 - \left( \frac{1}{n} \right)} \quad [7]$$

Where  $\theta_u$  is the liquid water content ( $\text{m}^3\text{m}^{-3}$ ),  $\theta_r$  is the residual total water content ( $\text{m}^3\text{m}^{-3}$ ),  $\theta_s$  is the saturated total water content ( $\text{m}^3\text{m}^{-3}$ ),  $g$  is the gravitational acceleration ( $\text{ms}^{-2}$ ), and  $\alpha$  and  $n$  are fitted model parameters.

The advantage of this approach is that the parameters that relate matric potential to water content can be used to determine the liquid water content. If the initial assumption is indeed correct (the relationship between capillary pressure and freezing point depression), this approach is a partially physically-based method since it is derived from the established dependence of phase change to pressure and temperature formalized in the Clapeyron equation. The word ‘partially’ is added because the soil water retention equation is an empirical description of capillary forces in a soil.

Soil water contains variable amounts of solutes however, which decreases the water’s freezing point. This would cause the prediction based on the Clapeyron relationship alone to be imprecise. Furthermore, as described before, since freezing expels solutes from water, liquid water in the presence of ice has increased solute concentration, which would further lower the freezing point. The degree to which osmotic potential effects make Clapeyron-based SFCs inaccurate is however unknown.

Hysteresis could affect the SFC in a similar way as it affects the SWRC, which would result in significantly different freezing and thawing curves (Amiri et

al., 2018a; Lara et al., 2021). This happens due to pore shape irregularities and hysteresis of contact angles, among other reasons. The author of this thesis proposes another factor of consideration, that of a different thawing temperature point of frozen water compared to the temperature at which the water under tensile stress froze. Once water turns to ice, capillary forces seize to act on the now solid water (Bogdan, 1998; van Oss et al., 2012). Consequently, the ice itself is not under tensile stress (negative pressure), and there is also potentially overburden pressure by the overlying soil. In that case, would the thawing temperature of ice not be closer to the standard thawing point at atmospheric pressure? The notion of a different thawing point in the soil compared to the freezing point has to the author's knowledge not been examined in earlier literature.

Several SFC expressions have been proposed that do not make use of the Clapeyron relationship but are purely reliant on empirically measured constants – these will be termed empirical approaches (Kurylyk & Watanabe, 2013). The simplest approach is a linear piecewise relationship between temperature and liquid water which has been found to reasonably approximate measured SFC datapoints (McKenzie et al., 2007; Kurylyk and Watanabe, 2013). Anderson and Tice (1972) developed an empirical power curve to express liquid water content as a function of temperature:

$$\theta_u = \frac{\rho_d}{\rho_w} \alpha_2 (-T)^\beta \quad [8]$$

Where  $\rho_d$  is the dry density of the soil ( $\text{kgm}^{-3}$ ) and  $\alpha_2$  and  $\beta$  are model parameters. The power curve has been used in several models and parameter values for a wide range of soils have been established, as well as a method to derive the parameters from the specific surface area of a soil (Kurylyk and Watanabe, 2013).

In the model SUTRA-ICE, an empirical exponential function for the liquid water content is implemented. This function has been suggested by McKenzie et al. (2007) based on work by Lunardini (1988):

$$\theta_u = \theta_r + (\theta_s - \theta_r) \exp \left[ - \left( \frac{T - T_0}{w} \right)^2 \right] \quad [9]$$

Where  $w$  is a fitting parameter.

It is difficult, however, to know the correct value for  $w$  in Equation 4 as very few soils have been parameterized through experimental work (Ren et al., 2017). Hence, it is a parameter that often requires calibration. Ren et al. (2017) provides a verification of four different SFC expressions on experimental data (the SFC expressions of Eq. 7, 8 and 9 included). The study shows that all three expressions work well, with some slightly better than others depending on soil type. Further systematic and repetitive experimental testing of SFC accuracy is however lacking in the literature. It therefore remains uncertain to what extent the aforementioned SFCs are generally applicable and in which cases adjustments are required, especially considering previous considerations on hysteresis, thawing temperature point, solute concentrations, and complex phase change physics at very low matric potentials.

### 2.3 Frozen soil: cryosuction

It is recognized for decades through experimental work that liquid water is drawn toward the frozen zone in a soil due to a lowering of matric potential, a process known as cryosuction (Harlan, 1973; Kaplar, 1970; Miller, 1980; Taber, 1930). The exact physicochemical causes of this water potential decrease in the frozen zone are complex and a reader new to the field of cryosuction might get confused and overwhelmed by the literature as vastly different theories are put forward. Miller (1980) is often cited for his fundamental work on cryosuction and frost heave. He for example notes that Soviet researchers diverged in important details on the mechanisms of frost heave, to which he adds: “if readers are dismayed by disarray among soil physicists who write about soil and water in English, (...) a translator encounters similar problems among scientists who write in Russian”. Even about his own work, Miller admits: “some of our thoughts may not survive closer scrutiny” (Miller, 1980).

Newman (1995) also observes a lack of consensus amongst soil scientists regarding cryosuction and writes that “numerous theories were proposed which attempted to describe the physics of soil freezing”, referring to the 1960s and 1970s. Miller (1980) wrote about the research of Edlefsen and

Anderson (1943) in looking for an adsorption force field in relation to freezing point depression: "their painstaking analysis of the influence of such a mechanism on freezing led to no useful interpretations and, if anything, discouraged most soil physicists from further efforts to understand soil freezing". In the report by Reed (1977), it is stated that there are various theories for water migration in frozen soil. He identified several motive forces in the literature behind the process, after which he simply concluded that "it is complicated".

More recent literature seems to ignore existing theoretical disparities and the inherent physical complexity of the freezing process (e.g., various review articles do not mention contrasting theories (Hayashi, 2013; Hohmann, 1997; Lundberg et al., 2016; Stähli, 2005). Yet, in those earlier decades (1940s to 1980s), the discussion seemed far from settled. The cause of varying theoretical approaches is possibly a result of the inherent complexity of the physics involved, different backgrounds of authors (e.g., geotechnical, hydrological, and soil scientific), loss of research interest (perhaps), and the difficulty of measuring matric potential and other properties of frozen soil – a common tensiometer for example does not function below 0 °C.

Below, an overview is given of different theories on water flux in freezing soil encountered in the literature, especially between the 1940s and 1980s, after which a discussion is provided.

#### *(1) Soil freezing = soil drying analogy*

The current dominant theory of cryosuction relies on the similitude of the water content against matric potential curve and the liquid water content against temperature curve. The theory assumes that ice has a similar effect as air on soil matric potential, because ice formation results in a new water interface at which tension is exerted, namely the ice-water interfacial tension (Koopmans & Miller, 1966). This proposed link led several scientists to conclude that the soil's matric potential can be calculated from its liquid water content whether the decrease in liquid water is due to drainage, evaporation, or due to freezing (Dall'Amico et al., 2011; Harlan, 1973; Miller, 1980). The ice pressure in that case is assumed to be atmospheric.



It was found however that the interfacial tension at the water-air interface is  $72 \text{ Nm}^{-2}$  (which is the same as for a water-vacuum interface) and approximately  $30 \text{ Nm}^{-2}$  at the ice-water interface, implying that the matric potential for a frozen soil at a certain liquid water content has to be reduced by a factor of 0.42 compared to the matric potential of a non-frozen soil with similar water content (Formanek et al., 1984; Hopke, 1980). The ice-air interfacial tension is  $90 \text{ Nm}^{-2}$  (Djikaev & Ruckenstein, 2017), but it likely has no effect on pore water pressure because ice is rigid.

A distinction is made in the literature between solid-solid contact (SS) and solid-liquid-solid contact (SLS) soils. The SS soils are assumed to be governed by capillary forces, while with SLS soils only adsorption plays a role. The 0.42 correction factor is then only necessary for SS soils, while with SLS soils the ice-water interfacial tension is deemed to be irrelevant because adhesive forces are dominant, hence no correction factor is required (Miller, 1980). This distinction is rather impossible to apply with real soil since nearly always both SS and SLS behaviour occurs (Azmatch et al., 2012). In any case, why would ice-water adhesion not matter for water flow in SLS soils in the first place? The rationale behind this seems elusive, since also in SLS soils there is a new interface at which capillary forces could act.

Nevertheless, whether the correction factor lies between 0.42 or 1, the implications of the theory are that the Clapeyron equation can be used to directly calculate matric potential from the soil's subzero temperature since it provides the corresponding liquid water content according when applied in an SFC (e.g., Eq. 7). For this reason, the Clapeyron equation has been incorporated into common SWRC equations to calculate matric potential, which gives the cryo-SWRC, for example (Dall'Amico et al., 2011):

$$\psi_f = \psi_w + \frac{L_f}{gT_0} (T - T_0) \quad [10]$$

Where  $\psi_w$  is the matric potential based on total water saturation and  $g$  is the gravitational constant (only included to convert pressure in water column height to its base unit of Pa – it has no physical influence on matric potential in frozen soil).

In summary, the freezing equals drying approach enables researchers to use a common soil water retention curve to estimate the matric potential at a certain freezing temperature through the Clapeyron equation.

### *(2) Vapour flow*

Some authors emphasize the role of vapor flow in frozen soil (Smith & Burn, 1987; S. Zhang et al., 2016). Although this does not replace other cryosuction theory, it adds a possible mechanism behind moisture migration and ice growth in the frozen zone. Through a combination of evaporation and condensation processes, a significant amount of water could be transported from the unfrozen to the frozen zone (e.g., over 10% of total moisture flux according to Zhang et al., 2016). Vapour flow is driven by thermal gradients, the larger the thermal gradient, the greater the vapor flux.

### *(3) Osmotic pressure*

According to Unold and Derk (2017), the assumption that cryosuction occurs because freezing equals drying (theory 1) lacks a clear description of the mechanisms behind it. Instead, these authors solely relate cryosuction to the osmotic effect, a perspective that can be traced back to Cass and Miller (1959). Unold and Derk (2017) state that freezing point depression results from non-uniform ion concentrations. Close to mineral surfaces, cations are bound, resulting in high ion concentration and thus lower freezing temperature. With increasing distance from a particle surface, the concentration in ions in the soil water decreases, and thereby the freezing temperature becomes closer to 0 °C accordingly.

When freezing of the water with lowest ion concentration commences, solutes are expelled, and the solute concentration of the remaining liquid water is increased. This increase results in a negative pore water pressure, which draws in water from the unfrozen zone with lower ion concentration. The process of increasing osmotic pressure with freezing is recognized by some other authors but is not seen as the sole cause of cryosuction (Burt & Williams, 1976b; Fuchs et al., 1978; Spaans & Baker, 1996).

### *(4) Water retention parameters altered by ice*

A different perspective on cryosuction is given by Noh et al. (2012), as they consider pore ice to alter the water retention parameters of the soil. They assume the ice itself does not induce flow of liquid water, but only alters the proportion of pore space that can be filled with air and liquid water. Essentially, they consider a newly formed pore geometry and pore size, at each specific ice content. A function is employed to calculate the empirical parameters of the van Genuchten equation ( $\alpha$  and  $n$ ) based on ice content. Each cryo-SWCC is thus a temporary relationship between liquid water content and matric suction, its parameters tied to ice content. The parameters change in such a way that suction in the frozen zone is increased, akin to a shift toward finer soil texture. The theory is based on the Kelvin Equation which relates matric potential to a specific pore radius (Eq. 6).

Noh et al. (2012) also considers the 9% increase in volume during phase change from water to ice, which further decreases the soil's pore sizes. Parameter changes to  $\alpha$  and  $n$  are also considered to be dependent on the initial total water content. Without reverting to further detail, the volumetric increase in ice content changes pore radius and thereby induces additional matric suction. The approach by Noh et al. (2012) is not verified experimentally but does present a novel approach that is different from the freezing equals drying approach (theory 1), although closer examination might reveal similarities at the level of pore-scale physics implicitly assumed.

Clark et al. (2015) used a similar method, albeit to greater simplicity. They considered ice also as part of the solid matrix, but ice content only changes the effective saturation of the pores:

$$S_e = \frac{\theta_u - \theta_r}{\theta_s - \theta_i - \theta_r} \quad [11]$$

Where  $S_e$  is the effective saturation.

The retention parameters  $\alpha$  and  $n$  remain unchanged. Subsequently, the van Genuchten equation is employed to calculate the matric potential based on effective saturation:

$$\psi_f = \frac{1}{a_{vg}} \left[ S e^{\frac{n_{vg}}{n_{vg}-1}} - 1 \right]^{\frac{1}{n_{vg}}} \quad [12]$$

This equation is incorporated into the broad SUMMA model (Structure for Unifying Multiple Modeling Alternatives) that encompasses atmospheric, river, biophysical and soil hydrologic processes at a large scale. Simplicity is obviously required for an integrated hydrological model.

#### *(5) Gibbs free energy decrease*

According to yet other authors, water migrates from larger unfrozen pores towards thinner water films in the frozen zone because in the thinner films water molecules are less mobile (Benoit & Bornstein, 1970; Henry, 2000). The reduction in mobility leads to a reduction in Gibbs' free energy of the water, hence water flows in the direction of decreasing free energy. Professor Housel in the discussion section of (Jumikis, 1957) similarly argues that the kinetic energy of water molecules is reduced in the frozen zone.

The cause of lower water mobility is attributed to a lowering of water temperature at the freezing front, in addition to the adhesive forces of water to ice resulting in a decrease of the molecular mobility of water. This is a perspective that Jumikis in response to Housel agrees on. House even states that he believes the concept of surface tension as a driving force for water migration to be a "myth" (Jumikis, 1957). It should be noted that the concept of free energy can and is also applied to capillary theory, but it differs here in its interpretation regarding water mobility.

#### *(6) Chemical action*

According to (Reed, 1977), Tsytoich (1975) describes work done on migration of water in freezing soil that showed the influence of psychochemical properties of soil surfaces. In the experiments, kaolin and montmorillonite clays were used to which water saturated with various exchange cations were added. It was found that moisture migration and heaving was greater with multivalent cations and less with univalent cations, owing to the role of chemical action at the interphases between solid and liquid (Tsytoich, 1975). Since this work is solely concentrated on two types

of clays, and further studies on the topic could not be easily found, these findings are not reproduced, and it thus remains unclear to what extent these results are applicable to a broader texture range and other water solutions.

### *(7) Supercooling*

Penner (1959) attributed moisture migration and heave in frozen soil to supercooling of pore water. Supercooling is different from freezing point depression because the water is in fact below the freezing point of water but there are no possibilities for ice nucleation. According to Penner, the confinement in small pores limits ice crystal growth, leading to supercooling of liquid water. Taber (1929) and Jackson et al. (1956) also stated that supercooled temperatures are required for a suction gradient in partly frozen soil. Specifically, these authors argued that the onset of ice nucleation at supercooled temperatures releases the energy required to induce moisture movement.

It is further stated by Research associate Torrence Martin in the discussion section of Penner (1959) that supercooling in a pore exists because pore size controls the probability of sufficient ice nucleation sites to initiate ice growth. Temperature must thus be further lowered below the freezing point to reach appreciable ice growth rate. Torrence Martin concludes that a method should be devised to differentiate between supercooling and freezing point depression in order to assess the importance of the supercooling phenomenon. He writes, regarding moisture migration in frozen soil: "if experiments show that there is no supercooling then some other source of energy must be found" (Penner, 1959).

### *(8) Rearrangement of water molecules*

Kaplar (1970) explains the occurrence of cryosuction in frozen soil the following alternative way. Molecular layers of water have a rigid structure when they are in contact with ice because of a high degree of polar orientation with the lattice. Adsorbed water on soil particles displays, according to him, similar structural rigidity. Once the adsorbed water freezes, the molecules undergo physical adjustment of position to fit into the crystal

lattice. Consequently, the force balance is disturbed, and liquid water molecules are attracted to fill the resulting void space. However, if permeability of the soil does not allow rapid filling of the void, air bubbles will fill the void space. This results in surface tension at the water-air interface, leading to further suction force (Kaplur, 1970). Experimental evidence of such a mechanism is not supplied, and the theory does not re-occur in other literature to this thesis' author's knowledge.

#### *(9) Restricted ice expansion*

According to Unold and Derk (2017), the work by Everett and Haynes (1965) describes moisture migration due to freezing as a result of restricted volume expansion of ice; supposedly, the cryosuction would equal the freezing pressure of the soil because of the restricted expansion. The original article however is not accessible digitally and was therefore not consulted. In addition, the theory lacks further explanation in Unold and Derk (2017) and does not seem to appear in other literature. Therefore, it is uncertain what the theory entails, and if it might have been a case of misquotation; however, for sake of completeness, the supposed theory is mentioned here.

#### *(10) Empirical approach*

In some approaches, matric suction is increased simply based on ice content through an empirical equation to simulate the effect of cryosuction on water redistribution (e.g., Zhang et al., 2007). There are no theoretical considerations involved, except for the fact that ice content and matric potential are assumed to be related.

The following empirical equation for cryosuction was for example developed by Kulik (1970):

$$\psi_f = \psi_w (1 + \Phi_i \theta_i)^2 \quad [13]$$

Where  $\psi_w$  (m) is the total matric potential of the soil (including the effect of cryosuction),  $\psi_w$  (m) is the matric potential due to total water content without the effect of possible ice present and  $\Phi_i$  is an empirical factor that represents the effect of ice on matric potential.

### *Discussion*

The diversity of theories and approaches indicates a lack of consensus on the physicochemical causes of cryosuction. Falsification of different hypotheses encountered in the literature has not been undertaken, thus they are still in consideration. Nevertheless, it will also be the case that some hypotheses are complementary rather than contradictory. For example, it seems reasonable to assume that osmotic potential decrease draws in additional water from the unfrozen zone. Also, adhesion and surface tension are logically affected by the presence of a solid phase of water, even if the precise nature at the pore-scale is still elusive.

Despite the plurality of proposed mechanisms, most recent authors assume that ice content and air content are equivalent in their effect on matric potential (theory 1) (Dall'Amico et al., 2011; Hansson et al., 2004; Larsbo et al., 2018; Watanabe & Osada, 2016), without explicitly mentioning or arguing that any of the other theories are thus incorrect. In a limited number of cases, the soil freezing equals drying approach predicted frozen soil water and heat transport satisfactorily (Newman & Wilson, 1997; Painter, 2011). Yet in many other cases with the same approach, an impedance factor had to be introduced to drastically reduce frozen soil permeability (Guymon et al., 1993; Hansson et al., 2004; Liu & Yu, 2011; Shoop & Bigl, 1997; Taylor & Luthin, 2011; X. Zhang et al., 2007), because otherwise the suction exaggerated the water content increase in the frozen zone. This could either indicate a discrepancy of the frozen soil permeability, or of the frozen soil matric potential itself.

One obvious problem that one encounters with the freezing equals drying theory is the analogy of air and ice in soil. In fact, since the water-air interface is equivalent to a water-vacuum interface, it implicitly implies that ice has no effect on water potential akin to a vacuum, i.e., surface tension is an inherent phenomenon of the water itself and because of the narrower space occupied by liquid water in frozen soil, this tension is increased. Does it truly not matter if a vacuum-water interface is replaced by a solid ice-water interface for liquid water potential? There exists molecular adhesion of water to ice,

which explains the decreased interfacial tension at the water-ice interface compared to a water-vacuum interface (factor 0.42).

Furthermore, the effective porosity of the soil is reduced upon freezing, i.e., the capillaries capable of holding air and liquid water are smaller. With theory 1, the increase in surface tension is subsequently considered as the driving force for moisture attraction due to the smaller capillary size; however, surface tension of water by itself does not cause capillary pressure if we consider Jurin's Law (Eq. 2)

Only in case of a contact angle smaller than 90 degrees does surface tension increase capillary pressure. If the contact angle is larger than 90 degrees, an increase in surface tension would only cause the water to be repelled more strongly by the capillary. Therefore, it is crucial to consider the contact angle of water on ice. Experiments have been too few to decisively determine this factor, and it is dependent on ice lattice geometry and other factors, which could also potentially show hysteretic behaviour (Gharedaghloo et al., 2020; Karlsson et al., 2019; Sarshar et al., 2013)).

Clearly, since the interfacial tension of the ice-water interface is lower than that of the water-vacuum interface by a factor of approximately 0.42, adhesion of water to ice has weakened the surface tension of water at the water-ice interface, and the contact angle must be lower than 90 degrees. Combined with the smaller capillary radius, a new adhesion and surface tension effect thus exists upon ice growth, and perhaps Jurin's Law could be employed to predict the new capillary pressure when ice is considered as (part of) the capillary wall. A thermodynamically equilibrated system with a clear physical boundary between water and ice is assumed, which might not hold in extremely tight spaces with complex pressure-controlled phase changes, possible pre-melting stages and tightly adsorbed water films.

Finally, the approach towards soil physics as capillary bundles might be inherently wrong, making it impossible to reconcile pore- and multipore-scale and molecular scale soil physical behaviour (Hunt et al., 2013). Soil pores have a complex three-dimensional shape compared to idealized capillary tubes. Perhaps physically more accurate consideration of soil



freezing requires a more advanced theory of soil physics, such as the pore network concept based on percolation theory (Berkowitz & Ewing, 1998)).

Regarding the other theories not discussed yet, there is simply lack of empirical evidence to begin with to ascertain their magnitude and validity. Closer inspection might reveal fundamental similarities of different theories, or flawed assumptions. Although certain processes are known to occur, such as the osmotic potential increase of liquid water, or vapour flow, it is hard to establish when these processes need to be accounted for to obtain accurate predictions.

It can be argued that current soil water transport models based on variations of Darcy's Law are empirical and semi-statistical rather than physical. These models are driven by parameters relating to soil water retention, relative permeability, and saturated hydraulic conductivity, which are based on empirical formulae and measurements of the average macroscale behaviour of soil volumes. There are no pore scale physics incorporated in such models, and the actual spatial complexity and heterogeneity of pore geometry cannot be accounted for. Few of such models could predict real cases well without some degree of calibration of empirical parameters. Add to this the questionable nature of capillary bundle theory, and soil water and heat transport models seem to mainly 'work' because of useful empirical relationships rather than fundamental physical equations.

Therefore, from a modelling perspective, empirical formulations relating to soil freezing might provide useful simulations not inferior to other quasi-physical approaches, and the question could be asked: is fundamental physical understanding necessary in the first place? Especially from the perspective of flood hazard prediction at the catchment scale, incorporating pore scale physics is a current impossibility.

Even the micro-heterogeneity of thermal conductivity at the pore scale is found to be impactful on resulting macroscale frozen soil behaviour because it determines the geometry of ice formation and resulting thermodynamic, as well as water potential, spatial processes (Amiri et al., 2018b). Concludingly, there is great opportunity to improve fundamental

understanding of frozen soil matric potential through cleverly designed experiments measurements at the (near) pore-scale level. How this knowledge could benefit current water and heat transport models is yet elusive however – at least until pore-scale modelling at relevant scales becomes feasible.

This thesis does not further focus on the physicochemical causes of cryosuction; instead, the approach in this research is pragmatic in that the goal was to obtain and use a functional water and heat transport model with phase change that satisfactorily simulates performed frozen soil column experiments, whether empirical or more physically based. Such a working model could subsequently be employed to understand frozen soil behaviour at the macroscale, even if underlying fundamental mechanisms of soil freezing at the molecular scale still require attention (as it does in virtually all soil water transport models given the deficiencies of the capillary bundle theory (Hunt et al., 2013).

## 2.4 Frozen soil: permeability reduction

In an unsaturated soil, air-filled pores are not part of the conductive channels for water flow. Permeability therefore decreases with decreasing water content since the number of pores that are conducting water decreases. Relative permeability functions exist to calculate the relationship between (liquid) water content and permeability based on empirical soil parameters; often, these parameters are the same as used for the SWRC. It is consensus that the filling of soil pores with ice has a similar effect on the soil's permeability as the filling of soil pores with air because freezing occurs in progressively smaller pores, and therefore liquid water content is used to estimate the soil's permeability (Kurylyk & Watanabe, 2013). The extent of this analogy is however uncertain. There is debate about the inclusion an ice impedance factor to further reduce the permeability of a frozen soil based on ice content (Newman & Wilson, 1997; Watanabe & Flury, 2008).

Jame and Norum (1980) noted that too much moisture migrated to the frozen zone if the freezing equals drying analogy for permeability was incorporated in a numerical model. They speculated that ice must have an additional effect on the blocking of flow paths which is not captured by the

simple presumed freezing-drying analogy. Therefore, they introduced an empirical ice impedance factor that further reduces permeability based on ice content:

$$K_f = 10^{-\Omega_i \theta_i} K_u \quad [14]$$

Where  $K_f$  ( $\text{ms}^{-1}$ ) is the hydraulic conductivity of (partly) frozen soil,  $K_u$  ( $\text{ms}^{-1}$ ) is the hydraulic conductivity based on the liquid water content,  $\theta_i$  is the volumetric ice content ( $\text{m}^3\text{m}^{-3}$ ) and  $\Omega_i$  is a dimensionless empirical factor of impedance. Zhang et al. (2007) found that including an impedance factor ( $\Omega_i = 17$ ) was crucial to accurately describe observed moisture transport in a freezing soil. Several variations of the impedance equation (Eq. 14) have been developed (e.g., Taylor and Luthin, 1978), but it is difficult to evaluate which predict better than others.

Shoop and Bigl (1997) suggested the following equation to determine  $\Omega_i$  based only on the saturated hydraulic conductivity:

$$\Omega_i = \frac{5}{4} (K_s - 3)^2 + 6 \quad [15]$$

Where  $K_s$  is the saturated hydraulic conductivity ( $\text{ms}^{-1}$ ).

Several authors followed the impedance factor approach introduced by Jame and Norum (e.g., Hromadka, 1987), Gosnik et al., 1988, Hansson et al., 2004). Gosnik et al. (1988) for example reported different values for the impedance factor: 8 for fine sands and silts, and 20 to 30 for coarse gravel soils.

There is critique on the impedance factor approach. According to Black and Hardenberg (1991), it is an arbitrary correction function and not physically based. Newman and Wilson (1994) are also sceptical of an ice impedance approach, because they found permeability to be well represented by a common relative permeability function. They speculated that the permeability – water content relationship might not have been accurate in studies that required an ice impedance factor. Empirical proof of incorrectness of studies using an ice impedance factor has not been provided, however. In addition, the number of studies that successfully

employed an impedance factor is numerous, making it hard to dismiss the impedance factor approach as inaccurate without substantiation.

It could be argued that the need of an ice impedance factor is logical. The assumption of similitude between liquid water – permeability relationships for frozen and non-frozen soil predisposes another assumption, namely that ice and air enter the exact same pores at progressively lower liquid water contents, and that their geometry (air bubble and ice crystal) is similar. This assumption has not been verified through pore-scale imaging techniques. Small-scale heterogeneity of thermal conductivity (Amiri et al., 2018b) could potentially cause ice to enter different pores than air would at similar liquid water content. Ice formation in pores due to phase change is a thermodynamic process, while air saturation can result from evaporation (thermodynamics) but mainly also because of soil water transport and thus it is a dissimilar physical process compared to pore ice growth. Given the different physics involved, it is only logical to assume ice and air filling of pores to be unlike to a certain degree. In addition, water expands ca. 9% when it turns into ice, which in small pores could potentially induce significant further restriction of flow paths. Also, ice crystal growth is dependent, amongst other factors, on heat transfer rate; therefore, different heat transfer rates might result in different ice lattice geometries and thus different permeability reductions (Azmatch et al., 2012).

The argument against the impedance factor as not being physically based does not hold. Approaches to soil water flux always entail averaging soil behaviour at a particular relevant scale. This necessitates the use of empirical parameters to represent pore-scale constitutive relationships such as between water content and permeability, and between water content and matric potential. If an empirical approach to frozen soil permeability agrees well with measurements, there is no reason to discard it. In fact, the common relative permeability function itself is an empirical equation to describe reduction in flow path connectivity upon desaturation. It would of course be more efficient and prudent to employ the least number of empirical parameters to correctly represent partly frozen soil water flux, hence it

would be beneficial if an ice impedance factor is not required – but that of course cannot be an argument of physics.

A factor that is also not considered is that the matric potential gradient induced by ice growth might have been overestimated, and not the permeability, in studies requiring an impedance factor. This would also result in overprediction of frozen zone water content. Adjusting frozen soil matric potential could have a similar effect as adjusting frozen soil permeability on the water flux. Lastly, it should be considered that frozen soil has a lower saturated permeability compared to unfrozen soil since the porosity of the soil has been reduced, i.e., the maximum permeability is lower. This has implications for numerical modelling approaches in which flow between cells, nodes or elements occurs; flow should never exceed the maximum permeability (e.g., the saturated soil permeability in frozen state). The presence of ice thus constitutes a soil structure discontinuity similar to the boundary between soil layers of different soil texture.

Alternatives to the above-mentioned methods of frozen soil permeability reduction have been developed. Tao and Gray (1994) for example used a power-curve relationship to relate normalized liquid saturation (as a function of ice content) to permeability based on the approach by Mualem (1976). Other approaches used complex laboratory testing to obtain permeability coefficients for the frozen zone (Konrad and Morgnestern, 1980; Oliphant et al., 1982).

The closure and opening of macropores has also been recognized as an important factor determining water flow in frozen soil by several studies (e.g. Mohammed et al., 2018; Holten, 2019; Pittman et al., 2020; Demand et al., 2019), which requires a dual porosity approach to incorporate in a numerical model. Macropores often allow infiltration to occur uninhibited into frozen soil because they drain before freezing commences.

In short, different approaches in the literature can be found towards frozen soil permeability, and as Newman and Wilson stated in 1994, “the literature shows that no single, acceptable method exists for determining the coefficient of permeability in partially frozen, unsaturated soil”. Almost 20

years later, Kurylyk and Watanabe (2013) also stated that it is a matter of ongoing research. To achieve progress in the matter, detailed pore-scale analysis of ice growth in soil pores should be undertaken to obtain more insight into reduction of flow path connectivity in frozen soils. Accurate prediction of frozen soil permeability is essential for flood prediction and mitigation.

## 2.5 Frozen soil: catchment hydrology

A popular categorization of infiltration capacity of frozen soil has been formulated by Gray et al. (1986) based on field experiments. They determined the following categories: 1) restricted infiltration: infiltration volumes are negligible due to concrete frost; 2) limited infiltration: infiltration occurs but is reduced due to a degree of ice saturation; and 3) unlimited infiltration: macropores and fractures allow all water to infiltrate. This categorization, however, obscures details about infiltration into frozen soil since infiltration is likely to occur along a gradient from unlimited to fully restricted depending on numerous factors such as ice content, soil temperature and soil texture. It has been found that higher ice saturation, and therefore higher initial saturation before freezing, decreases frozen soil infiltration capacity (McCauley et al., 2002; Hayashi, 2013). Further details on the effects of the environmental conditions combined with different soil types, such the shape of the relationship between initial saturation and eventual frozen soil infiltration, are lacking.

Several processes occur simultaneously in a freezing soil, such as the phase change of water with associated latent heat flux, capillary and gravitational flow, conduction of heat through the solid and liquid soil constituents, and the increase in matric potential of (partly) frozen soil volumes resulting in redistribution of liquid water (Ireson et al., 2013). Given the complex interactions of these processes, it is hard to predict how soil properties and environmental conditions (e.g., air temperature and initial soil moisture state) affect frozen soil infiltration capacity. Laboratory and field testing would be demanding in view of the many possible values of process parameters, further complicated by the difficulty of measuring ice and liquid water content in soils (Azmatch et al., 2012). The gain of most experimental

studies is therefore mostly qualitative rather than quantitative understanding, despite providing useful measurements and insights (Stähli et al., 1999).

Furthermore, an important question remains when frozen soil can be expected to have such a substantial impact on catchment hydrology. Despite a great deal of research on seasonally frozen soil, the relationship between frozen soil and a hydrological response at the catchment level remains poorly understood (Ala-Aho et al., 2021). Intuitively, it could be expected that the reduced permeability of frozen soil is reflected in the shape of a stream hydrograph. Since infiltration is impeded, more surface runoff would occur that flows quickly to streams. However, in a meta-review of catchment-scale studies, Ala-Aho et al. (2021) found the influence of frozen soil on catchment hydrology to be ambiguous: sometimes it had a clear effect, sometimes only to a minor extent, and sometimes not at all.

The task for hydrologists studying frozen soil is therefore to try to identify the environmental conditions during which frozen soil has an impact on hydrological partitioning in the landscape, and when it does not. This question is important because its answer has implications for flood hazard, erosion, contaminant transport, and groundwater flow. A few of the most important factors determining a catchment-scale frozen soil response would likely be soil type, vegetation cover, catchment size and surface topography, as well as time-variant factors such as air temperature, snow depth, melt- and rainfall rate, and soil ice content. Ala-Aho et al. (2021) provided a clue in their meta-analysis of frozen soil catchment responses: in case of deep snowpacks, and in case of extensive forest cover, the effect of frozen soil was unnoticed. With deep snowpacks and no midwinter melt events, the soil remains relatively dry and insulated against strong freezing temperatures (hence absence of frozen soil in the first place), and forest cover can lead to spatial patchiness in soil frost occurrence due to complex within-forest energy dynamics (DeWalle & Rango, 2008). Both these factors would cause meltwater to infiltrate despite cold conditions.

Other studies suggest that microtopography might also play a large role in determining the pathway of meltwater during frozen soil conditions (French

and Binley, 2004; Hayashi et al., 2003). These studies found that small depressions in the landscape (several centimetres deep in French and Binley, 2004, several meters deep in Hayashi et al., 2003) served as hotspots for focused infiltration. The evidence is however scarce and only entails these studies at different plot scales and with lack of repetition of plots. It is therefore unclear when microtopography could play a role, and what the magnitude of its effect might be. Also, the precise interplay of water transport, phase change and energy exchange processes during depression-focused infiltration remains unknown.

Mohammed et al. (2018) in a review study pointed out that macroporous soils most often allow infiltration to occur uninhibited despite freezing of the microporous soil matrix. Only during very cold soil conditions, macropores could be clogged with ice when infiltrating water freezes in-situ (Pittman et al., 2020). Therefore, when a landscape has a significant proportion of macroporous soil, a frozen soil effect on hydrological partitioning in the landscape might be absent.

This thesis tries to provide further insight into the role of soil conditions, soil type, microtopography, and macropores on frozen soil infiltration through numerical modelling of test scenarios.

## 2.6 Conclusion

Numerous hypotheses have been postulated in the literature, mostly between the 1940s and the 1990s, for three different aspects of frozen soil phenomena: freezing point depression, cryosuction, and permeability reduction. With reasonable success, the freezing point in a soil can be approximated based on the relationship between pressure and phase change, formalized in the Clapeyron equation. The explanation is that capillary pressure (tensile stress) acts as a negative pressure on the phase change diagram of water. Several outstanding knowledge gaps remain, however. Regarding cryosuction, there is a plurality of hypotheses of which none are systematically falsified through experiment. A strong link with pore- or molecular-scale physics would be needed in conjunction with empirical evidence to support a particular hypothesis.



Permeability reduction in frozen soil has been successfully modelled. Disagreement exists however regarding the question: does the standard relative permeability function based on liquid water content suffice to predict frozen soil permeability? Or do we require a special reduction in permeability based on ice content? The outcomes from different studies are not decisive. The pore-scale intricacies of ice crystal geometry are likely not appreciated well enough. In all likelihood, the complexity of soil, consisting of thousands to millions of pores per  $\text{cm}^3$ , necessitates empirical relationships to describe soil freezing until computer technology and numerical modelling techniques are capable of simulating fundamental molecular physics of complex porous systems at larger scales.

Frozen soil has an ambiguous role in catchment hydrology, with field and plot studies reporting no, mild, or strong effects on water partitioning in a landscape. Further study is needed to understand in which conditions frozen soil is expected to impede infiltration substantially at the scale of catchments. A few studies point to the role microtopography and macropores could play in obscuring a signal from frozen soil on stream hydrographs by allowing infiltration to occur locally despite reduced permeability in the landscape. Also, forest cover and snow pack depth has been found to influence the importance of frozen soil on catchment hydrology.

Despite significant gains in numerical modelling, scientific research performed on frozen soil is at hazard of losing coherency due to a large number of articles published during the past two decades without clear direction in terms of consensus on physical mechanisms and without clear improvement of physical understanding. The gap between soil hydrological models and pore-scale physics should be bridged. Meanwhile, a pragmatic approach that relies on empirical relationships could help to improve freezing algorithms for integrated hydrological models. Progress in this field is vital for the improvement of flood forecasting in catchments affected by soil freezing.

### 3. Numerical modelling of frozen soil: different approaches

*This chapter is based on the published paper: “Simulating water and heat transport with freezing and cryosuction in unsaturated soil: Comparing an empirical, semi-empirical and physically-based approach” by J.C. Stuurup, S.E.A.T.M. van der Zee, C.I. Voss and H.K. French in Advances in Water Resources, 2021, volume 149. For more detail on frozen soil theory (e.g., cryosuction, impedance factor, freezing point depression, and permeability), please see Chapter 2.*

#### 3.1 Introduction

The part of a soil that generally undergoes seasonal freezing and thawing extends from a few centimetres to about a meter or several meters below the surface (Loranger et al., 2017; Lundberg et al., 2016; Hayashi, 2013). This mostly comprises the unsaturated zone where moisture content and soil temperature respond to atmospheric dynamics on a relatively short timescale of hours to days (Carson, 1961). It has been demonstrated that the initial moisture and temperature state of the soil when freezing initiates affect frost depth and soil ice saturation (Ireson et al., 2013). Cryosuction is an important process in this context as it depends on initial moisture content, soil water retention characteristics and hydraulic conductivity (Miller and Black, 2003). The process entails the movement of moisture toward the frozen zone.

Different approaches have been developed to incorporate cryosuction, the soil freezing curve and permeability reduction into a numerical or mathematical model (Kurylyk and Watanabe, 2013). Examples include the models of Harlan (1973), Taylor and Luthin (1978), Ippisch (2001), Zhang et al. (2007) and Dall’Amico et al. (2011). Publicly available numerical models include a freezing module for HYDRUS-1D (Šimůnek et al., 1998), a beta version of SUTRA named SUTRA-ICE (McKenzie et al., 2007) and the atmosphere-plant-soil models SHAW (Flerchinger and Saxton, 1989) and COUP (Jansson and Karlberg, 2004). SUTRA-ICE does not currently include

the process of cryosuction and HYDRUS-1D freezing only works for unsaturated conditions.

Kurylyk and Watanabe (2013) noted that the history of frozen soil model development has been characterized by inconsistencies in nomenclature and methodology, in part due to different geotechnical and hydrological backgrounds. It remains unclear how different mathematical expressions and models for unsaturated soil freezing processes compare to each other in their ability to accurately represent an unsaturated frozen soil. An exception to this is the paper by Ren et al. (2017) in which the outcomes of different SFC equations are fitted to measurements on four different frozen soils. Regarding the reduction of permeability of frozen soil, there is debate about the use of a flow impedance factor based on ice content (Mohammed et al., 2018). Furthermore, previous models are often tested only on a single experimental dataset which did not include all relevant variables such as ice content and soil temperature (Mohammed et al., 2018; Kurylyk and Watanabe, 2013). As a result, confidence in model accuracy remains limited, and it remains unclear how the model would be parameterized for a different soil than the soil used in the experiment (e.g., the impedance factor).

Another unresolved question is whether an empirical approach towards unsaturated soil freezing and cryosuction could be adequate and how such an approach would compare to more physically-based models using the phase-change temperature-pressure relationship (Kurylyk and Watanabe, 2013). This question is relevant, as few multi-dimensional hydrological models, catchment-scale models or land-surface schemes have adopted approaches for unsaturated soil freezing, likely due to the complexity and often associated numerical instability of physically based simulation of unsaturated soil freezing.

In this study, we compare three different approaches for unsaturated soil freezing. These represent a fully empirical, a semi-empirical and a physically-based approach and entail different combinations of previously developed equations. The aim of this study is to compare and evaluate the performance and parameterization of each approach. Datasets from three experiments are used for testing, namely those of Mizoguchi (1990), Watanabe et al.

(2012) and Zhou et al. (2014). The latter two datasets contain measurements of ice content, liquid water content and soil temperature, which allows us to test for all relevant variables. We include a discussion of current points of debate concerning the governing equations for unsaturated frozen soil dynamics, as the different approaches rely on previous insights and developments in both empirical and physically-based equations.

## 3.2 Methods

### Model structure and assumptions

A numerical model was used that calculates heat and water transport for a one-dimensional soil profile with any number of layers. Vertical discretization of the layers was set to one centimetre with uniform soil properties for the entire column. Heat transport occurs at the top and bottom boundary, where a fixed temperature boundary can be set. There is no water flow possible across the model boundaries. The mathematical equations are solved through explicit difference calculation for the fluxes between soil volumes (Forward Euler Method). This method increases numerical stability and simplicity, but it requires high temporal discretization to maintain accuracy. Yang et al. (2009) successfully used a similar numerical method in their simulations of unsaturated flow governed by the Richards equation. In our case, it appeared to be an adequate model construct for the purpose of 1D “laboratory” type soil column simulations with freezing.

The model excludes osmotic processes and density changes of liquid water. Also, porosity and soil structure do not change with ice saturation as ice pressure is assumed to be constant.

### Unsaturated flow

Flow between soil volumes is governed by the Richard’s equation, here presented in its 1-dimensional form (Richards, 1931):

$$\frac{\partial \theta_t}{\partial t} = \frac{\partial}{\partial z} \left[ K_u(\theta_u) \left( \frac{\partial \psi_f}{\partial z} + 1 \right) \right] \quad [16]$$

Where  $\theta_t$  is the total water content (liquid and ice;  $\text{m}^3\text{m}^{-3}$ ),  $z$  is the elevation (m),  $\psi_f$  is the total matric potential including the effect of ice (m), and

$K_u(\theta_u)$  is the hydraulic conductivity ( $\text{ms}^{-1}$ ) as a function of the liquid water content (and also ice content if an impedance factor is used).

The matric potential of a soil volume is a state variable that depends on total water content, in our case given by the van Genuchten equation (van Genuchten, 1980):

$$\psi_w = \frac{1}{\alpha} \left[ \left( \frac{\theta_s - \theta_r}{\theta_t - \theta_r} \right)^{\frac{n}{n-1}} - 1 \right]^{\frac{1}{n}} \quad [17]$$

Where  $\alpha$  ( $\text{m}^{-1}$ ) and  $n$  are model parameters.

Hydraulic conductivity, the  $K_u(\theta_u)$  term in Eq. 16, is calculated with the following equation, which derives from the relationship between the relative permeability function of the Mualem – van Genuchten model (Mualem, 1976; van Genuchten, 1980), the saturated hydraulic conductivity and the liquid water content:

$$K_u = K_s \left( \frac{\theta_u - \theta_r}{\theta_s - \theta_r} \right)^{0.5} \left\{ 1 - \left[ 1 - \left( \frac{\theta_u - \theta_r}{\theta_s - \theta_r} \right)^{\left( \frac{n-1}{n} \right)} \right]^{\left( \frac{n-1}{n} \right)} \right\}^2 \quad [18]$$

Where  $K_u$  is the hydraulic conductivity of the soil ( $\text{ms}^{-1}$ ). The effect of temperature on hydraulic conductivity by affecting the viscosity of water is neglected.

### Energy exchange

There are three forms of energy exchange in the model that govern the energy balance: thermal conduction, advection and latent heat flux. These are expressed in the following general energy balance equation:

$$\begin{aligned} \frac{\partial T}{\partial t} [\theta_u \rho_w H_w + \theta_i \rho_i H_i + \theta_a \rho_a H_a + (1 - \varepsilon) \rho_s H_s] \\ + [(H_i - H_w)(T - T^*) - \Delta L_f] \left[ \left( \rho_i \frac{\partial \theta_i}{\partial T} \right) \frac{\partial T}{\partial t} \right] = \\ - \frac{\partial T}{\partial z} (\theta_u H_w \rho_w v) + \frac{\partial}{\partial z} \left( \bar{c} \frac{\partial T}{\partial z} \right) \end{aligned} \quad [19]$$

Where  $\rho_w$  is the density of water ( $\text{kgm}^{-3}$ ),  $H_w$  is the specific heat of water ( $\text{Jkg}^{-1}\text{K}^{-1}$ ),  $\rho_i$  is the density of ice ( $\text{kgm}^{-3}$ ),  $H_i$  is the specific heat of ice ( $\text{Jkg}^{-1}\text{K}^{-1}$ ),  $\theta_a$  is the volumetric air content,  $\rho_a$  is the density of air ( $\text{kgm}^{-3}$ ),  $H_a$  is the specific heat of air ( $\text{Jkg}^{-1}\text{K}^{-1}$ ),  $\varepsilon$  is porosity,  $\rho_s$  is the density of solid soil ( $\text{kgm}^{-3}$ ),  $H_s$  is the specific heat of solid soil ( $\text{Jkg}^{-1}\text{K}^{-1}$ ),  $\bar{c}$  is the average thermal conductivity of the soil ( $\text{Wm}^{-1}\text{K}^{-1}$ ),  $v$  is the flow velocity of liquid water ( $\text{ms}^{-1}$ ),  $L_f$  is the latent heat of fusion ( $\text{Jkg}^{-1}$ ),  $T$  is the temperature (K),  $T^*$  is the current freezing point of water (K), and  $z$  is the elevation (m).

Thermal dispersion is assumed to be negligible for heat transfer in small-scale unsaturated soil (Liu et al., 2014; Jouybari et al., 2020).

### Freezing approach: empirical version

The empirical approach quantifies the effect of cryosuction on flow and the effect of matric potential on freezing point depression without an underlying physical explanation. For the soil freezing curve, we use the exponential equation of McKenzie et al. (2007; Chapter 2, Eq. 8). Only the fitting parameter  $w$  is needed to approximate the freezing curve of a soil with this equation. The rationale for an empirical approach is that the model can easily be calibrated to better fit data. In addition, it is not affected by assumptions such as thermal equilibrium phase change which is the case for the physically-based SFC. Also, an empirical SFC can more easily be applied to non-colloidal soils via calibration.

To simulate cryosuction in the empirical version, we make use of Equation 9 (Chapter 2). Cryosuction entails both matric potential changes and the resulting flow of water. We assume the empirical cryosuction expression represents the observed upward flow correctly, not the matric potential changes itself; hence it incorporates a possible flow impedance effect due to ice content. This approach circumvents the numerical instability associated with the extreme hydraulic gradient at the frozen fringe when using the Clausius-Clapeyron relationship. By combining the exponential SFC equation and the empirical cryosuction expression, we thus have an empirical approach requiring two parameters,  $w$  for the SFC and  $\Phi_i$  for cryosuction. The question is whether  $\Phi_i$  can be generalized for a variety of soil types, or if it should be soil type specific. We will investigate

this by testing the empirical (and semi-empirical) approach on three different experimental datasets, later described. We will also include a small sensitivity analysis to the parameter  $\Phi_i$ .

#### Freezing approach: semi-empirical version

The semi-empirical approach that we use contains the same empirical expression for cryosuction, but it is combined with a physically-based expression for the SFC. We use Equation 2, shown above and originally formulated by Zhang et al. (2016), in which the Clausius-Clapeyron relationship is incorporated into the van Genuchten soil water retention expression. The freezing curve of the soil is hence determined by the common van Genuchten soil water retention parameters  $a$  and  $n$ . The only unsaturated freezing related parameter to be calibrated for the semi-empirical version is therefore  $\Phi_i$  for cryosuction.

#### Freezing approach: physically-based version

For the physically-based version, we use the expressions from Dall'Amico et al. (2011) to determine cryosuction. First, the freezing temperature is determined by:

$$T^* = T_0 + \frac{gT_0}{L_f} \psi_{totw} \quad [20]$$

Where  $T^*$  (K) is the freezing point of water at the current matric potential based on total water content,  $\psi_w$ , and  $g$  is the gravitational acceleration ( $\text{ms}^{-2}$ ). Subsequently, matric potential including the effect of ice is determined by the following expression:

$$\psi_f = \psi_w + \frac{L_f}{gT^*} (T - T^*) \quad [21]$$

If  $T \geq T^*$ , the equation collapses to  $\psi_f = \psi_w$ .

The van Genuchten based SFC (Chapter 2, Eq. 7) is used to determine the soil freezing curve. Hence, both matric potential and freezing point depression are based on the physical relationship between temperature and pressure. However, similar to other studies (Kurulyk and Watanabe, 2013), we found that the extreme hydraulic gradient at the frozen fringe led to a strong

overprediction of upward flow. Therefore, we developed a simple approach to solve this using the ice impedance factor combined with the concept of a soil structure discontinuity in the context of spatial discretization.

In any numerical model solving differential equations, soil water and heat transport need to be discretized in time and space. If water flows from a discretized location A to a location B, the hydraulic driving force between these points and the hydraulic conductivity of location A determine the flow rate. This premise would hold if the soil represented by location B has the same hydrological properties as location A. In case of ice in the soil however, the assumption of soil homogeneity cannot hold. If location B would be partly frozen, certain flow paths could be blocked as larger pores freeze first. The inflow rate is no longer dependent on the hydraulic conductivity of location A alone. Therefore, a special hydraulic conductivity reduction is needed for the frozen location that receives soil water.

We limited the flow rate of water to ice-filled soil volumes with the following formula, developed by Zhao et al. 2013:

$$K_m = 10^{-\Omega_i \frac{\theta_i}{\theta_t}} K_u \quad [22]$$

Where  $K_m$  is the maximum hydraulic conductivity ( $\text{ms}^{-1}$ ) for flow towards a frozen soil volume, and  $\Omega_i$  is the impedance factor for flowrate reduction due to ice in the soil pores. We will assess to which extent  $\Omega_i$  varies with soil type.

### Model testing

To ensure proper functioning of the numerical method, we successfully compared the output of the model to the established models SUTRA (Voss and Provost, 2002) and HYDRUS-1D (Šimůnek et al., 1998) for unsaturated flow and heat transport during nonfrozen conditions and for fully saturated frozen conditions (only SUTRA). The resulting comparisons are given in the appendix.

We make use of the experimental data of Mizoguchi (1990), Watanabe et al. (2012) and Zhou et al. (2014) to test the approaches for frozen unsaturated conditions. All experimental soil columns were insulated and closed systems. Frost heave was not observed in any of the experiments. The soil properties



and boundary conditions of the experiments are listed in Table 2. The parameters  $w$  and  $R_i$  were manually calibrated for each soil type. If a soil parameter was unknown, this was manually calibrated as well (mentioned in Table 2). For the datasets of Watanabe et al. (2012) and Zhou et al. (2014), we compare the empirical and the van Genuchten-based SFC to the measured liquid water contents at several subzero temperatures.

The simulated SFC's for Mizoguchi (1990) will also be shown, but without measured liquid water content for comparison. Regarding the  $\Phi_i$  parameter, we investigated whether a single empirical value could capture the cryosuction observed in the experiments. We tested for a range of  $\Phi_i$  values that would provide a water distribution that visually matched the experimental results; this range was between a value of 1 and 3. We include a small sensitivity test of the empirical cryosuction parameter to show how we established a single value for  $\Phi_i$  for all experiments.

Mizoguchi (1990) used a 20 cm high soil column filled with Kanagawa sandy loam. It was frozen from the top with a temperature of  $-6\text{ }^\circ\text{C}$ , while the soil had an initial temperature of  $6.7\text{ }^\circ\text{C}$ . Only total water content was measured in this experiment. Several authors used the dataset of Mizoguchi for model testing, such as Dall'Amico et al. (2011) and Hansson et al. (2008). We include the model results from Dall'Amico et al. (2011) for this experiment. By comparing the three versions to their model results, we can assess how well the different mathematical expressions compare with the approach of Dall'Amico, who used the Clausius-Clapeyron relationship to simulate cryosuction (Chapter 2, Eq. 9) with an equation splitting method combined with the numerical Newton method.

Furthermore, we will include the output from SUTRA-ICE for this experimental setup. SUTRA-ICE is a multi-dimensional saturated and unsaturated water and heat transport model that includes the depression of the freezing point of water, but not the process of cryosuction. By comparing the results of our model to SUTRA-ICE, we can assess the effect of cryosuction on simulated soil physics such as soil temperature and ice content.

Watanabe et al. (2012) did a freezing experiment on a soil column of 35 centimeters deep. The soil comes from the A horizon of a weeded fallow field and is characterized by a high porosity. Three different columns were prepared, each with a different initial water content: 0.31, 0.38 and 0.46. The column was brought to a homogenous temperature of 3.5 °C and subsequently frozen from the top with a temperature of -6.2 °C. The bottom of the column was in contact with a temperature element set to 2 °C. Measurements were done after 48 hours and included total water content and liquid water content.

Table 2. Parameters and variables used to numerically simulate the experiments of Mizoguchi (1990), Watanabe et al. (2012) and Zhou et al. (2014).

Parameter/ Variable	Mizoguchi (1990)	Watanabe et al. (2012)	Zhou et al. (2014)
$K_s$	3.19e-06	2.1e-06	3e-07*
$\epsilon$	0.535	0.617	0.467
$a_{vg}$ (m <sup>-1</sup> )	1.11	0.88	0.11
$n_{vg}$	1.48	1.36 <sup>#</sup>	2.2
$\theta_{res}$	0.05	0.006	0.05
Initial water content	0.34	0.31, 0.38, 0.46	0.16, 0.325
Initial T (°C)	6.7	3.5	3
Top T (°C)	-6	-6.2	-4.7, -4
Bottom T (°C)	No flux	2	3.5, 3.6
Thermal conductivity	0.55	0.4	1
Measurement times (hours)	12, 24, 50	48	24, 72
Soil texture type	Sandy loam	Silt loam	Loamy silt

\*Saturated hydraulic conductivity was not measured. Its current value is the result of an initial estimation for a loamy silt, subsequently manually calibrated. <sup>#</sup>This value was slightly adjusted from its measured value (1.25) to better fit the measured SFC points with the van Genuchten SFC function.

Zhou et al. (2014) performed a freezing soil column experiment on a sieved glacial till (sieve size 0.063 mm). The 24 cm high column initially had a

temperature of 3 °C and the experiment was performed with two different initial water contents, 0.16 and 0.325. For these two different initial water content setups, freezing temperatures of -4 and -4.7 °C were respectively applied at the top. Total water content, liquid water content, ice content and soil temperature were measured 24 and 72 hours after freezing started. The parameters for saturated hydraulic conductivity and thermal conductivity are unknown for this experiment and are therefore estimated based on soil type and subsequently slightly adjusted via manual calibration.

### 3.3 Results

#### Comparison of simulated SFC to measurements

The different SFC curves corresponding to the simulations and the different experiments are shown in Figure 4. With the experiment of Watanabe et al. (2012), the empirical SFC equation did not perform well without adjustment. When the measured residual water content during drying is used, the empirical SFC severely underpredicts the liquid water content (Figure 4). Therefore, we changed the unfrozen residual water content for the empirical SFC to 0.07 (SFC\_exp2) instead of 0.006 (SFC\_exp). After this adjustment, it is still apparent that the SFC underpredicts the liquid water content. As shown in Figure 4, a higher  $w$  value for the SFC does not solve the problem (SFC\_exp3), as it creates a too steep decrease in liquid water content with decreasing temperature. In general, the empirical SFC displays a near linear relationship between liquid water content and temperature that quickly reaches the residual water content at relatively high subzero temperature. The van Genuchten based SFC on the contrary, displays a more gradual decrease in liquid water content at lower subzero temperatures, and even at -8 °C the residual water content is not reached.

With the experiment of Zhou et al. (2014) the empirical SFC and the van Genuchten SFC represent the measured liquid water contents well. In the experiment of Mizoguchi (1990) no liquid water content measurements were performed to compare the results with, but it is also clear that the empirical SFC predicts reaching a residual water content at a much higher temperature than the van Genuchten based SFC. A crucial difference between the two SFC

approaches thus seems apparent in the high matric potential range, corresponding to low temperatures (below  $-1\text{ }^{\circ}\text{C}$ ).

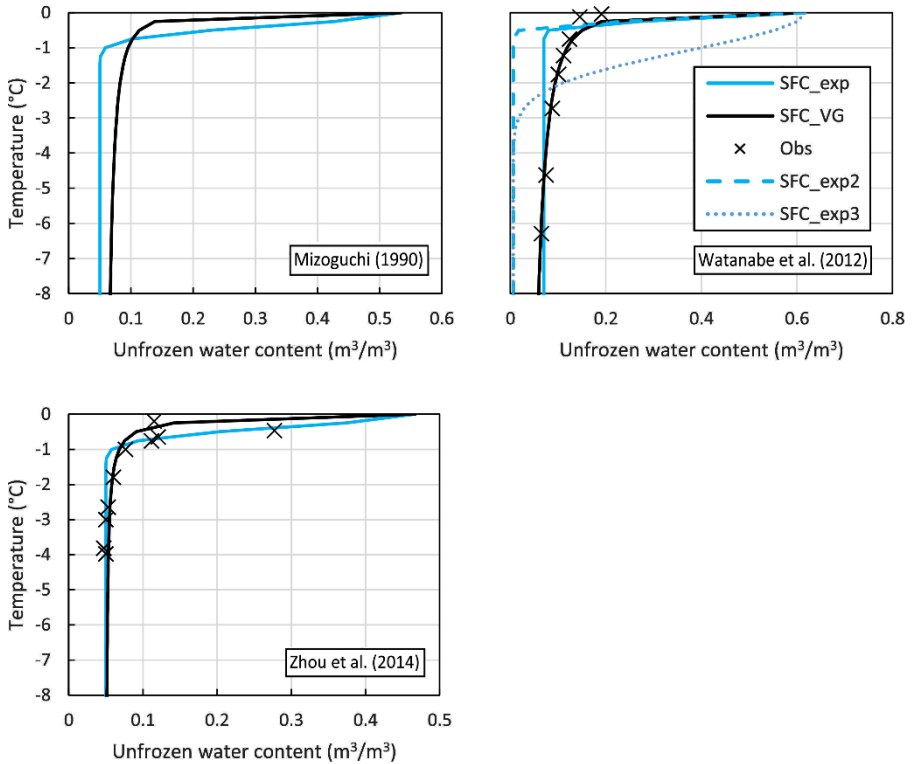


**Figure 4.** The exponential and van Genuchten based SFCs used in the simulations of each experiment, compared with the measurements of liquid water content at certain subzero temperatures in case of the experiments of Watanabe et al. (2012) and Zhou et al. (2014). For the experiment of Watanabe et al. (2012) also the exponential SFCs with a residual water content of 0.006 (SFC\_exp2) and a value of 1.5 for  $w$  (SFC\_exp3) are shown.

Table 3. Calibration results of frozen soil related parameters.

Parameter	Mizoguchi (1990)	Watanabe et al. (2012)	Zhou et al. (2014)
$w$ (SFC)	0.5	0.1	0.5
$\Phi_i$ (cryosuction)	1.8	1.8	1.8
$\Omega_i$ (impedance factor)	9	11	12

### Calibration results

The calibration results (Table 3) show that  $w$  varied for the different soil types used in the experiments. The  $\Phi_i$  parameter was kept at a fixed value of 1.8. To obtain accurate results, it was important to calibrate the impedance factor,  $R_i$ , for each soil type specifically as otherwise the predicted cryosuction was noticeably under- or overpredicted.

### Mizoguchi (1990)

The comparisons with the measurements of the experiment by Mizoguchi (1990) and the simulated outputs of the three approaches in this study, SUTRA-ICE and the numerical model by Dall'Amico et al. (2011) are shown in Figure 5. With all three approaches used in this study, the distribution of total water content after 12, 24 and 50 hours is in good agreement with measurements, each performing slightly better than the model of Dall'Amico et al. (2011). The variation amongst the empirical, semi-empirical and physically-based approaches is small. The depth to which cryosuction affects the water distribution in all simulations seems to align well with the measured water content profile.

As can be expected, SUTRA-ICE does not reproduce the cryosuction-based increase of total water content within the frozen zone. Also shown in Figure 5 are the ice contents and soil temperature profiles of our model and SUTRA-ICE. The frozen zone, as well as the zero-degree temperature isotherm, is deeper in the SUTRA-ICE simulation. Although the vertical extent of the frozen zone is larger, the ice content is lower in the SUTRA-ICE simulation compared to our model simulation.

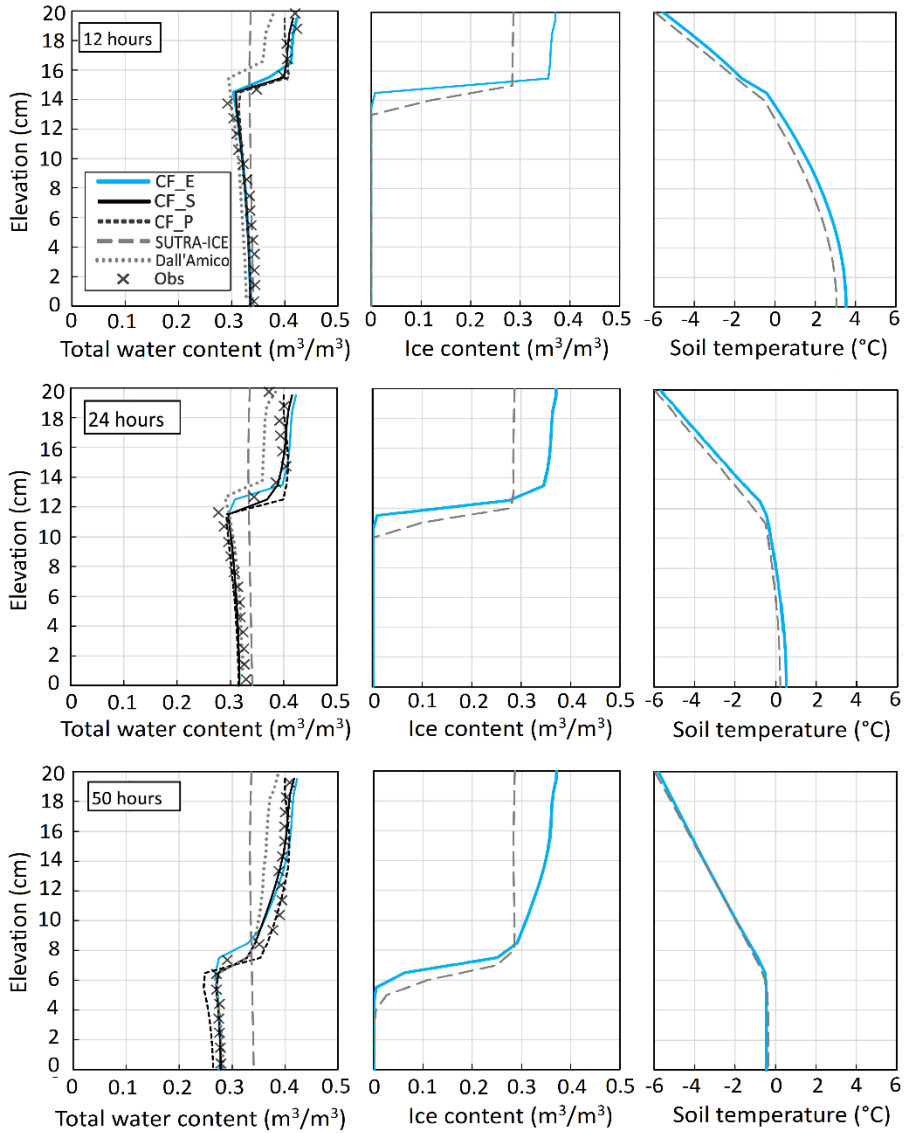


**Figure 5.** Measurements of total water content (Obs) in the experiment by Mizoguchi (1990) compared with the model outputs of Dall'Amico et al. (2011), SUTRA-ICE and CryoFlow for three different times after freezing started. Modelled ice content and temperature displayed as well. CF-E, -S and -P indicate empirical, semi-empirical and physically based approaches, respectively.

### Watanabe et al. (2012)

The comparison between simulated output the measurements in the experiment of Watanabe et al. (2012) are shown in Figure 6. All versions of the model perform reasonably well to simulate the observed total and liquid water contents for the three different initial water content setups. Some deviation can be seen with the empirical version, as the liquid water content is underpredicted. The liquid water content drops sharply above 23 centimeters elevation in the empirical version, while the other versions and the measurements display a more gradual decrease in liquid water content above this point.

### Zhou et al. (2014)

Figures 7 and 8 compare the output of the simulations to the experiment of Zhou et al. (2014) for two different initial water contents and at two different measurement times. In general, model results are in good agreement with observed values. All three versions predict the increase of water in the frozen zone and other output variables with reasonable accuracy. The variation amongst the different versions is noticeable but small. The model, however, struggles to capture some of the observed cryosuction in the lower initial water content setup, as there is a strong deviation of the total water content in the lower section of the freezing front after 3 days (Figure 7). The model in general predicts a mild increase of total water content with depth in the frozen zone, while the experimental data suggests that there was a steep increase in water content at the freezing front (depth 12 – 14 cm) after the first day. The physically-based version performed slightly better in this case than the empirical and semi-empirical approach. This could imply that the empirical cryosuction expression should take total water content into account to determine the effect of ice on matric potential. For this reason, we tested with an adapted cryosuction equation for the semi-empirical approach that is dependent on total water saturation:

$$\psi_t = \psi_w \left[ 1 + \frac{\theta_i}{\theta_t} C_i \right]^2 \quad [23]$$

Where  $C_i$  represents the effect of ice on matric potential. We found a value of 0.8 for  $C_i$  to match the observed cryosuction across the different

experiments. The result of substituting Eq. 13 (Chapter 2) with Eq. 23 is included in Figure 7 (CF\_S2). For all other cases, results remained roughly unchanged with Eq. 23 as the simulated cryosuction was similar; these results are therefore not shown. The adjusted equation captured the increase of cryosuction with depth better for the dry scenario, but only for the result after 72 hours.

### Sensitivity to the empirical cryosuction parameter

In addition to the calibrated value for  $\Phi_i$  of 1.8 the following values were tested; 1, 1.5, 2.5 and 3. We used these  $\Phi_i$  values in the simulations of several of the experimental setups with the empirical approach. The results are shown in Figure 9. It is clear that between a  $\Phi_i$  of 1 to 3, the results are within reasonable accuracy compared to measurements, but the midpoint covering the observed cryosuction in all experiments appears to be around the calibrated  $\Phi_i$  value of 1.8. The band of results differs for each experiment, as it is narrow below the frozen zone for Watanabe et al. (2012) and Mizoguchi (1990), but wide for Zhou et al. (2014).

## 3.4 Discussion

### General model performance

The model is capable of simulating three different unsaturated soil freezing experiments with reasonable accuracy. These experiments have different initial water content, freezing intensity and soil type. The three versions of the model predict the penetration depth of the freezing front with 1-centimeter accuracy in most cases. The ice content and total water contents are predicted reasonably well with an accuracy of about 0.05 ( $\text{m}^3/\text{m}^3$ ). It can thus be concluded that a simple freezing extension of a common soil water and heat transport model based on the Richard's equation is an adequate means of simulating freezing soil. The differences in accuracy amongst the empirical, semi-empirical and physically based approach are small, but noticeable. There is no approach that consistently performs better when considering all cases.



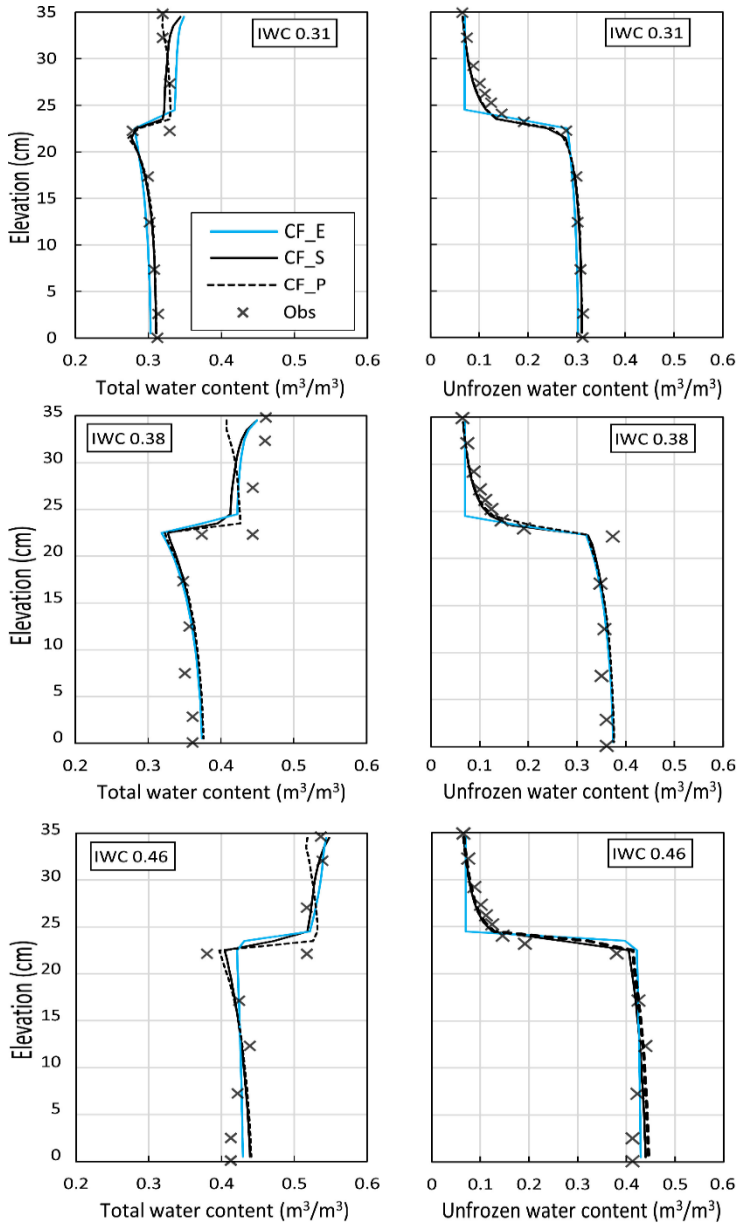


**Figure 6.** Measurements of total water content and liquid water content (Obs) after 48 hours in the soil freezing column experiment by Watanabe et al. (2012) with different initial water contents (IWC) and the output of the different model approaches (CF -E, -S and -P indicating empirical, semi-empirical or physically based approaches, respectively).

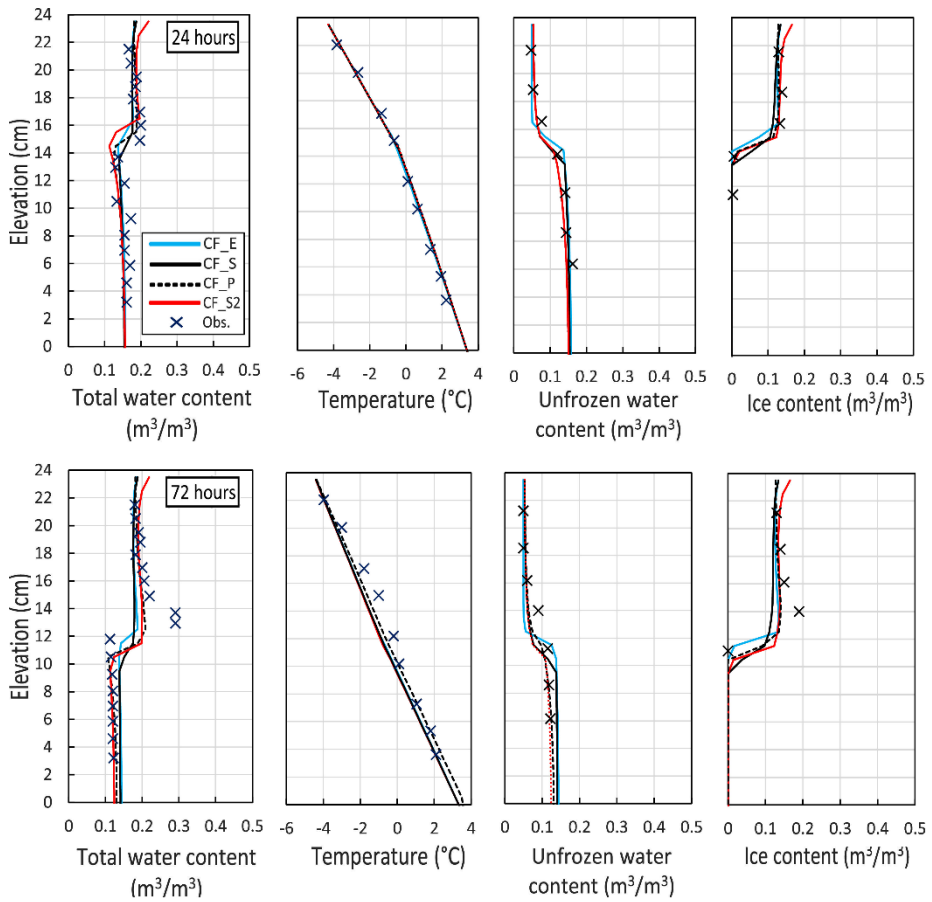


**Figure 7.** Measurements of Zhou et al. (2014) of a freezing soil column after 24 and 72 hours, compared with the model output of the different approaches (CF -E, -S and -P indicating empirical, semi-empirical or physically based approaches, respectively). Initial water content is 0.16. Results for an adapted cryosuction equation (Eq. 23) for the semi-empirical approach are included, designated as “CF\_S2”. Porosity of the soil is 0.47.

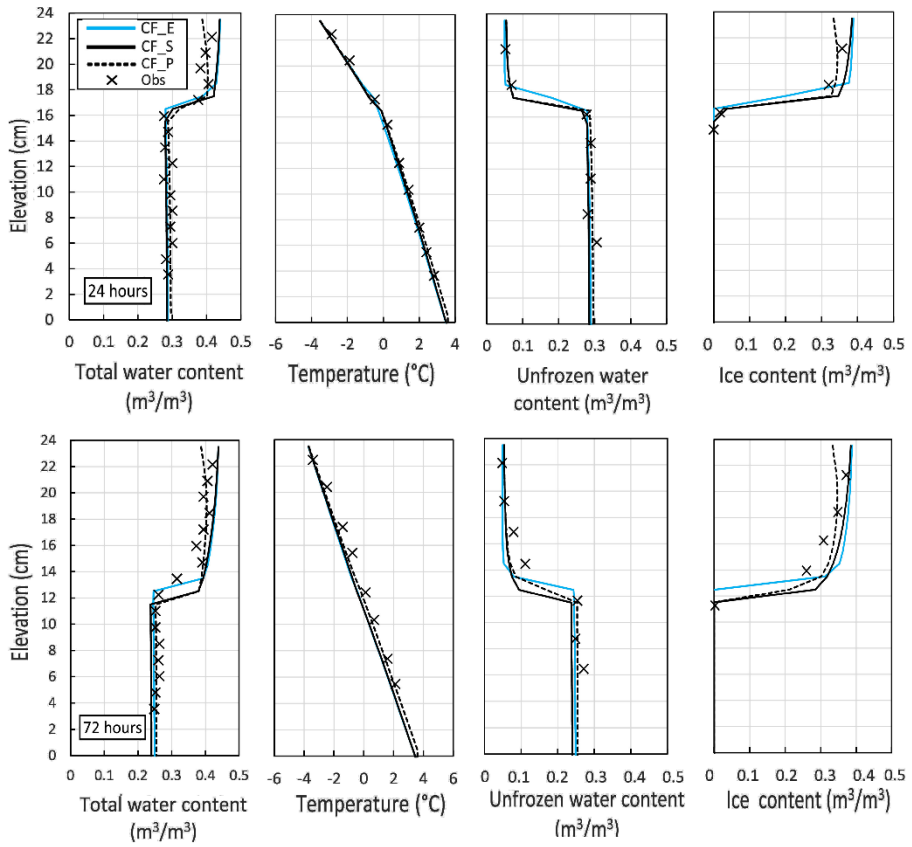


**Figure 8.** Comparison of measurements performed by Zhou et al. (2014) in their soil column freezing experiment and the output of the different approaches (CF -E, -S and -P indicating empirical, semi-empirical or physically based approaches, respectively) for total water content, temperature, liquid water content and ice content after 72 hours with an initial water content of 0.325. Porosity of the soil is 0.47.

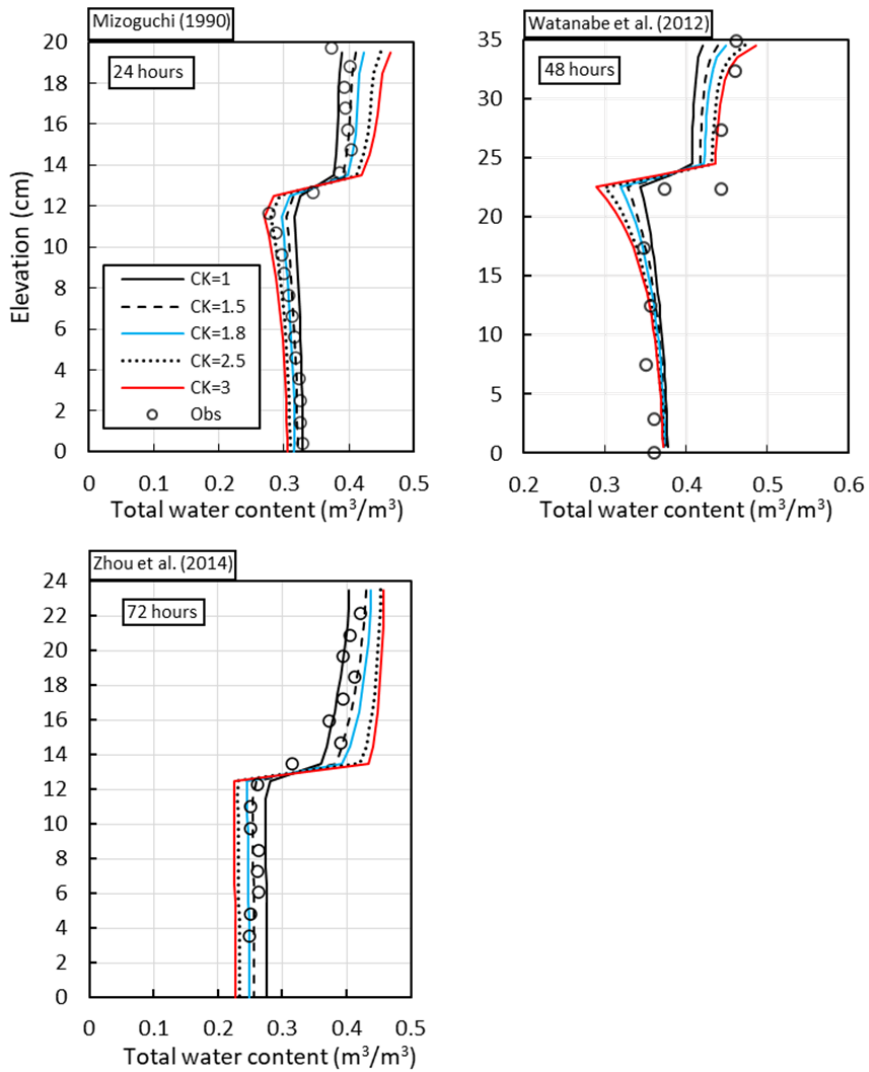


**Figure 9.** Sensitivity analysis of the  $\Phi_i$  parameter, using the empirical approach (CF\_E). Results are shown for the experiment of Mizoguchi (1990), Watanabe et al. (2012) with initial water content 0.38 and Zhou et al. (2014) with initial water content 0.325.  $\Phi_i$  was set to 1, 1.5, 1.8, 2.5 and 3.

## Empirical approach

The empirical SFC equation (McKenzie et al., 2007) combined with the empirical cryosuction equation (Kulik, 1978) circumvents the use of the more complex Clausius-Clapeyron relationship while the results show it can adequately capture the freezing process of unsaturated soil. A promising result is that a fixed parameter value for cryosuction ( $\Phi_i$ ), set to 1.8, simulated cryosuction well compared to measurements. Even though the experiments only represented three soil types, it suggests that in most cases – at least within the textural range of a sandy loam, silt loam and loamy silt, no soil type specific calibration would be required. This eases the applicability of this approach to a wide range of situations. Only one case showed underpredicted cryosuction, when the soil started with a low initial water content of 0.16. Adjusting the cryosuction equation (Chapter 2, Eq. 13) to include a dependency of the cryosuction effect on total water content (Eq. 23), improved the fit slightly. Such a dependency on total water content could be expected because there are significant changes in matric potential with changing liquid water content in the low water content range of a soil water retention curve; i.e. the effect of changes in ice content on matric potential could be stronger at low total water content.

The exponential SFC requires soil type specific calibration of the empirical SFC parameter ( $w$ ). It also became clear that though the empirical exponential SFC works well in most cases, it tends to underpredict the liquid water content in a fine soil - in this specific case, a loamy silt. The unfrozen residual water content is quickly reached at relatively high subzero temperature (between 0 and -1 °C). The residual liquid water content should be set to a different value than the unsaturated residual water content to avoid a drop to residual liquid water content too quickly. This unfortunately limits the applicability of the exponential SFC to soils with weak soil water retention if an accurate liquid water content, and thus ice content, is desired. In soils with strong soil water tension, such as clays and silts, the matric potential will increase significantly at lower liquid water contents, leading to a strong depression of the freezing point of water. For this reason, the exponential SFC could not capture the SFC of a silt loam well.

### Semi-empirical approach

The advantage of the semi-empirical approach is that it uses the empirical cryosuction equation, but it relies on the Clausius-Clapeyron relationship to determine the freezing point of water. This means the depression of the freezing point of water is thus based on the well-known physics of phase change. The van Genuchten based SFC in combination with the empirical cryosuction equation worked well in all cases considered, except for the low initial water content case. The van Genuchten based SFC captures the measured SFCs better than the empirical SFC equation and it provides a more realistic drop of liquid water content at low subzero temperatures. With this approach, residual liquid water content is reached at significantly lower subzero temperatures compared to the exponential SFC. Another benefit of the semi-empirical approach is that it does not require a special parameter for the SFC. Hence, only the  $\Phi_i$  parameter is needed. Since the empirical cryosuction equation predicts cryosuction well with a fixed value for  $\Phi_i$ , it is implied that this approach does not need calibration of a freezing related soil parameter.

### Physically-based approach

By limiting the flow of liquid water to the frozen zone with an impedance function, we were able to simulate cryosuction based on the Clausius-Clapeyron relationship in a simple numerical model with good accuracy. In all cases results were in good agreement with observations; only at the onset of freezing, the impedance factor tends to limit the flow towards the freezing front slightly too strongly in some cases. The main advantage of the physically-based approach is that it relies on the underlying physics of the temperature-pressure phase change relationship for both the freezing point depression and cryosuction, and it should therefore be widely applicable. The disadvantage is that, at least in our case, it requires reduction of flow to the frozen zone via an empirical impedance factor.

The impedance factor is an empirical, soil type specific parameter, and as we noted there is debate about the validity of its use. We used the impedance factor as a representation of reduced soil porosity in the frozen soil, akin to a soil heterogeneity. In our approach, the impedance parameter had to vary

for the different soil types in the experiment to capture the cryosuction process well. An alternative approach could be the dual porosity model used by Watanabe et al. (2010). A next step in a physically-based approach would likely involve changing the soil hydrological properties based on ice content, as it can be expected that the soil water retention parameters and saturated hydraulic conductivity would change with increasing ice content (Noh et al., 2012), but this would require further experimental study.

### The importance of simulating cryosuction

By comparing the results of our model to SUTRA-ICE, which does not simulate cryosuction, we could identify the effect it had on total water content, ice content and temperature. Cryosuction logically increases the total water content in the frozen zone. Accordingly, it slows down the freezing front as the heat capacity of the upper soil is increased and more energy is used for phase change. Consequently, in SUTRA-ICE, the freezing front progresses faster and the frozen zone becomes larger, though with a lower ice content. This implies that without cryosuction, the frozen zone has a higher permeability and more space for accommodating infiltrating water.

Of practical concern in flood hazard assessment, cryosuction thus strongly affects the infiltration capacity of a soil. Our study however is based on medium to fine textured soils in the range of loam and silt. It can be expected that for coarse soils such as sand, in which gravitational drainage significantly precedes cryosuction, the effect of cryosuction on total water content is strongly diminished. In very fine soils such as clays, cryosuction has been found to play a limited role as well due to very low hydraulic conductivity preventing water redistribution (Miller, 1980).

### 3.5 Conclusion

In this study, a simple 1D numerical model is used to simulate water and heat transport with phase change in unsaturated soil via three different approaches: empirical, semi-empirical and physically based. These approaches constitute new combinations of previously developed equations. The fully empirical approach uses an empirical exponential function for the soil freezing curve (SFC) and an empirical function for cryosuction. We found that the empirical SFC underpredicts liquid water

content for fine soils at low subzero temperatures (below  $-1\text{ }^{\circ}\text{C}$ ), leading to a loss of accuracy. The advantage of this approach is that it does not require accurate soil water retention parameters to work and that it does not rely on the assumptions associated with the Clausius-Clapeyron approach (such as thermal, phase and mechanical equilibrium).

The semi-empirical approach uses the van Genuchten soil water retention model combined with the Clapeyron relationship for the SFC, while cryosuction is based on the empirical equation. Since the cryosuction equation worked well with the same parameter value for a sandy loam, silt loam and loamy silt, the main advantage of this approach seems to be that calibration of a soil type related freezing parameter can be avoided. The van Genuchten-based SFC also performs better at temperatures below  $-1\text{ }^{\circ}\text{C}$ , as it more accurately links matric potential to the freezing point depression. Therefore, if correct liquid water content is desired for freezing soils with significant fine particle content, the semi-empirical approach is preferred. The physically based approach was used in our numerical scheme by regarding a frozen soil volume as a soil discontinuity. Similar to other studies, it was also necessary to use an impedance function in order to not overpredict upward flow (Kurylyk and Watanabe, 2013). The main advantage of this approach is that it is more physically based and therefore should be more widely applicable to different freezing circumstances, although it requires soil type calibration of the impedance factor.

The suggested approaches are useful for large-scale models in the simulation of frozen unsaturated soil. Depending on available soil data and model scale, an empirical, semi-empirical or physically-based approach could be preferred. Correct simulation of ice and water content is relevant in case of determining soil infiltration capacity and possible contaminant pathways. In addition, by simulating cryosuction correctly, it will be possible to predict zones of increased total water content which are thus susceptible to ice lensing and frost heave. Further modelling studies could investigate soil freezing and thawing dynamics in relation to actual infiltration of rain- and meltwater, which has received little attention. An important topic would for



example be freezing of infiltrating water, which would lower infiltration capacity but add significant amounts of energy as latent heat.

### 3.6 Acknowledgements

This research did not receive any specific grants from funding agencies in the public, commercial or not-for-profit sectors. Any use of trade, firm, or product names is for descriptive purposes only and does not imply endorsement by the U.S. Government.

## 4. Infiltration into frozen soil: controlling factors

*This chapter is based on the published paper: "The influence of soil texture and environmental conditions on frozen soil infiltration: a numerical investigation" by J.C. Stuurop, S.E.A.T.M. van der Zee, and H.K. French in Cold Regions Science and Technology, 2022, volume 194.*

### 4.1 Introduction

A popular categorization of infiltration capacity of frozen soil has been formulated by Gray et al. (1986) based on field experiments. They determined the following categories: 1) restricted infiltration: infiltration volumes are negligible due to concrete frost; 2) limited infiltration: infiltration occurs but is reduced due to a degree of ice saturation; and 3) unlimited infiltration: macropores and fractures allow all water to infiltrate. This categorization, however, obscures detail about infiltration into frozen soil since infiltration is likely to occur along a gradient from unlimited to fully restricted depending on numerous factors such as ice content, soil temperature and soil texture. It has been found that higher ice saturation, and therefore higher initial saturation before freezing, decreases frozen soil infiltration capacity (McCauley et al., 2002; Hayashi, 2013). Further details on the effects of the environmental conditions on different soil types, such the shape of the relationship between initial saturation and eventual frozen soil infiltration, are lacking.

Several processes occur simultaneously in a freezing soil, such as the phase change of water with associated latent heat flux, capillary and gravitational flow, conduction of heat through the solid and liquid soil constituents, and cryosuction - the increase in matric potential of (partly) frozen soil volumes resulting in redistribution of liquid water (Ireson et al., 2013). Given the complex interactions of these processes, it is hard to predict how soil properties and environmental parameters (e.g., air temperature and initial soil moisture state) affect frozen soil infiltration capacity. Laboratory and field testing would be demanding in view of the many possible values of process parameters, further complicated by the difficulty of measuring ice and liquid water content in soils (Azmatch et al., 2012). The gain of most experimental studies is therefore mostly qualitative rather than quantitative

understanding, despite providing useful measurements and insights (Stähli et al., 1999).

Regarding the temporal pattern of infiltration into frozen soil, Watanabe et al. (2012) observed three phases of frozen soil infiltration in their soil column experiment: (1) no infiltration due to in-situ freezing of infiltrating water, followed by (2) slow infiltration as water moves through the slowly thawing frozen zone and then (3) normal infiltration due to the progression of significant thaw. Zhao and Gray (1998) also proposed that infiltration rate changes with time, but quite differently: first, a short transient phase (several hours) when infiltration and heat transfer rate decrease rapidly, followed by a quasi-steady-state regime when changes in infiltration and heat transfer rate are small. These different results of Watanabe et al. (2012) and Zhao and Gray (1998) indicate that the temporal infiltration regime itself is likely dependent on soil type and environmental conditions.

Numerical simulation provides an opportunity to test a large number of soil parameters and environmental conditions in relation to frozen soil infiltration. It can help predict the response to freezing of different soil texture classes during different temperature and moisture conditions. The numerical calculations could also reveal possible hydrological threshold values at which freezing starts to have a significant effect on infiltration. While several numerical models have been created to simulate water and heat transport in variably-saturated frozen soils (Kurylyk and Watanabe, 2013), few models have been used to quantitatively explore the effect of various soil and environmental parameters on frozen soil infiltration capacity.

The study of thaw and infiltration into frozen soil with physically based numerical models, i.e., the end of winter and beginning of spring period, has received attention in the studies by Larsbo et al. (2019) and Mohammed et al. (2021). Numerical experiments with the dual-permeability model of Larsbo et al. (2019) found that percolation at the bottom of the soil column is dominated by preferential flow through macropores in a macroporous soil because the hydraulic conductivity of the micropore domain is reduced by ice. They also show that depending on energy transfer rate, macropores can be blocked by ice due to freezing of infiltrated water. Mohammed et al.

(2021) reached a similar conclusion as their modelling study demonstrates that freezing of infiltrated water along preferential flowpaths severely reduce infiltration.

In this study, we use an existing single-domain numerical code to simulate the freezing and thawing of variably-saturated frozen soil columns in combination with infiltration of melt- and rainwater. First, we assessed whether the numerical code, which has previously been tested on freezing soil column experiments (Stuuroop et al., 2021), could satisfactorily reproduce the full freeze-thaw temperature cycle of a laboratory soil column experiment as well as the infiltration pattern into a frozen soil. Subsequently, we performed a series of numerical 1D test simulations to investigate controlling factors on infiltration capacity of frozen soil, such as initial saturation, temperature boundary conditions and soil parameters. The results gave insight into the theoretical link between soil freezing and infiltration reduction, and the role soil and environmental parameters play herein. The focus lies on the soil matrix flow with a texture ranging from coarse to very fine are examined and environmental conditions are chosen to encompass a wide range of possible field situations.

## 4.2 Methods

### Numerical model

In this study we employed the semi-empirical version of the numerical model CryoFlow that is described in detail in Chapter 3 and in the Manual in the Appendix.

### Experimental validation

The numerical model had previously been tested on three experimental datasets of freezing soil columns (Stuuroop et al., 2021). To test the ability of the model to simulate the thermodynamic thawing process as well, we compared the results of the model to a full freeze-thaw cycle experiment by Wang et al. (2017) in which soil temperature was measured at different depths. In the experiment, a 20 cm column with silt soil at an initial temperature of 1 °C was periodically frozen and thawed from the top. The side walls were insulated, while the bottom temperature was kept at a

constant temperature of 1 °C. Freezing and thawing periods each lasted 24 hours, with temperatures of -5 and +5 °C imposed on top of the soil column. This was repeated until a total of 6 days. The grain size fractions of the soil were reported in the original study, but not the water retention parameters and hydraulic conductivity. We therefore used the Rosetta pedo-transfer function (Rosetta Lite version 1.1) of the software program Hydrus-1D (Šimůnek et al., 1998) to estimate the soil water retention parameters for the van Genuchten model ( $a = 0.021 \text{ cm}^{-1}$ ,  $n = 1.3475$  and residual water content = 0.01), the saturated hydraulic conductivity ( $1.1\text{e-}06 \text{ ms}^{-1}$ ) and porosity (0.4) based on the grain size fractions. In the original experiment, frost heave occurred, a process which is not simulated by the numerical model. A discrepancy could therefore be expected after repeated freeze-thaw cycles as initial soil properties could be changed. Thermal conductivity of solid soil particles was calibrated to  $1.5 \text{ WmK}^{-1}$ .

A second dataset (Pittman et al., 2020) was used to test the capability of the model to simulate the physics of infiltration into frozen soil. This provides experimental data of infiltration into frozen repacked soil columns. A few difficulties hamper a direct translation from experimental conditions to the model setup however. Soil water retention parameters are unknown. Therefore, these parameters were initially estimated with the Rosetta pedotransfer function from the reported bulk density and grain size fractions. Since repacking of the soil occurred after these soil properties were measured, we further adjusted the water retention parameters based on the liquid water content at a certain subzero temperature via the soil freezing curve (SFC) equation. For the same reason, we calibrated the saturated hydraulic conductivity of the topsoil layer as it was measured prior to repacking when the soil still contained macropores. Furthermore, the vertical distribution of the three soil layers of the soil column had to be estimated. The model was made to have only two soil layers for simplification because most relevant water dynamics occurred in the topsoil and the SFC suggested little difference between the middle and bottom layer.

In the experiment, a heat lamp was used to warm up the soil with  $250 \text{ Wm}^{-2}$ . Given the 10 cm water column on top of the soil during the infiltration experiment, it is unclear how much of this energy is absorbed by the top of the soil. Therefore, the amount of energy added to the top boundary was manually calibrated to roughly match the resulting topsoil temperature recorded in the experiment. This gave temporally varying energy transfer to the soil between  $50$  to  $150 \text{ Wm}^{-2}$  due to the infiltration of the water column. Solid grain thermal conductivity was manually calibrated to  $1 \text{ Wm}^{-1}\text{K}^{-1}$  to fit the temperature change rate. During the experiment, heat was added to the bottom of the soil column at an unknown timepoint and it is unclear how much energy this entails; we therefore ignored this since the main interest lies with the topsoil and we accept some discrepancy at the end of the experiment. Calibrated and estimated soil properties are later given in the Results section, Table 7. The original measurements of soil properties in the experiment are given in Table 4.

Table 4. Original soil properties measured in the frozen soil infiltration experiment by Pittman et al. (2020).

Soil layer	Bulk density ( $\text{kgm}^{-3}$ )	Porosity	Ks ( $\text{ms}^{-1}$ )	Particle size percentage (sand-silt-clay)
Top	1009	0.6	5.56e-06	9-62-29
Middle	1038	0.51	1.97e-08	11-64-26
Bottom	1044	0.51	1.16e-10	13-70-17

## Sensitivity testing of the model

### *Setup*

For the main goal of this study, we simulated a 50 cm deep soil column (soil textures and parameters defined in Table 6) exposed to varying temperatures and water input rates at the top boundary (Table 7), while the bottom boundary enabled free gravitational drainage. Water that does not infiltrate is removed from the surface and counted as non-infiltrated water, representing surface runoff in a hillslope situation (i.e., no ponding of water). The soil initially had a uniform temperature of  $1 \text{ }^\circ\text{C}$  and uniform total water

saturation. The first phase was a freezing period lasting 120 hours, representing various situations that occur during a natural freezing period before snow cover. During this period, a constant top boundary freezing temperature was varied (-0.25 to -4 °C) resulting in different levels of ice saturation. In addition, we varied the initial saturation (0.25 to 1) to represent different antecedent moisture conditions.

The freezing phase was followed by a thawing and water infiltration phase of varying time length. The thawing temperatures (0 to 4 °C) represent different energy exchange conditions between the soil and the snowpack or atmosphere. Water input rate varied between 0.25 to 4 mmh<sup>-1</sup>, thus ranging from low intensity snowmelt to high intensity combined snowmelt and rainfall (Rango and DeWalle, 2008). The total amount of water that was added to the soil was always 80 mm. The thaw/infiltration period therefore lasted from 20 to 320 hours depending on the water input rate. Temperature of the water input varied from 0 °C, common for snowmelt, to 2 °C.

In addition to the freeze and thaw scenarios, we performed simulations with the same initial saturation state and the same water input rate but without freezing. These simulations provided the infiltration if there had not been any freezing during the five days prior to water input. The total amount of infiltrated water into the soil column for the freezing scenario was subtracted from the amount of infiltration in the corresponding scenario without freezing; the resulting output variable is called *infiltration change due to freezing*. This variable is of particular interest, as it quantifies the specific effect of freezing on infiltration for a given soil type.

The soil texture classification triangle is shown in Figure 10 including the position of the soils we simulated. We considered the soil textures simulated to follow a rough gradient from coarse (soil 1) to very fine (soil 8) based on increasing water retention capacity and decreasing permeability. In addition, we considered soils 1 and 2 as coarse soils, soils 3 to 6 as intermediate soils and soils 7 to 8 as very fine soils.

All combinations of conditions in Table 5 were tested for each soil type, except for input water temperature. Water input temperature was initially

varied in the simulations (0 to 2 °C), but during testing we found it had no noticeable effect. To limit computational time, we therefore only tested water input temperature for soils 2, 3, 5 and 6.

Table 5. Soil parameters used in the different simulations. The values are based on soil cataloguing by Carsel and Parrish (1988).

Soil nr.	Soil type	Ksat (ms <sup>-1</sup> )	a (cm <sup>-1</sup> )	n	Porosity	Sres
1	Sand	3.3e-04	0.074	2.96	0.33	0.03
2	Loamy Sand	4.05e-05	0.124	2.28	0.41	0.057
3	Sandy Loam	1.23e-05	0.075	1.89	0.41	0.065
4	Sandy Clay Loam	3.63e-06	0.059	1.48	0.39	0.1
5	Silt Loam	1.25e-06	0.02	1.41	0.45	0.067
6	Silt	6.94e-07	0.016	1.37	0.46	0.034
7	Organic Layer	9.26e-07	0.013	1.20	0.766	0.01
8	Silty Clay	5.56e-08	0.005	1.09	0.36	0.07

Table 6. Initial and boundary conditions used in the simulations.

Variable	Value 1	Value 2	Value 3	Value 4	Value 5	Value 6	Value 7	Value 8
Initial $\theta_t$	0.25	0.3	0.4	0.5	0.6	0.75	0.9	1
Freeze T (°C)	-0.25	-0.5	-1	-2	-3	-4		
Thaw T (°C)	0	0.5	1	2	3	4		
Water input rate (mmh <sup>-1</sup> )	0.25	0.5	1	2	3	4		
Water input T (°C)	0	0.5	1	2				



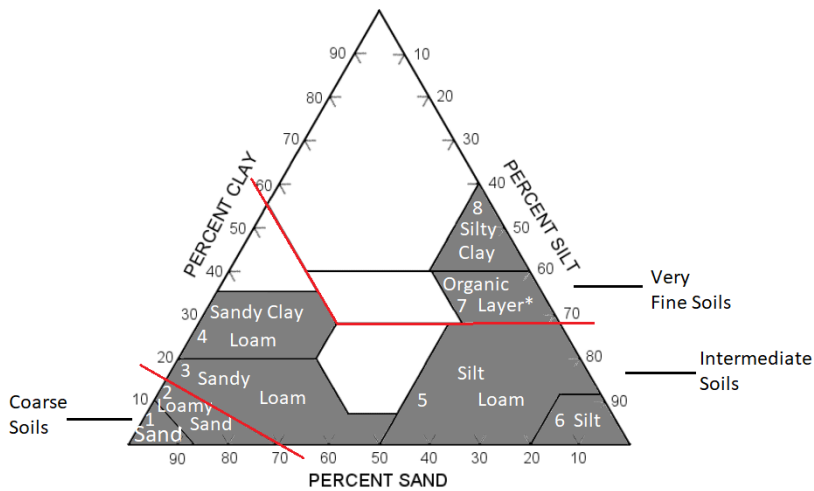


Figure 10. Soil texture classification triangle. The dark grey areas are soil types simulated in this study, with the numbers referring to the soils in Table 4. The large red lines distinguish between coarse, intermediate and very fine soils. \*Organic layer (soil 7) is placed in the area commonly classified as silty clay loam because of similar hydraulic properties.

Thermal conductivity of a soil is dependent on the water content and packing of the grains, their mineral and organic components, their connectivity and their shape (Zhang and Whang, 2017). The relationship with soil texture is therefore complicated. To simplify, we focused on how soil texture affects the infiltration capacity of a frozen soil and assumed all solid grains to have the same thermal conductivity of  $2.2 \text{ Wm}^{-1}\text{K}^{-1}$ . This represents an arbitrary midpoint value between minerals with a low (e.g. clay minerals and carbonates) and high thermal conductivity (e.g. quartz) (Cermak et al., 1982).

### Analysis

A large number of simulation results were obtained from all the scenarios (over 16,000). To visualize the output in a meaningful way, we created boxplots of relevant variables for each soil type. The output variables for the freezing phase were ice saturation of the entire soil profile, average temperature of the topsoil (upper 10 cm) and frost depth (the maximum depth at which ice is present). These boxplots provided insight into the effect of freezing by showing the full range of results as well as the medians and

quartiles. Regarding the output of the infiltration phase, boxplots were made for the total amount of infiltration during non-frozen conditions and the total amount of infiltration change due to freezing specifically. In addition, we plot the frequency of cases (%) for each soil type with 0, 25, 50 and 75% infiltration reduction due to freezing (function used:  $-100 \frac{\text{Infiltration change (mm)}}{\text{Total water input (80 mm)}}$ ). We also included time plots of cumulative infiltration, ice saturation and total saturation for a few chosen scenarios to illustrate different temporal infiltration regimes.

To get a better overview of the importance of the different environmental parameters for each soil type, we performed Spearman's rho correlation tests between infiltration change and each of the scenario variables (initial saturation, boundary temperature, water input rate and water input temperature). This test was preferred over the linear Pearson's correlation test because we expect a non-linear response in view of the non-linearity of the equations (e.g., soil freezing curve (Chapter 2, Eq. 7), cryosuction (Chapter 2, Eq. 13) and the Richards equation). We plotted the median values of infiltration reduction for each variable value to identify the shape of the relationship between variables and infiltration reduction for each soil type. Finally, we made cross-tabulations for the frequency of cases with over 75% infiltration reduction for each variable combination. These are provided in the Appendix. The cross-tabulations help identify thresholds for extreme infiltration reduction to occur.

## 4.3 Results & Discussion

### Experimental validation

The temperature profiles obtained from the simulations were in good agreement with measured temperatures during the first 48 hours at all three depths in the experiment of Wang et al. 2017 (Figure 11). This provides confidence that the freezing and thawing thermodynamic process was represented well by the numerical model. The increasing deviations after repeated freeze-thaw cycles we attributed to frost heave in the soil column of Wang et al. (2017). Frost heave alters pore and solid particle connectivity and general soil structure, thereby changing the soil's thermal conductivity.

It also affects heat capacity and latent heat flux due to the creation of ice lenses. Consequently, the thermal properties of the soil become time-variant (in addition to changes in water, ice and air saturation) and asynchronous temperature cycles can be expected. An alternative explanation for the increased discrepancy could be imperfections in boundary temperature control of the experiment.

The comparison of model output with the experimental data of Pittman et al. (2020) is shown in Figure 12 and 13. The values of soil properties used in these simulations are given in Table 7. Simulated results of liquid water content and temperature generally agreed well with the experimental data for both wet and dry initial conditions. Also, cumulative infiltration results of the model corresponded well to the measurements.

Despite the calibration involved to represent the experimental setup, these results provided confidence in the ability of the model to simulate the physics of infiltration into frozen soil, regarding both liquid water content and temperature development. However, the model failed to predict the liquid water content and temperature well after 7 days. This was likely due to an incongruence between soil properties in the experiment and calibrated or estimated soil properties in the simulation which becomes more apparent at longer runtimes. In addition, thermal boundary conditions were not accurately represented by the model because of uncertainty in the amount of radiation that heats up the topsoil, as well as the uncertainty of the amount of energy provided by the bottom heat source.

Table 7. Soil parameters used in the simulation of the frozen soil infiltration experiment by Pittman et al. (2020).

Soil layer (depth)	$\alpha$ (cm <sup>-1</sup> )	$n$	$K_s$ (ms <sup>-1</sup> )	$\theta_r$	$c_s$ (Wm <sup>-1</sup> K <sup>-1</sup> )	$\theta_s$
0 - 15 cm	0.53	1.56	6.27e-07	0.02	1	0.6
15 – 50 cm	0.04	1.61	1.97e-08	0.08	1	0.51

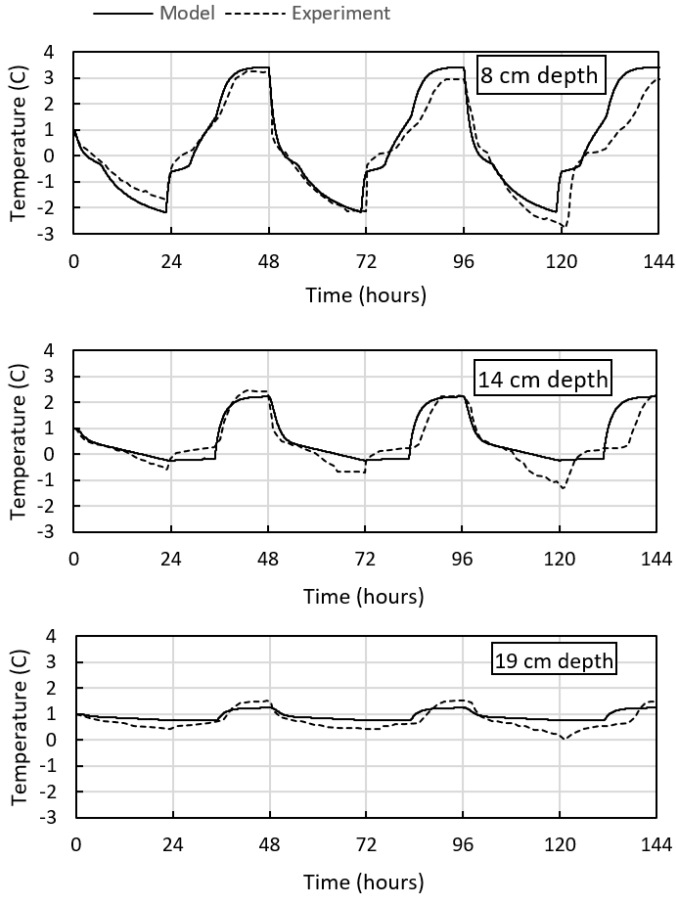


Figure 11. Measured soil temperatures at 8, 14 and 19 cm depth during repeated freeze-thaw cycles in the experiment by Wang et al. (2017) compared to the simulated temperature of the model.

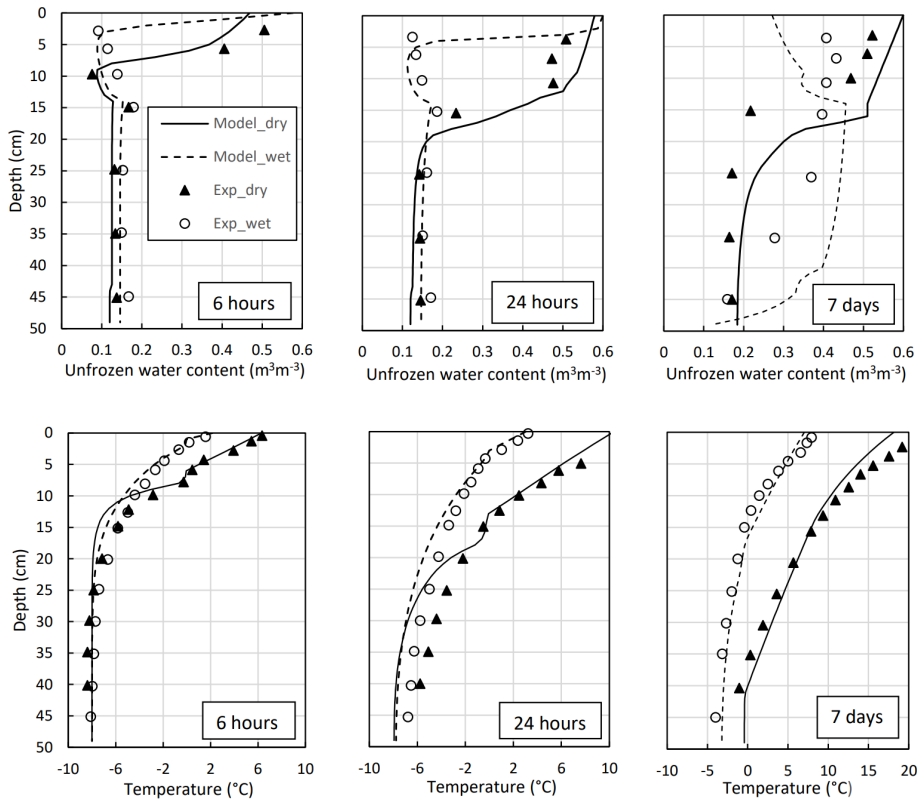


Figure 12. Comparison of model output with the measurements of Pittman et al. (2020) for both initially dry and wet frozen soil infiltration experiments. Exp stands for experimental measurements.

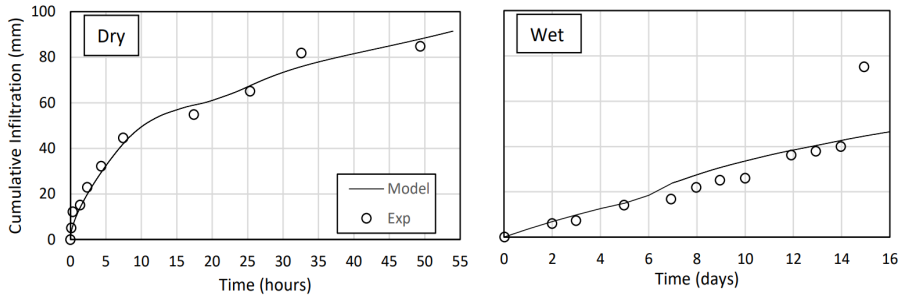


Figure 13. Plots of measured and modelled cumulative infiltration for initially dry (left) and wet (right) frozen soil experiments of Pittman et al. (2020). Exp stands for experimental measurements.

## Numerical experiments

Here we discuss the results of synthetic testing of different combinations of soil properties and boundary conditions. We describe the results of the freezing phase and the infiltration phase separately.

### *Differences after the freezing phase*

The state of the soil at the end of the freezing phase is summarized in Figure 14. We separately show the ice saturation (of the entire soil column), frost depth and average temperature in the topsoil (upper 10 cm). A case refers to a specific combination of the variables initial saturation and freezing temperature for a soil type.

### *Ice saturation*

It is apparent that soils with intermediate texture (soils 3 – 6) had the highest ice saturation after the freezing phase when looking at all cases combined in the boxplots; this concerns medians, upper quartiles and outliers (Figure 14a). These were the only soils which have cases with over 25% of the entire column saturated with ice. In comparison, the coarsest soils, soils 1 and 2, never had more than about 14% ice saturation of the column. With the very fine textured soils, soil 7 and 8, we observed the lowest medians of ice saturation, 0 and 3% respectively. Nevertheless, these soils had outlier cases in which ice saturation exceeded 15%. Furthermore, it was notable that the lowest value of ice saturation is higher for the coarse soils 1 and 2 (ca. 4%), while it was approximately 0% for the other soils. Lastly, we observed that the variability in ice saturation was highest for the intermediate soils.

These results demonstrated that intermediate soil textures potentially have higher ice saturation after the freezing phase compared to coarse and very fine soils. Given the large variability of the output, these soils were most sensitive to initial and boundary conditions. Characteristic of intermediate soils is that they have substantial water retention capacity, which prevents most of the pore water from flowing away due to gravity. Consequently, the pore water can freeze before it is drained. At the same time, the matric potential is not that strong to reduce the freezing point of water significantly, i.e., the soil freezing curve allows freezing to occur at mild subzero temperature. Lastly, these soils are most susceptible to cryosuction due to

moderate permeability combined with substantial water retention. This leads to increases in total water saturation and hence ice saturation in the freezing topsoil (e.g., Unold and Derk, 2017).

With the coarse soils, gravitational drainage leaves less pore water available for freezing. Small amounts of ice however always form during subzero temperature conditions. The reason is likely that the freezing point of water remains close to 0 °C in these coarse soils due to weak matric potential, allowing the remaining pore water to freeze. Contrarily, with the very fine soils, the freezing point of water is depressed strongly due to high matric potential which prevents a substantial amount of water from freezing. Only when the temperature for these soils becomes low enough, i.e., beneath the adjusted freezing point of water, phase change occurs.

#### *Topsoil temperature*

We focus on the topsoil (upper 10 cm) because this is where most of the thermodynamic freezing process occurs. Differences amongst soil types were observed in the lowering of topsoil temperature during the freezing phase, but there was no clear pattern related to soil texture. Instead, specific soil properties (Table 6) seem to have affected the heat transfer. Topsoil temperature was similar for soils 1 to 6, with soil 4 as a notable exception (Figure 14b). The sandy clay loam (soil 4) likely stood out as colder than the other soils after the freezing phase due to its low porosity combined with high residual water content. Low porosity implies a higher thermal conductivity because the solid particles have the highest thermal conductivity of all the soil constituents. The heat from the soil is therefore lost relatively rapid when the atmosphere (or snowpack) above is colder. Furthermore, low porosity results in a lower heat capacity due to the limited space for water. A high residual water content means that a significant portion of soil water always remains unfrozen, therefore involving less phase change. The reduction in latent heat flux facilitates temperature change.

For similar reasons prescribed to low porosity, the simulated silty clay (soil 8) became the coldest soil of all soils after the freezing phase. In addition, ice saturation with soil 8 was lowest due to the strong depression of the freezing point of water. This means there hardly was a latent heat flux, allowing for

rapid soil cooling. It was also noticeable that the low porosity soils were associated with higher sensitivity to the boundary temperature exemplified by the large variability in topsoil temperature output of soils 4 and 8.

Another anomalous topsoil temperature result could be seen with soil 7, the organic-rich soil. It had the highest median topsoil temperature and it was the only soil with frequent positive topsoil temperature cases at the end of the freezing phase. This is likely also explained by porosity as soil 7 had a high porosity (0.766). The large heat capacity of a water-logged highly porous soil slows down temperature change. At the same time, at low water saturation and thus high air saturation, the thermal conductivity is very low which also slows down freezing. It is not explained by a higher latent heat flux due to more pore water, since ice saturation after freezing was low for this soil.

#### *Frostdepth*

The pattern of frost depth results across soil types was different than the pattern of topsoil temperature results across soil types (Figure 14c). The frost depth was overall quite similar, but deepest with soils 2 to 6 for most cases (between 0 to 35 cm deep). Soil 7 had the least deep frost, likely because of the high porosity of the soil which leads to relatively warm soil temperature. Soil 8 on the other hand had exceptional outliers with deep frost (up to 49 cm deep). The freezing point of water was low in this soil type (silty clay). As a result, the ice saturation remained low with little latent heat flux, which made it possible to reduce the temperature in the deepest layers.

The minimum value of frost depth seen across cases was a bit deeper with soils 1, 2 and 3 compared to the other soils. Some ice always formed in these soils even with modest freezing temperatures because the freezing point of water was close to the freezing point of water at standard atmospheric pressure. Yet these soils did not have deep frost, likely because rapid drainage prior to freezing left the soil highly saturated with air. The air-filled topsoil acted as an insulator, slowing down the penetration of the freezing front.



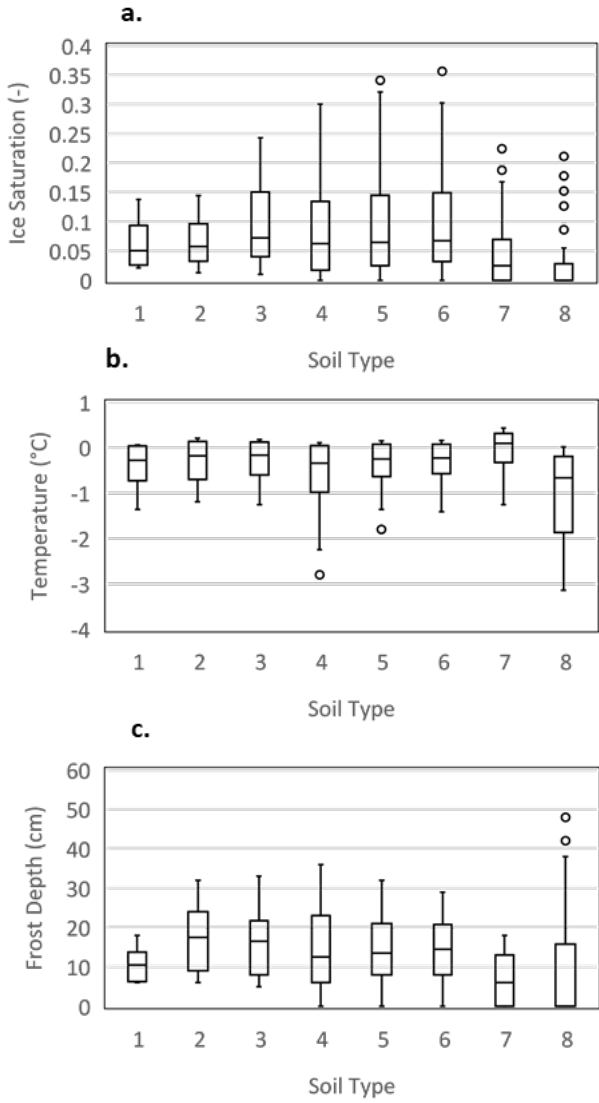


Figure 14. Boxplots of simulation results at the end of the freezing phase for each soil type of a) ice saturation; b) average temperature of the topsoil (upper 10cm); c) frost depth.

## Infiltration results

### *Overall results for the various soil types*

The unfrozen infiltration reference scenarios showed that the total amount of added water, 80 mm, always infiltrated with soils 1 to 4 (Figure 15a). Soil 5 had only a few unfrozen cases when not all water is infiltrating. With soils 6 and 7, infiltration during nonfrozen conditions varied from half to all the input water. Soil 8 never showed complete infiltration in the unfrozen scenarios with infiltration ranging from nothing to about half of all input water. These results were expected based on the lower permeability of the finer soil textures.

For the partly frozen scenarios, only with soil 1 (sandy soil) the total amount of added water infiltrated in all cases (Figure 15). The output for the other soils varied widely: ranging from cases with no infiltration to cases with full infiltration due to freezing. Differences across soil types were large. Firstly, soil 2 and 3 had infiltration reduction occurring only as outlier cases, meaning that specific circumstances were required to see an effect of freezing on infiltration. Secondly, soils in the intermediate texture range (soils 4 to 6) displayed the strongest reduction of infiltration due to freezing. Thirdly, regarding the finer soils, substantial infiltration reduction occurred with soil 7 but only to a small extent with soil 8.

The general pattern of strong infiltration reduction due to freezing for the intermediate soils was confirmed in Figure 16, in which the frequency of cases with a certain severity of infiltration reduction due to freezing is shown. Soil 4 had the highest frequency of cases (ca. 30%) in which infiltration reduction due to freezing was over 75% of the input water. Concludingly, the sandy clay loam (soil 4) was most severely affected in its infiltration capacity by freezing in our study.

The main reason for the major effect of freezing on infiltration capacity of intermediate soils (soils 4 to 6 specifically) is the substantial ice saturation of these soils caused by freezing as observed in the previous section. The high ice saturation results in a strong drop in permeability and reduced accommodation space for infiltrating water. Importantly, these soils are during unfrozen conditions already near the threshold for infiltration excess

overflow for various input rates, hence the permeability drop due to ice has significant impact. These results add information to the general notion that loamy and silty soils are most susceptible to the process of cryosuction and frost heaving (Hansson and Lundin, 2006).

Coarse soils have low ice saturation and hence higher permeability and more space for infiltrating water, leading to the result that freezing had little to no effect on infiltration. The infiltration into the silty clay (soil 8) was only mildly affected by freezing because of two major reasons: 1) unfrozen soil infiltration is already inhibited, hence further reduction in permeability has less compounding effect; 2) the freezing point of water is depressed strongly, leading to low ice saturation. The same applies to soil 7, the organic rich soil type, but with the exception that in several cases freezing did have a significant effect on infiltration. From the cross-tabulations in the Appendix, it follows that these cases concerned high initial saturation of soil 7 before the freezing phase.

#### *Temporal infiltration regimes*

Examples of the cumulative infiltration along with the development of ice content and total saturation with time are shown in Figure 17. These examples are selected to display the two different types of infiltration regime we observed. The example of soil 7 showed a two-phase infiltration pattern: infiltration rate decreased until it reaches a steady rate, similar to frozen soil infiltration as observed by Zhao and Gray (1998). The time it took to reach steady-state infiltration and the steady-state infiltration rate itself varied across cases, but only one example is shown here as this type of infiltration is not different from a normal infiltration curve into an unfrozen soil. First, the infiltration rate gradually decreased as the matric potential gradient becomes smaller. The second phase was characterized by a steady-state infiltration through the frozen zone at a rate lower than the saturated hydraulic conductivity due to the presence of ice. The heat transfer due to soil warming aligned with the progression of the wetting front as the ice rich zone lies exactly beneath the wetting front for all timepoints. The thawing rate was thus dictated by the maximum infiltration rate.

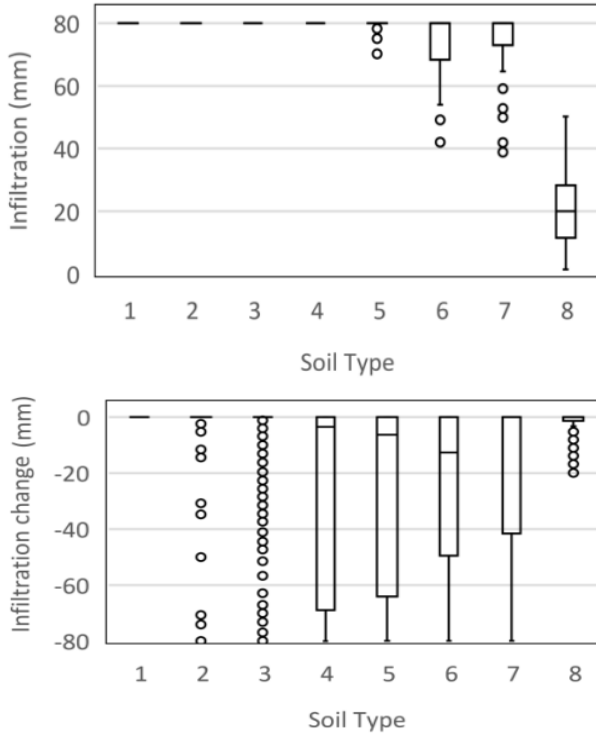


Figure 15. Boxplots for each soil type of amount of infiltration (mm) of input water under non-frozen conditions; and the change in the amount of infiltration (mm) due to frozen conditions.

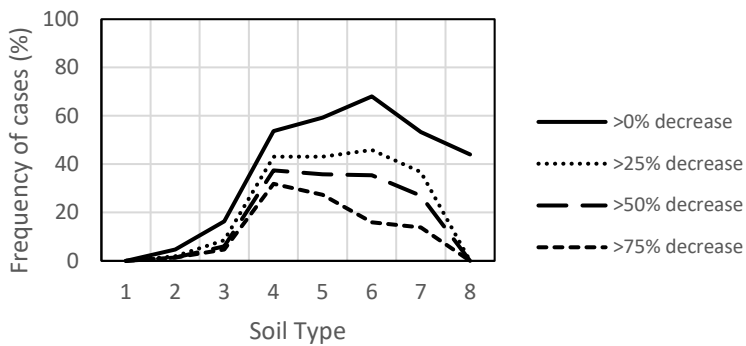


Figure 16. Graph showing the frequency of simulated cases (%) for each soil type in which a certain amount of infiltration reduction (% of total water input) due to freezing occurred.

It could be expected that during prolonged infiltration, the wetting front eventually would reach the unfrozen zone. At this point, infiltration would likely accelerate, but this was not observed within the simulated time periods of this study (maximum 320 hours). Below the wetting front, we observed that the ice melted at a consistent pace, likely due to heat from deeper and warmer layers in the soil. The meltwater then refroze deeper where the soil is still in the process of cooling. This phenomenon of downward ice migration occurred in both infiltration regimes, and it can be expected as soon as freezing from the top stops.

A three-phase infiltration regime could be observed in the examples of soil 4: first infiltration slowed down, followed by a temporary steady infiltration rate, and finally an increased infiltration rate until a steady-state situation. However, the results for the three different cases of soil 4 shown in Figure 17 varied a lot both in length of the different phases and in their infiltration rates. In the case of Figure 17b, there was a modest increase in ice saturation after 1h causing the penetration of the wetting front to slow down in phase 2. It turned into a slightly higher steady-state infiltration rate again when thawing causes most of this increased ice saturation below the wetting front to disappear after 96h.

A large local increase in ice saturation could be observed in Figure 17c, when the soil had been frozen more severely (-3 instead of -2 °C) and the input rate was higher (2 instead of 0.5 mmh<sup>-1</sup>). The colder soil and faster addition of water caused significant freezing of infiltrating water. Consequently, the wetting front hardly moved downward during phase 2. During this phase, most of the infiltration excess overland flow could be expected. The final phase starts when the heat from above connected to the ice rich layer and caused it to thaw. As a result, the infiltration rate increased. The slightly wobbly pattern observed in the plot was likely an artefact of numerical discretization of the thin highly ice-saturated layer.

In the case of Figure 17d, the increase in ice saturation was severe and occurred immediately in the top few centimeters of the soil. This was the result of near absence of thaw (0 °C top temperature boundary) resulting in a quick halt of the wetting front at the frozen infiltrated water layer. After

24h the heat from the top boundary temperature slowly initiated melting. The infiltration rate thereby transitioned to phase 3 but not clearly within the timespan of the simulated water input event. Only about 2 of the 80 mm water infiltrated, meaning that most of the melt- and rainwater became surface runoff.

The three-phase infiltration regime is different from the three frozen soil infiltration phases described by Watanabe et al. (2011). They observed the first phase as having no infiltration at all, followed by slow infiltration and rapid infiltration, respectively. It is possible the different first phase of the infiltration regime in their experiment was the consequence of a permanent 15-cm constant head at the top of the column, causing instant sealing of the topsoil due to in-situ freezing. A more realistic slow water input rate does not lead to such immediate ice sealing, instead the local ice saturation increases gradually, allowing infiltration during the first phase. Additionally, the topsoil boundary had a temperature of  $-6\text{ }^{\circ}\text{C}$  in the experiment of Watanabe et al. (2011), leading to rapid in-situ freezing. This might be unrealistically cold for most field situations.

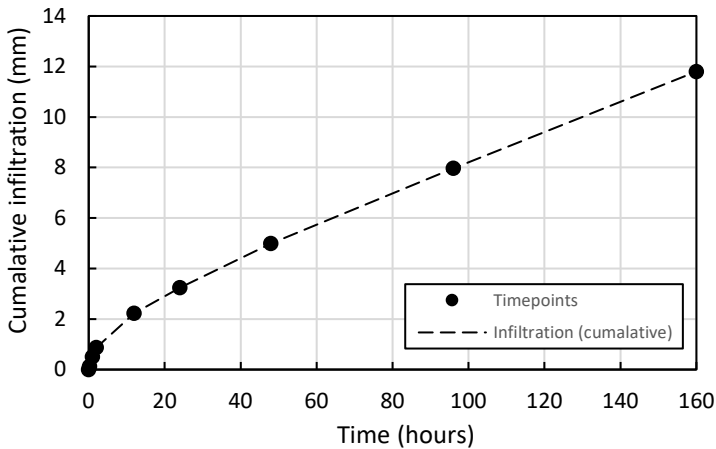
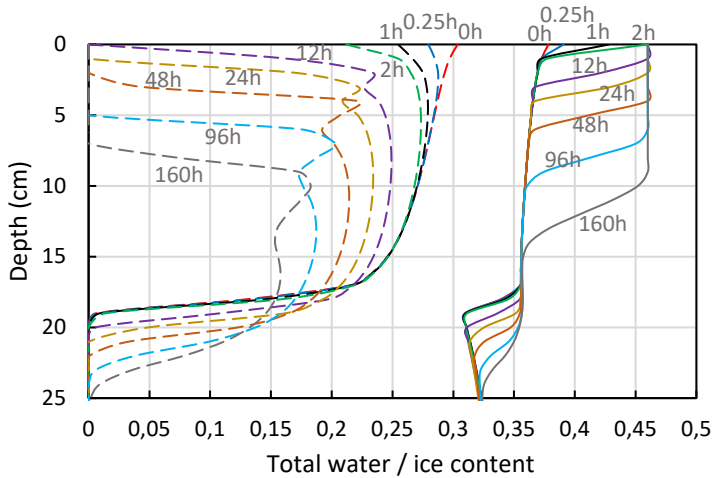
### Scenario variables

The scenario variables studied include initial saturation, freezing temperature, thawing temperature, water input rate and water input temperature. The statistically significant Spearman correlation coefficients for the relationship between the variables and infiltration change for each soil type are plotted in Figure 18 ( $p < 0.01$ ). All correlations that were not significant ( $p \geq 0.01$ ) were put to a value of 0 (i.e., no relationship). Input water temperature had no significant Spearman correlation with infiltration change due to freezing for all soils ( $p > 0.01$ ). It is therefore omitted from Figures 18 and 19. The median values of infiltration change due to freezing are plotted in Figure 19 against each of the other variable values. In the appendix, the frequency of cases with extreme infiltration reduction due to freezing ( $>75\%$ ) are shown for each combination of variable values.

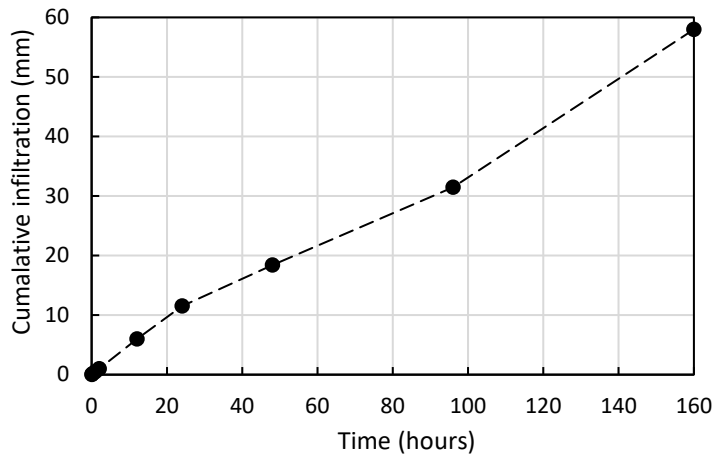
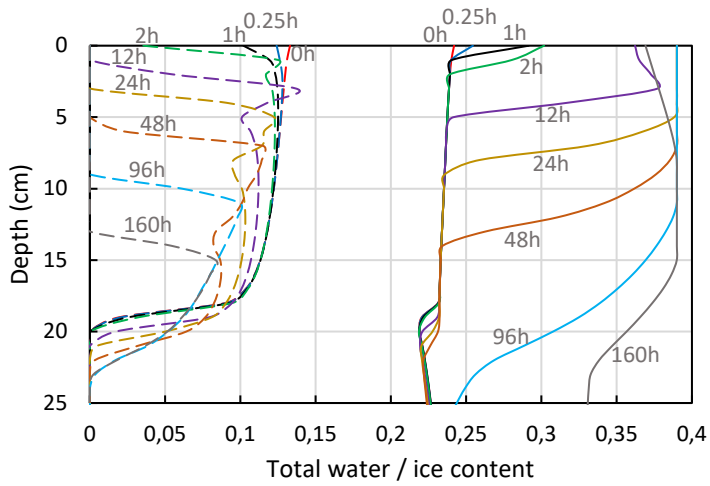
### *Initial saturation*

In our simulations, initial saturation was the most important factor determining the impact of freezing on infiltration into frozen ground (Figure

18), a similar finding as other studies (e.g., Watanabe and Osada, 2017; Zhao et al., 2013). A particularly strong relationship between reduced infiltration and initial saturation existed for soils 4 to 7 (Spearman's  $\rho > 0.6$ ). The more pore water initially present, the higher the potential ice saturation and the more the permeability and accommodation space for infiltrating water are reduced.

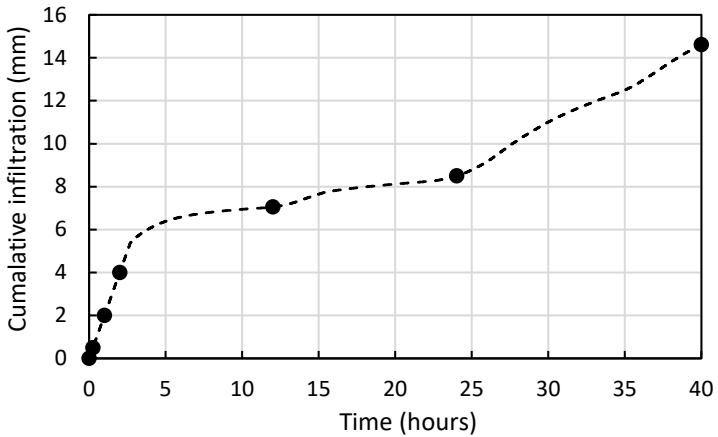
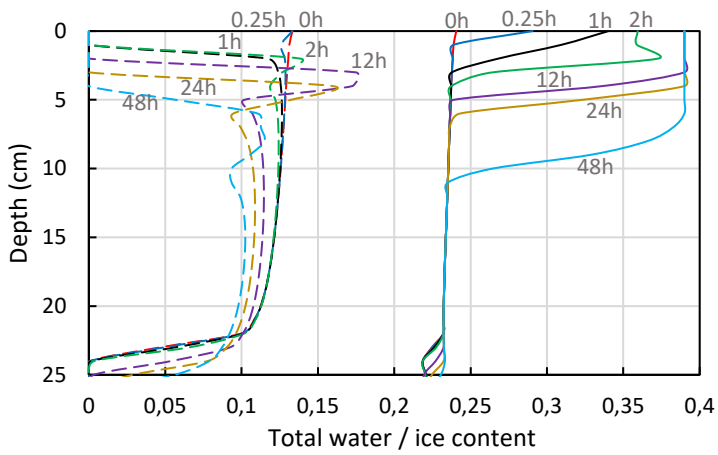


a. Soil 7, initial saturation: 0.75, freezing temperature:  $-3\text{ }^{\circ}\text{C}$ , thawing temperature:  $0.5\text{ }^{\circ}\text{C}$ , inflow rate:  $0.5\text{ mmh}^{-1}$ .

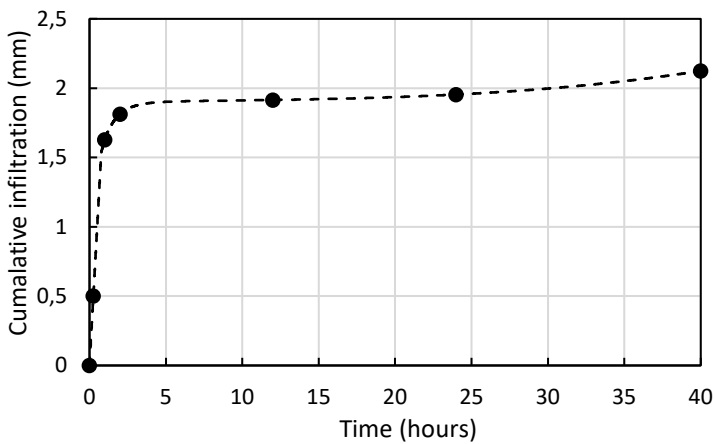
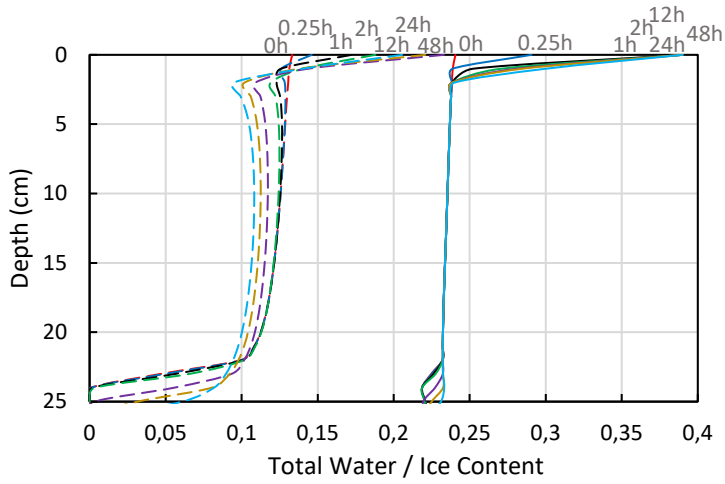


**b.** Soil 4, initial saturation: 0.6, freezing temperature:  $-2\text{ }^{\circ}\text{C}$ , thawing temperature:  $0.5\text{ }^{\circ}\text{C}$ , inflow rate:  $0.5\text{ mmh}^{-1}$ .





c. Soil 4, initial saturation: 0.6, freezing temperature: -3 °C, thawing temperature: 0.5 °C, inflow rate: 2 mmh<sup>-1</sup>.



**d.** Soil 4, initial saturation: 0.6, freezing temperature:  $-3\text{ }^{\circ}\text{C}$ , thawing temperature:  $0\text{ }^{\circ}\text{C}$ , inflow rate:  $2\text{ mmh}^{-1}$ .

Figure 17. Plots of total water and ice saturation through time, as well as cumulative infiltration, for different scenarios and soil types (a-d). These are selected examples to demonstrate different temporal frozen soil infiltration regimes.

With soil 4 however, median infiltration reduction was weaker at 0.75 than at 0.6 initial saturation, and weaker at 1.0 than at 0.9 initial saturation,

resulting in a sinusoidal type of relationship between 0.6 and 1.0 initial saturation (Figure 19a). The same pattern could be found in the cross-tabulations in the Appendix, in which different variable combinations are shown. This effect of higher initial saturation seemed to occur irrespective of the values of the other variables. With soil 7 a similar phenomenon could be observed as the median infiltration reduction is weaker at 1.0 than at 0.9 initial saturation (Figure 19a). This phenomenon could be explained by the presence of two opposing processes: an increase in latent heat flux and heat capacity due to more initial pore water slows down temperature change leading to lower ice saturation, while more initial porewater also causes higher thermal conductivity and potentially higher ice saturation since more loosely held water is available. Apparently at these specific higher initial saturation values, the energy cost is stronger than the potential volumetric increase in ice saturation. This finding demonstrates the sensitivity of the freezing process to specific circumstances, antecedent conditions, and the intricate balance of processes involved.

#### *Freezing temperature*

A temperature threshold could be identified for most soils; above this value, infiltration change due to freezing was minimal. Below the threshold, the relationship between freezing temperature and median infiltration change was mostly linear with gradually more infiltration reduction with decreasing temperature (Figure 19b). The threshold was at  $-0.5$  °C for soils 4, 5 and 6, while with soil 7 it lies at  $-2$  °C. For the other soils, no relationship could be observed due to the low number of cases with infiltration change. The decrease in infiltration with lower temperature below the threshold could be explained by a few factors. The lower the temperature of the soil, the higher the potential ice saturation as dictated by the soil freezing curve. Also, the faster freezing rate at lower temperature means that water can be immobilized quicker before it drains. Furthermore, a colder soil thaws slower and has more potential to experience infiltrating water freezing in-situ.

#### *Thawing temperature*

A non-linear relationship could be observed between thawing temperature and median infiltration change for most soils (Figure 19c). Increasing the

thawing temperature from 0 to 1 °C substantially decreased the number of cases with strong infiltration reduction due to freezing. Above 1 °C (0.5 °C for soils 7 and 8), an even higher thawing temperature had less effect. The crucial temperature range for effective thaw thus seemed to lie between 0.5 to 1 °C for most soils. Above the threshold boundary temperature sufficient energy was transferred to raise the soil temperature above the freezing point of water. If the boundary temperature was too low, the soil remains cold and frozen, and the potential for infiltrating water freezing in-situ is high. In practice, infiltration is therefore strongly inhibited when a snowpack exists on top of the soil. A melting snowpack has a temperature of about 0 °C (Rango and DeWalle, 2008), while the soil itself is insulated from the air. Top boundary thawing temperatures above 0 °C represent situations with snowpack free conditions whereby the atmosphere and solar radiation provide energy to the soil. In those cases, frozen soil infiltration can be much enhanced due to thaw.

#### *Inflow rate*

Intermediate soil textures displayed a stronger correlation between inflow rate and infiltration change due to freezing than both finer and coarser soils. The correlation only existed for soils 3 to 7, ranging from a Spearman's rho of 0.17 for soil 3 to about 0.32 for soil 5 (Figure 18). A threshold for the effect on median infiltration change could also be observed (Figure 19d). The strongest decrease in infiltration occurred between 0.5 to 2 mmh<sup>-1</sup> water input with soils 4 to 6. Below 0.5 mmh<sup>-1</sup> input rate, the median infiltration change was zero. Above 2 mmh<sup>-1</sup>, the effect of higher input rate diminished, except for soil 7. The role of water input rate thus seemed straightforward: the higher the input rate, the more likely it was that the infiltration capacity of frozen soil is exceeded. However, with soils that already experience infiltration rate excess during the unfrozen reference scenarios, a very high input rate leads to a comparatively less strong effect of pore ice on infiltration.

Concludingly, with a low water input rate, water can often still infiltrate into frozen soil. However, the data in the Appendix showed that infiltration could

still be severely inhibited if the soil is highly saturated before freezing, or if the soil is cold enough to cause freezing of infiltrating water.

*Extreme cases*

The appendix displays the cross-tabulations for each variable combination and the frequency of cases with over 75% infiltration reduction due to freezing. The highest number of cases was for most soils associated with a low boundary thawing temperature, especially at 0° C. This underscores the importance of thawing and the opposing process of infiltrating water freezing in-situ with its effect on subsequent infiltration. Infiltrating water freezes readily in still frozen soil because the available pore space has less matric potential. Furthermore, most of the extreme cases occurred when freezing temperature was lower than -0.5 or -1 °C and initial saturation was at least 0.6 or 0.75. In some cases, such as with soil 4, a higher initial saturation (0.75 compared to 0.6, and 1.0 compared to 0.9) corresponded to less extreme infiltration reduction cases. This is similar to the earlier finding on the effect of specific values of higher initial saturation. In practice, the extreme cases show the conditions during which flood and erosion hazard are highest.

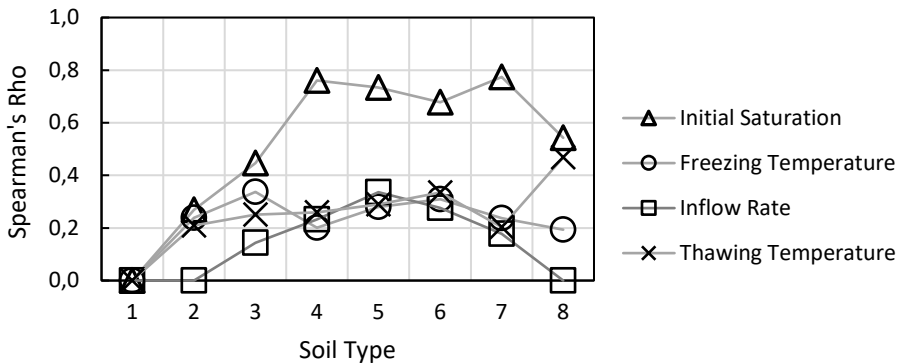
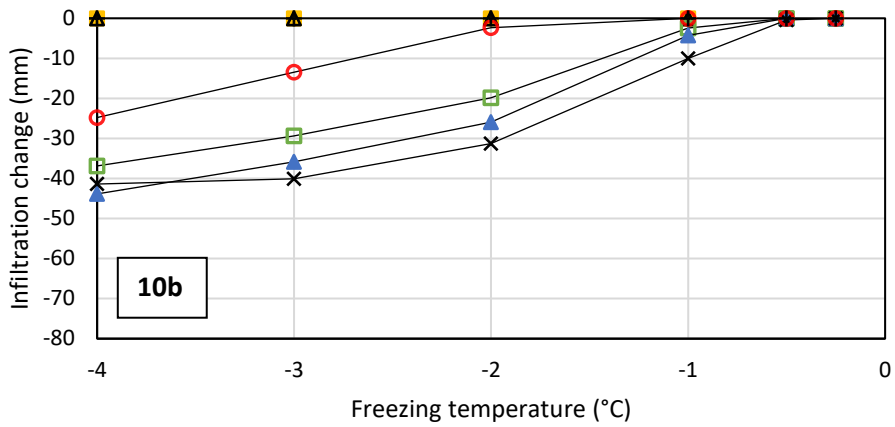
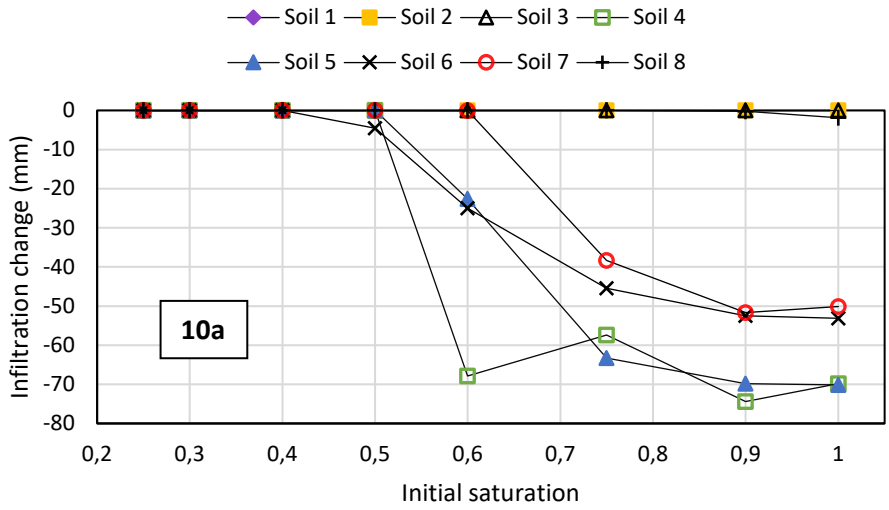


Figure 18. Plot of Spearman's Rho correlation coefficients for the relationship between each environmental variable and the reduction in infiltration due to freezing for each soil type ( $p < 0.01$ ). Non-significant correlation coefficients ( $p > 0.01$ ) were plotted as having the value 0.



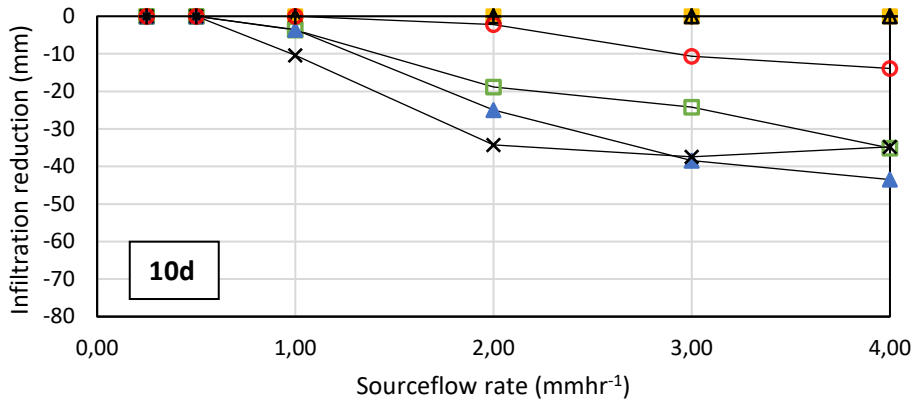
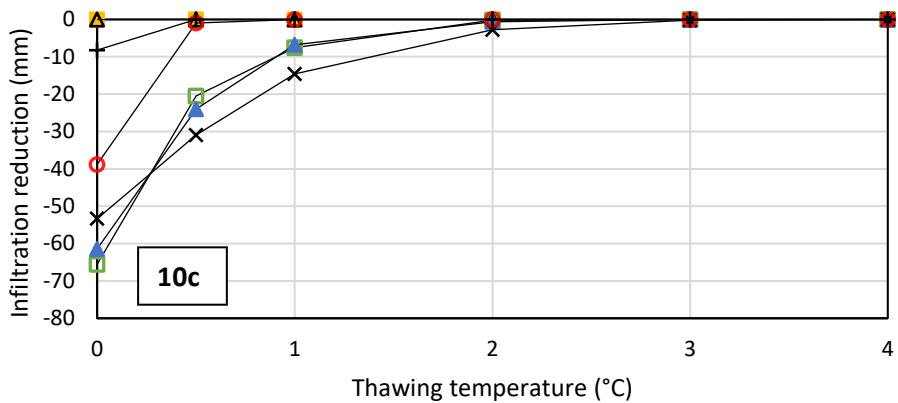


Figure 19. Median values of infiltration reduction due to freezing (%) for input variable values of initial saturation (a), freezing temperature (b), thawing temperature (c) and inflow rate (d).

### Uncertainty

This study did not include simulation of preferential flow through macropores. It has been found in previous studies that macropores often allow infiltration to occur uninhibited into a frozen soil because macropores rarely saturate with ice (Mohammed et al., 2018). Under specific circumstances, infiltrating water could however freeze within macropores and lead to ice blockage of preferential flow (Mohammed et al., 2021). Despite the importance of macropores for frozen soil infiltration, the focus

of this study is on the soil matrix and the effect of various single-domain soil parameters.

Also not considered in this study was alteration of pore structure due to frost heave. The prediction of frost heave has received a lot of attention (Lein et al., 2019), but there is less knowledge of its influence on soil hydrological properties. An experimental study by Leuther and Schlüter (2021) shows that clay content is important in determining the effect of freeze-thaw cycles on pore structure. They also demonstrate changes in soil water retention and hydraulic conductivity due to soil structure change. There is however too little empirical information yet to derive constitutive relationships between soil freezing and soil hydrological properties.

Furthermore, it is uncertain whether the empirical parameter  $\Phi_i$  for cryosuction (Chapter 2, Eq. 12) had a value of 1.8 for all soil types due to lack of empirical data. Based on Stuurup et al. (2021) it is however suggested that  $\Phi_i$  functions as a constant independent of soil texture. Lastly, soil thermal conductivity between soil types in our simulations could only differ due to differences in porosity and water, ice, and air content. Although these are major factors determining soil thermal conductivity, other possible changes in thermal conductivity were not considered such as different solid grain thermal conductivities.

## Outlook

The modelling exercise performed in this study provided several clues as to how temperature, soil texture, initial water content and water input rate play a role in determining frozen soil infiltration capacity. These are theoretical results based on the equations that represent the thermodynamics of freezing and thawing as well as transport of water in porous media. Further empirical validation is needed based on experimental work. This study could provide a framework for more focused experiments to expand the empirical knowledge on frozen soil infiltration. Similar soil types could for example be used to verify that infiltration into intermediate textured soils is most affected. The same boundary and initial conditions could be recreated for a smaller number of test columns, to investigate if similar effects as we have



modelled are observed. Of particular interest could be the role initial saturation plays, as well as the importance of freezing of infiltrating water.

#### 4.4 Conclusion

Comparison with experimental data suggested the model is capable of simulating infiltration into frozen soil. Numerical simulation of a high number of synthetic test cases provided insight into the freezing, thawing and infiltration process of various soil types during different boundary conditions. The most important findings are listed below.

- Intermediate soil textures had the highest ice saturation after the freezing phase compared to coarse and fine soils and therefore the strongest reduction in infiltration capacity due to freezing. Coarse soils were hardly affected but very fine soils to some extent depending on specific conditions.
- A two-phase infiltration regime existed when the thawing front during infiltration did not overtake the wetting front and no significant amount of infiltrating water froze in-situ. At first, infiltration was fast until the soil was highly saturated. Subsequently, there was slow steady-state infiltration through the frozen zone. This infiltration pattern is similar to normal infiltration into unfrozen soil.
- A three-phase infiltration regime existed when a substantial amount of infiltrating water froze in-situ. First, infiltration rate decreased as ice saturation increased. Secondly, there was quasi-steady state infiltration with a very slow rate due to frozen infiltrated water. Thirdly, infiltration rate increased when the thawing front connected to the frozen infiltrated water. Significant surface runoff could be expected during phase 1 and 2 due to the frozen infiltrated water.
- Large differences existed concerning the effect of environmental parameters (initial saturation, freezing temperature, thawing temperature and water input rate) on frozen soil infiltration for various soil types. Overall, initial saturation was one of the most important factors affecting frozen soil infiltration capacity. Water input temperature had no effect. Threshold values were identified at which frozen soil infiltration capacity started to become increasingly

affected, e.g. initial saturation of 0.6 and 0 °C top boundary temperature during infiltration for most intermediate soil types.

- Cases of severe infiltration reduction due to freezing were for most soils associated with an initial saturation of at least 0.6 or 0.75, an absence of thaw (0 °C top boundary temperature) and a freezing temperature of at least -0.5 or -1 °C for five days; differences between soil types should be considered.
- Low soil porosity facilitated soil cooling and thereby led to increased chances of infiltrating water freezing in-situ, while high porosity slowed down soil cooling.
- Ice migrated slowly downward during the infiltration and thawing phase through refreezing of melted ice deeper in the soil.

The results of this study are based on numerical simulation and therefore provide theoretical insight into the freezing and infiltration dynamics of a homogenous 1-dimensional soil column. The simulations provide a framework for further experimental work to validate or falsify our findings. This study also provides insight into the intricate and complicated physics of frozen soil infiltration with many tipping points and processes steering in different directions. A drawback of our approach is the lack of structural soil change during freezing and the absence of preferential flow. The current reality is that little information exists to be able to predict a change in hydraulic properties due to freeze-thaw cycles. Our results should therefore be considered uncertain for cases in which frost heave is expected. It should also be considered that our results show the link between various parameters in the absence of macropores; the case of preferential flow requires further specific attention.

## 5. The role of microtopography and macropores

*This chapter is based on the yet unpublished manuscript “The effect of microtopography and macropores on frozen soil infiltration dynamics” by J.C. Stuurup, S.E.A.T.M. van der Zee and Helen K. French.*

### 5.1 Introduction

It is well known that freezing of soil lowers a soil’s infiltration capacity. Ice that grows in the pores of a soil results in a blocking of flow paths and reduced accommodation space for infiltrating water (Garstka, 1945). A landscape receiving large water input (rain or snowmelt) during reduced soil infiltration capacity is vulnerable to flooding (Fang and Pomeroy, 2016; Zuzel et al., 1982). An important question is therefore when frozen soil can be expected to increase flood hazard. Despite a great deal of research on seasonally frozen soil however, the relationship between frozen soil and a hydrological response at the catchment level remains poorly understood (Ala-Aho et al., 2021).

At the laboratory soil column and field plot scale, experiments have shown that freezing of soil reduces infiltration (e.g., Saadat et al., 2020; Pittman et al., 2020). The higher the ice content of the soil, the lower the permeability of the soil (McCauley et al., 2002). It would therefore seem likely that this reduced permeability during frozen conditions is reflected in the response of a stream hydrograph to water input. However, in a meta-review of catchment-scale studies, Ala-Aho et al. (2021) found the influence of frozen soil on catchment hydrology to be ambiguous: sometimes it had a clear effect, sometimes only to a minor extent, and sometimes not at all. The least impact of frozen soil was observed with deep snowpacks, or extensive forest cover. With deep snowpacks and no midwinter melt events, the soil remains relatively dry and insulated against strong freezing temperatures, whereas forest cover can lead to spatial patchiness in soil frost occurrence due to complex within-forest energy dynamics.

To improve our predictive capacity, we need to identify the environmental conditions during which soil freezing has an impact on hydrological partitioning in the landscape. It is important because of implications for flood

hazard, erosion, contaminant transport, and groundwater flow. A few of the most important factors determining a catchment-scale frozen soil response would likely be soil type, vegetation cover, catchment size and surface topography, as well as time-variant factors such as air temperature, snow depth, melt- and rainfall rate, and soil ice content.

A numerical model study of 1D non-macroporous soil columns concluded that for intermediate soil textures, there is a strong effect of freezing on infiltration capacity, while for sandy and clayey soils the influence was much less (Stuuroop et al., 2021b). Their study also indicated threshold values for initial soil moisture, air temperature during freezing and thawing, and infiltration rate. At these threshold values, frost drastically reduces infiltration. These threshold factors might already partly explain different hydrological responses to frozen soil due to variations in soil type and weather conditions. In short, the hydrological response cannot be simplified to a binary principle, frozen or unfrozen soil, given variations in environmental conditions.

Other studies suggest that microtopography plays a role in determining the pathway of meltwater during frozen soil conditions (French and Binley, 2004; Hayashi et al., 2003). These studies found that small depressions in the landscape (several centimetres deep in French and Binley, 2004, several meters deep in Hayashi et al., 2003) served as hotspots for focused infiltration. The precise interaction between melt water transport, infiltration, phase change and energy exchange processes causing this phenomenon is still not well understood. Potentially, focused infiltration reduces the amount of surface runoff that would otherwise occur.

Mohammed et al. (2018) in a review study pointed out that macroporous soils likely allow infiltration to occur uninhibited despite freezing of the soil matrix. This is because macropores hardly clog with ice: water drains rapidly, leaving little time for phase change. Only during very cold soil conditions, macropores could get filled with ice as the infiltrating water freezes in-situ (Pittman et al., 2020). Further study is required to examine such effects of macropores on frozen soil in a landscape setting,.

In this study, we focus on the role of microtopographic depressions and macropore presence on influencing the effect of frozen soil on infiltration. With the help of a numerical model, we examine the infiltration during frozen soil conditions for various soil types and weather circumstances in the presence or absence of small depressions and macroporous soil. The hypotheses that micro-depressions and macropores reduce flood hazard during frozen soil conditions will thus be tested. The modelling results will also shed light on the underlying physical processes that could explain the effect of micro-depressions and macropores on frozen soil dynamics.

## 5.2 Methods

### Numerical model

A two-dimensional model for water and heat transport including phase change and cryosuction was used for this study. The model is adopted from the 1D model described in Stuurop et al. (2021a) which includes a detailed explanation of the model and tests against laboratory experiments. The model simulates water and heat transport including phase changes between water and ice. There are three variants of the model; here we used the semi-empirical version as it requires the least number of empirical parameters (see Stuurop et al. (2021a)). Water flow was based on the Richards Equation for unsaturated flow (Richards, 1931). The energy balance equation for heat transport including thermal conduction, advection and latent heat transfer is given in Chapter 3, Equation.

The thermal conductivity was calculated as the geometric mean of the sum of thermal conductivities of all soil constituents. The van Genuchten model (van Genuchten, 1980) was used to simulate soil water retention. Cryosuction was simulated through the empirical equation developed by Zhang et al. (2007) and Kulik (1978) (see Chapter 2, Equation 9). The Clausius-Clapeyron relationship was incorporated into the van Genuchten equation to relate the liquid water content of the soil, to soil temperature (see Chapter, Equation).

Instead of the original surface temperature boundary of the model, we employed a more realistic soil-atmosphere energy exchange boundary in this

study based on the following equation for sensible heat convection (DeWalle and Rango, 2008):

$$Q_a = \rho_a H_a C_h u_a (T_a - T_s) \quad [24]$$

Where  $Q_a$  is the energy exchange between the atmosphere and soil (J),  $\rho_a$  is the density of air ( $\text{kgm}^{-3}$ ),  $H_a$  is the specific heat of air ( $\text{Jkg}^{-1}\text{K}^{-1}$ ),  $C_h$  is the bulk transfer coefficient for sensible heat,  $u_a$  is the windspeed at height  $z_a$  ( $\text{ms}^{-1}$ ),  $T_a$  is the air temperature at height  $z_a$  ( $^{\circ}\text{C}$ ) and  $T_s$  is the soil surface temperature ( $^{\circ}\text{C}$ ). The measurement height of atmospheric variables,  $z_a$ , is set to 2 m in our model.

Short-wave and long-wave radiative transfer is not taken into account. This would overcomplicate the parametrization of the model (e.g., albedo, vegetation cover), as well as require additional data input (e.g., solar radiation, cloudiness). We consider the omission of these types of radiative transfer to be unproblematic because of their small extent in winter / snowmelt conditions, and the uniform absence of these radiative transfers for all scenarios simulated.

For simplicity, we only assume stable atmospheric conditions. The bulk transfer coefficient for sensible heat under a stable atmosphere can then be calculated with the following equation (DeWalle and Rango, 2008):

$$C_{hn} = k^2 \left[ \ln \left( \frac{z_a}{z_0} \right) \right]^{-2} \quad [25]$$

Where  $k$  is von Karmin's constant (0.4) and  $z_0$  is the aerodynamic roughness of the soil surface (m). For our simulations, we assume bare soil conditions, which gives the value of 0.005 m for  $z_0$  (van der Kwast et al. 2013).

The model excludes shortwave- and longwave radiation exchange between the soil and atmosphere. These are strongly time-variant and would depend on cloud cover, slope angle and direction, shading, longitude and latitude, and time of the year. Hence, we reduce complexity and focus on quantifying the effect of sensible and latent heat exchange with the atmosphere.

Water that cannot infiltrate flows on the surface toward the micro-depression (10 cm deep and wide) or out of the model domain (scenario

without micro-depression). Surface flow velocity is calculated using Manning's Equation (Manning, 1891):

$$v = \frac{1}{n_2} h^{\frac{5}{3}} s^{0.5} \quad [26]$$

Where  $v$  is the surface flow velocity ( $\text{ms}^{-1}$ ),  $n_2$  is the Manning coefficient ( $\text{ms}^{-1}$ ),  $h$  is the surface water height (m) and  $s$  is the slope ( $\text{mm}^{-1}$ ).

When water reaches the micro-depression, it starts to fill the micro-depression space, hence creating a micro-pond. When the micro-depression is full, additional water is counted as surface runoff. In case of a smooth-surface scenario (no micro-depression), water that reaches the vertical model boundary is counted as surface runoff. The atmosphere-soil boundary at the bottom of the micro-depression shifts to an atmosphere-pondwater boundary when water fills the micro-depression, and a pondwater-soil boundary at the bottom of the micro-depression then exists.

For the energy balance within the micro-depression, equation 1 is valid but the thermal conductivity of water is replaced by the heat transfer coefficient of water to simulate convective heat transfer. In addition, solid grain and air contents are turned to 0, hence all energy transfer is within the water or ice in pond.

### Model geometry and parameters

The geometry of the model with simulated water fluxes is shown in Figure 20. The system is assumed to be symmetrical, hence no flow occurs below the midpoint of the pond. In reality, there would be a sequence of micro-depressions slope downward, leading to accumulation of overflow the further downslope. Here we are only interested in the dynamics of one isolated micro-depression. Parameter values are given in Table 8.

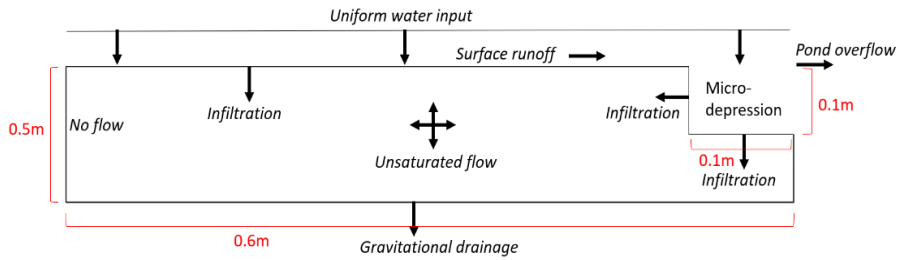


Figure 20. Geometry of the 2D model for the micro-depression scenarios. Simulated water fluxes are shown. The surface of the model has a slope angle of 0.04. The system is simulated as symmetrical, one half shown.

Table 8. Parameter values used in the model.

Slope angle	0.04
Manning's n	0.02
Freezing point of water	0 °C
Cryosuction constant ( $\phi_i$ )	1.8
Thermal conductivity solid grains	2.2 Wm <sup>-1</sup> K <sup>-1</sup>
Thermal conductivity water	0.6 Wm <sup>-1</sup> K <sup>-1</sup>
Thermal conductivity ice	2.22 Wm <sup>-1</sup> K <sup>-1</sup>
Thermal conductivity air	0.024 Wm <sup>-1</sup> K <sup>-1</sup>
Heat transfer coefficient water	1000 Wm <sup>-2</sup> K <sup>-1</sup>
Specific heat solid grains	840 Jkg <sup>-1</sup> K <sup>-1</sup>
Specific heat water	4182 Jkg <sup>-1</sup> K <sup>-1</sup>
Specific heat ice	2108 Jkg <sup>-1</sup> K <sup>-1</sup>
Specific heat air	1003 Jkg <sup>-1</sup> K <sup>-1</sup>
Density of solid grains	2648 kgm <sup>-3</sup>
Density of water	1000 kgm <sup>-3</sup>
Density of ice	916 kgm <sup>-3</sup>
Density of air	1.2754 kgm <sup>-3</sup>
Latent heat of fusion	33400 Jkg <sup>-1</sup>
Windspeed	3 ms <sup>-1</sup>
Aerodynamic roughness	0.005 m



## Scenarios

### *Micro-depression*

Different scenarios were developed to test the effect of a micro-depression on frozen soil infiltration during various boundary conditions and for various soil types. The configurations of initial and boundary conditions for each scenario can be found in Table 9. Broadly, the scenarios can be classified as time-variant freeze-thaw conditions and time-invariant freeze-thaw conditions; in the former case, freezing and thawing (with water input) alternate in time, while in the latter case thaw follows once after freezing, hence without any recurrence of freezing conditions (and no refreezing of water). Furthermore, the intensity and duration of freezing is varied amongst the scenarios, as well as the thaw intensity and water input rate during the snowmelt/rainfall phase. Also, the extent of time between the last moment of pre-freezing water input and the initiation of freezing (air temperature  $< 0^{\circ}\text{C}$ ) is varied (meaning soil water has varying timespans to drain before freezing), in addition to variations in the extent of time between the onset of thaw (air temperature  $> 0^{\circ}\text{C}$ ) and the start of water input (meaning soil ice has varying timespans to thaw before water is added to the soil).

We further classify the time-invariant freeze-thaw scenarios as slow and quick, referring to the timespan between freezing and water input boundary condition changes. Slow means that soil moisture has time to drain before freezing starts after last water input, in addition to energy exchange with the atmosphere, before water input starts. Quick means that freezing starts immediately after the last water input, and water input starts directly again after freezing. The chronology of the different boundary conditions as well as their values are given in Figure 21. An overview of boundary condition values for each scenario is given in Table 9.

Three soil types were selected for the simulations based on prior research by Stuurup et al. (2021b), because these soil types displayed significant effects of freezing on infiltration capacity: a sandy clay loam, a silt loam, and a silt (Table 10); we preserved the numbering of the soils of the original article.

An extra set of scenarios was run after completion of simulation of the 17 scenarios, because we wanted to identify the possible role of water input

rate. We performed model simulations with 1, 3, and 4 mmhr<sup>-1</sup> water input for scenario SC9, soil type 4.

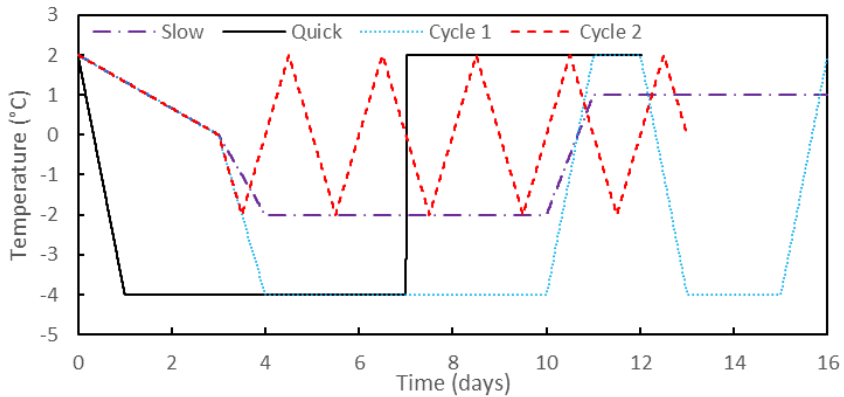


Figure 21. Different temporal modes of temperature boundary conditions simulated. See Table 9 for the corresponding scenarios.

Table 9. Modelled scenarios. Temporal temperature modes are clarified in Figure 21.

Scenario nr. (SC)	Freezing temperature (°C)	Thawing temperature (°C)	Water input rate (mmhr <sup>-1</sup> )	Temporal temperature mode
1	-2	0	1	Slow
2	-2	0.5	2	Slow
3	-2	0.5	1	Slow
4	-2	1	1	Slow
5	-4	2	1	Slow
6	-2	2	1	Slow
7	-2	0.5	2	Quick
8	-2	0.5	1	Quick
9	-4	1	2	Quick
10	-2	1	2	Quick
11	-2	1	1	Quick
12	-4	2	2	Quick

<b>13</b>	-4	2	1	Quick
<b>14</b>	-2	1	2	Cycle 1
<b>15</b>	-2	1	1	Cycle 1
<b>16</b>	-4	2	1	Cycle 1
<b>17</b>	-2	2	1	Cycle 2

Table 10. Soil hydraulic properties, including van Genuchten parameters, of the soils simulated in this study. Symbols.

<b>Soil nr.</b>	<b>Soil type</b>	<b>Ks(ms<sup>-1</sup>)</b>	<b><math>\alpha</math> (cm<sup>-1</sup>)</b>	<b>n</b>	<b>Porosity</b>	<b><math>\theta_r</math></b>
<b>4</b>	Sandy Clay Loam	3.63e-06	0.059	1.48	0.39	0.1
<b>5</b>	Silt Loam	1.25e-06	0.02	1.41	0.45	0.067
<b>6</b>	Silt	6.94e-07	0.016	1.37	0.46	0.034
<b>NA</b>	Macropore	6.00e-03	0.1	2	0.9	0.01

### *Macropores*

The 17 scenarios described above were also used for the macropore simulations. To simulate the presence of a macropore: a 20 cm-deep vertical zone of 1.7 cm width, with gravel-like soil hydraulic properties surrounded by finer soil matrix(silt loam). A total of three such macropore zones were simulated, accounting for 9% of the upper soil area (Figure 22). The macropore properties were directly derived from macropore samples in a study by Mohammed et al. (2018) in which they studied the simulation of macropores during frozen conditions (Table 10). In addition to the 17 scenarios, we included 3 macroporous scenarios with extreme freezing to gain more understanding of conditions in which macropores might not permit infiltration into frozen soil (SC1 setup, air freezing temperatures adjusted: -4, -6, and -8 °C).

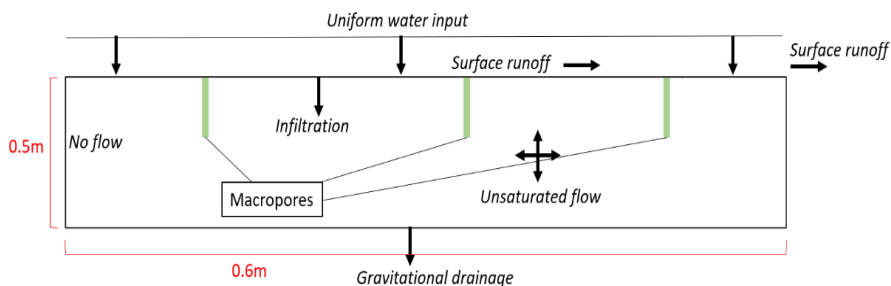


Figure 22. Geometry of the 2D model for the macroporous soil scenarios. Simulated water fluxes are shown. The green zones are macroporous soil. The surface of the model has a slope angle of 0.04 and macroporous zones are 1.7 cm wide.

### Output results

All scenarios were modelled with and without macropores, and with and without a micro-depression, in order to isolate the effect of the micro-depression and macropores. We subtracted the total infiltration measured in the microtopographic or macroporous cases from each corresponding smooth-surface case to obtain our main result of the study: the change in infiltration during frozen conditions due to the presence of the micro-depression or macropores.

For the micro-depression cases, we also calculated the proportions of total infiltration that occurred along the sloping surface, the wall of the pond, and the floor of the pond (Figure 20). This provides information on the manner through which either more or less water infiltrated into the soil. Finally, we made detailed graphs of total water content, ice content and soil temperature for specific scenario results to further illustrate the apparent physics involved.

## 5.3 Results

### Micro-depressions

#### Overall results

The change in amount of infiltration due to the presence of the micro-depression for each scenario is given in Figure 23. The result shows that the effect of the micro-depression on infiltration, compared to the reference

case, ranges from a substantial increase to a reduction. With the cyclical freeze-thaw scenarios (SC14 to SC17), the increase in infiltration by the micro-depression is overall strongest, while the scenarios with a temporal delay in freezing after wetting of the soil showed the weakest effect of the micro-depression on infiltration (SC1 to SC6). Reduced infiltration only occurred in a few cases, most cases showed increased or no infiltration change. The change in infiltration due to the micro-depression could range to up to 40% of total water added (120 mm).

In Figure 24 we can see the total amount of infiltration that occurred in each scenario with and without a micro-depression, as well as the proportion of infiltration that entered the soil at three different locations in the micro-depression case (along the slope, at the floor of the micro-depression, and at the walls of the micro-depression). The importance of each type of infiltration (slope, floor or wall) differs per scenario. In one case for example, the micro-depression increased infiltration by allowing water to enter the soil at its floor (SC17, soil 6). In another case, the micro-depression increased infiltration at the slope itself, hence the micro-topographic influence reached further than the immediate surrounding soil of the pond itself (SC15, soil 4). Finally, in yet another case most additional infiltration occurred laterally into the wall of the micro-depression, instead of vertically downward into the floor (SC3, soil 5). Possible physical causes of such infiltration dynamics are examined in more detail in section 3.2.

Boxplots of infiltration change for several scenario variables are shown in Figure 25. In most cases, the micro-depression improved infiltration for sandy clay loam (soil 4), and less often with silt loam and silt, respectively (soil 5 and 6). However, the highest infiltration increase occurred with the silt (soil 6), demonstrating the complex sensitivity of the frozen soil infiltration process to specific combinations of initial conditions, boundary conditions and soil properties. Severe reduction of infiltration due to the micro-depression only occurred with the silt (soil 6).

The number of days to freezing air temperatures after wetting played an important role. When frost occurred directly after wetting the soil, the micro-depression increased infiltration more than when freezing started three days

after wetting. The higher water input of  $2 \text{ mmhr}^{-1}$  led to more improved infiltration due to the micro-depression, compared to  $1 \text{ mmhr}^{-1}$  water case. The role of variable air freezing temperature is less clear, although most significant infiltration increases due to the micro-depression were observed at  $-2 \text{ }^{\circ}\text{C}$  instead of  $-4 \text{ }^{\circ}\text{C}$ . A significant decrease in infiltration also only occurred during milder freezing ( $-2 \text{ }^{\circ}\text{C}$  instead of  $-4 \text{ }^{\circ}\text{C}$ ). With an air temperature of  $0 \text{ }^{\circ}\text{C}$  during the water input phase (hence, absence of strong thaw), the micro-depression had little to no effect on infiltration.

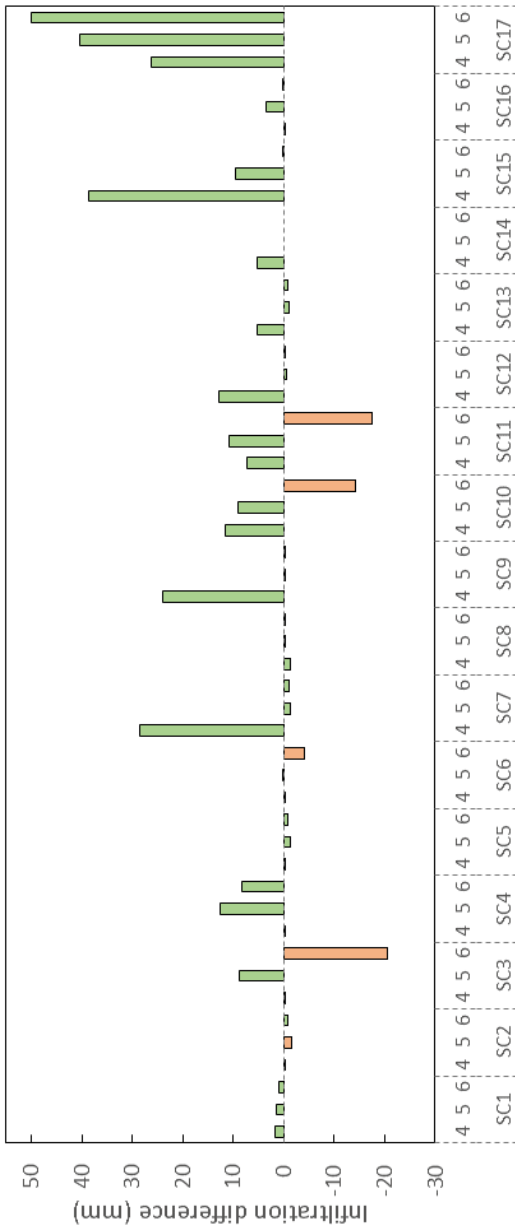


Figure 23. Total infiltration (mm) compared to reference model (infiltration difference) without micro-depression for each scenario (green = positive, orange = negative). Rotate the thesis 90 degrees clockwise to see the graph.

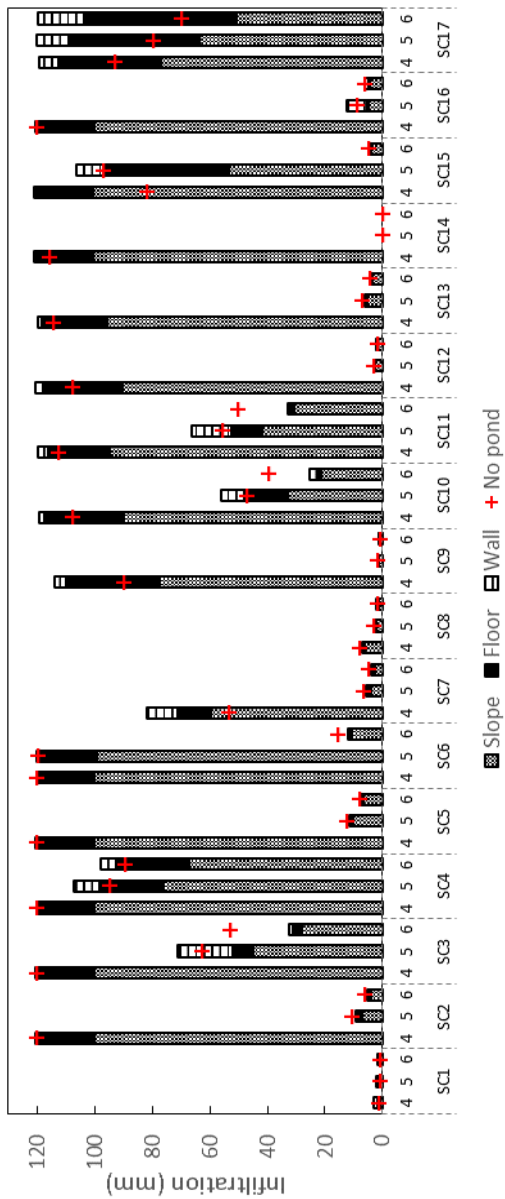


Figure 24. Total infiltration in each scenario for the micro-depression and smooth-surface (no pond) cases with distinction of location of infiltration: slope, floor and walls. Rotate the thesis 90 degrees clockwise to see the graph.



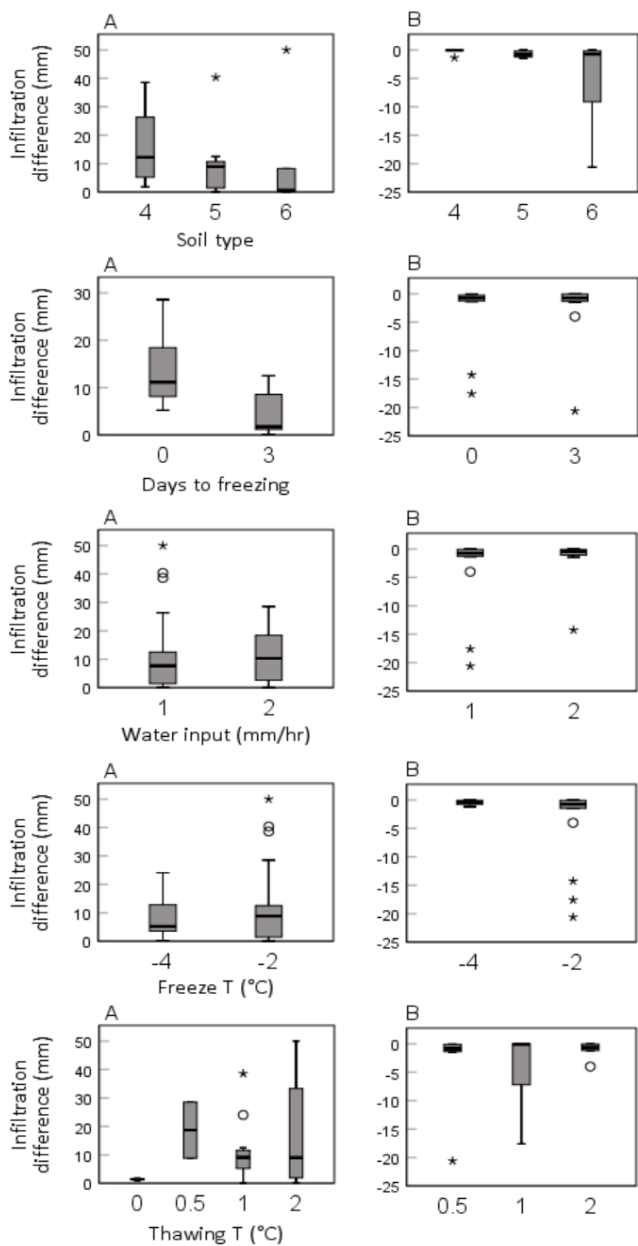


Figure 25. Boxplots of infiltration difference (mm) for different variable configurations; the A column entails infiltration increases, the B column infiltration decreases. Infiltration difference is the total infiltration (mm) compared to the reference model without micro-depression.

### *Specific cases*

In this section we explore how in some specific scenarios the micro-depression affected the spatial distribution of soil temperature, total water content and ice content in the soil profiles. These specific cases are selected based on their spatial infiltration differences: infiltration was either improved through infiltration along the slope, lateral infiltration along the micro-depression wall, or vertical infiltration into the floor of the micro-depression. We also examine a case in which infiltration substantially decreased due to the micro-depression in more detail.

#### *Slope infiltration (case: SC15 soil 4)*

In this case, there is more water infiltrating along the slope when a micro-depression is present than without a micro-depression. Soil conditions just before water input starts, are shown in Figure 26. The frozen soil had at this moment already been exposed to an air temperature of 1 °C for 24 hours. The area around the micro-depression is slightly warmer. Furthermore, while ice was concentrated around the micro-depression, it started to melt there. The ice saturation along the slope itself is also slightly lowered close to the micro-depression, providing a “gap” in the topsoil ice saturation. There is also a drier zone beneath the soil here that runs oblique downward along the ice-rich zone.

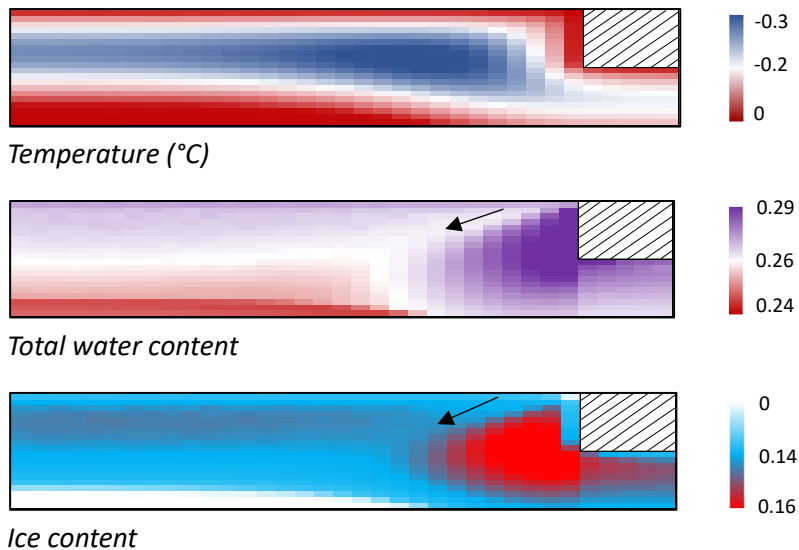


Figure 26. Temperature, total water content and ice content in the upper 22 cm of the whole 2D soil profile, after 1 day of positive air temperature (prior, the air temperature was at subzero degrees) (S, soil 4). Notice the non-linear colour scale.

#### *Wall infiltration (case: SC3 soil 5)*

The conditions at the end of the simulation for the wall infiltration case, hence after water input, are shown in Figure 27. It can be seen that the soil beneath the micro-depression is coldest, whereas the wall is warmest. Furthermore, there is still ice in the soil beneath the micro-depression, while there is no ice present in the wall. In Figure 28 we observe that the pond was completely filled with water for several days, until after approximately 3.5 days the pond level started to drop.

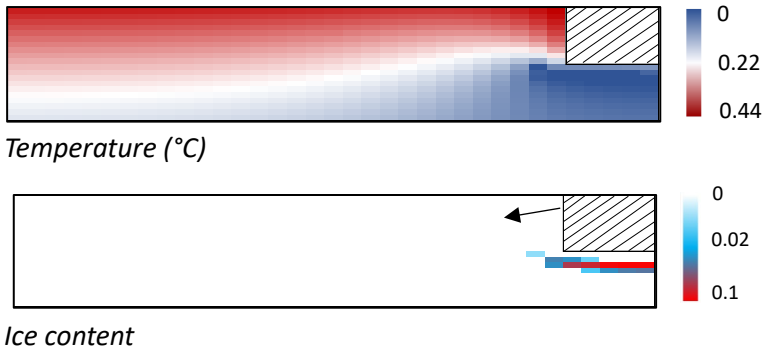


Figure 27. Temperature and ice content in the upper 22 cm of model the end of the full simulation (hence, after water input) (SC3, soil 5). Notice that the colour scale is not linear.

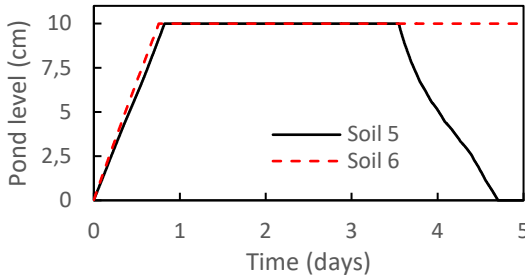


Figure 28. Pond level in the micro-depression from the start of water input to the end of the simulation for Scenario 3, soils 5 and 6.

#### *Floor infiltration (SC17, soil 5)*

This case concerns diurnal freezing and thawing. Most infiltration occurred vertically downward into the floor of the micro-depression. The conditions in the soil 2.5 days into the freeze-thaw cycle are shown in Figure 29. The cold front beneath the pond is much shallower than beneath the slope and adjacent to the wall. Also, vertical infiltration beneath the pond is in progress, as we see the wetting front moving downward. There is no ice beneath the pond, while there is ice beneath the slope and adjacent to the wall.

Figure 30 displays the diurnal pattern of pond filling and draining, as well as the soil ice content immediately beneath the pond and the ice layer

thickness inside the pond over time. The pond never overflows. A pattern can be observed: when the pond is dry, soil ice content starts to increase. As the pond gets filled with water, soil ice content decreases again. During the first two freeze-thaw cycle, the pond doesn't dry out completely and the soil ice content drops to zero instead of increasing again during the freezing phase. The ice in the pond itself forms only a short-lived thin layer of maximum 1.5 mm.

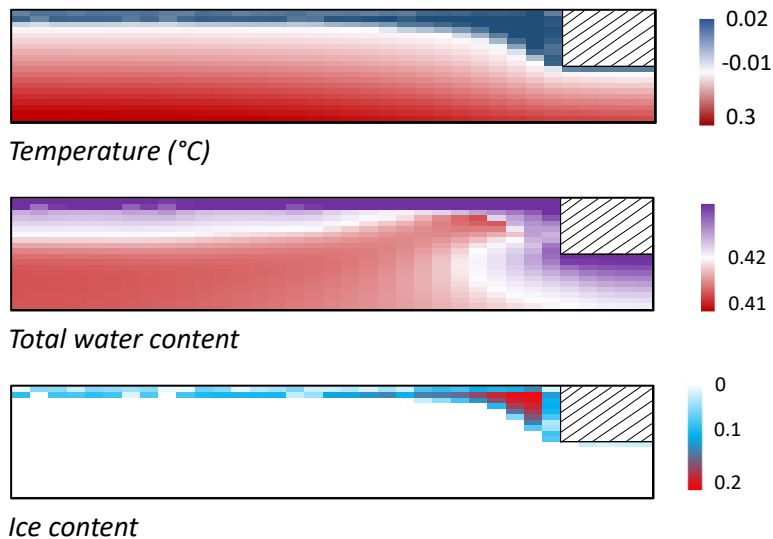


Figure 29. Temperature, total water content and ice content in the upper 22 cm of the whole 2D soil profile after 2.5 days of diurnal freeze-thaw cycles (SC17, soil 5). Notice that the colour scale is not linear.

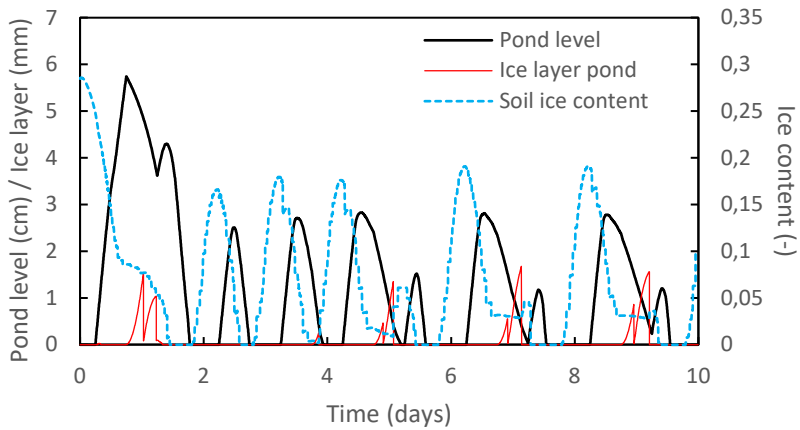


Figure 30. Water level in the micro-pond (cm), soil ice content directly beneath the pond, and ice layer thickness on the floor of the pond over time in Scenario 17, soil 6 (silt). Time 0 is the start of the diurnal freeze-thaw cycles.

#### *Reduced infiltration (SC17, soil 6)*

The micro-depression negatively affecting infiltration is demonstrated with this case. Figure 31 displays the soil conditions at the end of the freezing phase, hence with maximum ice saturation and coldest temperatures during the entire simulation. The ice saturation along the wall of the micro-depression is noticeably highest, as well as the total water content. A dry zone has formed between the top ice layer and the liquid water below. The soil is coldest adjacent to the micro-depression, and this cold extends obliquely into the soil.

There is still ice present in the soil around the micro-depression at the end of the full simulation, hence after water input (Figure 32). The ice beneath the slope melted earlier than the ice in the soil surrounding the micro-depression (Figure 33). The ice at the corner point of the micro-depression floor never melted completely.

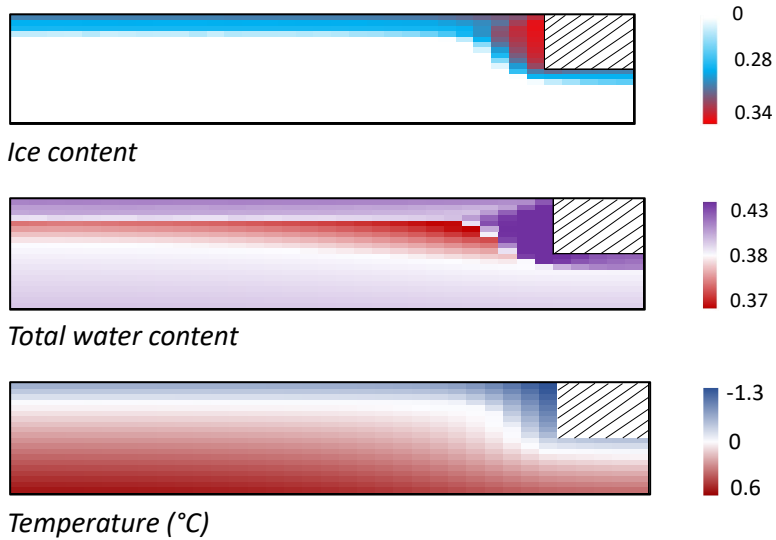


Figure 31. Temperature, total water content and ice content in the upper 22 cm of the whole 2D soil profile at the end of the freezing phase (Scenario 17, soil 6). Notice that the colour scale is not linear.

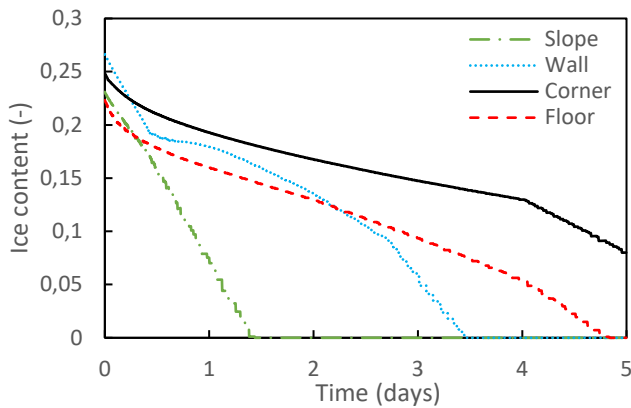


Figure 32. Ice content over time from the onset of thawing and water input to the end of the simulation, for various locations in the soil profile (Scenario 17, soil 6). Corner refers to the intersection between the wall and the floor of the micro-depression.



*Ice content*

Figure 33. Ice concentration at the end of the simulation in the whole 2D-soil profile (Scenario 17, soil 6). Black indicates ice.

### *Water input scenarios*

For the specific case of Scenario 9 soil 4, it can be seen that there is a non-linear relationship between the effect of the micro-depression on frozen soil infiltration and the water input rate (Figure 34). The strongest effect is seen at  $2\text{mmhr}^{-1}$ , whereas less or more water input decreases the importance of the micro-depression regarding infiltration, especially at high water input rates.

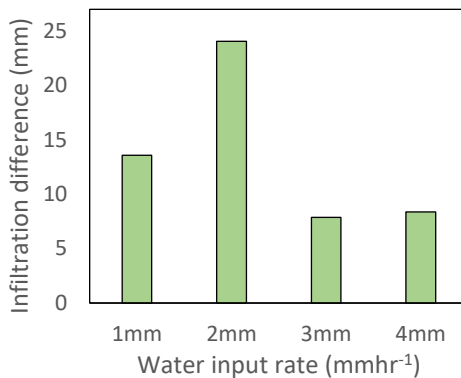


Figure 34. Infiltration difference due to the presence of the micro-depression compared to the smooth surface case for different water input rates in case Scenario 9 soil 4.

### **Macropores**

The results for the scenarios with macropores are straightforward: in all cases all water infiltrated despite frozen conditions. Only with one scenario,



when the air temperature was set to -8 °C, did not all water infiltrate; only 40% of total water input infiltrated. The difference between the ice content at the end of the simulation between the -4° C and -8 °C cases is shown in Figure 35. The ice content reached near maximum value in the upper element in the -8 °C case, while it was zero in the -4 °C case.

0.27	0.27	0.88	0.26	0.27
0.24	0.23	0.00	0.22	0.23

0.24	0.24	0.00	0.23	0.23
0.21	0.24	0.00	0.23	0.21

Figure 35. Final ice content at the end of the simulation for a macropore zone and surrounding soil matrix; upper table: -8 °C case, lower table: -4 °C case. The macropore zone is in the middle column of elements; each element is 1.1 by 1.7 cm in z- and x- directions respectively. Blue-white-red gradient applied from maximum to minimum values.

## 5.4 Discussion

The results of the synthetic simulations showed that the effect of a micro-depression is highly dependent on weather and soil textural conditions. Micro-depression effect on frozen soil infiltration ranged from a substantial increase (up to 40% of water input), to no change, to a reduction in infiltration. The reduction in infiltration occurred only in a few cases however, with the majority of cases showing no infiltration change or increased infiltration. With cyclical freeze-thaw scenarios (SC14 to SC17), the effect of increasing infiltration was overall strongest. When freezing did not occur within three days after the last moment of wetting the soil, the micro-depression was less influential because the topsoil could drain. It therefore seems key for a micro-depression to affect infiltration capacity in a landscape that the antecedent moisture level is high.

The infiltration capacity of the sandy clay loam was more often affected by the micro-depression than the silt loam and the silt, suggesting that this soil is more sensitive in its frozen soil capacity to micro-topographic effects. Most likely, the ice in the sandy clay loam more readily melts at milder air temperature due to weaker matric potential, hence an effect of the micro-

depression by changing soil thermal dynamics is more quickly reflected in changes in ice saturation. The results further suggest that only the silt soil was at hazard of an increase in flood hazard due to micro-depression presence. A possible explanation is that this soil drains poorly, thus the topsoil remains waterlogged, while cryosuction could be strong because of the fine soil texture. Consequently, the soil surrounding the the micro-depression becomes high in ice saturation when the cold front progresses both vertically and laterally into the soil. In general, we found cryosuction to be of impact, because we always observed increased total water content surrounding the micro-depression after freezing.

Furthermore, the micro-depression played a large role during moderate water input rate ( $2 \text{ mmhr}^{-1}$ ). During low or high water input rate, it had less effect on frozen soil infiltration. This is likely explained by the following. With low water input rate, frozen soil infiltration can already occur more easily without a micro-depression, while with a high water input rate the micro-depression cannot improve infiltration capacity enough to match the rainfall intensity. Next, there also needs to be positive heat transfer from the air to the soil via the micro-depression (air temperature  $> 0 \text{ }^\circ\text{C}$ ), otherwise the micro-depression has no effect. Therefore, when thawing of frozen soil cannot occur, which is the case with insulating snow cover, micro-topography likely has little effect.

To further explain the frozen soil dynamics in response to microtopography, we must first summarize its theoretical effect:

- (1) A micro-depression becomes a wetter zone in the landscape because surface runoff will accumulate there, after which it can infiltrate at a slower rate into the surrounding soil. Therefore, the following are true for a micro-depression zone:
  - a) A wetter soil will have higher ice saturation and thus lower permeability.
  - b) A wetter soil has higher heat capacity, thus cools or heats up more slowly.
  - c) A wetter soil has higher thermal conductivity, thus transfers heat or cold more rapidly.

- d) A wetter soil can have higher ice saturation, and thus larger latent heat flux, preventing lower soil temperatures during freezing. The reverse would be true during thawing.
- (2) If the micro-depression is not fully filled with water, the soil around it is more exposed to heat transfer from the air (or snow) than the soil beneath a flat surface, because heat transfer can occur in two directions instead of one. Consequently, the soil around an empty micro-depression becomes colder or warmer (depending on air (or snow) – soil temperature difference). This results in the following:
- a) The soil freezes or thaws more rapidly here.
  - b) Cryosuction will pull liquid water toward the soil around the micro-depression because it is the coldest zone in the soil profile.
- 3) If the micro-depression is filled with water, the soil beneath is insulated against freezing or thawing because the water in the pond has high heat capacity.

The results show how different energy transfer and water flow mechanisms might be predominant during different weather and soil textural conditions. We saw for example that because the micro-depression area becomes more thawed than surrounding soil, infiltration is sometimes improved along the slope in front of the micro-depression. In other cases, the water in the pond could infiltrate laterally into the soil because it had thawed while the soil beneath the bottom of the pond remained saturated with ice, owing to the insulating effect of the pond water. In yet other cases, infiltration was improved because the pond could drain vertically downward into the soil. In this case the walls were cold and frozen but the floor of the micro-depression was warmer and unfrozen, owing to the pond water insulating the soil during a diurnal freeze-thaw cycle.

In case of macroporous soil, the synthetic simulations showed that infiltration can be expected to occur uninhibited. This supports the findings of studies by e.g., Demand et al. (2019) and Watanabe and Kugisaki (2017).

Water could simply bypass the frozen soil matrix by infiltrating deep into the soil via the macropores. The macropores remain free of ice because they drain rapidly. When freezing initiates, the macropores are already desaturated. However, if the soil temperature becomes very cold, water infiltrating into the macropores freezes in-situ. In that case, the macropores become blocked with ice and infiltration is suddenly inhibited. The latter has also been found by Mohammed et al. (2021).

These simulations are performed in a highly synthetic and simplified modelling environment. The results we obtained about the effect of a single micro-depression are therefore not easily extrapolated to the landscape scale. In a landscape, boundary conditions are highly time-variant, and also include wind patterns, solar radiation and snowpack dynamics that we did not take into account. Furthermore, microtopographic geometry will be more complex than the simple structure we simulated. We did not take factors into account relating to slope angle, soil roughness, different micro-depression depths, among others. Nevertheless, by studying synthetic cases, we can reduce complexity and study basic physical principles of microtopographic and macroporous frozen soil condition.

As noted in the introduction, sometimes frozen soil is found to influence catchment hydrology, and sometimes it does not (Ala-Aho et al., 2021). The outcomes of the synthetic simulations provide part of an answer to this question: when microtopographic depressions are present, focused infiltration could sometimes occur despite frozen conditions, hence there will be no signal of frozen soil at the catchment level. Another part of the answer would be the presence of macropores, which allow infiltration to occur unimpeded despite frozen conditions, except in extreme cold scenarios. Further research could expand on our simulations and modelling approach. The results of this study could further serve as a starting point for further experimental research or serve as theoretical background for empirical studies.

## 5.5 Conclusion

The simulation results of synthetic test cases showed that micro-depressions (10 cm deep) can influence infiltration into frozen soil in a landscape. The

range of outcomes is however extremely varied, indicating that an effect of a micro-depression is highly sensitive to weather and soil textural conditions. Especially with repeated freeze-thaw cycles, the effect on improving infiltration seems to be largest. Importantly, the effect of the micro-depression is high when antecedent soil moisture level (prior to freezing) is high. A reduction in infiltration can sometimes also occur, which seemed to be dependent on soil texture. It only occurred with a silt soil type and in 3 out of 51 cases. The most frequent improvement of infiltration due to the micro-depression was seen in the sandy clay loam soil.

The micro-depression affected infiltration by changing the water and energy dynamics of the surrounding soil. In some cases, ice saturation beneath the pond was high, leading to lateral infiltration along the pond walls. In other cases, the slope adjacent to the micro-depression thawed, resulting in higher infiltration capacity there. Contrastingly, in yet other cases the walls of the pond were saturated with ice while beneath the pond the soil was ice-free and infiltration could occur vertically downward. This demonstrates the intricacies of the physics involved and the sensitivity of those physical processes to result in either colder or warmer, and thus more or less ice saturated, soil conditions. Furthermore, after freezing, total water content was highest surrounding the micro-depression, suggesting an important role played by cryosuction. The increased total water and ice saturation explains why in some rare cases, the micro-depression increased flood hazard.

Macroporous soil was found to allow for all water to infiltrate during frozen conditions, except for extreme cold scenarios. Therefore, a part of the answer as to why frozen soil sometimes does and sometimes does not affect catchment-scale water partitioning, could be the presence of microtopography and macropores. In case of rough micro-topographic terrain present under certain weather and soil conditions, focused infiltration might decrease flood hazard in a landscape. Macroporous soil can also be expected to prevent a signal of frozen soil at the catchment level. The results presented here are based on synthetic scenarios within a limited range of conditions, and should thus serve as a basis for further empirical study or improved theoretical understanding.



## 6. Cryosuction and water migration within frozen soil

*This short chapter is in current form not a draft for publication. It is included in the thesis because it gives a useful overview of cryosuction dynamics in response to various boundary conditions and soil properties.*

### 6.1 Introduction

Cryosuction is an important process that results in water redistribution in frozen soil. It can lead to substantial increases of ice content in the frozen zone, and it is the main process responsible for the phenomenon of frost heave. A frozen soil in which cryosuction causes a large upward flux of liquid water is thus both at hazard of having strongly reduced infiltration capacity, as well as losing soil structural integrity. It is therefore important to understand the context in which cryosuction can be expected to have a large influence on water transport. In this mini-chapter, the effect of cryosuction on water migration in frozen soil is studied through numerical modelling of test scenarios with a focus on different soil types and different boundary conditions.

### 6.2 Methods

The semi-empirical version of the CryoFlow model is used (see Chapter 3, and the manual in the Appendices). The model setup for the experiment of Zhou et al. (2014) is used as a “baseline” for comparative simulations: a 24 cm soil column with a top temperature of -4 °C and a bottom temperature of 3.5 °C (for details, see Chapter 3). To highlight the importance of geometry, boundary conditions and soil type, the following contrasting test scenarios were applied to the original setup:

- Bottom boundary at 100 cm versus 24 cm depth.
- Top temperature boundary at -1 °C versus -4 °C.
- Sandy soil type versus a silty soil type.

The parameters and conditions that were used for the test scenarios are summarized in Table 11. The sandy soil parameters are taken from soil properties catalogued by Carsel and Parrish (1988).

Table 11. Parameter and variable values used for different test scenarios. All simulation scenarios are repeated with the properties of a sandy soil (listed in the last column) and are performed with two different initial water contents.

Parameter/ variable	Baseline scenario	Slow Freezing (SF) scenario	Deep scenario	Sandy soil
$K_{sat}$	3e-07	3e-07	3e-07	8.25e-05
$\epsilon$	0.47	0.47	0.47	0.43
$a$	0.0011	0.0011	0.0011	0.145
$n$	2.2	2.2	2.2	2.68
$\theta_{init}$	0.16, 0.325	0.16, 0.325	0.16, 0.325	
$\theta_{res}$	0.05	0.05	0.05	0.045
$T_{init}$	3	3	3	
$T_{top}$	-4	-1	-4	
$T_{bot}$	3.5	3.5	3.5*	
$c$ (soil)	1	1	1	1
$w$	0.5	0.5	0.5	0.3 <sup>#</sup>
Soil column depth (cm)	24	24	100	

\*The bottom temperature boundary is located at 24 cm depth (not at 100 cm).

<sup>#</sup>This is an estimated value for sand. Because sand has lower matric pressures, it is expected that the freezing point of water remains closer to zero (i.e.  $w$  has a smaller value).

## 6.3 Results

The results of the test scenarios are displayed in Figure 36 and described below.

### Higher top temperature

The change in top temperature from -4 to -1°C has the following effect for the silt soil: the freezing front reaches a depth of 2 centimeters instead of 15 centimeters. Significantly less water has been drawn towards the freezing front. However, it is noticeable that with the initially dryer soil, the water content in the upper 1 cm frozen zone is higher (albeit very shallow frost). This water is to a degree still unfrozen, and as a result the ice content is not



higher. Logically, the zero-degree temperature isotherm reaches substantially less depth with the warmer top temperature.

#### Initial water content

The zero-degree isotherm reaches deeper soil when the initial water content is low. Interestingly therefore, the vertical extent of frost is larger with a drier initial state. In general however, ice saturation and the extent of cryosuction are substantial only in the case of a high initial water content.

#### Soil depth

When the impermeable layer is located at 100 cm instead of 24 cm depth, the results for total water content, liquid water content, ice content and soil temperature in the silt after 24 hours remained unchanged, except in the case of a higher initial water content (0.325 instead of 0.16). The liquid water content between the frozen zone and 24 cm depth was higher. It is observed that cryosuction was still active at this timepoint, and extended simulation time displayed a sustained but slow increase in total water content at the freezing front (not displayed).

#### Sandy soil

The simulation results for the same test scenarios but with sandy soil properties are shown in Figure 37 (with results for the silt soil included for comparison). In general, there is substantially less upward flow and lower ice content in the sandy soil compared to the silty soil. However, the vertical extent of the frozen zone is slightly larger even though the soil temperature profiles are similar. It is also notable that ice content first decreases, and then increases again with depth for the base configuration.

The deeper bottom boundary has a large effect, contrary to the case with a silt soil. There is hardly ice in the frozen zone, with rapidly decreasing ice

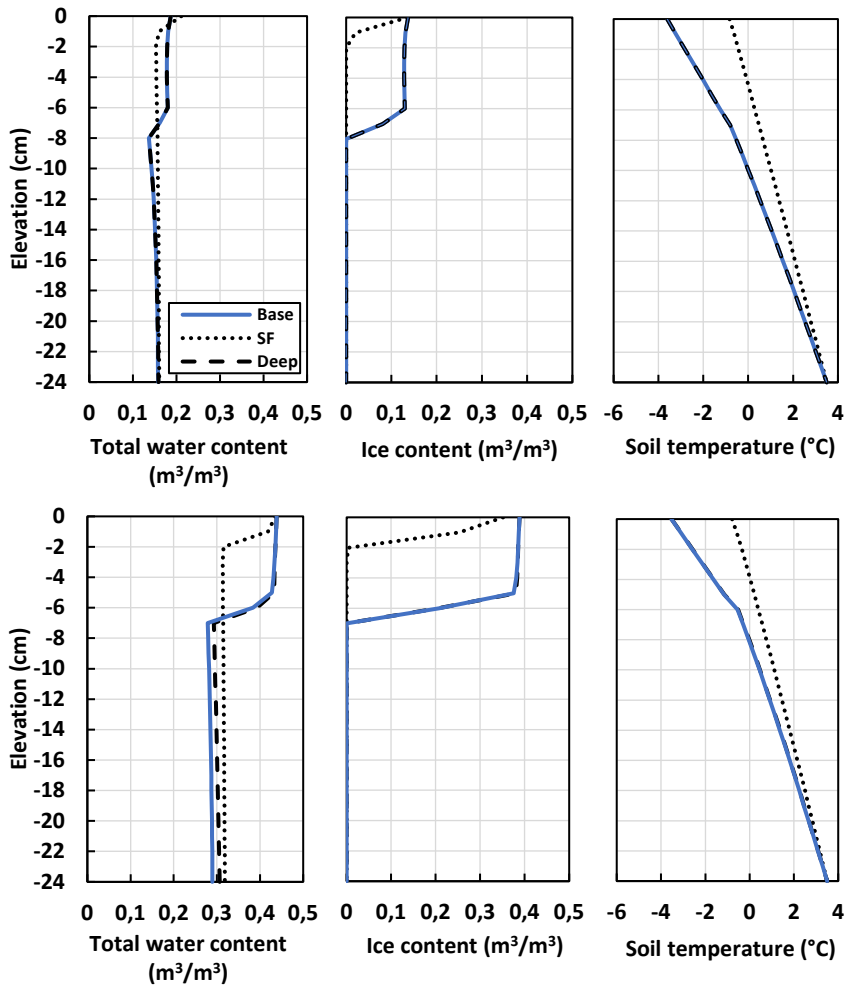


**Figure 36.** Results for three simulation scenarios applied to a silty soil. Table 11 lists the parameters and boundary conditions for each scenario. The upper graphs show the results for simulations with an initial water content of 0.16, the lower graphs for an initial water content of 0.325. 'Deep' is the scenario with a deeper bottom boundary and 'SF' is the slower freezing scenario with a warmer top temperature. 'Baseline' represents the same setup as used in the experiment by Zhou et al. Porosity of the soil is 0.47.

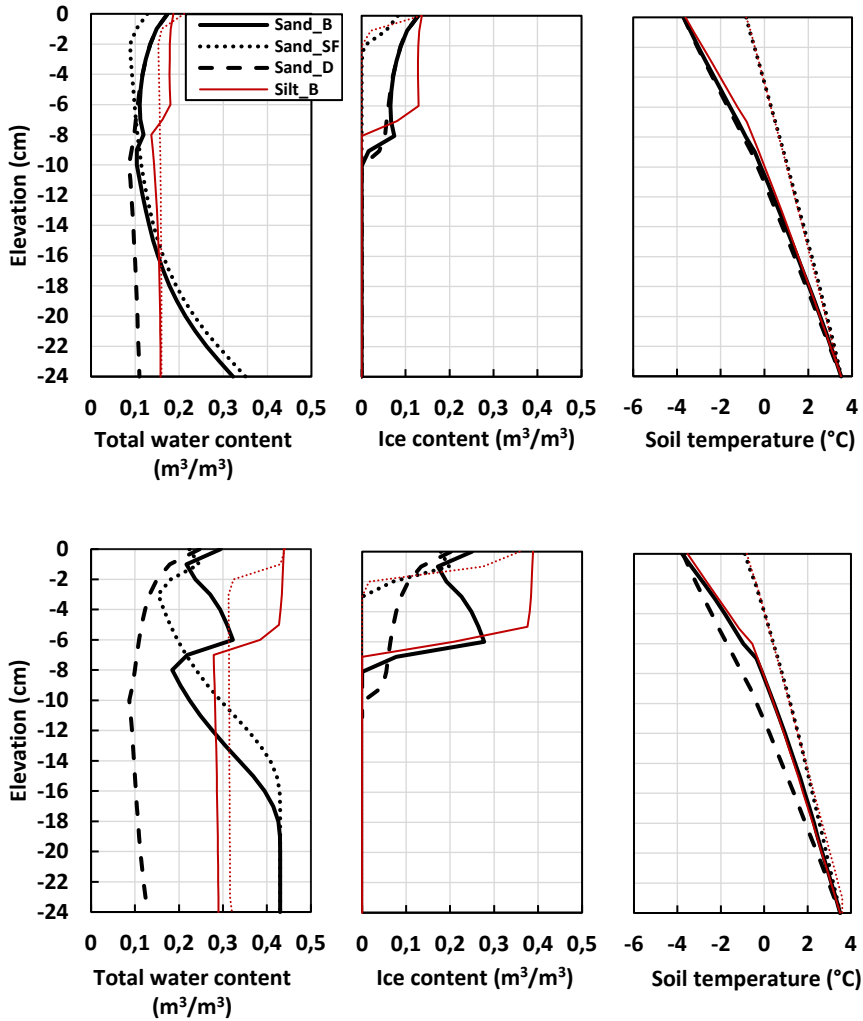


**Figure 37.** Simulation results for a sandy soil with three different scenarios. ‘Sand\_B’ stands for the baseline experimental setup (Table 11) but in this case with a sandy soil type. ‘Sand\_SF’ is the scenario with a milder freezing temperature and ‘Sand\_D’ is the scenario with a deeper bottom boundary, in both cases with a sandy soil type (Table 11). Also shown are the

'baseline' and 'SF' results for the silty soil, 'Silt\_B' and 'Silt\_SF' respectively (similar to Figure 6). Porosity of the sand is 0.43, while of the silt it is 0.47.

content with depth. The total water content drops quickly from the top downward as well. Also, the sub-zero temperature isotherm penetrates slightly deeper into the soil, leading to minor ice formation at greater depth. Furthermore, an increase of ice content near the freezing front deeper in the sand is noticeable in the colder (baseline) scenario, something that does not occur in the simulated silty soil. Another observation is that the water contents in the lower part of the shallow sand profiles (15-24 cm depth) are substantially higher compared to the silty soil, while being substantially lower at 10-24 cm depth in the deeper 100 cm sand profile.

## 6.4 Discussion

Cryosuction increases the total water content higher in the profile where freezing occurs. It slows down the freezing front as the heat capacity of the upper soil is increased and more heat is used in the phase change from water to ice. Cryosuction also decreases soil permeability by increasing the ice content of the soil.

Initial water content is of importance in determining eventual ice and water contents. Higher initial water contents are also associated with slower freezing rates given the increased heat capacity and larger latent heat flux required for phase changes. Correspondingly, cryosuction transports more water in wet soils than in dry soils. The frozen zone however reaches more depth in dry soils.

Top boundary temperature controls frost depth, upward flow and ice saturation for both the sandy and silty soils. A three-degree Celsius temperature difference (-1 to -4 °C) moves the frost line to 2 cm instead of 15 cm depth (24 hour freezing period). However, it was shown that with the silty soil and a warmer top temperature, cryosuction might be sustained for a longer time period than what was simulated, which would lead to high water contents in the frozen zone. The slower rate of freezing thus actually allows for more water to be drawn towards the freezing front because a

source of liquid water beneath the freezing front is maintained, and permeability is not too strongly diminished for water migration to occur.

Within the sand, initial soil water flows downward due to gravity before cryosuction could cause it to flow upward. Only a sand with shallow depth subjected to high freezing rate would experience significant ice saturation and cryosuction, because the liquid water is stored at such a shallow depth that cryosuction can transport it upward. This finding might be relevant to an agricultural setting, in which ploughing creates a more hydraulically permeable layer overlying compacted soil (Lundekvam, 2007), or in the case of constructed soil systems such as raingardens (Dussaillant et al., 2004) and intensive green roofs (Mentens et al., 2006),

A 'frost formation window' in a soil might be a useful concept, i.e. the time starting from the last water input (i.e., initial conditions) to the onset of freezing temperatures (i.e., boundary conditions) until snow cover insulates the soil. Two directionally opposite processes occur during this time window, namely gravitational and capillary downward flow versus cryosuction-induced upward flow. In practice this means that the days after the last rainfall event until a significant snow cover develops strongly influence eventual soil ice content, which will eventually affect infiltration capacity during the snow melt period. The simulation analyses show that several factors affect this 'conflict' between upward and downward flow, such as the depth of liquid water availability. These reflections and results are important, because an increase in cryosuction will increase flood hazard through reduction of storage space for infiltrating water and a reduction in infiltration capacity due to increased ice content (decreased permeability).

## 7. Snowmelt erosion and flooding in a small agricultural catchment

*This chapter is based on the published paper “Groundwater seepage causes surface runoff and erosion during snowmelt in a tile-drained agricultural catchment: field observations and modelling analysis” by J.C. Stuurop, S.E.A.T.M. van der Zee, T.K. Thijs and H.K. French in CATENA volume 220A, 2023.*

### 7.1 Introduction

The hydrology of cold climate regions is significantly impacted by snowfall. When the snow that built up during Winter melts in Spring, a large amount of liquid water is released into the environment. Most of this water either infiltrates into the subsurface or becomes surface runoff (Rango and DeWalle, 2008). The soil is potentially still frozen during the snow melting period, which could impede infiltration. Due to the large flux of melt water, the hazard of erosion of fertile soil is high (McCool, 2020). Furthermore, stream levels often rise rapidly leading to a hazard of flooding (Kundzewicz et al., 2010). Nutrient loss during the snowmelt period in agricultural environments is also high (Deelstra et al., 2009), as well as leaching of contaminants, resulting in a degradation of stream and lake water quality (Fučík et al., 2011). The snowmelt event therefore poses a hydrological challenge for society and agricultural environments in particular.

Numerous studies have been performed on snowmelt mechanisms with a focus on snowmelt-runoff models and streamflow forecasting in mountainous catchments. Low-lying agricultural areas in more temperate zones with shallow snow cover have received somewhat less attention (Starkloff, 2017). Insights from studies in high mountain catchments are not easily translated to low-lying agricultural settings because in cultivated areas the topography is less steep, the catchment scale is often smaller, the weather conditions are milder and manmade interventions are substantial

(e.g., ploughing, tile drainage and crop growth). At the same time, cultivated areas in cold-climate countries are often considered vital by national governments, such as in Norway, since arable land in those regions is scarce (Flaten, 2001).

Existing studies in low-lying agricultural areas have demonstrated the significant impact of snowmelt on erosion. For example, Lundekvam et al. (1998) concluded that snowmelt-induced erosion can lead to considerable soil loss in southern Norway. They identified the effect of tillage methods and the timing of tillage, noting that a high hazard of erosion was associated with autumn ploughing. According to their study, leaving plant residue over the winter provided the best protection against soil loss. Deelstra et al. (2009) showed that large losses of nitrogen and phosphorus from agricultural soils to streams occur in Nordic agricultural catchments at the end of winter. Comparable effects of snowmelt on erosion and water quality have been found across the world in cold-climate and relatively low-lying agricultural areas such as in Russia (Yakutina et al., 2015; Maltsev and Yermolaev, 2020), the United States (Hoffman et al., 2019), Germany (Ollesch et al., 2006), Scotland (Wade and Kirkbride, 1998), Poland (Rodzik et al., 2009), Canada (Su et al., 2011) and northeast China (Tang et al., 2021).

Frozen soil is a factor sometimes recognized as enhancing soil erosion due to snowmelt (Banaszuk et al., 2013). In addition, rain on snow is mentioned to increase overland flow and erosion hazard (Zuzel et al., 1982). Specific to the agricultural setting, tile drainage has been found to lead to rapid loss of nutrients and contaminants to streams even though it seems to decrease overland flow and erosion (Banaszuk et al., 2013). Melt water reaching the stream via drainage pipes bypasses possible buffer strips and vegetation traps that could have otherwise filtered out nutrients and pollutants. Furthermore, rill and ephemeral gully erosion are mentioned as the most frequent type of erosion due to snowmelt, because during large water influx events sheet erosion is often limited (Øygarden, 2001; Tang et al., 2021). The rills and ephemeral gullies created during snowmelt are usually removed by farmers when spring tillage starts (Øygarden, 2001).

Apart from important insights mentioned above, it is difficult to further synthesize snowmelt erosion studies because of differences between study sites such as topography, soil type, agricultural practices and weather conditions. Furthermore, annual variations in snowmelt intensity and corresponding erosion are large, owing to differences in snow depth, rainfall, melt rate and frozen soil occurrence. Øygarden (2001) noted that soil erosion events have certain multiyear recurrence intervals, making it difficult to consistently do research on major snowmelt-induced erosion. Also, many studies observed the end-result effects of snowmelt erosion such as soil loss volumes, stream sediment discharge and water quality indicators. While providing valuable information on snowmelt erosion hazard, it does not provide direct insight into the in-situ snowmelt erosion process related to water partitioning in the landscape (i.e., infiltration, overland flow and subsurface flow). Especially what happens to the meltwater in the subsurface warrants further study.

In this paper, a particular snowmelt period is documented in which subsurface flow played a critical role concerning the fate of melt water in the landscape. The study area is a tile-drained agricultural catchment in southern Norway where field and UAV-based observations were made during the snowmelt period. The aim of this paper is to shed light on the various ways soil erosion can be triggered during wintertime hydrological conditions. This is done through a combination of observations and modelling, and through comparison with prior erosion studies in the catchment (Starkloff, 2017; Starkloff et al., 2018). Specifically, this paper addresses the potentially large role of groundwater seepage in surface and subsurface erosion.

Groundwater modelling with MODFLOW was performed to help understand the cause of seepage during snowmelt. The model provided useful information on the influence of several variables such as the spatial snow melt pattern (i.e., spatially varying recharge), melt and rainfall rates (recharge rate), and hydrological soil properties on seepage volumes and its spatial distribution. The second aim of this paper is therefore to identify environmental controls on groundwater seepage during snowmelt.



## 7.2 Methods

### Study area

The study area is situated in southern Norway in the Skuterud catchment (4.5 km<sup>2</sup>; 59.67°N, 10.83°E; Figure 38). The catchment consists of approximately 60% agriculture with cereal production (wheat, barley, and rye), followed by 33% pine forest and 7% urban area (Kværnø et al., 2007). A sub-catchment called Gryteland (0.29 km<sup>2</sup>) is the focus area of this study. The elevation of Gryteland is between 106 and 141 meters above sea level with numerous gentle slopes (max. 15%). Part of the agricultural area is tile-drained, but the exact drainage lay-out is not documented.

The arable land of Skuterud consists of marine sediments in the textural range of clay loam and silty clay loam. Isostatic uplift after the last glacial period caused these sediments to rise above sea level (Sauer et al., 2009). On the fringes of the agricultural plots and in the surrounding forests, sandy shore deposits are found. Several undeveloped gullies exist in the marine sediments in the form of connected shallow depressions in the landscape. These undeveloped gullies are clearly visible on a digital terrain model of the subcatchment (Figure 39). These “semi-gullies” are part of the land cultivated by the farmer.

Mean annual temperature in the area is 5.3 °C and mean annual precipitation is 785 mm (Thue-Hansen and Grimenes, 2015). The snow melt events studied in this paper occurred in the months February and March in 2019.

### Unmanned Aerial Vehicle (UAV) photography

Aerial photos of the subcatchment Gryteland were frequently made during the snowmelt period with an Unmanned Aerial Vehicle (UAV), model Parrot Anafi, which carried a 21-megapixel 1/2.4-inch CMOS sensor camera. Flights were planned with the Pix4Dcapture flight planner Android application and nadir photos were set to have an overlap of 80 to 85% depending on the amount of direct sunlight present. Flight altitude

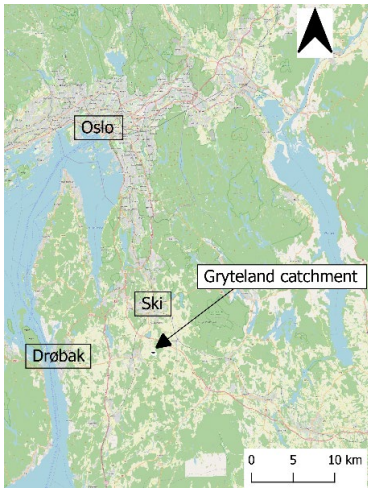


Figure 38. Location of Gryteland catchment in southern Norway. Source: Open Street Map.

was set to 65 meters resulting in a ground sampling distance of 2.17 cm per pixel. The software Pix4Dmapper was used to create an orthomosaic and digital terrain model (DTM) from the images. Ground control points (GCPs) were manually added and tied to recognizable points in the images, which were corners of houses and the midpoint of a manhole. The coordinates of these GCPs, as well as their elevations, were determined with the publicly available terrain map of Norway at [norgeskart.no](http://norgeskart.no) from Kartverket.

The resulting orthomosaics and DTMs were visualized with QGIS software. The flights were performed on an almost daily basis, depending on weather conditions. The rasterized DTM elevations of the snow-covered catchment of different dates were subtracted from each other to get an indication of the spatial snow ablation pattern, to be used later as a proxy for spatially distributed recharge in the groundwater model. To achieve correct subtraction of the DTMs, manual snow depth measurements were compared to specific points on the DTMs. Subsequently, the snow depth map was calibrated through subtraction or addition based on the difference between the DTM and ground measurements. Visual cues on the orthomosaic, mainly snow cover disappearance, were further used as a confirmation of snow melt pattern in the DTMs. The orthomosaics were also used to identify overland flow.

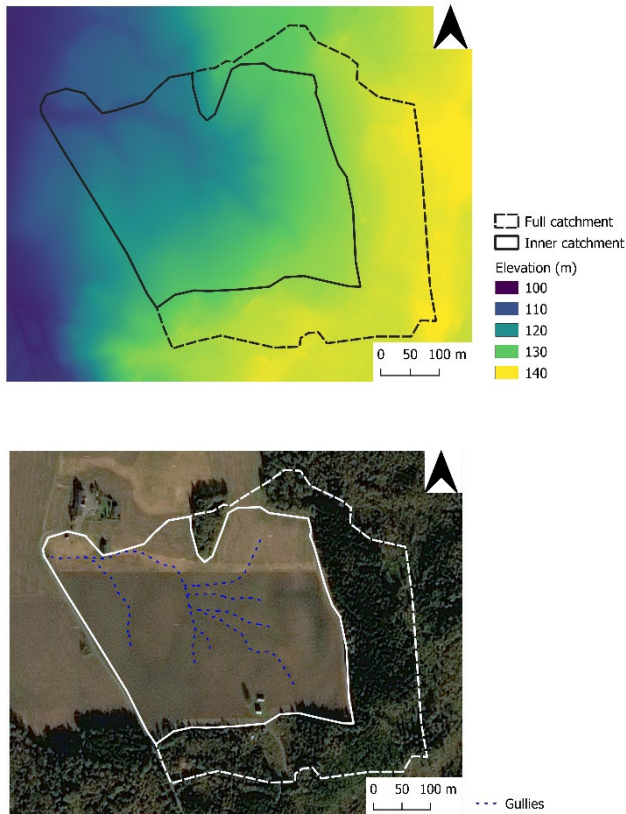


Figure 39. Digital elevation model (upper; kartverket.no) and satellite image of the Gryteland subcatchment (lower; Yandex Maps, 2007). The undeveloped gullies are visible as connected shallow depressions in the landscape. The inner catchment excludes the forested areas from which water is led away from the agricultural area via ditches and drainpipes.

### Manual snow measurements

Manual measurements of snow density, snow water equivalent (SWE) and snow depth were performed with a snow core sampler and measuring stick along a fixed trajectory. The trajectory was chosen to encompass a variety of slopes and depressions in the central area of the Gryteland subcatchment. A second trajectory was later established (19 February) to incorporate

sampling of forest effects at the southern edge (later shown in Figure 48). Furthermore, local observations were made of surface runoff and erosion.

### Monitoring stations

At the northwestern edge of the Gryteland subcatchment, a flume with water level sensor has been installed to measure discharge ( $\text{m}^3\text{s}^{-1}$ ) from surface runoff that accumulates in the semi-gully system. A water level sensor is also present in the main drainpipe that leads the water from all drainage pipes in Gryteland toward the stream of Skuterud. Air temperature was also recorded at the station. The discharge ( $\text{m}^3\text{s}^{-1}$ ) from the stream of Skuterud was recorded before it enters lake Østensjøvannet in the north. The weather station of the Norwegian University of Life Sciences (NMBU) was used to get information on solar radiation, soil temperature and precipitation. It is located approximately 3 kilometres southeast of Gryteland. Soil temperature is measured at 2, 5, 10, 20, 50 and 100 cm depth. Because of similarities in snow depth, soil type and weather circumstances at the two locations, we assume the soil temperatures measured at the weather station give a good indication of soil temperature in Gryteland.

### Prior snowmelt erosion studies

During the winters of 2013, 2014 and 2015 snowmelt erosion studies were undertaken in the Gryteland subcatchment. The results of these can be found in Starkloff (2017). The same environmental variables were measured during those winters as with this study, but without frequent UAV-based observations. The results of this study will be compared to the data collected during those three winters to assess why in certain circumstances we did or did not observe erosion.

In the winter of 2015, the hypothesis was that frozen soil had a significant impact on infiltration and surface runoff generation (Starkloff, 2017). To test this specific hypothesis, we employed the 1-dimensional water and heat transport model with freezing for the unsaturated zone by Stuurop et al. (2021). We used the measured soil temperature, water content, soil properties and rainfall rates of Starkloff (2017) as input for the model. We also included a scenario in which the same variables were used but with a positive soil temperature throughout the simulation in order to compare the

frozen circumstances to the unfrozen scenario. The results of these simulations would either demonstrate an effect or no effect of the 2015 winter temperature conditions on infiltration.

### Simulating groundwater flow

The groundwater model MODFLOW (version 2005) was used for the simulations of snowmelt recharge and saturated subsurface flow. The model setup was based on the Gryteland subcatchment, but with the forested part excluded, from here referred to as the “inner catchment” (Figure 39). Ditches exist along the entire forest edge which collect ground- and surface water coming from the forest. The ditches lead the water away from the agricultural land and toward a manhole connected to the drainage system.

The elevation raster data from the DEM of the Norwegian Mapping authorities (Kartverket) (1 meter resolution) was used for the surface elevation of the model. Although bedrock is exposed in the outer parts of the catchment, the depth to bedrock in the inner catchment is unknown; the same is the case for the depth of soil layers. We chose an arbitrary value of 10 meters depth below the surface for the impermeable bottom boundary of the model to allow for sufficient space for a groundwater table to form. To simplify the overall soil type pattern in the horizontal direction, we employed a gradually decreasing saturated hydraulic conductivity in the model with increasing distance from the forested areas in the east/southeast (Appendix, Figure A) roughly based on the presumed distribution of sediments (Figure 40). We disregarded changes in soil properties in the vertical direction and assumed gradual transitions of sediments due to decades of agricultural tillage.

Not exactly known was the spatial coverage of the drainage pipes. We assumed that the area that displays significant subsurface seepage at the surface level does not contain an effective drainage system (broken, blocked or absent), because the drainage pipes would otherwise have prevented the rise in water table toward the surface. This assumption resulted in a spatial drainage system that covered the western half of the catchment (Appendix, Figure A). The drained area was given a drain boundary condition located at a depth of 1 meter below the surface (the ploughing depth was about 25

cm); in practice, the water table in this area can thus not rise toward the surface. In the rest of the simulated catchment, any water that would make the water table rise above the surface is immediately removed and counted as seepage.

Prior to the snowmelt period, we performed a steady-state simulation with recharge to the groundwater at 30% of annual precipitation to obtain an initial water table for the snowmelt simulations. For the snow melt period, the recharge was based on snow melt measurements and included spatial variation; we assumed all water recharged the groundwater, since infiltration excess overland flow was not observed. Given the number of estimates and simplifications used in the model, we do not assume the model setup to be an exact simulation of Gryteland but rather a relevant analogy as a partly drained groundwater system with a similar soil property distribution.

In addition to the simulation based on the setup mentioned, we included several scenarios in which we varied catchment properties. This helped to understand if and how certain variables influenced the groundwater seepage pattern. The scenarios considered are spatially homogeneous versus spatially heterogeneous hydraulic conductivity distribution, spatially heterogeneous versus spatially homogeneous snow depth and melt rate, and no tile drainage versus tile drainage. We also included a rainfall event of 56 mm for 3 days to compare the snowmelt results with a substantial rainfall event. The detailed setups of the scenarios simulated are summarized in Table 12.

Finally, we also simulated the recharge during the winters of 2013, 2014, and 2015 for which the data can be found in Starkloff (2017). Because only snow depth changes were documented in those prior winters, we calculated the meltwater loss based on an estimated snow water content of 20%. The goal was to assess whether the simulations would agree with the 2013, 2014 and 2015 observations that no groundwater seepage would occur under those winter circumstances.

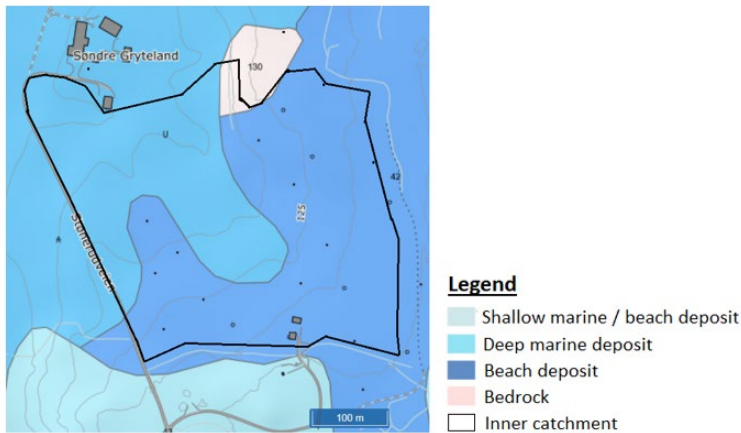


Figure 40. Sediment map from the Geological Survey of Norway.

Table 12. Additional scenarios simulated to study the influence of several variables on groundwater seepage. The base simulation (not a scenario) covers the 2019 winter conditions with spatially varying recharge and spatially varying hydraulic conductivity.

Scenario	Configuration
Homogeneously distributed sandy loam	One K-value for the entire area, set to $1.23e-05 \text{ ms}^{-1}$
Homogeneously distributed loam	One K-value for the entire area, set to $3.63e-06 \text{ ms}^{-1}$
Homogeneously distributed silty clay loam	One K-value for the entire area, set to $1.94e-07 \text{ ms}^{-1}$
Homogeneously distributed snowmelt recharge	No recharge multiplier used for different areas
No drainage	The drain boundary condition is removed
Rainfall	Instead of snowmelt, there is 3 days of water input equal to 56 mm of rain
2013-2014-2015 winters	Adjusted the water input according to data from Starkloff (2017).

## 7.3 Results

### Snow depth distribution

The maximum snow depth during the 2018-2019 winter was observed on 08 February. Figure 41 displays the snow depth map, including the calculated SWE based on snow density measurements in the field along the main snow course. An uneven distribution of snow cover depth can be observed on the snow depth map. We grouped the different snow depths into three regions. The snow depth distribution has implications for shallow groundwater recharge. Based on local snow density measurements, it is estimated that the full range of total water storage in the snowpack locally varied from 70 to 120 mm.

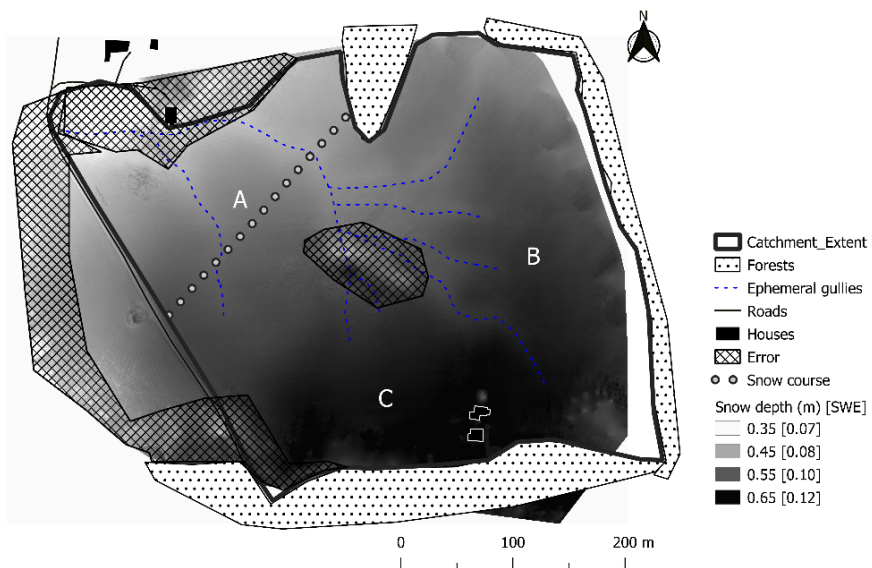


Figure 41. Snow depth distribution in the Gryteland sub-catchment at February 08, based on UAV-derived elevation data and local manual measurements.



### Weather and snow melting conditions

The air temperature during the snow melt period (2019) is given in Figure 42, together with the soil temperature at the weather station (2 cm depth). It is observed that the soil was not significantly frozen as the temperature remained approximately 0 °C at the soil – snow interface during the melting season. Therefore, we deemed it unlikely that substantial ice saturation affected the infiltration of melt- and rainwater. The soil temperature started to rise again when the snow cover fully disappeared on the March 22.

We distinguished six different snow melt periods (Table 13). The manual snow depth measurements, together with daily rainfall totals and snowmelt totals, are given in Figure 42. The full melting period lasted from February 08 to March 22 for the largest part of the catchment; some areas had longer lasting snow cover. The first snow cover already disappeared on the 27<sup>th</sup> of February. A cold weather spell followed that brought new snow cover of approximately 15 cm depth, which was uniformly distributed over the catchment. The melting of this second snow cover started on the 19<sup>th</sup> of March and lasted 3 days. From the first snow cover, an estimated total of approximately 105 mm of water was released, while from the second snow cover only about 36 mm was released. There was intermittent rainfall, with high intensity rainfall occurring early in the snow melt period between February 08 and 10. Another notable rain-on-snow event occurred on March 17, but it was followed by snowfall the same night.

A complicating factor was rain on snow, as part of the rain is absorbed by the snow. This increases the density and therefore SWE of the snow and leads to a double count of water input to the soil, since part of the rainfall became later snowmelt; therefore, the total water input in our simulations is overestimated.

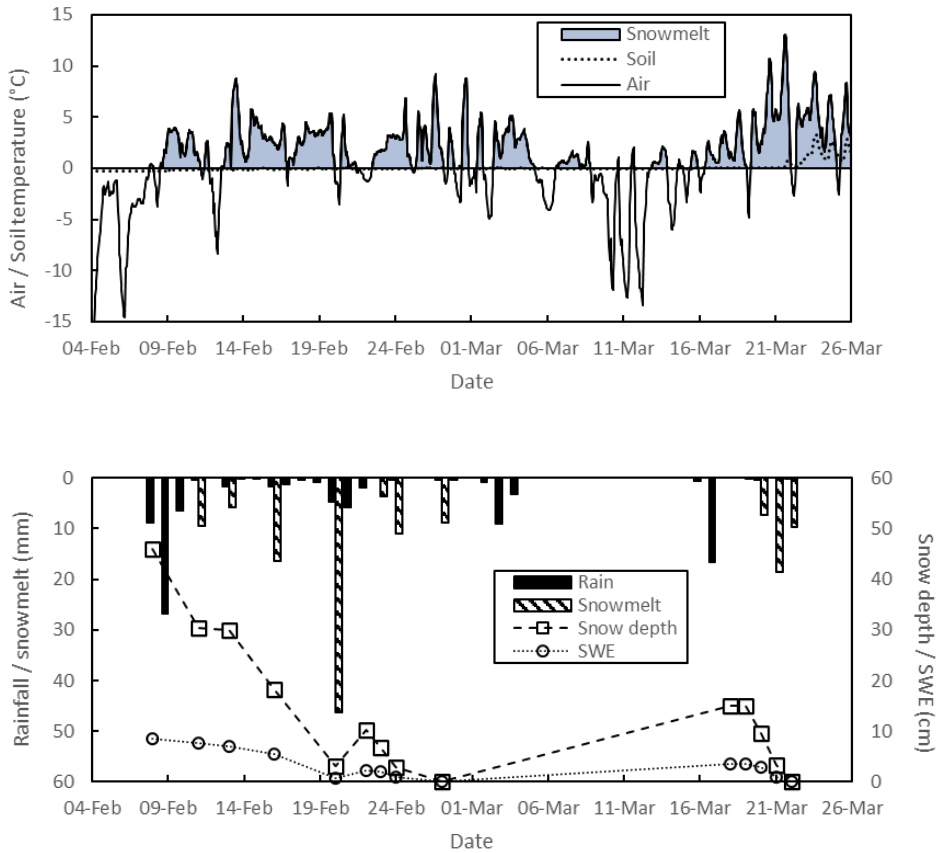


Figure 42. Upper graph: air temperature and soil temperature measurements (2 cm depth) during February and March (2019). The blue area indicates positive air temperature and thus potential snowmelt. Lower graph: rainfall and snowmelt, manual snow depth and manual SWE measurements. Rainfall is given as mm per day, while snowmelt is the cumulative snowmelt (mm) between measurement points.

Table 13. Different snowmelt events distinguished based on weather observations and snow measurements. For each period the average air temperature, solar radiation, total rainfall and total snowmelt is given.

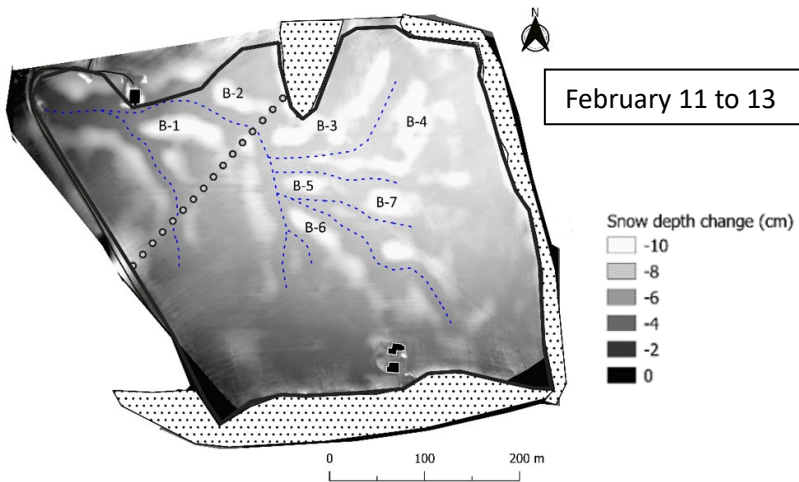
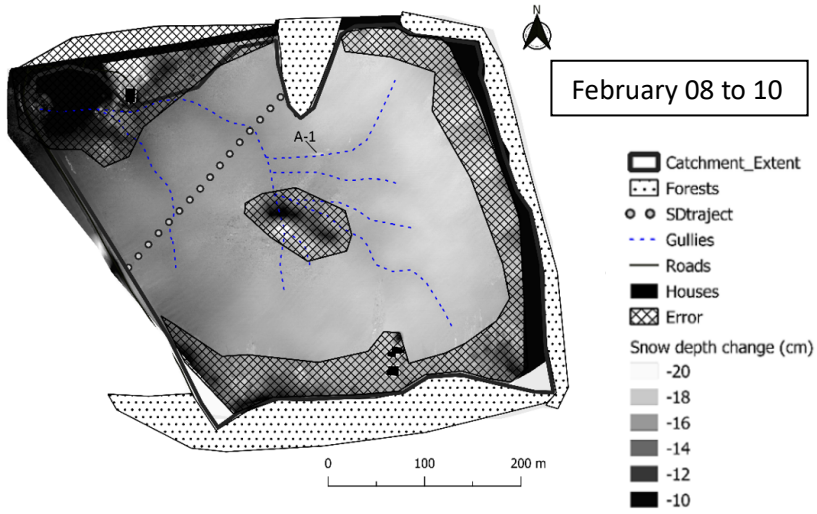
Snowmelt period	Average Air temperature (°C)	Solar radiation (Wm <sup>-2</sup> )	Rainfall (mm)	Snowmelt (mm)
08 – 10 February	2.0	99.4	39.5	9.4
11 – 13 February	4.1	135.4	3.8	5.7
14 – 16 February	3.3	100.3	1.5	16.4
17 – 20 February	3.3	102.9	2.4	46.2
22 – 27 February	2.4	117.0	1.8	23.6
19 – 22 March	5.8	264.0	0.3	35.7

### Spatial snowmelt pattern

The snow depth change maps were created from the UAV photographs for the snowmelt between February 08 and 10, February 11 and 13, and February 08 and 19. For other UAV-mapping dates, the photogrammetric procedure failed due to insufficient contrast in the images. Previous studies suggest that direct solar radiation is necessary to be able to make good quality photogrammetric reconstruction of snow-covered surfaces (Chiba and Thiis, 2016). We consider these maps as an indication of the melt pattern, rather than accurate values of snowmelt. Snow depth change does not equate to snowmelt, as snow metamorphism also leads to snow depth reduction. Nevertheless, measurements along the snow course, as well as observations of visual snow cover changes from the orthomosaics, provide confidence in the relative distribution of snow melt rates derived from the UAV-based DTMs (Figure 43 and 41).

The snow ablation pattern was fairly homogeneously distributed for the February 08 to 10 melt event (Figure 43). A notable feature in the February 08 to 10 map is marked as "A-1", as all snow cover disappeared here. This is a spring that became active during snow melt, releasing warm groundwater (measured to be 2.6 °C) which melted the snow locally. The melt pattern for February 11 to 13 and 08 to 19 was different. Numerous areas with higher snow ablation are visible, marked with a letter and number combination (Figure 43). These higher snow ablation areas correspond to slopes across the catchment which are predominantly southern to western facing. The southern and south-eastern parts of the catchment experienced slower melt, likely because they were in the shade of surrounding forest. Observed melt patterns are confirmed by orthomosaics of the catchment (Figure 44). In addition, three springs could be identified on the orthomosaic from which groundwater exfiltrated.

The combination of spatial maximum snow depth differences as well as spatial differences in snow melt rate imply that different parts of the catchment received different water fluxes. While rainfall is usually homogeneously distributed over an area without forest canopy, in case of snowmelt the pattern is heterogeneous. In this case, the faster melt rate and deeper snow cover for a large part occurred in the area with coarser soil.



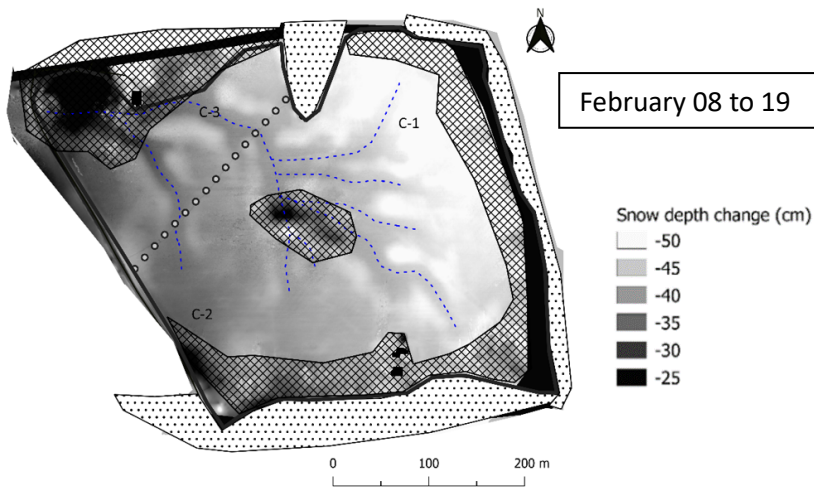


Figure 43. Snow depth change maps for different snow melting periods. A letter and number combination in the map indicates a noticeable feature, an area with increased or decreased snowmelt rate, that could be seen in the orthomosaics in Figure 44.

### Surface runoff and erosion

A total of five springs were detected in the catchment. These are marked on the orthomosaic in Figure 45 and photographs of several springs are shown in the Appendix. Spring A entailed an area, not a single source, with water exfiltrating from the subsurface. It is located along a knickpoint in topography combined with a change in soil texture from coarse to fine (Figure 40). At springs B and E water came from cavities in the ground (width between 10-30 cm, depth > 40 cm). These holes indicated subsurface erosion in the form of soil piping. Several similar holes were observed in the larger Skuterud catchment. Spring C was an area of seepage on a slope face, while Spring D was a small cavity (5 cm width).

All surface runoff observed in the field and on the UAV-photographs originated from the springs. The surface runoff flowed toward the semi-gully system and exited the sub-catchment via the flume outlet. Measured discharge at the flume, as well as from the main drainpipe, is given in Figure 46. Major surface runoff was observed only on the 21<sup>st</sup> of March when there

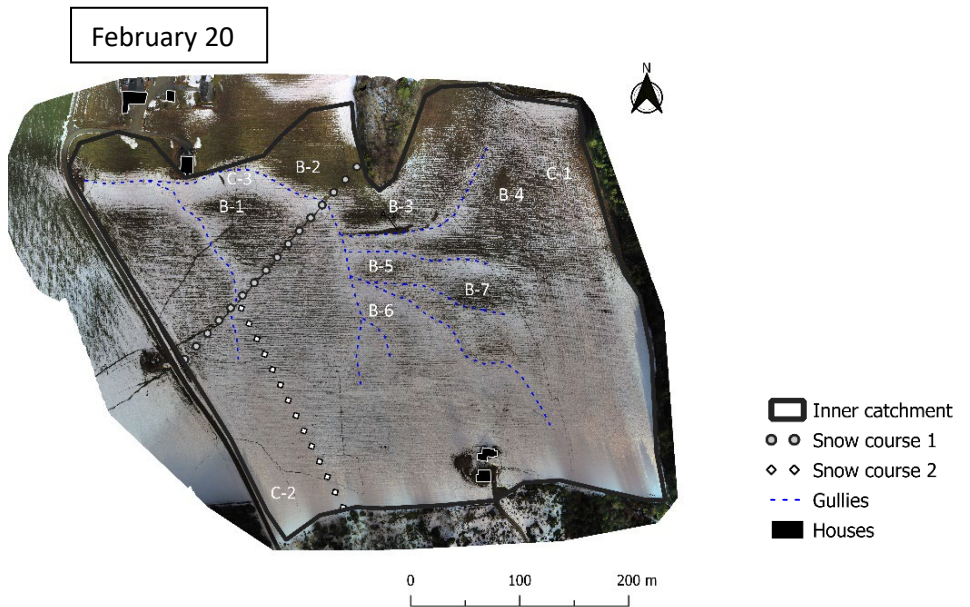
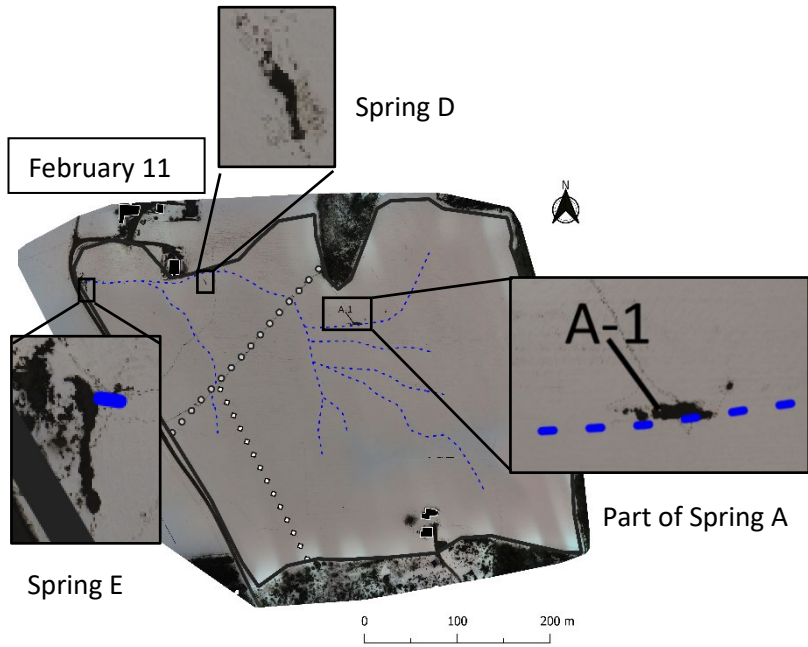


Figure 44. Orthomosaics of the Gryteland catchment for two different dates constructed with the UAV-photographs.

was visible streamflow in the gullies (Figure 45). This is confirmed by the flume discharge peak that day. On the 21<sup>st</sup> of March, a large area of spring A became active and was noted as the major source of surface water. Prior snowmelt events did not cause significant observable surface runoff, whereas the drainpipe did carry substantial amounts of water during prior snowmelt events (Figure 46).

Similar large-scale seepage during rainfall has not been observed or recorded in the sub-catchment in prior studies. In this study, the amount of water released into the catchment during the snow melt season equalled approximately 25% of the average annual precipitation. The surface runoff due to groundwater seepage in Gryteland did not affect the streamflow in Skuterud noticeably (Figure 47). The discharge pattern of the stream correlated well with the discharge of the drainpipe, suggesting that the streamflow is dictated by tile drainage rather than exfiltrated groundwater.

After the 21<sup>st</sup> of March, significant erosion marks could be observed downhill from the springs. An example of such erosion near spring A is shown in Figure 48. Several rills and gullies had formed in this region with a braided pattern. The rills and gullies were between 10 to 50 cm wide and several cm deep with many smaller rills higher up in the catchment.

### Comparison with prior snowmelt erosion studies in Gryteland

The current winter documented in this study was different from the winters between 2013 and 2015 for various variables (Table 14). Snow cover was deeper in 2019, providing a larger water input compared to the prior study periods. Combined with the amount of rainfall that occurred during the melt season, the total water input was 186 mm in 2019 compared to 97, 135, 78 mm for 2013, 2014, 2015 respectively. Also, the total melting period in 2019 was temporally more spread out with a total of 21 days compared to 8, 7, 4 days in 2013, 2014, 2015 respectively.

Only in the current study winter (2019) and in 2015 was substantial soil erosion observed, but with different causes attributed to it. In 2015, the



cause of erosion was thought to be a total of 28 mm of rain on snow-free

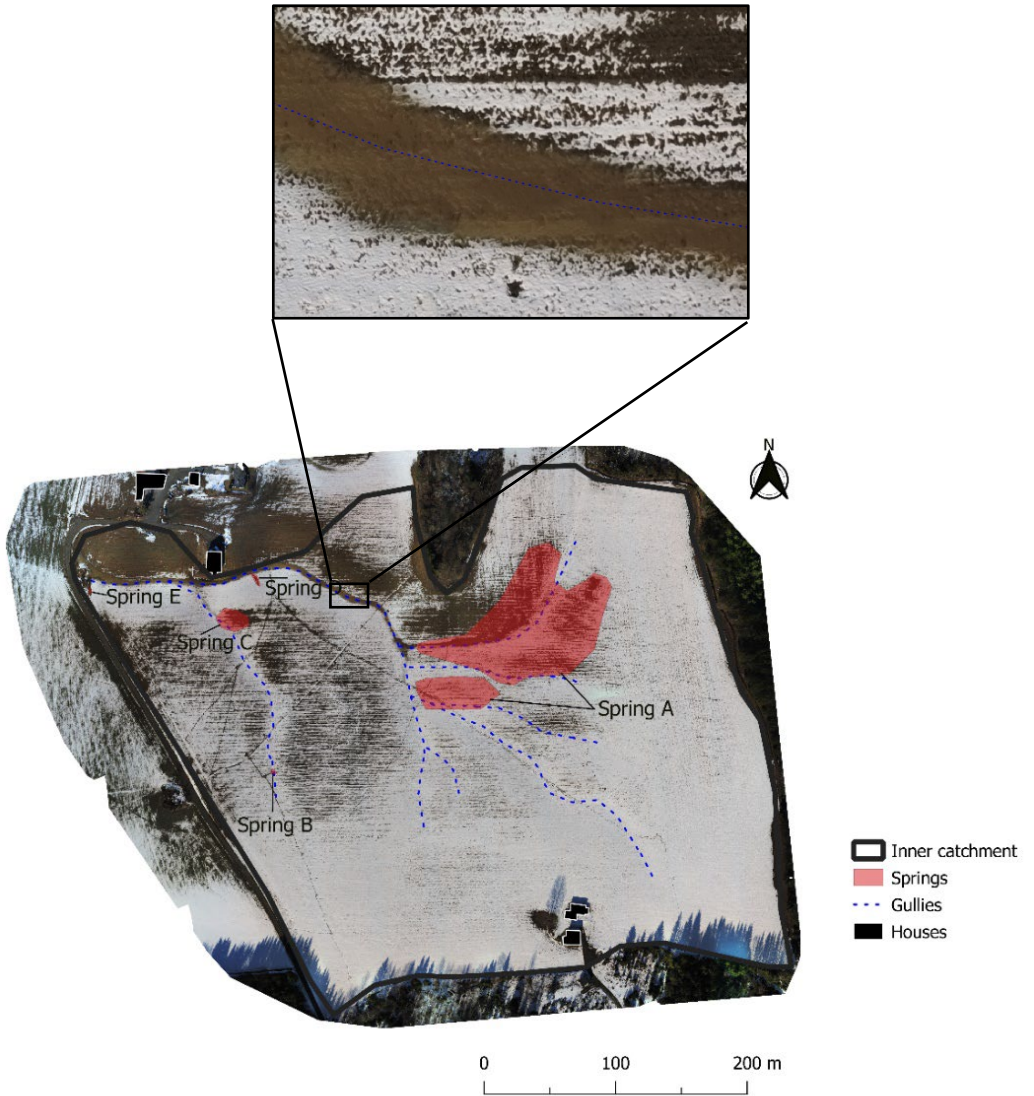


Figure 45. Orthomosaic of Gryteland capturing the seepage event on March 21. Areas with active seepage are marked in red.

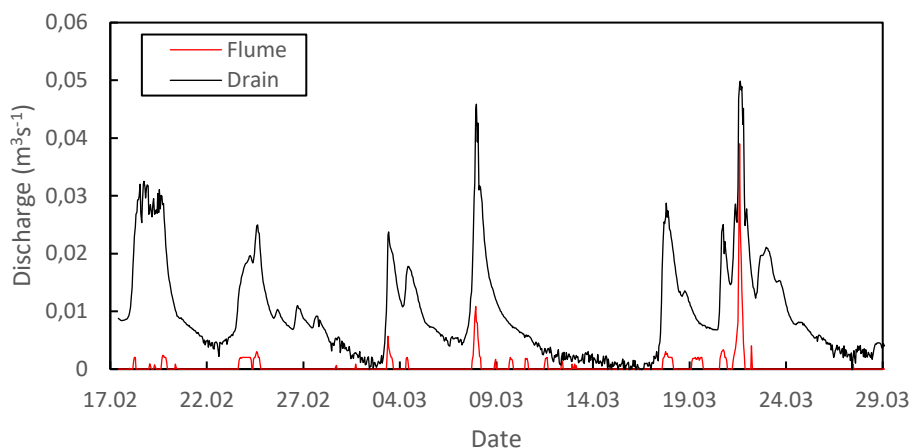


Figure 46. Discharge measurements in the flume (surface runoff) and main drainpipe of Gryteland. Since the surface runoff is mainly due to groundwater seepage, it can be considered a measurement of volumetric groundwater seepage rate.

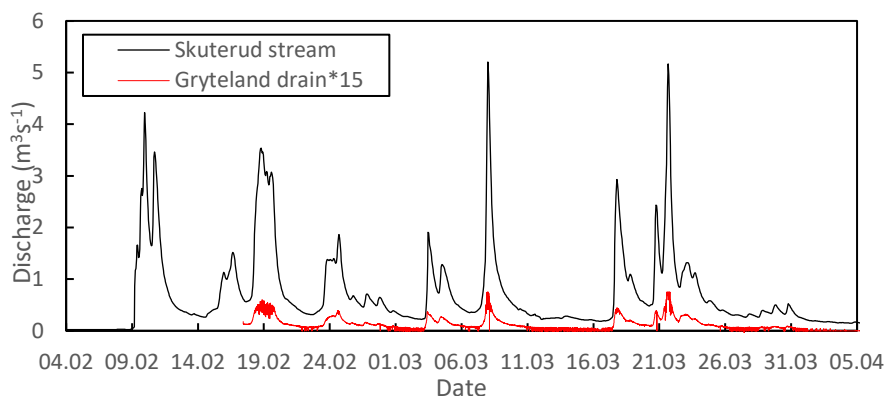


Figure 47. Discharge measurements of the larger stream in the full catchment (Skuterud) compared with the discharge (multiplied by 15) of the main drainpipe in the Gryteland subcatchment for the study period in 2019. Data: Agricultural Environmental Monitoring Programme (JOVA), Norway.



Figure 48. Erosion marks in the landscape photographed by the UAV. The gullies to the left are approximately 20 cm wide, while the larger gully on the right is approximately 50 cm wide.

frozen soil that did not infiltrate well (Starkloff, 2018). The erosion occurred in the main depressions in the landscape due to overland flow accumulating there. In the current study winter, the cause was groundwater seepage and no in-situ infiltration excess overland flow was observed. The erosion gullies also had a more braided pattern in 2019, leading to a broader surface area being affected (ca. 4.2 meters width in the depressions). In 2015, the gullies were deep but narrow; the width of erosion in the depressions was about 40 cm (Figure 49; Starkloff, 2017). Furthermore, the soil was not frozen in 2019 compared to 2015.

The modelling results for the unsaturated zone, based on the 2015 frozen soil situation, are shown in Table 15. The hypothesis that frozen soil caused significant surface runoff during that winter is not rejected. A similar amount of total discharge is predicted by the model compared to measured discharge at the flume. During unfrozen conditions, the model predicted that all 28 mm rainwater in 2015 would have infiltrated.

### Modelling results

The spatial snowmelt recharge was roughly based on the observed snowmelt pattern (study winter 2019). Figure 50 provides the background snowmelt recharge values that were used. In the model we distinguished different areas that received less or more recharge compared to the background value (Appendix, Figure B), based on the spatial differences we found.

Table 14. Comparison of environmental conditions during different study winters.  
 \*\*there were two temporally separate snow covers during this winter.

	2013	2014	2015	2019
Significant soil erosion?	No	No	Yes	Yes
Rainfall (mm)	42	105	28	49
Total SWE (mm)*	55	30	50	137
Total water input (mm)	97	135	78	186
Frozen soil during water input?#	No	No	Yes	No
Melting period (days)	8	7	4	18 & 3**
Attributed cause of erosion	-	-	Rain on frozen soil	Groundwater seepage

Table 15. Results for the 1D unsaturated zone model for the frozen soil condition of winter 2015.

Total water input:	28 mm
Total water input not infiltrated (frozen soil conditions 2015):	15.6 mm
Total water input not infiltrated (unfrozen scenario):	0 mm
Total volumetric surface runoff inner Gryteland catchment (frozen soil model):	2527 m <sup>3</sup>
Total discharge measured at the Gryteland catchment outlet:	2594 m <sup>3</sup>



Figure 49. Left: photograph of erosion marks in 2015 (eroded gully width: 40 cm; Starkloff, 2017), right: UAV-photograph of erosion in the same gully in 2019 (eroded gully width: 420 cm).

#### *Comparison of model results with field observations*

The map in Figure 51 shows the area with simulated groundwater seepage at its peak (21<sup>st</sup> of March) when the western part of the catchment was subjected to tile drainage. The simulated area corresponds well to the observed zone of seepage in the orthomosaics (Spring A). In the simulation,

groundwater seepage occurred along the undeveloped gullies where the water table rose above the surface level during snowmelt. It is also the zone where the hydraulic conductivity decreases westward, causing flow velocity to decrease. Consequently, the hydraulic head locally increases with the water received from the east. Without the need for further calibration of parameters, the pattern of seepage was already accurately simulated.

The temporal pattern of groundwater seepage in the simulation is shown in Figure 52. It can be seen that the major seepage event occurred March 21 to 22, corresponding well to the observed surface runoff in the field on March 21. The total discharge at the flume and the total exfiltrated groundwater discharge are given in Table 16. In the field, the discharge happened quicker and with a higher peak discharge compared to the simulation, but the total discharge due to the March 20-21 melt event is similar. Before this date, the model predicted minor but increasing seepage over time. In the field, any such minor seepage was not picked up at the flume as discharge, although the disappearance of snow cover in the spring areas (Figure 44) does suggest seepage indeed occurred prior to 20-21 March.

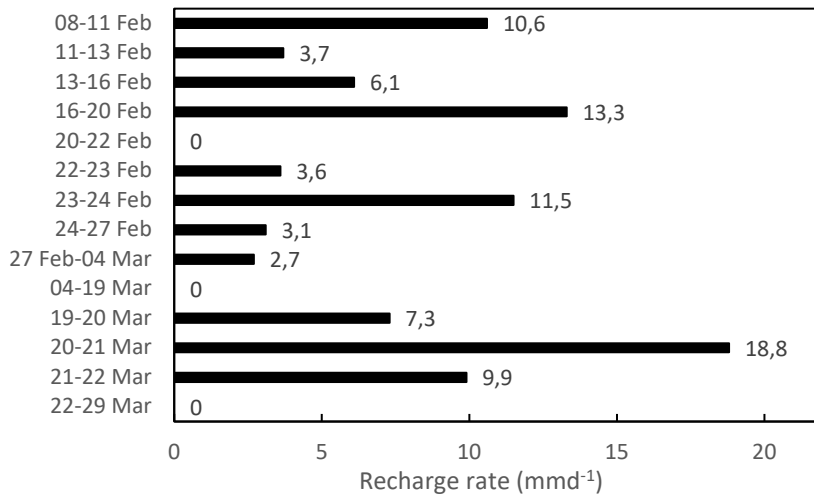


Figure 50. Background recharge rates used in the simulations, varied through time according to different snowmelt episodes (winter 2019).

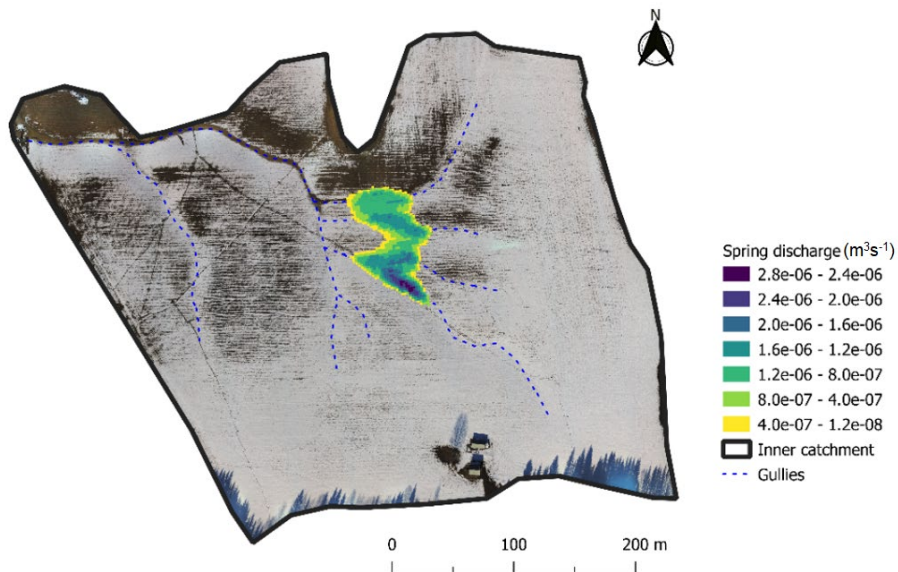


Figure 51. Simulated spring discharge for each grid cell ( $4\text{m}^2$ ) at March 22, 00:00, shown on the March 21 orthomosaic of the Gryteland catchment (2019).

Table 16. Measured total flume discharge and total simulated seepage discharge after the 20<sup>th</sup> of March compared.

Flume total measured discharge ( $\text{m}^3$ ) (20/03-21/03)	672
Simulated total seepage discharge ( $\text{m}^3$ ) (20/03-21/03)	221
Simulated total seepage discharge ( $\text{m}^3$ ) (20/03-29/03)	523

### *Simulated scenarios results*

In Figure 53 we see the simulated groundwater seepage area when tile drainage would be absent. A much larger surface area received groundwater and a significantly higher total amount of groundwater exfiltrated, ca. 3 times more compared to the partly tile drained catchment (Figure 54). The existing springs C, D and E marked on the orthomosaics (Figure 45) fall within the simulated seepage area. It could also be observed that rainfall of 56 mm

in 3 days caused groundwater seepage when tile drainage was absent (Figure 54), while with the tile drainage active, rainfall did not cause seepage.

The results of the different scenarios in which hydraulic conductivity is varied, are given in Figure 52 and Figure 54. It can be observed that if the soil properties would be homogeneously distributed across the catchment, much less to no seepage occurs. Furthermore, when the snowmelt-induced groundwater recharge is spatially homogeneous, the amount of seepage and potential for erosion is also lower (Figure 54).

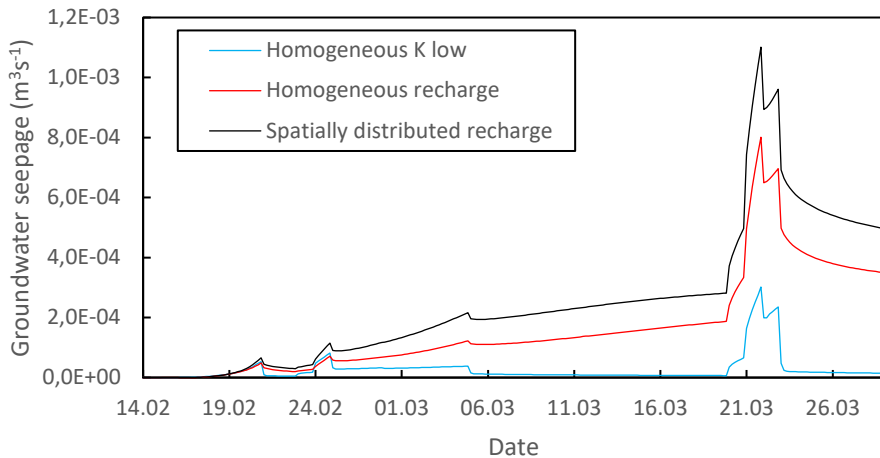


Figure 52. Simulated groundwater discharge rate ( $\text{m}^3\text{s}^{-1}$ ) at the surficial seepage zones. Different scenarios are included in which groundwater discharge was not 0. Spatially distributed recharge is the baseline simulation that represents the field measured snowmelt circumstances of February and March, 2019.



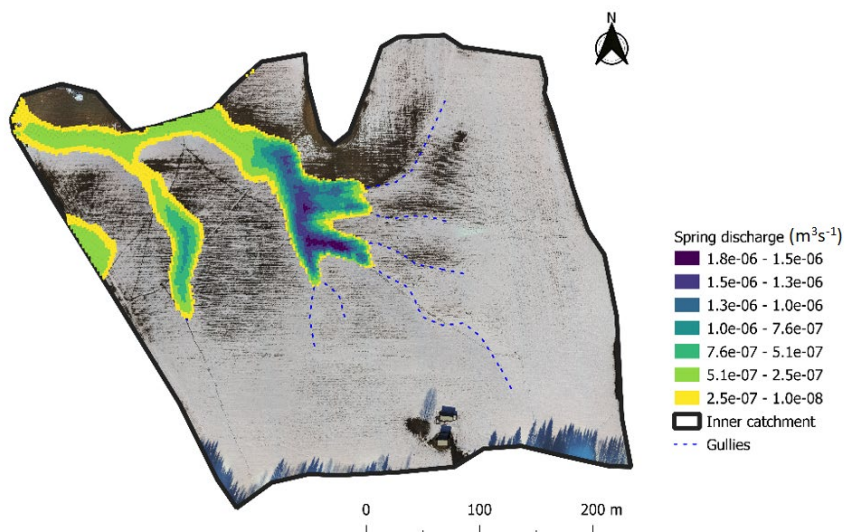


Figure 53. Simulated spring discharge for each grid cell ( $4\text{m}^2$ ) at March 22, 00:00, shown on the March 21 orthomosaic of the Gryteland catchment, for the scenario without tile drainage.

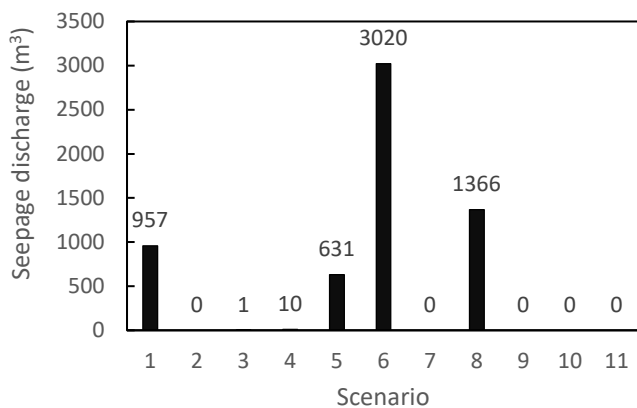


Figure 54. Total seepage discharge that occurred during each simulated scenario. Scenario numbers are explained in Table 17.

Table 17. Scenario numbers with descripts (used in Figure 17).

Scenario Number	Scenario description
1	Baseline (spatially distributed recharge, spatially varying $K_s$ )
2	Homogeneous $K_s$ (sandy loam)
3	Homogeneous $K_s$ (loam)
4	Homogeneous $K_s$ (silty clay loam)
5	Homogeneous recharge
6	No drainage (heterogeneous recharge and $K_s$ )
7	Rainfall (with drainage)
8	Rainfall (without drainage)
9	2013 winter
10	2014 winter
11	2015 winter

## 7.4 Discussion

### Field measurements and observations in 2019

During the winter of 2019 there was moderate snow cover (ca. 40 cm) that melted at an increasing rate during the melt season, likely because initial energy gained by the snowpack first satisfied the cold content of the snow (Rango and DeWalle, 2008), and because air temperature and solar radiation increased with the progression of the melting season. The deepest snow cover and highest melt rates were mostly found in the region with coarser soil. This implied that a large amount of water infiltrated into an unsaturated zone with good permeability. Shallow groundwater recharge was thus expected to be most voluminous and rapid in these regions. The landscape configuration of slopes (higher or lower solar irradiation) and forest cover (shading), as well as the wind pattern, thus influence the spatial coupling between water input and groundwater flow in conjunction with the spatial variation in soil hydraulic properties.

The soil was not frozen during the current study winter (2019), likely because the insulating snow cover kept the soil temperature close to 0 °C at the snowpack base. Since the soil was unfrozen, infiltration of melt- and

rainwater could occur unimpeded. Rainwater was also partly absorbed by the snowcover itself. The absence of visible infiltration-excess overland flow in the field supports the notion that all rain- and meltwater infiltrated.

Groundwater seepage was observed throughout the melting period. The active groundwater springs were easily detected as patches without snow cover in an otherwise snow-covered landscape due to the advection of heat. Some seepage areas coincided with subsurface erosion in the form of soil piping. In a sudden event late in the melt season, a large quantity of water exfiltrated from a seepage area, causing noticeable erosion of topsoil for one or two days. A substantial discharge peak was registered at the catchment outlet, confirming the sudden nature of the event.

We did not identify an above-ground cause for the sudden large-scale groundwater seepage. The water input (rainfall and snowmelt) was not of a larger volume compared to earlier in the melt season, especially since this concerned a second snow cover that was less deep than the first snow cover (ca. 15 vs 45 cm). Our hypothesis therefore is that a certain storage threshold was exceeded in the subsurface leading to intensive seepage, a possible explanation we further tested through modelling.

The surface erosion due to groundwater seepage is of concern, as fertile topsoil was lost and nutrients and potentially contaminants were quickly discharged into the Skuterud stream, eventually reaching nearby lakes and the Oslofjord. Furthermore, subsurface erosion due to soil piping created the unexpected concern of danger for humans, livestock, and wild animals because of the possibility of accidental stepping into subsurface holes. To our knowledge, there are no other studies that reported surface or subsurface erosion due to groundwater seepage in response to snowmelt.

### Comparison with earlier winters

The different results for the winters 2013, 2014, 2015 and 2019 demonstrate the interannual variability of snowmelt and erosion processes. The factors of importance that determine whether surface erosion occurs seem to be frozen soil and volume of water input (rainfall and snowmelt totals combined). Substantial overland flow occurred in the winter of 2015 with

only a moderate rain event, and Starkloff (2017) hypothesized that ice saturation of the soil impeded infiltration leading to the erosion event. Our unsaturated zone simulation for winter 2015 confirmed this hypothesis: infiltration was impeded. The influence of frozen soil on reducing infiltration is well known on the laboratory scale or via numerical modelling (Appels et al., 2017; Stuurup et al., 2022), but in-situ flooding and erosion evidence is scarce.

In prior winters before this study, when no flooding or erosion occurred, the water input was likely too small to cause significant groundwater seepage. The MODFLOW results for the winters of 2013, 2014 and 2015, wherein no groundwater seepage was observed, underline this hypothesis.

The type of surface erosion was different depending on the cause of overland flow. With the frozen soil event in 2015, the erosion gullies were deep but narrow, limiting the spatial extent of topsoil erosion. This likely indicates short-lived fast flowing water. During the groundwater seepage event of 2019, surface erosion occurred in a spatially broader area in the form of braided gully networks, suggestion the flow might have been slower but longer lasting. Both types of erosion events are of concern however, especially since the rain on frozen soil concerned only a moderate rainfall amount and intensity (28 mm, maximum 2 mm/hr; Starkloff, 2017).

### Implications of the modelling results

The MODFLOW modelling results show a similar large-scale groundwater seepage event as was observed in the field. The temporal match of the initiation groundwater seepage is near exact, and the spatial extent is also similar. This underscores the idea that a threshold was reached in the subsurface by repeated addition of water from rainfall and snowmelt over the 1.5-month period (February – March). Crossing the threshold meant that the water table intersected with knickpoints in topography, leading to groundwater seepage. Without the final water input (15 cm of snow cover melting), this event would not have occurred according to the groundwater model. In case of significant rainfall and no other water source (56 mm in 3 days), the model shows that the water input is too low to cause seepage.

With the model results for the 2019 winter, the seepage event is more spread out in time than was measured at the flume. The cause of groundwater stagnation in the model was the decrease of horizontal hydraulic conductivity in the downstream direction. Groundwater could therefore exfiltrate gradually. In reality, there might have been additional subsurface processes at work, such as subsurface erosion, preferential flow and pressure build-up. To understand the precise cause of the sudden nature of the event however requires further study.

The alternative scenarios that were modelled show the major effects of tile drainage, spatial distribution of soil hydraulic properties, and spatial distribution of snowmelt. It was found that tile drainage prevented a substantial amount of groundwater-seepage and subsequent overland flow and erosion during the snowmelt season by routing groundwater directly toward the main stream of Skuterud. Geomorphological evolution through erosion of the semi-gully system is therefore hampered.

With spatially homogeneous hydraulic conductivity (high or low) the groundwater seepage was small to negligible. This result provides a clue as to why groundwater seepage occurred at all, namely the transition from coarser beach deposits to finer deep marine deposits. As the groundwater flow in the horizontal direction stagnates, the local hydraulic head increases, until it matches the surface elevation. The fact that the decrease in hydraulic conductivity coincides with a drop in elevation is also important because it facilitates the intersection of the water table with the surface level. This finding implies that similar agricultural settings with coarse beach deposits in higher areas and finer marine deposits in lower areas -a common situation in postglacial uplifted regions of Scandinavia (Sauer et al., 2009)-, could expect groundwater-seepage induced overland flow and erosion.

Lastly, the modelling confirms the earlier described coupling between spatially distributed snowmelt and groundwater flow. The deepest snow cover and highest melt rates were on the coarsest soils that delivered most of the water for the seepage event. Without this spatial coupling between snowmelt recharge and soil properties, the groundwater seepage would have been weaker.

## 7.5 Conclusion

Field measurements and observations together with UAV-photography were carried out during the snowmelt period in an agricultural catchment in southern Norway. The observations coincided with a significant erosion event caused by seepage of groundwater in response to snowmelt. Three previous field campaigns during winters in the same catchment only recorded one instance of surface erosion due to rain on frozen ground. We hypothesized that in the current study, which had much higher snowmelt volumes, a threshold of water storage in the subsurface was exceeded, subsequently leading to groundwater seepage.

Numerical modelling confirmed the occurrence of the seepage event in response to a final input of melt water to the subsurface. Field observations and simulations further revealed that groundwater seepage occurred along the transition from coarser to finer sediments. A reduction in groundwater flow velocity caused the water table to rise locally. The modelling also revealed that the spatial distribution of snow cover and snow melt rate influenced the seepage event because the deepest snow cover and highest melt rates corresponded to the area with the coarsest soil, leading to rapid groundwater recharge. Numerical modelling also revealed that without tile drainage, the undeveloped gully system would likely receive larger quantities of groundwater and undergo more severe erosion.

The combination of field observations and relatively simple numerical groundwater modelling proved promising to capture and explain the non-yearly erosion event of the 2019 melt season. From our study, it could follow that seepage-induced erosion in postglacial isostatically uplifted marine sediments where agriculture is performed is at serious hazard of flooding and erosion with a multi-year recurrence interval. Since a lot of agriculture in southern Norway and other parts of Scandinavia takes place in such a landscape, the process of surface and subsurface erosion due to groundwater seepage after snowmelt warrants further study. The non-yearly occurrence of the erosion event makes a focused study difficult, but questions about its recurrence frequency, its widespread occurrence in

northern regions, and its underlying hydrological causes are relevant with regards to conservation of fertile soil and flood protection.

## 8. Discussion & Conclusion

The aim of the research in this PhD project was to better understand to what extent frozen soil conditions could increase flood hazard in a landscape through infiltration and storage capacity reduction. A model was developed to simulate freezing of unsaturated soil, and different modelling approaches were tested. The model was subsequently used to understand infiltration and storage capacity reduction during various frozen soil conditions in both 1D and 2D cases. Snowmelt flooding in an actual landscape was also studied and the frozen soil model was applied to the case-study in addition to a groundwater model to understand causes of observed overland flow. Furthermore, an overview was drafted of current understanding and knowledge gaps related to the physics of frozen unsaturated soil.

### *Modelling approach and soil freezing physics*

The numerical model (CryoFlow) based on the Forward Euler Method was successful in replicating frozen soil behaviour from several experiments to a satisfactory degree. None of the different mathematical approaches tested stood out in being more reliable or accurate than the other. However, one approach required the least number of empirical parameters, and thus it was preferred and adopted for the rest of the research. This approach was called the “semi-empirical” approach: the liquid water content was related to soil temperature based on thermodynamic phase change formalized in the Clapeyron relationship, but the change in matric potential due to freezing was calculated with an empirical equation.

The empirical cryosuction equation provided consistently good results with a fixed value for its empirical parameter ( $\Phi_i = 1.8$ ). It is difficult to explain why the function would work with a universal parameter, given the missing link to fundamental physics at the molecular interface of ice and water. It should also be noted that the parameter both includes matric potential changes and permeability reduction because pressure gradients drive flow velocity for which the parameter was calibrated, so it might not be an accurate reflection of either. In any case, an empirical approach can be useful even in absence of thorough physical justification, if it is well tested. The limited number of test cases is too scarce to be able to draw strong



conclusions about the universal applicability of the cryosuction equation with a fixed constant, however. Yet, with a pragmatic approach, and considering other frozen soil models are often tested on even less experimental datasets (one or two datasets, to the Author's knowledge), the semi-empirical version of the CryoFlow model was deemed adequate to explore the dynamics of frozen soil infiltration.

Some researchers might prefer the physically based approach that was also developed with CryoFlow, in which the matric potential in frozen soil is directly related to the Clapeyron relationship by assuming freezing equals drying in its effect on matric potential. The supposed analogy is however unproven and rather unrealistic according to the current author's viewpoint; this is discussed in more detail in Chapter 2. At least the matric potential cannot be exactly equal given the different physical processes involved (crystal ice growth creating new interfacial tensions versus air entering pores).

Considering a model that would incorporate the freezing equals drying approach as truly physically based might also be misleading because soil water retention is in the first place determined by an empirical equation irrespective of the physically based Clapeyron relationship. Also, while Darcy's Law can be derived from the fundamental Navier-Stokes equation, this would only be applicable for steady and noncompressible flow conditions in media with uniform porosity, thus not with water transport in real soil. Therefore, even the fundamental flow equation of soil water transport models is a phenomenologically derived constitutive relationship (Neuman, 1977). In any case, approaches toward soil freezing remain speculative until falsification of first principle-based hypotheses is undertaken to reconcile soil freezing behaviour with pore-scale and atomic-scale physics.

In this research, we also found that an impedance factor (Chapter 2, Eq. 14) was required to prevent overprediction of water flow to the frozen zone when the freezing equals drying analogy for the soil's matric potential was used (i.e., only reducing permeability based on liquid water content was insufficient). This is a similar find as some studies (e.g., Harlan, 1973; Jame &

Norum, 2008; Dall'Amico et al., 2011), while others found the impedance factor to be unnecessary (Newman & Wilson, 1997; Painter, 2011). There has been debate and criticism surrounding the impedance factor (Kurylyk & Watanabe, 2013). Two notions could be added to the debate: 1) exact similitude of frozen and unfrozen soil permeability solely based on liquid water content is illogical given the fundamental differences between soil drying and freezing physics; 2) overprediction of flow toward the frozen zone might also be the result of overprediction of frozen soil matric potential, not overestimation of permeability.

This thesis did not provide new theory nor empirical evidence to advance our understanding of fundamental soil freezing physics, but it did present an updated overview, rediscussed 'forgotten theories', and added several notions for consideration. The plurality of hypotheses about physicochemical causes of cryosuction for instance (Chapter 2) remains unaddressed. The current results of the model CryoFlow do however provide some level of confidence in our ability to simulate frozen soil dynamics of a soil column despite a lack of accurate understanding of the physics involved. Even if first principles are absent from a model, which is already the case with macroscopic soil water transport models at any rate, it can rely on empirical relationships to be useful. In the context of flood hazard mitigation, predictability is ultimately more important than physical understanding.

The knowledge gained from the different model versions, and from the literature review, could aid in the improvement of numerical models simulating frozen soils, which will ultimately improve simulation of infiltration and storage capacity reduction due to freezing.

#### *Flood hazard due to frozen unsaturated soil: reduction of infiltration capacity*

The application of the model to a wide range of scenario cases revealed the sensitivity of frozen soil infiltration dynamics to several variables (Chapters 3, 4 and 5). The effects of these variables according to the simulations are summarized below.

### Soil type

If we broadly categorize soil texture into coarse, intermediate and very fine soils (see Chapter 4 for details on the soil types), then according to the CryoFlow model, intermediate soils are most at hazard of having reduced infiltration due to freezing. These soils had the highest ice saturation after the freezing phase, suggesting that cryosuction drew in liquid water toward the freezing front. This higher ice saturation lowers the soil's permeability. Also, these soils hold water against gravitational drainage, while the freezing temperature is only mildly depressed, meaning that soil water could freeze to ice and thus be immobilized before it could flow downward.

In coarse soils, liquid water drains too quickly for cryosuction to have an effect; in principle, these soils are also drier before freezing starts, unless freezing occurs briefly after the soil has been wetted. Therefore, despite the weak or near-absent freezing point depression in coarse soils, there is no strongly reduced infiltration capacity due to freezing. In case of extreme cold soil temperature, e.g., several degrees below zero, coarse soil could still experience severe infiltration impedance due to infiltrating water freezing in-situ. It should also be noted that infiltration could also still be impeded due to refreezing of meltwater within snowpacks above or on top of the soil surface (Stähli et al., 2004).

With very fine soils, freezing had less effect on infiltration for a simple reason: infiltration capacity in such soils is already low, leading to little additional reduction in infiltration during common water input rates. Only with very slow water input which would normally not exceed the soil's infiltration capacity, could freezing make a clear difference by lowering the infiltration capacity of a very fine soil even further. Also, because of the very low matric potential in fine soils, the freezing point deviates substantially from 0 °C, thus requiring rather low temperatures for the soil to freeze. Furthermore, cryosuction often has minimal effect with very fine soils – at least at short timescales, because the soil's inherent low permeability slows down water transport toward the frozen zone.

### Temperature

It is hardly worth mentioning that the lower the temperature, the higher the

ice content in a soil, and thus the lower the infiltration capacity. A few nuances could be added to this simple logic however based on the simulation results. Firstly, soils with lower porosity cool faster than higher porosity soils. The lower the porosity the higher the soil's thermal conductivity, the lower the heat capacity, and the smaller the latent heat flux because of lower saturated water content. Soils with lower porosity therefore demonstrated faster response of soil temperature to boundary temperature conditions. Lower porosity soils thus have potentially more reduced infiltration capacity during freezing temperature conditions compared to soils with higher porosity (all other hydraulic properties hypothetically being equal). It should be noted that permeability and matric potential of the soil have an impact on soil temperature as well by controlling water flux and phase change.

Secondly, the simulations identified threshold temperature values at which freezing started to have a stronger effect on infiltration. For example, infiltration was limited severely if top boundary freezing temperature was at least below  $-0.5\text{ }^{\circ}\text{C}$  for a sandy clay loam, and  $-2\text{ }^{\circ}\text{C}$  for an organic rich soil horizon. This is explained by the depression of the freezing point in both soils; it required lower than  $0\text{ }^{\circ}\text{C}$  temperature for the water under tensile stress (negative pressure) to freeze.

Thirdly, the freezing rate itself played a role: the faster the soil freezes, the more water is turned to immobile ice before it can drain, thus the higher the ice content. Faster freezing can result from rapidly declining top boundary temperatures (i.e., quickly going from positive to negative air temperature), from very low boundary temperatures (this creates a large temperature gradient between air and soil), or from high thermal conductivity of the soil.

Fourthly, the colder a soil becomes, the higher the likelihood of infiltrating water freezing in-situ. This phenomenon is a decisive factor in increasing flood hazard, as it can quickly clog pores in the topsoil with ice. It can cause macropores, which normally allow water to infiltrate easily despite frozen conditions, to fill with ice and thereby drastically reduce infiltration.

Finally, the temperature boundary conditions during snowmelt and/or rainfall play an important role because thaw and infiltration often occur

simultaneously. When infiltration proceeds more rapid than thawing of the pore ice, infiltration is inhibited. Therefore, when temperature boundary conditions at the top remain below 1 °C (for most soil types tested), infiltration was reduced substantially; above this threshold value, pore ice thawed, and infiltration was improved. In case of snowpacks of sufficient depth (e.g., 20 cm), the soil receives little energy from the atmosphere due to the snow's insulating effect, which would prevent thaw of the soil frost. Melt- or rainwater reaching the topsoil through percolation in a snowpack might thus infiltrate with more difficulty. However, if snowpacks formed before significant freezing of the soil occurred, the insulation effect would work the other way around: infiltration capacity remains high because the soil is insulated against freezing air temperatures (Hardy et al., 2001).

#### Initial moisture conditions

The amount of water present in the soil at the onset of freezing is crucial for the eventual infiltration and storage capacity of the soil. Logically, the higher the initial water content of the soil, the higher the potential ice saturation, and thus the lower the infiltration and storage capacity. A few nuances could be added, however. In some specific cases, a high initial water content led to less infiltration reduction due to freezing compared to a lower initial water content (e.g., 0.75 compared to 0.6 initial saturation for a sandy clay loam). It is unclear how realistic such physical behaviour is, but it results from the complex interplay between thermal conduction, heat capacity and latent heat flux in the numerical model.

With more pore water present, there is more water available to turn to ice, and at a less depressed freezing point because water in larger pores is under less tensile stress. At the same time, more pore water implies a higher heat capacity of the soil, and more water turning to ice leads to a stronger latent heat flux. These two factors slow down temperature change, and thus might reduce the eventual ice content compared to lower initial water content. In most simulated cases however, it could be seen that higher initial moisture content leads to higher ice contents and thus higher flood hazard. Specifically, with an initial saturation of at least 0.6 to 0.75 (threshold value), most frozen soils tested experienced strong reduction in infiltration.

### Water input rate

Another important variable of influence on frozen soil infiltration dynamics was the rate at which water was supplied to the surface of the soil. Between a water input rate of 0.5 to 2 mmh<sup>-1</sup> the effect of frozen conditions on infiltration was strongest. The higher the input rate for finer soils, the less the effect of freezing, because during unfrozen conditions the water input would already exceed the soil's infiltration capacity. In other cases, higher water input rate would lead to less infiltration. This means that rainfall on frozen ground is more likely to lead to flood hazard than snowmelt, because rainfall rate usually exceeds snowmelt rate (Zaqout et al. 2023). However, the sheer amount of snowmelt could still exceed the storage space in the unsaturated zone even if infiltration capacity is not exceeded, and the presence of soil frost reduces the storage space.

With slower water input rate, water could still infiltrate despite frozen conditions for most soil types. However, in very cold situations, the slow infiltrating water potentially freezes in-situ, thereby reducing infiltration capacity. In such a scenario, overland flow still occurred, and flood hazard was therefore increased.

### Microtopography

The effect of microtopography on infiltration during frozen conditions can be large but ultimately depends on various other variables such as soil type and air temperature, at least in the case of the 10 cm wide and deep simulated micro-depression. In some cases, infiltration was improved because the simulated micro-depression became a site of focused infiltration, usually due to more rapid thaw of soil ice at or near the micro-depression. This effect was strongest during cyclical freeze-thaw scenarios. Furthermore, the effect of improving infiltration by the micro-depression was strongest for a sandy clay loam soil, and less strong with a coarser silt loam or finer silt soil. Also, the micro-depression mainly improved infiltration if thawing temperature conditions were present.

In a few specific cases with the silt soil type, the micro-depression reduced the amount of infiltration during frozen conditions. This was likely due to higher ice content in the soil. The micro-depression froze faster because of

its larger exposure to the atmosphere (increased atmosphere-soil surface contact length compared to a flat situation). The stronger freezing in turn drew in more water from the unfrozen zone due to cryosuction. Furthermore, an ice-layer could form on top of the soil within the micro-depression during cyclical freeze-thaw conditions because the water is standing still. This would also temporarily impede infiltration.

The simulations showed that the effect of a micro-depression is intricately tied to thermodynamic and water transport processes. Depending on specific configurations of atmospheric variables, soil conditions and soil type, micro-topography could in some frozen soil cases reduce flood hazard according to the model compared to an analogue frozen situation with a flat surface. And in very specific cases, the micro-topography increased flood hazard compared to the flat-surface case. These assertions require further empirical evidence to be supported as the scenarios simulated were highly synthetic cases.

#### Macropores

The results with macro-porous soil were straightforward: in most cases, the presence of macropores negates any reduction in infiltration due to freezing temperatures. It required extreme cold soil temperatures ( $< -8$  °C) for overland flow to occur with a macro-porous soil. The explanation of the limited effect of freezing is that macropores are drained before phase change initiates. Only with extreme cold temperatures could infiltrating water freeze in-situ and fill macropores with ice. In catchments with abundant macro-porous soil, flood hazard would thus only be increased when the soil has reached sufficiently low temperatures to cause in-situ freezing of infiltrated water.

#### Temporal conditions

Another important factor to consider is time, especially the amount of time between the last moment of water input to a soil, and the moment freezing temperatures are reached. The shorter this timeframe, the higher the likelihood of still moist conditions in the soil, and thus an increased potential for high ice contents. Also, the duration of freezing conditions is of importance. The longer the freezing period, the deeper the frost

penetration. The CryoFlow model also revealed that the amount of time a frozen soil can thaw before water is supplied to its surface influences the eventual infiltration.

Lastly, it was found that cyclical patterns of freezing and thawing can have a strong impact on infiltration. It means that infiltrated water supplied during the thawing phase can refreeze in the topsoil during the freezing phase. This creates an ice-rich topsoil layer which will impede water infiltration during subsequent periods. It should thus be noted that frozen soil infiltration dynamics are tied to snowpack dynamics (not simulated), since snowpacks are also subjected to cyclical freeze-melt cycles.

*Case-study: snowmelt runoff and erosion an agricultural landscape*

Fieldwork in a small agricultural catchment revealed how groundwater flow patterns during snowmelt can cause flooding and erosion. Even if the soil was not frozen, the sheer quantity of snowmelt caused the groundwater table to intersect with sloping surfaces. Groundwater modelling confirmed that a certain tipping point was reached in water storage in the subsurface. While there was no overland flow during most of the snowmelt period, during a final melting phase of snow cover, a large quantity of water seeped out of the ground from various springs.

It was suggested through numerical modelling that the transition from beach deposits to finer marine sediments played a role in stagnating groundwater flow near knickpoints in topography. Such spatial distribution of sediments is typical of some agricultural areas of Norway and Sweden. During three previous study winters, the groundwater seepage event did not occur because of shallower snowpacks and thus less meltwater. This implies the flooding and erosion event due to groundwater seepage is not an annually recurring event.

For an earlier overland flow event during another winter, it was hypothesized that frozen soil conditions caused flooding and erosion. Numerical modelling with CryoFlow confirmed that the conditions of that year would have resulted in frozen soil with significantly lowered infiltration capacity. Total predicted surface discharge according to the CryoFlow model matched well



with surface runoff measurements. This shows that modelling infiltration capacity reduction due to freezing with a numerical model can indeed aid to predict overland flow and thus flood hazard.

Flooding and erosion extent were not the same for the different winters, likely resulting from different overland flow velocities. It was furthermore found that the spatial distribution of snow depth and snowmelt influenced the groundwater seepage event. Most meltwater was supplied to regions with coarser soil, allowing rapid recharge of the groundwater.

It is not easy to generalize from catchment-based studies. However, the study identifies different possible causes of flooding and erosion during the snowmelt period. Frozen soil could impede infiltration in an agricultural tile-drained landscape, resulting in overland flow and gully erosion. And even in the absence of frozen soil, the rise of the water table toward the surface due to the large amount of meltwater infiltrating can cause flooding and erosion. In that case, the main research question regarding the influence of frozen soil becomes irrelevant, since flooding can be induced by the sheer quantity of the meltwater flux entering the soil resulting in a large volume of groundwater seepage, i.e., subsurface flow became important irrespective of overland flow.

Still, if the soil would have been frozen, it could have reduced the meltwater infiltration and thus the volume of groundwater seepage. In that case, in-situ overland flow might be more important than groundwater seepage, which could as we have seen, alter the extent of erosion.

### *Limitations*

This PhD project mostly consisted of numerical modelling. The main drawback of the modelling approach is the lack of soil structural changes upon ice growth. Frost heave is an important phenomenon that impacts the hydraulic properties of the soil (Lundin, 1990). The current lack of empirical equations to predict those changes in hydraulic properties make the coupling of frost heave to water and heat transport in a model difficult. Further research is needed to derive relationships between frost heave and soil hydraulic properties such as changes to the soil's permeability, porosity and

soil water retention parameters. In specific situations, the assumption of decreased infiltration capacity might not hold for thawing frost-heaved soils, and the simulated infiltration capacities might be wrong.

Another limitation of the PhD research is the application of the model to a large number of test cases without experimental verification. Although the model is tested on various experimental datasets, the scenarios are synthetic and often had unrealistic boundary conditions. It remains unclear to which extent the results would be in line with actual dynamics of a frozen soil in a real catchment. Nevertheless, the synthetic scenarios revealed the inner workings of the model and showed how, according to current empirical and physical equations combined, freezing of soils would impact infiltration. The results could also lead to more focused experimental efforts to falsify the findings of this research. Unfortunately, the large quantity of variable combinations as was tested with the CryoFlow model is not feasible to be reproduced in laboratory studies. This underscores the usefulness to exhaust numerical resources for the purpose of exploring the interplay of freezing and infiltration which ultimately has implications for flood hazard prediction and mitigation, among other land management concerns.

What also could be considered a limitation is that the complexity of frozen soil thermal conductivity was ignored in this PhD research. To isolate the effect of certain variables on frozen soil infiltration dynamics, it was deemed acceptable to use a simple thermal conductivity function based on the geometric mean of the thermal conductivities of soil constituents. More accurate and elaborate thermal conductivity equations exist for soil in unfrozen state, but these often require several empirical constants (Dong et al, 2015) and thus increase parameter complexity of the model. Also, empirical thermal conductivity equations are not developed yet for soil in a frozen state.

In reality, thermal conductivity of frozen soil would have varied more than what the model simulated. The discrepancy is likely small however because air and water content are the major controlling factors on soil thermal conductivity, and the impact of these factors were incorporated in the

numerical model. Simulations revealed the importance of water content and porosity on soil thermodynamics accordingly.

### *Conclusion and outlook*

This PhD project provided insights into the conditions in which increased flood hazard due to a frozen unsaturated zone could be expected through infiltration and storage capacity reduction. The knowledge gained from the numerical model itself could be of interest for integrated catchment-scale hydrological models, in which simplified schemes for soil freezing are incorporated. The numerical algorithm, as well as the physical and empirical equations which the model CryoFlow consists of, could be further simplified for integration into hydrological models. The results are also instructive for flood hazard management in areas with seasonal frost occurrence through the insight provided into the conditions that increase frozen soil flood hazard.

The main message of the simulated scenarios is that a specific combination of factors should be looked out for at which infiltration due to frozen conditions is inhibited strongly. In simplified terms, these conditions would entail soil types of intermediate soil texture such as loamy soils, wet antecedent moisture conditions before freezing, absence of microtopographic depressions and macropores, low thawing temperatures during the liquid water input phase, repeated freeze-thaw cycles, and moderate to high liquid water input rates during the snowmelt and/or rainfall period.

Future studies could try to couple soil freezing dynamics to snowpack dynamics. Snowpacks control soil temperature and water input. Liquid water could also be stored within the snowpack itself. An ice layer could then form on top of the soil that prevents water from infiltrating into the soil. In cases without a snowpack, the soil is vulnerable to freezing due to the lack of insulation (Decker et al., 2003). Especially if rain would fall on bare soil that has been frozen deeply in the absence of snow, the hazard of flooding can be high (Shanley & Chalmers, 1999).

The modelling also revealed that empirical and semi-empirical formulations work well to predict water transport, phase change and soil temperature when compared to experimentally frozen soil columns. Refinement, simplification, and parametrization of empirical and semi-empirical relationships would in the short-term likely be useful for the improvement of catchment-based flood predictions. Further testing could for example be done with the empirical cryosuction equation to assess the universality of its empirical parameter.

There are also research opportunities to advance our understanding of the pore-scale physics of freezing, and to reconcile macroscopic water transport and phase change with fundamental physical understanding of freezing point depression, matric potential change, and permeability change due to ice growth in the soil.

On another note, the link between frozen soil and flood hazard could gain heightened importance in the future due to climate change. There are predictions that frost depth and frost frequency could increase due to reductions in snowfall and higher frequency of rain on frozen soil episodes (Zaqout et al., 2023; Zhu et al., 2019). This highlights the importance of further study of frozen soil conditions that could impair infiltration and increase flood hazard.

#### *Beyond Earth: soil freezing on other planetary bodies*

In our field of science, we are mainly dealing with water on Earth. Ultimately, hydrological processes take place throughout the Universe on other planetary bodies. The water dynamics on our planet are only one example. By disentangling our understanding of hydrology from Earth we could learn more about fundamental assumptions and theories, and to what extent they have been biased to our planet. It is known that hydrological processes are taking place on other celestial bodies such as Mars (Grotzinger, 2009), the Lunar crust (Robinson & Taylor, 2014), Venus (in the past; Kane et al., 2019), moons of Jupiter and Saturn (Gaidos & Nimmo, 2000; Waite et al., 2009), comets and meteorites (Alexander et al., 2018), and likely exoplanets (Seager, 2013). The moon Titan for example has landscaping hydrological processes but with liquid methane instead of water.

Soil freezing dynamics on other planets should be explored through numerical modelling (and later experimentation) to understand the role of gravity and other Earth-specific parameters on the freezing and thawing processes in soils. Especially given the complex nature of pore-scale physical phase change processes, such research might provide useful insights. Does gravity play a role, for example, by altering soil cohesion and affecting the weight of water? Such efforts could be part of a broader off-planet hydrological research endeavour to learn more about hydrology on our own planet, but also to benefit future colonization of terrestrial bodies that will rely on local soil water-plant systems. A starting point could be experiments with the freezing of capillaries in zero gravity aboard the International Space Station.



## 9. Conclusion diagram

Table 18. Simplified overview of the major research results concerning the various factors related to frozen-soil-induced flood hazard increase according to the numerical model CryoFlow. The following assumption underlies these results: water that cannot infiltrate due to soil freezing becomes overland flow and thus increases flood hazard. For the full list of applicable assumptions, see Chapter 1, Section 3. For more nuanced details on the results, see Chapter 4, 5, and 8.

<b>Factor</b>	<b>Role</b>	<b>Highest increase of flood hazard</b>
Soil type	Important	Medium soil textures
Initial saturation (at start of freezing)	Important	>0.6 or >0.75 (depending on soil type)
Freezing temperature	Important	<-0.5 or <-2 °C (depending on soil type; <-8 °C for macropores)
Freezing duration	Important	> Multiple days
Thawing temperature	Important	<1 °C
Time between water input and subsequent thawing	Important	> Several hours
Water input rate	Important	0.5 to 2 mmhr <sup>-1</sup> (higher rates as well)
Water input temperature	Not important	
Diurnal freeze/thaw regime	Important	Frequent recurring freeze-thaw episodes
Microtopography	Important	Smooth, flat surface
Macropores	Important	No macropores

## 10. Epilogue

There was once a mouse who dreamed of forests tall and crooked. In one of those dreams, the little creature scurried through bushes and undergrowth in search of flavourful berries and acorns he had never tasted before.

“How do you know these berries and acorns to truly exist?” a friend of the mouse once asked, when he heard about the dream.

“I do not know if they exist, for dreams are not empirical evidence, alas they are only fantasy. But nothing can be ruled out that is not yet observed, but neither does it make sense to pretend existence.”

During fieldwork one day, the same mouse ran past my measurement equipment while I was measuring the weight of the snowpack. He asked with curiosity what I was doing, and what was the need of it all. I patiently explained my research, and what I was trying to find out.

“Mm yes, but dear lad, what will become of it?” the mouse asked. I did not understand the question at first, but then I explained to him that I would publish my findings in a journal, and with a few more of such publications, I would obtain my doctoral degree. The mouse was rather inquisitive and kept asking about all the details of my academic endeavours. I explained about co-authorship, the practice of citations, the impact factor of a journal, the practice of the PhD defence, and the general pathways of the academic career. The mouse eagerly listened as the snow melted beneath our feet.

It was a day of grey clouds drifting past the sky with an occasional ray of sunlight in between the gaps. I offered the mouse some of my raisins which he eagerly accepted. He apologized for not having anything to offer in return.

As the sun was setting, the time had come for the mouse to move along. He had family in wait for an evening meal. When he scurried through the snow, the little creature looked back at me and said with kindness:

“You are not scientists.”



## 11. References

References are sorted per chapter.

### Chapter 1

- Apel, H., Aronica, G.T., Kreibich, H. & Thielen, A.H. (2008). **Flood risk analyses—how detailed do we need to be?** *Natural Hazards*, 49: 79–98. <https://doi.org/10.1007/s11069-008-9277-8>
- Berghuijs, W. R., Woods, R. A., & Hrachowitz, M. (2014). **A precipitation shift from snow towards rain leads to a decrease in streamflow.** *Nature Climate Change*, 4(7): 583–586. <https://doi.org/10.1038/nclimate2246>
- Burt, T. P., & Williams, P. J. (1976). **Hydraulic conductivity in frozen soils.** *Earth Surface Processes*, 1(4): 349–60. <https://doi.org/10.1002/ESP.3290010404>
- Chang, H., & Franczyk, J. (2008). **Climate change, land-use change, and floods: toward an integrated assessment.** *Geography Compass*, 2: 1549-1579. <https://doi.org/10.1111/j.1749-8198.2008.00136.x>
- Chen, A. S., Djordjević S., Leandro, J., & Savić, D. A. (2010). **An analysis of the combined consequences of pluvial and fluvial flooding.** *Water Science & Technology*. 62 (7): 1491–1498. <https://doi.org/10.2166/wst.2010.486>
- Cobby, D., Morris S., Parkes, A., & Robinson, V. (2009). **Groundwater flood risk management: advances towards meeting the requirements of the EU floods directive.** *Journal of Flood Risk Management*, 2(2): 111-119. <https://doi.org/10.1111/j.1753-318X.2009.01025.x>
- Ferreira, C.S.S., Walsh, R.P.D., Steenhuis, T.S., Shakesby, R.A., Nunes, J.P.N., Coelho, C.O.A. & Ferreira, A.J.D. (2015). **Spatiotemporal variability of hydrologic soil properties and the implications for overland flow and land management in a peri-urban Mediterranean catchment.** *Journal of Hydrology*, 525: 249-263. <https://doi.org/10.1016/j.jhydrol.2015.03.039>
- French, H. K., Hardbattle, C., Binley, A., Winship, P., & Jakobsen, L. (2002). **Monitoring snowmelt induced unsaturated flow and transport using**

- electrical resistivity tomography.** *Journal of Hydrology*, 267(3–4): 273–284. [https://doi.org/10.1016/S0022-1694\(02\)00156-7](https://doi.org/10.1016/S0022-1694(02)00156-7)
- Graybeal, D. Y., & Leathers, D. J. (2006). **Snowmelt-Related Flood Hazard in Appalachia: First Estimates from a Historical Snow Climatology.** *Journal of Applied Meteorology and Climatology*, 45(1): 178–193. <https://doi.org/10.1175/JAM2330.1>
- Hartman, M. D., Baron, J. S., Lammers, R. B., Cline, D. W., Band, L. E., Liston, G. E., & Tague, C. (1999). **Simulations of snow distribution and hydrology in a mountain basin.** *Water Resources Research*, 35(5): 1587–1603. <https://doi.org/10.1029/1998WR900096>
- Hayashi, M., van der Kamp, G., & Schmidt, R. (2003). **Focused infiltration of snowmelt water in partially frozen soil under small depressions.** *Journal of Hydrology*, 270(3–4): 214–229. [https://doi.org/10.1016/S0022-1694\(02\)00287-1](https://doi.org/10.1016/S0022-1694(02)00287-1)
- Hayhoe, H. N., Pelletier, R. G., & Coote, D. R. (1995). **Estimating snowmelt runoff erosion indices for Canada.** *Journal of Soil and Water Conservation*, 50(2): 174–179. <https://www.jswnonline.org/content/50/2/174>
- Hernández-Atencia, Y., Peña, L.E., Muñoz-Ramos, J., Rojas, I. & Álvarez, A. (2023). **Use of soil infiltration capacity and stream flow velocity to estimate physical flood vulnerability under land-use change scenarios.** *Water*, 15. <https://doi.org/10.3390/w15061214>
- Ippisch, O. (2001). ***Coupled transport in natural porous media.*** PhD thesis, Rupertus Carola University of Heidelberg. <https://doi.org/10.11588/HEIDOK.00001872>
- Leal, M., Ramos, C. & Pereira, S. **Different types of flooding lead to different human and material damages: the case of the Lisbon Metropolitan Area.** *Natural Hazards*, 91: 735–758. <https://doi.org/10.1007/s11069-017-3153-3>
- Li, H., Gao, H., Zhou, Y., Xu, C., Ortega, R.Z., Nils Roar Sælthun, M. (2020). **Usage of SIMWE model to model urban overland flood: a case study**

- in Oslo. *Hydrology Research*, 51(2): 366–380.  
<https://doi.org/10.2166/nh.2020.068>
- Li, P., Sheng, M., Yang, D., & Tang, L. (2019). **Evaluating flood regulation ecosystem services under climate, vegetation and reservoir influences.** *Ecological Indicators*, 107.  
<https://doi.org/10.1016/j.ecolind.2019.105642>
- Lundberg, A., & Halldin, S. (2001). **Snow interception evaporation. Review of measurement techniques, processes, and models.** *Theoretical and Applied Climatology*, 70(1–4): 117–133.  
<https://doi.org/10.1007/S007040170010>
- Mohammed, A. A., Kurylyk, B. L., Cey, E. E., & Hayashi, M. (2018). **Snowmelt infiltration and macropore flow in frozen soils: overview, knowledge gaps, and a conceptual framework.** *Vadose Zone Journal*, 17(1): 1–15.  
<https://doi.org/10.2136/VZJ2018.04.0084>
- Mohammed, A. A., Pavlovskii, I., Cey, E. E., & Hayashi, M. (2019). **Effects of preferential flow on snowmelt partitioning and groundwater recharge in frozen soils.** *Hydrology and Earth System Sciences*, 23(12): 5017–5031. <https://doi.org/10.5194/HESS-23-5017-2019>
- O’Neill, K. (1983). **The physics of mathematical frost heave models: a review.** *Cold Regions Science and Technology*, 6(3): 275–291.  
[https://doi.org/10.1016/0165-232X\(83\)90048-4](https://doi.org/10.1016/0165-232X(83)90048-4)
- Pourali, S. H., Arrowsmith, C., Chrisman, N., Matkan, A. A. & Mitchell, D. (2014). **Topography Wetness Index Application in Flood-Risk-Based Land Use Planning.** *Applied Spatial Analysis and Policy*, 9: 39-54.  
<https://doi.org/10.1007/s12061-014-9130-2>
- Sarsembayeva, A., & Collins, P. E. F. (2017). **Evaluation of frost heave and moisture/chemical migration mechanisms in highway subsoil using a laboratory simulation method.** *Cold Regions Science and Technology*, 133: 26–35. <https://doi.org/10.1016/J.COLDREGIONS.2016.10.003>
- Shanley, J. B., & Chalmers, A. (1999). **The effect of frozen soil on snowmelt runoff at Sleepers River, Vermont.** *Hydrological Processes*, 13: 1843-1857. [https://doi.org/10.1002/\(SICI\)1099-1085\(199909\)13:12/13](https://doi.org/10.1002/(SICI)1099-1085(199909)13:12/13)

- Starkloff, T., Hessel, R., Stolte, J., & Ritsema, C. (2017). **Catchment Hydrology during Winter and Spring and the Link to Soil Erosion: A Case Study in Norway.** *Hydrology*, 4(1): 15.  
<https://doi.org/10.3390/HYDROLOGY4010015>
- Zaqout, T., Andradóttir, H.Ó., Sørensen, J. (2023). **Trends in soil frost formation in a warming maritime climate and the impacts on urban flood hazard.** *Journal of Hydrology*, 617(A): 128978.  
<https://doi.org/10.1016/j.jhydrol.2022.128978>
- Zhang, S., Teng, J., He, Z., & Sheng, D. (2016). **Importance of vapor flow in unsaturated freezing soil: a numerical study.** *Cold Regions Science and Technology*, 126: 1–9.  
<https://doi.org/10.1016/J.COLDREGIONS.2016.02.011>
- Zhu L., Ives, A.R., Zhang, C., Guo, Y., Radeloff V.C. (2019). **Climate change causes functionally colder winters for snow cover-dependent organisms.** *Nature Climate Change*, 9: 886-893.  
<https://doi.org/10.1038/s41558-019-0588-4>

## Chapter 2

- Anderson, D.M., Tice, A.R. (1972). **Predicting liquid water contents in frozen soils from surface area measurements.** *Highway Research Record*, 393: 12-8.
- Azmatch, T. F., Segó, D.C., Arenson, L.U., Biggar, K.W. (2012). **New ice lens initiation condition for frost heave in fine-grained soils.** *Cold Regions Science and Technology*, 82: 8-13.  
<https://doi.org/10.1016/j.coldregions.2012.05.003>
- Carson, J. E. (1961). **Soil temperature and weather conditions.** *AEC Research and Development Report, ANL-6470. Argonne National Laboratory, Argonne, Ill.*
- Dall'Amico, M., Endrizzi, S., Gruber, S., Rigon R. (2011). **A robust and energy-conserving model of freezing variably-saturated soil.** *Cryosphere*, 5(2): 469-484. <https://doi.org/10.5194/tc-5-469-2011>
- Demand, D., Selker, J.S., Weiler, M. (2019). **Influences of macropores on infiltration into seasonally frozen soil.** *Vadose Zone Journal*, 18(1). <https://doi.org/10.2136/vzj2018.08.0147>
- Durner, W. (1994). **Hydraulic conductivity estimation for soils with heterogeneous pore structure.** *Water Resources Research*, 30: 211-223. <https://doi.org/10.1029/93WR02676>
- Evans, S. G., Ge, S., Voss, C.I., Molotch, N.P. (2018). **The role of frozen soil in groundwater discharge predictions for warming alpine watersheds.** *Water Resources Research*, 54(3): 1599-1615.  
<https://doi.org/10.1002/2017WR022098>
- Flerchinger, G.N., Saxton, K.E. (1989). **Simultaneous heat and water model of a freezing snow-residue-soil system I. Theory and development.** *Transactions of the ASAE*, 32(2): 565-571.
- French, H.K., Hardbattle, C., Binley, A., Winship, P., Jakobsen, L. (2002). **Monitoring snowmelt induced unsaturated flow and transport using electrical resistivity tomography.** *Journal of Hydrology*,

267(3-4): 273-284. [https://doi.org/10.1016/S0022-1694\(02\)00156-7](https://doi.org/10.1016/S0022-1694(02)00156-7)

- French, H.K., Binley, A. (2004). **Snowmelt infiltration: monitoring temporal and spatial variability using time-lapse electrical resistivity**. *Journal of Hydrology*, 297(1-4): 174-186.  
<https://doi.org/10.1016/j.jhydrol.2004.04.005>
- van Genuchten, M. (1980). **A closed-form equation for predicting the hydraulic conductivity of unsaturated soils**. *Soil Science Society of America Journal*, 44(5): 892-898.  
<http://dx.doi.org/10.2136/sssaj1980.03615995004400050002x>
- Jouybari, N.F., Lundström, T.S., Hellström, J.G.I. (2020). **Investigation of thermal dispersion and intra-pore turbulent heat flux in porous media**. *International Journal of Heat and Fluid Flow*, 81.  
<https://doi.org/10.1016/j.ijheatfluidflow.2019.108523>
- Liu, G., Zhou, Z., Li, Z., Zhou, Y. (2014). **Analysis and experimental study on thermal dispersion effect on small scale saturated porous aquifer**. *Energy*, 67: 411-421.  
<https://doi.org/10.1016/j.energy.2013.12.06>
- Hansson, K., Šimůnek, J., Mizoguchi, M., Lundin, L., van Genuchten, M.T. (2004). **Water flow and heat transport in frozen soil. Numerical solution and freeze-thaw applications**. *Vadose Zone Journal*, 3(2): 693-704. <https://doi.org/10.2136/vzj2004.0693>
- Harlan, R.L. (1973). **Analysis of coupled heat-fluid transport in partially frozen soil**. *Water Resources Research*, 9(5): 1314-1323.  
<https://doi.org/10.1029/WR009i005p01314>
- Hayashi, M., van der Kamp, G., Schmid, R. (2003). **Focused infiltration of snowmelt water in partially frozen soil under small depressions**. *Journal of Hydrology*, 270: 214-229.  
[https://doi.org/10.1016/S0022-1694\(02\)00287-](https://doi.org/10.1016/S0022-1694(02)00287-)

- Hayashi, M. (2013). **The cold vadose zone. Hydrological and ecological significance of frozen-soil processes.** *Vadose Zone Journal*, 12(4).  
<https://doi.org/10.2136/vzj2013.03.0064>
- Holten, R. (2019). **The effect of freezing and thawing on water flow and pesticide leaching in partially frozen soil: soil column experiments and model development.** PhD Thesis. Ås: Norwegian University of Life Sciences.
- Ippisch, O. (2001). **Coupled transport in natural porous media.** PhD Thesis. Rupertus Carola University of Heidelberg.
- Ireson, A. M., van der Kamp, G., Ferguson, G., Nachshon U., Wheater, H.S. (2013). **Hydrogeological processes in seasonally frozen northern latitudes: understanding, gaps and challenges.** *Hydrogeology Journal*, 21(1): 53-66.  
<https://doi.org/10.1007/s10040-012-0916-5>
- Jame, Y.W., Norum, D.I. (1972). **Phase composition of a partially frozen soil.** Division of Hydrology, College of Engineering, University of Saskatchewan, Saskatoon; Research Paper 11.
- Jansson, P.E., Karlberg, L., (2004). **Coupled heat and mass transfer model for soil-plant-atmosphere systems.** Stockholm, Sweden: Royal Institute of Technology, Department of Civil and Environmental Engineering.
- Koopmans, R. W., Miller, R. D., (1966). **Soil freezing and soil water characteristic curves.** *Soil Science Society of America Proceedings*, 30(6): 680-685.  
<https://doi.org/10.2136/sssaj1966.03615995003000060011x>
- Kulik, V. Y. 1978. **Water Infiltration into Soil (in Russian).** *Gidrometeoizdat*.
- Kurylyk, B.L., Watanabe, K. (2013). **The mathematical representation of freezing and thawing processes in variably-saturated, non-deformable soils.** *Advances in Water Resources*, 60: 160-177.  
<https://doi.org/10.1016/j.advwatres.2013.07.016>

- Li, Q., Sun, S., Xue, Y. (2010). **Analyses and development of a hierarchy of frozen soil models for cold region study.** *Journal of Geophysical Research*, 115 (D03107) 1-18. <https://doi.org/10.1029/2009JD012530>
- Loranger, B., Scibilia, E., Hoff, I., Aksnes, J., Skoglund, K. (2017). **Evaluation of Norwegian gradation based regulation for frost susceptibility of crushed rock aggregates in roads and railways.** The 10th International Conference on the Bearing Capacity of Roads, Railways and Airfields (BCRRA 2017)
- Lunardini, V.J. (1988). **Freezing of soil with a liquid water content and variable thermal properties.** Hanover, NH: U.S. Army Corps of Engineers Cold Regions Research and Engineering Laboratory.
- Lundberg, A., Ala-Aho, P., Eklo, O., Klöve, B., Kværner, J., Stumpp, C. (2016). **Snow and frost: implications for spatiotemporal infiltration patterns - a review.** *Hydrological Processes*, 30(8): 1230-1250. <https://doi.org/10.1002/hyp.10703>
- Lundin, L. (1990). **Hydraulic properties in an operational model of frozen soil.** *Journal of Hydrology*, 118: 289–310. [https://doi.org/10.1016/0022-1694\(90\)90264-X](https://doi.org/10.1016/0022-1694(90)90264-X)
- Ma, W., Zhang, L., Yang, C. (2015). **Discussion of applicability of the generalized Clausius-Clapeyron equation and the frozen fringe process.** *Earth-Science Reviews*, 142: 49-59. <https://doi.org/10.1016/j.earscirev.2015.01.003>
- McKenzie, J. M., Voss, C.I., Siegel, D.I. (2007). **Groundwater flow with energy transport and water-ice phase change: Numerical simulations, benchmarks, and application to freezing in peat bogs.** *Advances in Water Resources*, 30(4): 966-983. <https://doi.org/10.1016/j.advwatres.2006.08.008>
- Miller, R.D. (1980). **Freezing phenomena in soils.** In Hillel, D. (ed.) *Application of Soil Physics*, Academic Press. 254-299.



- Miller, R.D., Black, P.B. (2003). **Redistribution of water in terrestrial soils at subfreezing temperatures. A review of processes and their potential relevance to Mars.** *Journal of Geophysical Research*, 108(E4). <https://doi.org/10.1029/2002JE001873>
- Mizoguchi, M. (1990). **Water, heat and salt transport in freezing soil** (in Japanese). PhD thesis. Graduate School of Agricultural and Life Sciences, University of Tokyo.
- Mohammed, A. A., Kurylyk, B.L., Cey, E.E., Hayashi, M. (2018). **Snowmelt infiltration and macropore flow in frozen soils: overview, knowledge gaps, and a conceptual framework.** *Vadose Zone Journal*, 17(1): 1-15. <https://doi.org/10.2136/vzj2018.04.0084>
- Mualem, Y. (1976). **A new model predicting the hydraulic conductivity of unsaturated porous media.** *Water Resources Research*, 12: 513-522.
- Newman, G, Wilson, G. (1997). **Heat and mass transfer in unsaturated soils during freezing.** *Canadian Geotechnical Journal*, 34: 63–70.
- Noh, J. H., Lee, S.R., Park, H. (2012). **Prediction of Cryo-SWCC during Freezing Based on Pore-Size Distribution.** *International Journal of Geomechanics*, 12(4): 428-438. <https://doi.org/10.1139/t96-085>
- Pittman, F., Mohammed, A., and Cey, E. (2020). **Effects of antecedent moisture and macroporosity on infiltration and water flow in frozen soil.** *Hydrological Processes*, 34: 795-809. <https://doi.org/10.1002/hyp.13629>
- Rango, A., DeWalle, D.R. (2008). **Principles of Snow Hydrology.** Cambridge: Cambridge University Press.
- Richards, L.A. (1931). **Capillary conduction of liquids through porous mediums.** *Physics*, 1(5): 318-333. <https://doi.org/10.1063/1.1745010>

- Ren, J. P., Vanapalli, S.K., Han, Z. (2017). **Soil freezing process and different expressions for the soil-freezing characteristic curve.** *Sciences in Cold and Arid Regions*, 9(3). <https://doi.org/221-228>.  
10.3724/SP.J.1226.2017.00221
- Shoop, S. A., and Bigl, S. R. (1997). **Moisture migration during freeze and thaw of unsaturated soils: Modeling and large scale experiments.** *Cold Regions Science And Technology*, 25: 33–45.  
[https://doi.org/10.1016/S0165-232X\(96\)00015-8](https://doi.org/10.1016/S0165-232X(96)00015-8)
- Šimůnek, J., Šejna, M., van Genuchten, M. T. (1998). **The HYDRUS-1D software package for simulating the one-dimensional movement of water, heat, and multiple solutes in variably-saturated media. Version 1.0.** IGWMC – TPS – 70, International Ground Water Modeling Center, Colorado School of Mines, Golden, Colorado.
- Stähli, M. (2006). **Freezing and thawing phenomena in soils.** In Encyclopedia of Hydrological Sciences. Hoboken, NJ: John Wiley & Sons. <https://doi.org/10.1002/0470848944.hsa075>
- Spaans, E.J.A. Baker, J.M. (1996). **The soil freezing characteristic: its measurement and similarity to the soil moisture characteristic.** *Soil Science Society of America Journal*, 60: 13-9.
- Taylor, G.S., Luthin, J.N. (1978). **A model for coupled heat and moisture transfer during soil freezing.** *Canadian Geotechnical Journal*, 15: 548–555. <https://doi.org/10.1139/t78-058>
- Voss, C. I., Provost, A.M. (2002; Version of September 22, 2010), **SUTRA, A model for saturated-unsaturated variable-density ground-water flow with solute or energy transport.** U.S. Geological Survey Water-Resources Investigations Report 02-4231, 291 p.
- Watanabe, K., Flury M. (2008). **Capillary bundle model of hydraulic conductivity of frozen soil.** *Water Resources Research*, 44(12). <https://doi.org/10.1029/2008WR007012>

- Watanabe, K., Kito, T., Sakai, M., Toride, N. (2010). **Evaluation of hydraulic properties of a frozen soil based on observed liquid water contents at the freezing front.** *Journal of Japanese Society of Soil Physics*, 116: 9-18.
- Watanabe, K., Kito, T., Dun, S., Wu, J.Q., Greer, R.C., Flury, M. (2012). **Water infiltration into a frozen soil with simultaneous melting of the frozen layer.** *Vadose Zone Journal*, 12(1).  
<https://doi.org/10.2136/vzj2011.0188>
- Watanabe, K., Osada, Y. (2017). **Simultaneous measurement of liquid water content and hydraulic conductivity of partially frozen soil near 0 °C.** *Cold Regions Science and Technology*, 142: 79-84.  
<https://doi.org/10.1016/j.coldregions.2017.08.002>
- Williams, P.J., Smith, M.W. (1989). **The Frozen Earth. Fundamentals of geocryology.** Cambridge: Cambridge University Press.
- Woo, M.K. (2012). **Permafrost Hydrology.** Berlin: Springer-Verlag.
- Yang, D., Zhang, T., Zhang, K., Greenwood, D.J., Hammond, J.P., White, P.J. (2009). **An easily implemented agro-hydrological procedure with dynamic root simulation for water transfer in the crop-soil system. Validation and application.** *Journal of Hydrology*, 370(1-4): 177-190.  
<https://doi.org/10.1016/j.jhydrol.2009.03.005>
- Zhang, X., Sun, S.F., Xue, Y. (2007). **Development and testing of a frozen soil parameterization for cold region studies.** *American Meteorological Society*, 8: 690-701. <https://doi.org/10.1175/JHM605.1>
- Zhang, S., Teng, J., He, Z., Sheng, D. (2016). **Importance of vapor flow in unsaturated freezing soil. A numerical study.** *Cold Regions Science and Technology*, 126.  
<https://doi.org/10.1016/j.coldregions.2016.02.011>
- Zhao, Y., Nishimura, T., Hill, R., Miyazaki, T. (2013). **Determining hydraulic conductivity of air-filled porosity in an unsaturated frozen soil by the**

**multistep outflow method.** *Vadose Zone Journal*, 12(1).

<https://doi.org/10.2136/vzj2012.0061>

Zhou, X., Zhou, J., Kinzelbach, W., Stauffer, F. (2014). **Simultaneous measurement of liquid water content and ice content in frozen soil using gamma ray attenuation and TDR.** *Water Resources Research*, 50(12): 9630 – 9655. <https://doi.org/10.1002/2014WR015640>

### Chapter 3

Amiri, E. A., Craig, J. R., & Kurylyk, B. L. (2018a). **A theoretical extension of the soil freezing curve paradigm.** *Advances in Water Resources*, 111: 319–328. <https://doi.org/10.1016/J.ADVWATRES.2017.11.021>

- Anderson, D., & Tice, A. R. (1973). **Predicting liquid water contents in frozen soils from surface area measurements.** No. 393, 12–18 (1972). *Journal of Terramechanics*, 10(2): 105. [https://doi.org/10.1016/0022-4898\(73\)90017-7](https://doi.org/10.1016/0022-4898(73)90017-7)
- Azmatch, T. F., Sego, D. C., Arenson, L. U., & Biggar, K. W. (2012). **Using soil freezing characteristic curve to estimate the hydraulic conductivity function of partially frozen soils.** *Cold Regions Science and Technology*, 83–84: 103–109. <https://doi.org/10.1016/J.COLDREGIONS.2012.07.002>
- Benoit, G. R., & Bornstein, J. (1970). **Freezing and thawing effects on drainage.** *Soil Science Society of America Journal*, 34(4): 551–557. <https://doi.org/10.2136/SSSAJ1970.03615995003400040007X>
- Berghuijs, W. R., Woods, R. A., & Hrachowitz, M. (2014). **A precipitation shift from snow towards rain leads to a decrease in streamflow.** *Nature Climate Change*, 4(7): 583–586. <https://doi.org/10.1038/nclimate2246>
- Blachere, J. R., & Young, J. E. (1972). **The Freezing Point of Water in Porous Glass.** *Journal of the American Ceramic Society*, 55(6): 306–308. <https://doi.org/10.1111/J.1151-2916.1972.TB11291.X>
- Bogdan, A. (1998). **Thermodynamics of the curvature effect on ice surface tension and nucleation theory.** *The Journal of Chemical Physics*, 106(5): 1921. <https://doi.org/10.1063/1.473329>
- Burt, T. P., & Williams, P. J. (1976a). **Hydraulic conductivity in frozen soils.** *Earth Surface Processes*, 1(4): 349–360. <https://doi.org/10.1002/ESP.3290010404>
- Dall'Amico, M., Endrizzi, S., Gruber, S., & Rigon, R. (2011). **A robust and energy-conserving model of freezing variably-saturated soil.** *Cryosphere*, 5(2): 469–484. <https://doi.org/10.5194/TC-5-469-2011>
- Djikaev, Y. S., & Ruckenstein, E. (2017). **Self-consistent determination of the ice-air interfacial tension and ice-water-air line tension from**

- experiments on the freezing of water droplets.** *Journal of Physical Chemistry C*, 121(30): 16432–16439. <https://doi.org/10.1021>
- Fisher, E. A. (2002). **The Freezing of Water in Capillary Systems.** *The Journal of Physical Chemistry*, 28(4): 360–367.  
<https://doi.org/10.1021/J150238A006>
- Formanek, G. E., McCool, D. K., & Papendick, R. I. (1984). **Freeze-Thaw and Consolidation Effects on Strength of a Wet Silt Loam.** *Transactions of the ASAE*, 27(6): 1749–1752. <https://doi.org/10.13031/2013.33040>
- French, H., & Binley, A. (2004). **Snowmelt infiltration: monitoring temporal and spatial variability using time-lapse electrical resistivity.** *Journal of Hydrology*, 297(1–4): 174–186.  
<https://doi.org/10.1016/J.JHYDROL.2004.04.005>
- French, H. K., Hardbattle, C., Binley, A., Winship, P., & Jakobsen, L. (2002). **Monitoring snowmelt induced unsaturated flow and transport using electrical resistivity tomography.** *Journal of Hydrology*, 267(3–4): 273–284. [https://doi.org/10.1016/S0022-1694\(02\)00156-7](https://doi.org/10.1016/S0022-1694(02)00156-7)
- Fuchs, M., Campbell, G. S., & Papendick, R. I. (1978). **An analysis of sensible and latent heat flow in a partially frozen unsaturated soil.** *Soil Science Society of America Journal*, 42(3): 379–385.  
<https://doi.org/10.2136/SSSAJ1978.03615995004200030001X>
- Good, R. J., (1992). **Contact angle, wetting, and adhesion: a critical review.** *Journal of Adhesion Science and Technology*, 6(12).
- Gharedaghloo, B., Berg, S. J., & Sudicky, E. A. (2020). **Water freezing characteristics in granular soils: Insights from pore-scale simulations.** *Advances in Water Resources*, 143: 103681.  
<https://doi.org/10.1016/J.ADVWATRES.2020.103681>
- Graybeal, D. Y., & Leathers, D. J. (2006). **Snowmelt-related flood hazard in appalachia: first estimates from a historical snow climatology.** *Journal of Applied Meteorology and Climatology*, 45(1): 178–193.  
<https://doi.org/10.1175/JAM2330.1>

- Guymon, G. L., Berg, R., & Hromadka, T. (1993). **Mathematical model of frost heave and thaw settlement in pavements**. Report. U.S. Army Cold Regions Research and Engineering Laboratory Hanover, New Hampshire 03755-1290.
- Hansson, K., Šimůnek, J., Mizoguchi, M., Lundin, L.-C., & Genuchten, M. Th. van. (2004). **Water flow and heat transport in frozen soil: numerical solution and freeze–thaw applications**. *Vadose Zone Journal*, 3(2): 693–704. <https://doi.org/10.2136/VZJ2004.0693>
- Harlan, R. L. (1973). **Analysis of coupled heat-fluid transport in partially frozen soil**. *Water Resources Research*, 9(5): 1314–1323. <https://doi.org/10.1029/WR009I005P01314>
- Hartman, M. D., Baron, J. S., Lammers, R. B., Cline, D. W., Band, L. E., Liston, G. E., & Tague, C. (1999). **Simulations of snow distribution and hydrology in a mountain basin**. *Water Resources Research*, 35(5): 1587–1603. <https://doi.org/10.1029/1998WR900096>
- Hassanizadeh, S. M., & Gray, W. G. (1993). **Thermodynamic basis of capillary pressure in porous media**. *Water Resources Research*, 29(10): 3389–3405. <https://doi.org/10.1029/93WR01495>
- Hayashi, M. (2013). **The Cold Vadose Zone: Hydrological and Ecological Significance of Frozen-Soil Processes**. *Vadose Zone Journal*, 12(4). <https://doi.org/10.2136/VZJ2013.03.0064/91440>
- Hayashi, M., van der Kamp, G., & Schmidt, R. (2003). **Focused infiltration of snowmelt water in partially frozen soil under small depressions**. *Journal of Hydrology*, 270(3–4): 214–229. [https://doi.org/10.1016/S0022-1694\(02\)00287-1](https://doi.org/10.1016/S0022-1694(02)00287-1)
- Hayhoe, H. N., Pelletier, R. G., & Coote, D. R. (1995). **Estimating snowmelt runoff erosion indices for Canada**. *Journal of Soil and Water Conservation*, 50(2): 174–179. <https://www.jswnonline.org/content/50/2/174>

- Henry, K. S. (2000). **A Review of the Thermodynamics of Frost Heave.** Report. Engineer Research and Development Center Hanover, Cold Regions Research and Engineering Lab.  
<https://apps.dtic.mil/sti/citations/ADA381842>
- Hohmann, M. (1997). **Soil freezing — the concept of soil water potential. State of the art.** *Cold Regions Science and Technology*, 25(2): 101–110.  
[https://doi.org/10.1016/S0165-232X\(96\)00019-5](https://doi.org/10.1016/S0165-232X(96)00019-5)
- Hopke, S. W. (1980). **A model for frost heave including overburden.** *Cold Regions Science and Technology*, 3(2–3): 111–127.  
[https://doi.org/10.1016/0165-232X\(80\)90016-6](https://doi.org/10.1016/0165-232X(80)90016-6)
- Hosler, C. L., & Hosler, C. R. (1955). **An investigation of the freezing of water in capillaries.** *Eos, Transactions American Geophysical Union*, 36(1): 126–132. <https://doi.org/10.1029/TR036I001P00126>
- Huang, Y., Zhu C., Wang, L., Cao, X., Su, Y., Jiang, X., Meng, S. Zhao, J., Zeng, X.C. (2016). **A new phase diagram of water under negative pressure: The rise of the lowest-density clathrate s-III.** *Science Advances*, 2(2).
- Hunt, A. G., Ewing, R. P., & Horton, R. (2013). **What’s wrong with soil physics?** *Soil Science Society of America Journal*, 77(6): 1877–1887.  
<https://doi.org/10.2136/SSAJ2013.01.0020>
- Ippisch, O. (2001). **Coupled transport in natural porous media.** PhD thesis, Rupertus Carola University of Heidelberg.  
<https://doi.org/10.11588/HEIDOK.00001872>
- Jones, H. C., & Getman, F. H. (1903). **The Molecular-lowering of the Freezing-point of Water produced by concentrated Solutions of certain Electrolytes.** *Zeitschrift Für Physikalische Chemie*, 46U(1): 244–286. <https://doi.org/10.1515/ZPCH-1903-4619>
- Jumikis, A. R. (1957). **The Effect of Freezing on a Capillary Meniscus.** *Highway Research Board Bulletin*, 168: 116–122.
- Jurin, J. (1718). **II. An account of some experiments shown before the Royal Society; with an enquiry into the cause of the ascent and**



- suspension of water in capillary tubes.** *Philosophical Transactions of the Royal Society of London*, 30(355): 739–747.  
<https://doi.org/10.1098/RSTL.1717.0026>
- Kaplar, C. W. (1970). **Phenomenon and mechanism of frost heaving.** *Highway Research Record. U.S. Army Cold Regions Research and Engineering Laboratory, Hanover, New Hampshire.*
- Karlsson, J. O. M., Braslavsky, I., & Elliott, J. A. W. (2019). **Protein-Water-Ice Contact Angle.** *Langmuir*, 35(23): 7383–7387.  
<https://doi.org/10.1021/ACS.LANGMUIR.8B01276>
- Koopmans, R. W. R., & Miller, R. D. (1966). **Soil Freezing and Soil Water Characteristic Curves.** *Soil Science Society of America Journal*, 30(6): 680–685.  
<https://doi.org/10.2136/SSSAJ1966.03615995003000060011X>
- Kruse, A. M., Darrow, M. M., & Akagawa, S. (2017). **Improvements in Measuring Liquid water in Frozen Soils Using the Pulsed Nuclear Magnetic Resonance Method.** *Journal of Cold Regions Engineering*, 32(1): 04017016. [https://doi.org/10.1061/\(ASCE\)CR.1943-5495.0000141](https://doi.org/10.1061/(ASCE)CR.1943-5495.0000141)
- Kurylyk, B. L., & Watanabe, K. (2013). **The mathematical representation of freezing and thawing processes in variably-saturated, non-deformable soils.** *Advances in Water Resources*, 60: 160–177.  
<https://doi.org/10.1016/J.ADVWATRES.2013.07.016>
- de Laplace, P.S., (1805). **Supplément au dixième livre du Traité de Mécanique Célest.** *Traité de Mécanique Céleste*, 4.
- Lara, R. P., Berg, A. A., Warland, J., & Parkin, G. (2021). **Implications of measurement metrics on soil freezing curves: A simulation of freeze–thaw hysteresis.** *Hydrological Processes*, 35(7): e14269.  
<https://doi.org/10.1002/HYP.14269>
- Larsbo, M., Holten, R., Eklo, O. M., Stenrod, M., & Jarvis, N. (2018). **A model for water flow in macroporous soils under freezing and thawing**

- conditions.** *EGUGA*, 20, 13422.  
<https://ui.adsabs.harvard.edu/abs/2018EGUGA..2013422L/abstract>
- Liu, Z., Muldrew, K., Wan, R. G., & Elliott, J. A. W. (2003). **Measurement of freezing point depression of water in glass capillaries and the associated ice front shape.** *Physical Review E*, 67(6): 061602.  
<https://doi.org/10.1103/PhysRevE.67.061602>
- Liu, Z., & Yu, X. (2011). **Coupled thermo-hydro-mechanical model for porous materials under frost action: Theory and implementation.** *Acta Geotechnica*, 6(2): 51–65. <https://doi.org/10.1007/S11440-011-0135-6>
- Lundberg, A., Ala-Aho, P., Eklo, O., Klöve, B., Kværner, J., & Stumpp, C. (2016). **Snow and frost: implications for spatiotemporal infiltration patterns – a review.** *Hydrological Processes*, 30(8): 1230–1250.  
<https://doi.org/10.1002/HYP.10703>
- Lundberg, A., & Halldin, S. (2001). **Snow interception evaporation. Review of measurement techniques, processes, and models.** *Theoretical and Applied Climatology*, 70(1–4): 117–133.  
<https://doi.org/10.1007/S007040170010>
- Luo, S., Likos, W. J., & Lu, N. (2021). **Cavitation of Water in Soil.** *Journal of Geotechnical and Geoenvironmental Engineering*, 147(8): 04021079.  
[https://doi.org/10.1061/\(ASCE\)GT.1943-5606.0002598](https://doi.org/10.1061/(ASCE)GT.1943-5606.0002598)
- Mazur, P. (1977). **The role of intracellular freezing in the death of cells cooled at supraoptimal rates.** *Cryobiology*, 14(3): 251–272.  
[https://doi.org/10.1016/0011-2240\(77\)90175-4](https://doi.org/10.1016/0011-2240(77)90175-4)
- Miller, R. D. (1980). **Freezing Phenomena in Soils.** *Applications of Soil Physics*, 254–299. <https://doi.org/10.1016/B978-0-12-348580-9.50016-X>
- Mohammed, A. A., Kurylyk, B. L., Cey, E. E., & Hayashi, M. (2018). **Snowmelt Infiltration and Macropore Flow in Frozen Soils: Overview,**

- Knowledge Gaps, and a Conceptual Framework.** *Vadose Zone Journal*, 17(1): 1–15. <https://doi.org/10.2136/VZJ2018.04.0084>
- Mohammed, A. A., Pavlovskii, I., Cey, E. E., & Hayashi, M. (2019). **Effects of preferential flow on snowmelt partitioning and groundwater recharge in frozen soils.** *Hydrology and Earth System Sciences*, 23(12): 5017–5031. <https://doi.org/10.5194/HESS-23-5017-2019>
- Morrow, N. R., & Szabo, J. O. (1970). **Physics and thermodynamics of capillary.** *Industrial and Engineering Chemistry*, 62(6): 32–56. <https://doi.org/10.1021/IE50726A006/ASSET/IE50726A006>
- Newman, G. P., & Wilson, G. W. (1997). **Heat and mass transfer in unsaturated soils during freezing.** *Canadian Geotechnical Journal*, 34(1): 63–70. <https://doi.org/10.1139/T96-085>
- O’Neill, K. (1983). **The physics of mathematical frost heave models: A review.** *Cold Regions Science and Technology*, 6(3): 275–291. [https://doi.org/10.1016/0165-232X\(83\)90048-4](https://doi.org/10.1016/0165-232X(83)90048-4)
- Or, D., Tuller, M. (2002). **Cavitation during desaturation of porous media under tension.** *Water Resources Research*, 38(5): 1061. <https://doi.org/10.1029/2001WR000282>
- Painter, S. L. (2011). **Three-phase numerical model of water migration in partially frozen geological media: Model formulation, validation, and applications.** *Computational Geosciences*, 15(1): 69–85. <https://doi.org/10.1007/S10596-010-9197-Z>
- Reed, M. A. (1977). **Frost heaving rate of silty soils as a function of pore size distribution: interim report.** *JTRP Technical Reports*. <https://doi.org/10.5703/1288284313953>
- Ren, J., Vanapalli, S. K., & Han, Z. (2017). **Soil freezing process and different expressions for the soil-freezing characteristic curve.** *Sciences in Cold and Arid Regions*, 9(3): 221–228. <https://doi.org/10.3724/SP.J.1226.2017.00221>

- Sarsembayeva, A., & Collins, P. E. F. (2017). **Evaluation of frost heave and moisture/chemical migration mechanisms in highway subsoil using a laboratory simulation method.** *Cold Regions Science and Technology*, 133: 26–35. <https://doi.org/10.1016/J.COLDREGIONS.2016.10.003>
- Sarshar, M. A., Swarctz, C., Hunter, S., Simpson, J., & Choi, C. H. (2013). **Effects of contact angle hysteresis on ice adhesion and growth on superhydrophobic surfaces under dynamic flow conditions.** *Colloid and Polymer Science*, 291(2): 427–435. <https://doi.org/10.1007/S00396-012-2753-4>
- Shanley, J. B., & Chalmers, A. (1999). **The effect of frozen soil on snowmelt runoff at Sleepers River, Vermont.** *Hydrological Processes*, 13: 1843–1857. [https://doi.org/10.1002/\(SICI\)1099-1085\(199909\)13:12/13](https://doi.org/10.1002/(SICI)1099-1085(199909)13:12/13)
- Shoop, S. A., & Bigl, S. R. (1997). **Moisture migration during freeze and thaw of unsaturated soils: modeling and large scale experiments.** *Cold Regions Science and Technology*, 25(1): 33–45. [https://doi.org/10.1016/S0165-232X\(96\)00015-8](https://doi.org/10.1016/S0165-232X(96)00015-8)
- Smith, M. W., & Burn, C. R. (1987). **Outward flux of vapour from frozen soils at Mayo, Yukon, Canada: results and interpretation.** *Cold Regions Science and Technology*, 13(2): 143–152. [https://doi.org/10.1016/0165-232X\(87\)90052-8](https://doi.org/10.1016/0165-232X(87)90052-8)
- Sorby, H. C. (1859). **XIX. On the freezing-point of water in capillary tubes.** *The London, Edinburgh, and Dublin Philosophical Magazine and Journal of Science*, 18(118): 105–108. <https://doi.org/10.1080/14786445908642731>
- Spaans, E. J. A., & Baker, J. M. (1996). **The soil freezing characteristic: its measurement and similarity to the soil moisture characteristic.** *Soil Science Society of America Journal*, 60(1): 13–19.
- Stähli, M. (2005). **Freezing and thawing phenomena in soils.** *Encyclopedia of Hydrological Sciences*.

- Starkloff, T., Hessel, R., Stolte, J., & Ritsema, C. (2017). **Catchment hydrology during winter and spring and the link to soil erosion: a case study in Norway.** *Hydrology*, 4(1): 15.  
<https://doi.org/10.3390/hydrology4010015>
- Suzuki, S. (2011). **Dependence of liquid water content in unsaturated frozen clay soil on initial soil moisture content.** *Soil Science and Plant Nutrition*, 50(4): 603–606.  
<https://doi.org/10.1080/00380768.2004.10408518>
- Taber, S. (1930). **The mechanics of frost heaving.** *The Journal of Geology*, 38(4): 303–317. <https://doi.org/10.1086/623720>
- Taylor, G. S., & Luthin, J. N. (2011). **A model for coupled heat and moisture transfer during soil freezing.** *Canadian Geotechnical Journal*, 15(4): 548–555. <https://doi.org/10.1139/T78-058>
- Tsytoovich, N. A. (1975). **The mechanics of frozen ground.** Scripta Book Co.
- van Oss, C. J., Giese, R. F., Wentzek, R., Norris, J., & Chuvilin, E. M. (2012). **Surface tension parameters of ice obtained from contact angle data and from positive and negative particle adhesion to advancing freezing fronts.** *Journal of Adhesion Science and Technology*, 6(4): 503–516. <https://doi.org/10.1163/156856192X00827>
- Watanabe, K., & Flury, M. (2008). **Capillary bundle model of hydraulic conductivity for frozen soil.** *Water Resources Research*, 44(12).  
<https://doi.org/10.1029/2008WR007012>
- Watanabe, K., & Osada, Y. (2016). **Comparison of hydraulic conductivity in frozen saturated and unfrozen unsaturated soils.** *Vadose Zone Journal*, 15(5): 1–7. <https://doi.org/10.2136/VZJ2015.11.0154>
- Watanabe, K., & Wake, T. (2009). **Measurement of liquid water content and relative permittivity of frozen unsaturated soil using NMR and TDR.** *Cold Regions Science and Technology*, 59(1): 34–41.  
<https://doi.org/10.1016/J.COLDREGIONS.2009.05.011>

- Vera, F., Rivera, R., Romero-Maltrana, D., Villanueva J. (2016). **Negative Pressures and the First Water Siphon Taller than 10.33 Meters.** *PLoS One*, 11(4): e0153055.  
<https://doi.org/10.1371/journal.pone.0153055>
- Williams, P. (1967). **Properties and behaviour of freezing soil.** *Norwegian Geotechnical Institute, Published Report.*
- Williams, P. J. (1964). **Liquid water content of frozen soils and soil moisture suction.** *Géotechnique*, 14(3): 231–246.  
<https://doi.org/10.1680/GEOT.1964.14.3.231>
- Yong, R. N. (1964). **Soil suction effects on partial soil freezing.** *McGill University, Report.*
- Young, T. (1805). **An essay on the cohesion of fluids.** *Philosophical Transactions of the Royal Society of London*, 95: 65-87.  
doi:10.1098/rstl.1805.0005. S2CID 116124581
- Zhang, S., Teng, J., He, Z., & Sheng, D. (2016). **Importance of vapor flow in unsaturated freezing soil: a numerical study.** *Cold Regions Science and Technology*, 126: 1–9.  
<https://doi.org/10.1016/J.COLDREGIONS.2016.02.011>
- Zhang, X., Sun, S. F., & Xue, Y. (2007). **Development and Testing of a Frozen Soil Parameterization for Cold Region Studies.** *Journal of Hydrometeorology*, 8(4): 690–701. <https://doi.org/10.1175/JHM605.1>

## Chapter 4

- Ala-Aho, P., Autio, A., Bhattacharjee, J., Isokangas, E., Kujala, K., Marttila, H., Menberu, M., Meriö, L.-J., Postila, H., Rauhala, A., Ronkanen, A.-K., Rossi, P.M., Saari, M., Torabi Haghighi, A., Kløve, B. (2021). **What conditions favor the influence of seasonally frozen ground on hydrological partitioning? A systematic review.** *Environmental Research Letters*, 16: 043008.  
<https://doi.org/10.1088/1748-9326/abe82c>
- Azmach, T. F., Sego, D.C., Arenson, L.U., Biggar, K.W. (2012). **New ice lens initiation condition for frost heave in fine-grained soils.** *Cold Regions Science and Technology*, 82: 8-13.  
<https://doi.org/10.1016/j.coldregions.2012.05.003>
- Blackburn, W. H., Pierson, F. B., Seyfried, M.S. (1990). **Spatial and temporal influence of soil frost on infiltration and erosion of sagebrush rangelands.** *Journal of the American Water Resources Association*, 26: 991-997.  
<https://doi.org/10.1111/j.1752-1688.1990.tb01434.x>
- Carsel, R. F., Parrish, R.S. (1988). **Developing joint probability-distributions of soil-water retention characteristics.** *Water Resources Research*, 24(5): 755-769.  
<https://doi.org/10.1029/WR024i005p00755>
- Cermak, V., Rybach, L. (1982). **Thermal Properties**, in: *Angenheister, G., Cermák, V., Hellwege, K.-H., Landolt, H. (Eds.), Zahlenwerte und Funktionen aus Naturwissenschaft und Technik: Neue Serie. — Numerical Data and Functional Relationships in Science and Technology: New Series c.* Springer, Berlin, 310–314.
- Coles, A.E., McDonnell, J.J. (2018). **Fill and spill drives runoff connectivity over frozen ground.** *Journal of Hydrology*, 558: 115-128. <https://doi.org/10.1016/j.jhydrol.2018.01.016>
- French, H.K., , C., Binley, A., Winship, P., Jakobsen, L. (2002). **Monitoring snowmelt induced unsaturated flow and transport using**

- electrical resistivity tomography.** *Journal of Hydrology*, 267(3-4): 273-284.  
[https://doi.org/10.1016/S0022-1694\(02\)00156-7](https://doi.org/10.1016/S0022-1694(02)00156-7)
- van Genuchten, M. (1980). **A closed-form equation for predicting the hydraulic conductivity of unsaturated soils.** *Soil Science Society of America Journal*, 44(5): 892-898.  
<http://dx.doi.org/10.2136/sssaj1980.03615995004400050002x>
- Granger, R.J., Gray, D.M., Dyck, G.E. (1984). **Snowmelt infiltration to frozen prairie soils.** *Canadian Journal of Earth Sciences*, 22: 464-72.  
<https://doi.org/10.1139/e84-073>
- Gray, D.M., Granger, R.J. (1986). **In situ measurements of moisture and salt movement in freezing soils.** *Canadian journal of Earth Sciences*, 23(5): 696 – 704. <https://doi.org/10.1139/e86-069>
- Gray, D.M., Granger, R.J., Landine, P.G. (1986). **Modelling snowmelt infiltration and runoff in a prairie environment.** In *Proceedings of the Cold Regions Hydrology Symposium*, Kane D.L. (ed.). AWRA, Bethesda, MD; 427-438.
- Hansson, K., Lundin, L. (2006). **Equifinality and sensitivity in freezing and thawing simulations of laboratory and in situ data.** *Cold Regions Science and Technology*, 44(1): 20 – 37.  
<https://doi.org/10.1016/j.coldregions.2005.06.004>
- Hayashi, M. (2013). **The cold vadose zone. Hydrological and ecological significance of frozen-soil processes.** *Vadose Zone Journal*, 12(4).  
<https://doi.org/10.2136/vzj2013.03.0064>
- Ireson, A. M., van der Kamp, G., Ferguson, G., Nachshon U., Wheeler, H.S. (2013). **Hydrogeological processes in seasonally frozen northern latitudes: understanding, gaps and challenges.** *Hydrogeology Journal*, 21(1): 53-66.  
<https://doi.org/10.1007/s10040-012-0916-5>



- Jones, H.G., Pomeroy, J.W. (2001). **Early spring snowmelt in a small boreal forest watershed: influence of concrete frost on the hydrology and chemical composition of streamwaters during rain-on-snow events.** 58<sup>th</sup> Eastern Snow Conference Ottawa, Ontario, Canada 209-218.
- Kane, D.L., Stein, J. (1983). **Water movement into seasonally frozen soils.** *Water Resources Research*, 19(6): 1547 – 1557.  
<https://doi.org/10.1029/WR019i006p01547>
- Kulik, V. Y. 1978. **Water Infiltration into Soil** (in Russian).  
 Gidrometeoizdat.
- Kurylyk, B.L., Watanabe, K. (2013). **The mathematical representation of freezing and thawing processes in variably-saturated, non-deformable soils.** *Advances in Water Resources*, 60: 160-177.  
<https://doi.org/10.1016/j.advwatres.2013.07.016>
- Larsbo, M., Holten, R., Stenrød, M., Eklo, O.M., Jarvis, N. (2019). **A dual-permeability approach for modeling soil water flow and heat transport during freezing and thawing.** *Vadose Zone Journal*, 18.  
<http://dx.doi.org/10.2136/vzj2019.01.0012>
- Lein, W.A., Slone, S.M., Smith, C.E., Bernier, A.P. (2019). **Frost depth penetration and frost heave in frost susceptible soils.** In: *International Airfield and Highway Pavements Conference 2019*.
- McCauley, C.A., White, D.M., Lilly, M.R., Nyman, D.M. (2002). **A comparison of hydraulic conductivities, permeabilities and infiltration rates in frozen and unfrozen soils.** *Cold Regions Science and Technology* 34(2): 117-125.  
[https://doi.org/10.1016/S0165-232X\(01\)00064-7](https://doi.org/10.1016/S0165-232X(01)00064-7)
- Miller, R.D. (1980). **Freezing phenomena in soils.** In Hillel, D. (ed.) *Application of Soil Physics*, Academic Press. 254-299.
- Mohammed, A. A., Kurylyk, B.L., Cey, E.E., Hayashi, M. (2018). **Snowmelt Infiltration and Macropore Flow in Frozen Soils: Overview,**

- Knowledge Gaps, and a Conceptual Framework.** *Vadose Zone Journal*, 17(1): 1-15. <https://doi.org/10.2136/vzj2018.04.0084>
- Mohammed, A.A., Cey, E.E., Hayashi, M., Callaghan, M.V., Park, Y-J., Miller, K.L., Frey, S.K. (2021). **Dual-permeability modelling of preferential flow and snowmelt partitioning in frozen soils.** *Vadose Zone Journal*, 20. <https://doi.org/10.1002/vzj2.20101>
- Mualem, Y. (1976). **A new model predicting the hydraulic conductivity of unsaturated porous media.** *Water Resources Research*, 12: 513-522.
- Nyberg, L., Stähli, M., Mellander, P., Bishhop, K.H. (2001). **Soil frost effects on soil water and runoff dynamics along a boreal forest transect: 1. Field investigations.** *Hydrological Processes*, 15: 909-926. <https://doi.org/10.1002/hyp.256>
- Pittman, F., Mohammed, A., Cey, E. (2020). **Effects of antecedent moisture and microporosity on infiltration and water flow in frozen soil.** *Hydrological Processes*, 34: 795-809. <https://doi.org/10.1002/hyp.13629>
- Rango, A., DeWalle, D.R. (2008). **Principles of Snow Hydrology.** Cambridge: Cambridge University Press.
- Richards, L.A. (1931). **Capillary conduction of liquids through porous mediums.** *Physics*, 1(5): 318-333. <https://doi.org/10.1063/1.1745010>
- Stähli, M., Jansson, P., Lundin, L. (1999). **Soil moisture redistribution and infiltration into sandy soils.** *Water Resources Research*, 35(1): 95-103. <https://doi.org/10.1016/j.jhydrol.2016.12.032>
- Stähli, M. (2017). **Hydrological significance of soil frost for pre-alpine areas.** *Journal of Hydrology*, 546: 90-102. <https://doi.org/10.1016/j.jhydrol.2016.12.032>
- Šimůnek, J., Šejna, M., van Genuchten, M. T. (1998). **The HYDRUS-1D software package for simulating the one-dimensional movement of**

**water, heat, and multiple solutes in variably-saturated media.**

**Version 1.0.** IGWMC – TPS – 70, International Ground Water Modeling Center, Colorado School of Mines, Golden, Colorado.

- Starkloff, T. (2017). **Winter hydrology and soil erosion processes in an agricultural catchment in Norway.** PhD thesis. Wageningen: Wageningen University.
- Stuurop, J.C., van der Zee, S.E.A.T.M., Voss, C.I., French, H.K. (2021). **Simulating water and heat transport with freezing and cryosuction in unsaturated soil. Comparing an empirical, semi-empirical and physically-based approach.** *Advances in Water Resources*, 149. <https://doi.org/10.1016/j.advwatres.2021.103846>
- Unold, F., Derk, L. (2017). **Cryosuction – A model to describe the mechanism during ground freezing.** *PanAm Unsaturated Soils*, 2017: 290-299. <https://doi.org/10.1061/9780784481691.029>
- Wang, Q., Liu, J., Wang, L. (2017). **An experimental study on the effects of freeze-thaw cycles on phosphorus adsorption-desorption processes in brown soil.** *RSC Advances*, 7: 37441-37466. <https://doi.org/10.1039/C7RA05220K>
- Watanabe, K., Osada, Y. (2017). **Simultaneous measurement of liquid water content and hydraulic conductivity of partially frozen soil near 0 °C.** *Cold Regions Science and Technology*, 142: 79 – 84. <https://doi.org/10.1016/j.coldregions.2017.08.002>
- Watanabe, K., Kito, T., Dun, S., Wu, J.Q., Greer, R.C., Flury, M. (2012). **Water infiltration into a frozen soil with simultaneous melting of the frozen layer.** *Vadose Zone Journal*, 12(1). <https://doi.org/10.2136/vzj2011.0188>
- Williams. P.J., Smith, M.W. (1989). **The Frozen Earth. Fundamentals of geocryology.** Cambridge: Cambridge University Press.

- Zhang, X., Sun, S.F., Xue, Y. (2007). **Development and testing of a frozen soil parameterization for cold region studies.** *American Meteorological Society*, 8: 690-701. <https://doi.org/10.1175/JHM605.1>
- Zhang, N., Wang, Z. (2017). **Review of soil thermal conductivity and predictive models.** *International Journal of Thermal Sciences*, 117: 172 – 183. <https://doi.org/10.1016/j.ijthermalsci.2017.03.013>
- Zhao, L., Gray, D.M. (1998). **A parametric expression for estimating infiltration into frozen soils.** *Hydrological Processes*, 11(13): 1761 – 1775. [https://doi.org/10.1002/\(SICI\)1099-1085\(19971030\)11:13<1761::AID-HYP604>3.0.CO;2-O](https://doi.org/10.1002/(SICI)1099-1085(19971030)11:13<1761::AID-HYP604>3.0.CO;2-O)
- Zhao, Y., Nishimura, T., Hill, R., Miyazaki, T. (2013). **Determining hydraulic conductivity for air-filled porosity in an unsaturated frozen soil by the multistep outflow method.** *Vadose Zone Journal*, 12(1): 1-10. <https://doi.org/10.2136/vzj2012.0061>

## Chapter 5

- Ala-Aho, P., Autio, A., Bhattacharjee, J., Isokangas, E., Kujala, K., Marttila, H., Menberu, M., Meriö, L. J., Postila, H., Rauhala, A., Ronkanen, A. K., Rossi, P. M., Saari, M., Haghghi, A. T., & Klove, B. (2021). **What conditions favor the influence of seasonally frozen ground on hydrological partitioning? A systematic review.** *Environmental Research Letters*, 16(4): 043008. <https://doi.org/10.1088/1748-9326/ABE82C>
- Demand, D., Selker, J. S., & Weiler, M. (2019). **Influences of Macropores on Infiltration into Seasonally Frozen Soil.** *Vadose Zone Journal*, 18(1): 1–14. <https://doi.org/10.2136/VZJ2018.08.0147>
- DeWalle, D. R., & Rango, A. (2008). **Principles of snow hydrology.** Cambridge: Cambridge University Press.
- Fang, X., & Pomeroy, J. W. (2016). **Impact of antecedent conditions on simulations of a flood in a mountain headwater basin.** *Hydrological Processes*, 30(16): 2754–2772. <https://doi.org/10.1002/HYP.10910>
- French, H., & Binley, A. (2004). **Snowmelt infiltration: Monitoring temporal and spatial variability using time-lapse electrical resistivity.** *Journal of Hydrology*, 297(1–4): 174–186. <https://doi.org/10.1016/J.JHYDROL.2004.04.005>
- Garstka, W. U. (1944). **Hydrology of small watersheds under winter conditions of snow-cover and frozen soil.** *Eos, Transactions American Geophysical Union*, 25(6): 838–874. <https://doi.org/10.1029/TR025I006P00838>
- Genuchten, M. Th. van. (1980). **A Closed-form Equation for Predicting the Hydraulic Conductivity of Unsaturated Soils.** *Soil Science Society of America Journal*, 44(5): 892–898. <https://doi.org/10.2136/SSSAJ1980.03615995004400050002X>
- Hamada, A., Ashraf A.E., Elawady, A. Lin, W.E. (2014). **State-of-the-Art Knowledge about Behaviour of Transmission Line Structures under Downbursts and Tornadoes.** Conference: 2014 International

Conference on Advances in Wind and Structures (AWAS14) -  
ACEM14At: Busan, Korea.

Hayashi, M., van der Kamp, G., & Schmidt, R. (2003). **Focused infiltration of snowmelt water in partially frozen soil under small depressions.** *Journal of Hydrology*, 270(3–4): 214–229.  
[https://doi.org/10.1016/S0022-1694\(02\)00287-1](https://doi.org/10.1016/S0022-1694(02)00287-1)

Manning, R. (1891). **On the flow of water in open channels and pipes.** Transactions of the Institution of Civil Engineers of Ireland. 20: 161–207.

McCauley, C. A., White, D. M., Lilly, M. R., & Nyman, D. M. (2002). **A comparison of hydraulic conductivities, permeabilities and infiltration rates in frozen and unfrozen soils.** *Cold Regions Science and Technology*, 34(2): 117–125. [https://doi.org/10.1016/S0165-232X\(01\)00064-7](https://doi.org/10.1016/S0165-232X(01)00064-7)

Mohammed, A. A., Cey, E. E., Hayashi, M., & Callaghan, M. v. (2021). **Simulating preferential flow and snowmelt partitioning in seasonally frozen hillslopes.** *Hydrological Processes*, 35(8): e14277.  
<https://doi.org/10.1002/HYP.14277>

Mohammed, A. A., Kurylyk, B. L., Cey, E. E., & Hayashi, M. (2018). **Snowmelt Infiltration and Macropore Flow in Frozen Soils: Overview, Knowledge Gaps, and a Conceptual Framework.** *Vadose Zone Journal*, 17(1): 1–15. <https://doi.org/10.2136/VZJ2018.04.0084>

Pittman, F., Mohammed, A., & Cey, E. (2020). **Effects of antecedent moisture and macroporosity on infiltration and water flow in frozen soil.** *Hydrological Processes*, 34(3): 795–809.  
<https://doi.org/10.1002/HYP.13629>

Richards, L. A. (2004). **Capillary conduction of liquids through porous mediums.** *Physics*, 1(5): 318. <https://doi.org/10.1063/1.1745010>

Saadat, S., Frankenberger, J., Bowling, L., & Ale, S. (2020). **Evaluation of surface ponding and runoff generation in a seasonally frozen drained agricultural field.** *Journal of Hydrology*, 588.  
<https://doi.org/10.1016/J.JHYDROL.2020.124985>

- Stuuroop, J. C., van der Zee, S. E. A. T. M., & French, H. K. (2022). **The influence of soil texture and environmental conditions on frozen soil infiltration: A numerical investigation.** *Cold Regions Science and Technology*, 194: 103456.  
<https://doi.org/10.1016/J.COLDREGIONS.2021.103456>
- Stuuroop, J. C., van der Zee, S. E. A. T. M., Voss, C. I., & French, H. K. (2021). **Simulating water and heat transport with freezing and cryosuction in unsaturated soil: Comparing an empirical, semi-empirical and physically-based approach.** *Advances in Water Resources*, 149: 103846. <https://doi.org/10.1016/J.ADVWATRES.2021.103846>
- Walter U. Garstka (1945): **Hydrology of Small Watersheds under Winter Conditions of SnowCover and Frozen Soil**, Transactions American Geophysical Union of 1944, part VI, pages 838-871, May 1945.
- Watanabe, K., & Kugisaki, Y. (2017). **Effect of macropores on soil freezing and thawing with infiltration.** *Hydrological Processes*, 31(2): 270–278.  
<https://doi.org/10.1002/HYP.10939>
- Zhang, X., Sun, S. F., & Xue, Y. (2007). **Development and Testing of a Frozen Soil Parameterization for Cold Region Studies.** *Journal of Hydrometeorology*, 8(4): 690–701. <https://doi.org/10.1175/JHM605.1>
- Zuzel, J. F., Allmaras, R. R., & Greenwalt, R. (1982). **Runoff and soil erosion on frozen soils in northeastern Oregon.** *Journal of Soil and Water Conservation*, 37(6): 351–354.  
<https://www.jswconline.org/content/37/6/351>

## Chapter 6

- Carsel, R. F., & Parrish, R. S. (1988). **Developing joint probability distributions of soil water retention characteristics.** *Water Resources Research*, 24(5): 755–769. <https://doi.org/10.1029/WR024I005P00755>
- Dussailant, A. R., Wu, C. H., & Potter, K. W. (2004). **Richards Equation Model of a Rain Garden.** *Journal of Hydrologic Engineering*, 9(3): 219–225. [https://doi.org/10.1061/\(ASCE\)1084-0699\(2004\)9:3\(219\)](https://doi.org/10.1061/(ASCE)1084-0699(2004)9:3(219))
- Lundekvam, H. E. (2007). **Plot studies and modelling of hydrology and erosion in southeast Norway.** *CATENA*, 71(2): 200–209. <https://doi.org/10.1016/J.CATENA.2007.03.004>
- Mentens, J., Raes, D., & Hermy, M. (2006). **Green roofs as a tool for solving the rainwater runoff problem in the urbanized 21st century?** *Landscape and Urban Planning*, 77(3): 217–226. <https://doi.org/10.1016/J.LANDURBPLAN.2005.02.010>
- Zhou, X., Zhou, J., Kinzelbach, W., & Stauffer, F. (2014). **Simultaneous measurement of liquid water content and ice content in frozen soil using gamma ray attenuation and TDR.** *Water Resources Research*, 50(12): 9630–9655. <https://doi.org/10.1002/2014WR015640>



## Chapter 7

- Appels, W.M., Coles, A., McDonnell, J.J. (2017). **Infiltration into frozen soil: From core-scale dynamics to hillslope-scale connectivity.** *Hydrological Processes*, 32: 66-79. <https://doi.org/10.1002/hyp.11399>
- Banaszuk, P., Krasowska, M., Kamocki, A. (2013). **Transport of contaminants in agricultural catchments during snowmelt: buffer strips vs. preferential flow paths.** *Ecohydrology & Hydrobiology*, 13(1): 31-40. <https://doi.org/10.1016/j.ecohyd.2013.03.005>
- Chiba, T., Thiis, T. (2016). **Accuracy of Snow Depth Measurements on Roofs measured with Photogrammetry.** Conference: International Conference on Snow Engineering 2016, Nantes, France.
- Deelstra, J., Kværnø, S.H., Granlund, K., Sileika, A.S., Gaigalis, K., Kyllmard, K. and Vagstada, N. (2009). **Runoff and nutrient losses during winter periods in cold climates— requirements to nutrient simulation models.** *Journal of Environmental Monitoring*, 11: 602-609. DOI: 10.1039/b900769p
- Flaten, O. (2001). **Food security and international trade: The Norwegian case.** Conference: 77<sup>th</sup> EAAE Seminar / NJF Seminar No. 325, August 17-18, 2001, Helsinki.
- Fučík, P., Kaplická, P., Kvítek, T., Peterková, J. (2011). **Dynamics of Stream Water Quality during Snowmelt and Rainfall – Runoff Events in a Small Agricultural Catchment.** *Clean Soil Air Water*, 40(2): 154-163.
- van Genuchten, M. (1980). **A closed-form equation for predicting the hydraulic conductivity of unsaturated soils.** *Soil Science Society of America Journal*, 44(5): 892-898. <http://dx.doi.org/10.2136/sssaj1980.03615995004400050002x>

- Granger, R.J., Gray, D.M., Dyck, G.E. (1984). **Snowmelt infiltration to frozen prairie soils**. *Canadian Journal of Earth Sciences*, 22: 464-72. <https://doi.org/10.1139/e84-073>
- Gray, D.M., Granger, R.J., Landine, P.G. (1986). **Modelling snowmelt infiltration and runoff in a prairie environment**. In *Proceedings of the Cold Regions Hydrology Symposium*, Kane D.L. (ed.). AWRA, Bethesda, MD; 427-438.
- Hayashi, M. (2013). **The cold vadose zone. Hydrological and ecological significance of frozen-soil processes**. *Vadose Zone Journal*, 12(4). <https://doi.org/10.2136/vzj2013.03.0064>
- Hoffman, A.R., Polebitski, A.S., Penn, M.R., Busch, D.L. (2019). **Long-term Variation in Agricultural Edge-of-Field Phosphorus Transport during Snowmelt, Rain, and Mixed Runoff Events**. *Journal of Environmental Quality*, 48(4): 931-940. <https://doi.org/10.2134/jeq2018.11.0420>
- Jones, H.G., Pomeroy, J.W. (2001). **Early spring snowmelt in a small boreal forest watershed: influence of concrete frost on the hydrology and chemical composition of streamwaters during rain-on-snow events**. 58<sup>th</sup> Eastern Snow Conference Ottawa, Ontario, Canada 209-218.
- Kindzewicz, Z.W., Luger, N., Dankers, R., Hirabayashi, Y., Döl, P., Pińskwar, I., Dysarz, T., Hochrainer, S., Matczak, P. (2010). **Assessing river flood hazard and adaptation in Europe – review of projections for the future**. *Mitigation and Adaptation Strategies for Global Change*, 15: 641-656. <https://doi.org/10.1007/s11027-010-9213-6>
- Kværnø, S.H., Haugen, L.E., Børresen, T. (2007). **Variability in topsoil texture and carbon content within soil map units and its implications in predicting soil water content for optimum workability**. *Soil & Tillage Research*, 95: 332-347.

- Lundekvam, H., Skøien, S. (1998). **Soil erosion in Norway. An overview of measurements from soil loss plots.** *Soil Use and Management*, 14: 84-89.
- Maltsev, K., Yermolaev, O. (2020). **Assessment of soil loss by water erosion in small river basins in Russia.** *CATENA*, 195: 104726.  
<https://doi.org/10.1016/j.catena.2020.104726>
- McCool, D.K. (2020). **Erosion: Snowmelt. Chapter in: Managing Soils and Terrestrial Systems**, CRC Press 2020, second edition.
- Ollesch, G., Kistner, I., Meissner, R., Lindenschmidt, K-E. (2006). **Modelling of snowmelt erosion and sediment yield in a small low-mountain catchment in Germany.** *CATENA*, 68(2-3): 161-176.
- Øygarden, L., Deelstra, J., Blankenberg, A.G.B., Hauge, A., Kitterød, N.O., Eggestad, H.O. (2011). **Runoff and mitigation measures in agricultural catchment under climate change in Norway.** In: Kelman, I. (Ed.), *Municipalities Addressing Climate Change, A Case Study of Norway*. 25-49. Nova Science Publisher.
- Parker, G. (1976). **On the cause and characteristic scales of meandering and braiding in rivers.** *Journal of Fluid Mechanics*, 76(3): 457-480.
- Richards, L.A. (1931). **Capillary conduction of liquids through porous mediums.** *Physics*, 1(5): 318-333. <https://doi.org/10.1063/1.1745010>
- Rango, A., DeWalle, D.R. (2008). **Principles of Snow Hydrology.** Cambridge: Cambridge University Press.
- Rodzik, J., Furtak, T., Zglobicki, W. (2009). **The impact of snowmelt and heavy rainfall runoff on erosion rates in a gully system, Lublin**

- Upland, Poland.** *Earth Surface Processes and Landforms*, 34(14): 1938-1950.
- Sauer, D., Schüllli-Maurera, I., Sperstad, R., Sørensen, R., Stahr, K. (2009). **Albeluvisol development with time in loamy marine sediments of southern Norway.** *Quaternary International*, 209(1-2): 31-43.  
<https://doi.org/10.1016/j.quaint.2008.09.007>
- Starkloff, T. (2017). **Winter hydrology and soil erosion processes in an agricultural catchment in Norway.** PhD thesis. Wageningen: Wageningen University.
- Starkloff, T., Stolte, J., Hessel, R., Ritsema, C., Jetten, V. (2018). **Integrated, spatial distributed modelling of surface runoff and soil erosion during winter and spring.** *CATENA*, 166: 147-157.  
<https://doi.org/10.1016/j.catena.2018.04.001>
- Stuurop, J.C., van der Zee, S.E.A.T.M., Voss, C.I., French, H.K. (2021). **Simulating water and heat transport with freezing and cryosuction in unsaturated soil. Comparing an empirical, semi-empirical and physically-based approach.** *Advances in Water Resources*, 149.  
<https://doi.org/10.1016/j.advwatres.2021.103846>
- Stuurop, J.C., van der Zee, S.E.A.T.M., French, H.K. (2022). **The influence of soil texture and environmental conditions on frozen soil infiltration: A numerical investigation.** *Cold Regions Science and Technology*, 194.  
<https://doi.org/10.1016/j.coldregions.2021.103456>
- Su, J.J., van Bochove, E., Thériault, G., Novotna, B., Khaldoune, J., Denault, J.T., Zhou, J., Nolin, M.C., Hu, C.X., Bernier, M., Benoy, G., Xing, Z.S., Chow, L. (2011). **Effects of snowmelt on phosphorus and sediment losses from agricultural watersheds in Eastern Canada.** *Agricultural Water Management*, 98(5): 867-876.  
<https://doi.org/10.1016/j.agwat.2010.12.013>

- Tang, J., Liu, G., Xie, Y., Duan, X., Wang, D., Zhang, S. (2021). **Ephemeral gullies caused by snowmelt: A ten-year study in northeastern China.** *Soil and Tillage Research*, 212.  
<https://doi.org/10.1016/j.still.2021.105048>
- Thue-Hansen, V., Grimenes, A.A. (2015). **Metereologiske Data for Ås 2014.** Norwegian University of Life Sciences, Norway.
- Yakatina, O.P., Nechaeva, T.V., Smirnova N.V. (2015). **Consequences of snowmelt erosion. Soil fertility, productivity and quality of wheat on Greyzemic Phaeozem in the south of West Siberia.** *Agriculture, Ecosystems & Environment*, 200: 88-93.  
<https://doi.org/10.1016/j.agee.2014.10.021>
- Wade, R.J., Kirkbride, P. (1998). **Snowmelt-generated runoff and soil erosion in Fife, Scotland.** *Earth Surface Process and Landforms*, 23(2): 123-132. [https://doi.org/10.1002/\(SICI\)1096-9837\(199802\)23:2<123::AID-ESP818>3.0.CO;2-D](https://doi.org/10.1002/(SICI)1096-9837(199802)23:2<123::AID-ESP818>3.0.CO;2-D)
- Zuzel, J.F., Allmaras, R. R., Greenwalt, R. (1982). **Runoff and soil erosion on frozen soils in northeastern Oregon.** *Journal of Soil and Water Conversation*, 37(6): 351-354.

## Chapter 8

- Berkowitz, B., & Ewing, R. P. (1998). **Percolation theory and network modeling applications in soil physics.** *Surveys in Geophysics*, 19(1): 23–72. <https://doi.org/10.1023/A:1006590500229>

- Decker, K. L. M., Wang, D., Waite, C., & Scherbatskoy, T. (2003). **Snow Removal and Ambient Air Temperature Effects on Forest Soil Temperatures in Northern Vermont.** *Soil Science Society of America Journal*, 67(4): 1234–1242. <https://doi.org/10.2136/SSSAJ2003.1234>
- Dong, Y., McCartney, J. S., & Lu, N. (2015). **Critical Review of Thermal Conductivity Models for Unsaturated Soils.** *Geotechnical and Geological Engineering*, 33(2): 207–221. <https://doi.org/10.1007/S10706-015-9843-2>
- Gaidos, E. J., & Nimmo, F. (2000). **Tectonics and water on Europa.** *Nature*, 405(6787): 637–637. <https://doi.org/10.1038/35015170>
- Grotzinger, J. (2009). **Beyond water on Mars.** *Nature Geoscience*, 2(4): 231–233. <https://doi.org/10.1038/ngeo480>
- Hardy, J. P., Groffman, P. M., Fitzhugh, R. D., Henry, K. S., Welman, A. T., Demers, J. D., Fahey, T. J., Driscoll, C. T., Tierny, G. L., Nolan, S. (2001). **Snow depth manipulation and its influence on soil frost and water dynamics in a northern hardwood forest.** *Biogeochemistry*, 56: 151–174.
- Harlan, R. L. (1973). **Analysis of coupled heat-fluid transport in partially frozen soil.** *Water Resources Research*, 9(5): 1314–1323. <https://doi.org/10.1029/WR009I005P01314>
- Jame, Y. -W, & Norum, D. I. (1980). **Heat and mass transfer in a freezing unsaturated porous medium.** *Water Resources Research*, 16(4): 811–819. <https://doi.org/10.1029/WR016I004P00811>
- Journal, A. I., Stähli, M., Bayard, D., Wydler, H., Flüher, H., & Flüherà, H. (2004). **Snowmelt Infiltration into Alpine Soils Visualized by Dye Tracer Technique.** *Arctic, Antarctic, and Alpine Research*, 36(1): 128–135. [https://doi.org/10.1657/1523-0430\(2004\)036](https://doi.org/10.1657/1523-0430(2004)036)
- Kane, S. R., Arney, G., Crisp, D., Domagal-Goldman, S., Glaze, L. S., Goldblatt, C., Grinspoon, D., Head, J. W., Lenardic, A., Unterborn, C., Way, M. J., & Zahnle, K. J. (2019). **Venus as a Laboratory for Exoplanetary Science.** *Journal of Geophysical Research: Planets*, 124(8): 2015–2028. <https://doi.org/10.1029/2019JE005939>

- Kurylyk, B. L., & Watanabe, K. (2013). **The mathematical representation of freezing and thawing processes in variably-saturated, non-deformable soils.** *Advances in Water Resources*, 60: 160–177.  
<https://doi.org/10.1016/J.ADVWATRES.2013.07.016>
- Lundin, L. C. (1990). **Hydraulic properties in an operational model of frozen soil.** *Journal of Hydrology*, 118(1–4): 289–310.  
[https://doi.org/10.1016/0022-1694\(90\)90264-X](https://doi.org/10.1016/0022-1694(90)90264-X)
- Neuman, S. P. (1977). **Theoretical derivation of Darcy's law.** *Acta Mechanica*, 25(3–4): 153–170. <https://doi.org/10.1007/BF01376989>
- Newman, G. P., & Wilson, G. W. (1997). **Heat and mass transfer in unsaturated soils during freezing.** *Canadian Geotechnical Journal*, 34(1): 63–70. <https://doi.org/10.1139/T96-085/ASSET/T96-085>
- O', C. M., Alexander, D., Mckeegan, K. D., Altwegg, K., Blanc, M., Morbidelli, A., Alibert, Y., Elkins-Tanton, L., Estrada, P., Hamano, K., Lammer, H., Raymond, S., Schönbächler, M., Mckeegan, K. D., & Altwegg, K. (2018). **Water Reservoirs in Small Planetary Bodies: Meteorites, Asteroids, and Comets.** *Space Science Reviews*, 214(1): 1–47.  
<https://doi.org/10.1007/S11214-018-0474-9>
- Painter, S. L. (2011). **Three-phase numerical model of water migration in partially frozen geological media: Model formulation, validation, and applications.** *Computational Geosciences*, 15(1): 69–85.  
<https://doi.org/10.1007/S10596-010-9197-Z>
- Robinson, K. L., & Taylor, G. J. (2014). **Heterogeneous distribution of water in the Moon.** *Nature Geoscience*, 7(6): 401–408.  
<https://doi.org/10.1038/ngeo2173>
- Seager, S. (2013). **Exoplanet habitability.** *Science*, 340(6132): 577–581.  
<https://doi.org/10.1126/SCIENCE.1232226>
- Shanley, J. B., & Chalmers, A. (1999). **The effect of frozen soil on snowmelt runoff at Sleepers River, Vermont.** *Hydrological Processes*, 13: 1843–1857. [https://doi.org/10.1002/\(SICI\)1099-1085\(199909\)13:12/13](https://doi.org/10.1002/(SICI)1099-1085(199909)13:12/13)
- Waite, J. H., Lewis, W. S., Magee, B. A., Lunine, J. I., McKinnon, W. B., Glein, C. R., Mousis, O., Young, D. T., Brockwell, T., Westlake, J., Nguyen, M. J.,

Teolis, B. D., Niemann, H. B., McNutt, R. L., Perry, M., & Ip, W. H. (2009). **Liquid water on Enceladus from observations of ammonia and 40Ar in the plume.** *Nature*, 460(7254): 487–490.  
<https://doi.org/10.1038/nature08153>

Zaqout, T., Andradóttir, H.Ó., Sørensen, J. (2023). **Trends in soil frost formation in a warming maritime climate and the impacts on urban flood hazard.** *Journal of Hydrology*, 617(A): 128978.  
<https://doi.org/10.1016/j.jhydrol.2022.128978>

Zhu L., Ives, A. R., Zhang, C., Guo, Y., Radeloff V. C. (2019). **Climate change causes functionally colder winters for snow cover-dependent organisms.** *Nature Climate Change*, 9: 886-893.  
<https://doi.org/10.1038/s41558-019-0588-4>



## 12. Appendices

### Appendix A. Chapter 3

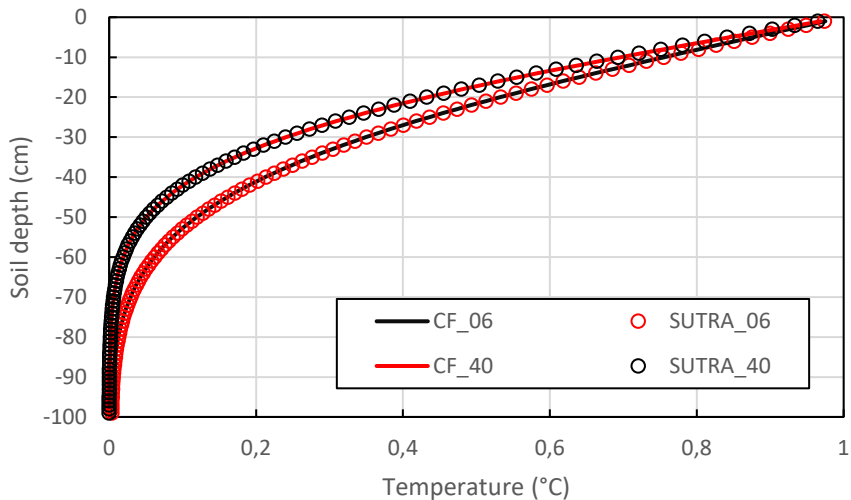
#### Comparison of model basic energy and water transport with SUTRA and HYDRUS1D

SUTRA was originally developed for saturated and unsaturated groundwater flow of variable density with solute or energy transport, but it has been extended to include the freeze-thaw process (beta version used, called SUTRA-ICE). It uses Galerkin finite element and finite difference methods. HYDRUS-1D is a model used for water, heat and solute flow in variably saturated media. Its numerical solver is based on Galerkin type linear finite elements. Both models have been in the public domain for decades and have been applied to numerous case studies.

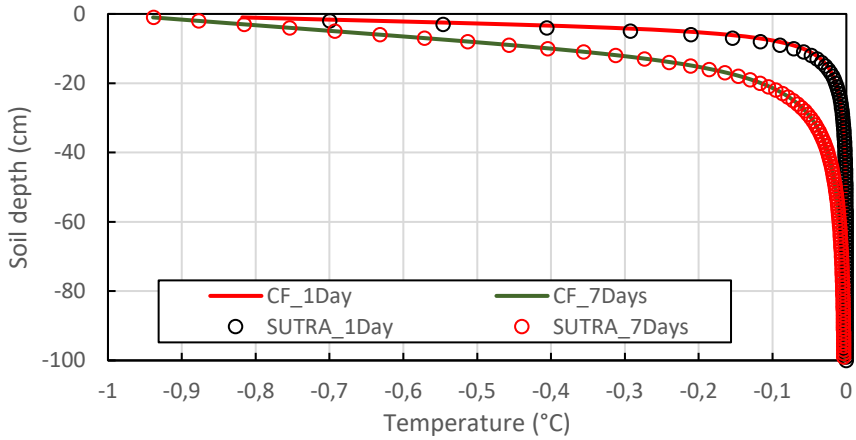
For the comparisons with our model, we set up a 1D model domain with a vertical extent of 1 meter, a no-flux (energy or water) bottom boundary (at a depth of 1 m) and constant top boundary conditions (at an elevation of 0 m). We chose different scenarios to test the unsaturated flow, heat conduction, latent heat flux and advection. Parameters and other conditions are listed in Table A for the six scenarios considered (parameter constants used are listed in Table 2 in the main text). Results are shown in Figures A-E. These show a nearly identical fit between output of HYDRUS1D or SUTRA-ICE for all cases considered compared to the model used in this study (empirical approach used, designated with “CF”).

Table A. Parameter and variable values used in the comparative scenario simulations with the model used in this study (CF), SUTRA-ICE and HYDRUS-1D (only scenario 4).

Parameter/ variable	Scenario 1 (warming - unsaturated)	Scenario 2 (warming - saturated)	Scenario 3 (freezing - saturated)	Scenario 4 (thawing - saturated)	Scenario 5 (infiltration)	Scenario 6 (advection)
$K_{sat}$ ( $ms^{-1}$ )	1e-05	1e-05	1e-05	1e-05	2.89e-06	2.89e-06
$\epsilon$	0.4	0.4	0.4	0.4	0.4	0.4
$a$ ( $cm^{-1}$ )	0.145	0.145	0.145	0.145	0.036	0.036
$n$	2.68	2.68	2.68	2.68	1.56	1.56
$\theta_{init}$	0.06	0.4	0.4	0.4	0.10	0.10
$\theta_{res}$	0.01	0.01	0.01	0.01	0.01	0.01
$w$ (SFC)			0.5	0.5		
$T_{init}$ ( $^{\circ}C$ )	0	0	0	-1	1	0
$T_{top}$ ( $^{\circ}C$ )	1	1	-1	1		
$c_{soil}$ ( $Wm^{-1}K^{-1}$ )	1.5	1.5	1.5	1.5	1.5	1.5
Source Flow					2 mm/hr	5 mm/hr
Source T ( $^{\circ}C$ )						5
Simulation time	24 hrs	24 hrs	168 hrs	72 hrs	168 hrs	48 hrs



**Figure A.** Comparison of simulated temperatures after 24 hours of the model used in this study and SUTRA-ICE with two different initial water contents (0.06 and 0.4; scenario 1 and 2, respectively), a top boundary of 1 °C and uniform initial temperature of 0 °C. CF is the empirical version of the model used in this study.



**Figure B.** Comparison of simulated temperatures after 24 and 168 hours of the model used in this study and SUTRA-ICE with a top boundary of  $-1\text{ }^{\circ}\text{C}$  and a uniform initial temperature of  $0\text{ }^{\circ}\text{C}$  (scenario 3). CF is the empirical version of the model used in this study.

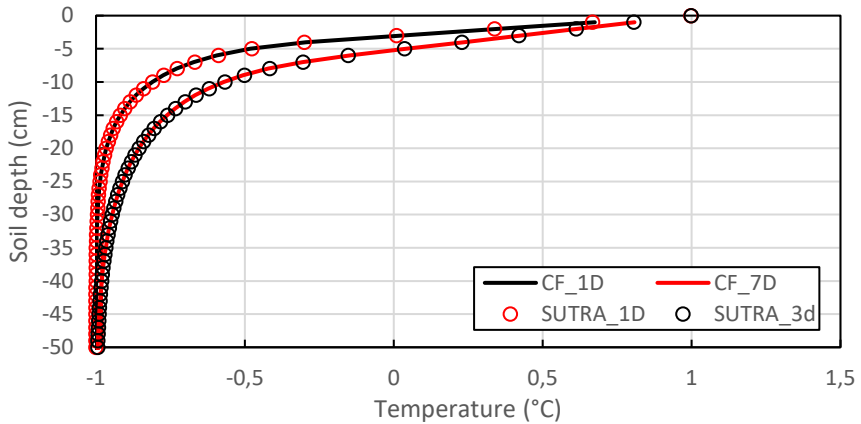


**Figure C.** Comparison of simulated temperatures after 24 and 72 hours of the model used in this study and SUTRA-ICE with a top boundary of  $1\text{ }^{\circ}\text{C}$  and a uniform initial temperature of  $-1\text{ }^{\circ}\text{C}$  (scenario 4). Only 0 to 50 cm depth shown of total 100 cm depth in the simulation. CF is the empirical version of the model used in this study.

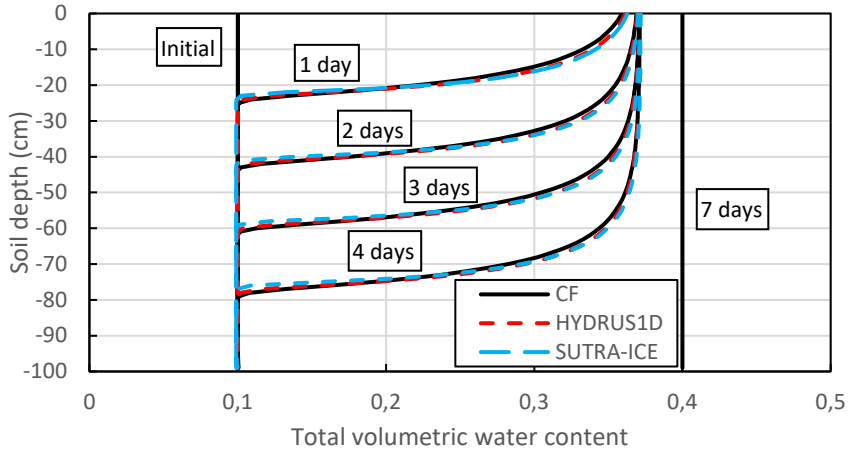


**Figure D.** Comparison of simulated water contents after 1, 2, 3, 4 and 7 days of the model used in this study, HYDRUS1D and SUTRA-ICE with a top boundary sourceflow of 2 mm per hour (scenario 5). CF is the empirical version of the model used in this study.

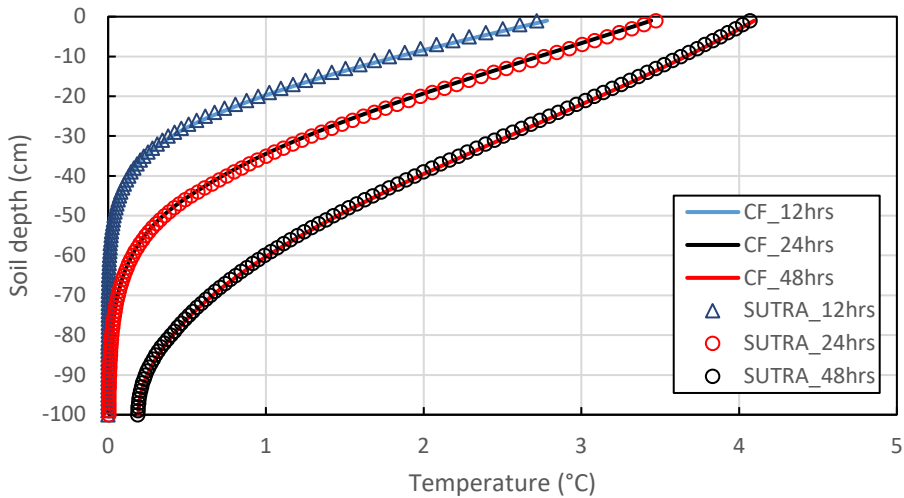


**Figure E.** Comparison of simulated temperature after 12, 24 and 48 hours of the model used in this study and SUTRA-ICE with a top boundary sourceflow of 5 mm per hour with a water temperature of 5 °C and no specified temperature boundaries (scenario 6). CF is the empirical version of the model used in this study.

## Appendix B. Chapter 4

Cross-tabulations showing the number of cases for each variable combination in which infiltration reduction due to freezing was at least 75%. A red-white colour gradient is applied to each cross-tabulation, with white being the lowest value, red the highest value. The total number of cases in which each variable combination occurred is also given.

Total cases: 36		Initial Saturation					
Soil Type	Freezing Temperature	0.40	0.50	0.60	0.75	0.90	1.00
2	-4.00				4	4	4
	-3.00				3	4	4
3	-4.00			3	8	9	9
	-3.00			3	5	5	8
	-2.00			2	5	6	6
	-1.00				3	4	3
	-.50					1	2
4	-4.00		5	27	24	34	31
	-3.00		5	27	23	34	30
	-2.00			27	23	31	26
	-1.00			27	16	27	20
	-.50			23	10	22	11
	-.25			20	6	15	7
5	-4.00	2	8	13	27	32	34
	-3.00		5	12	27	31	32
	-2.00		4	11	25	28	29
	-1.00		3	10	19	23	24
	-.50			6	10	15	16
	-.25			3	6	9	9
6	-4.00	3	5	8	16	21	22
	-3.00	2	5	8	15	20	20
	-2.00	1	4	6	13	17	18
	-1.00		2	5	9	11	13
	-.50		1	2	4	7	7
	-.25			1	2	4	4
7	-4.00		2	5	12	22	23
	-3.00		1	5	10	22	22
	-2.00			2	9	19	19
	-1.00			1	6	14	14
	-.50				3	9	9
	-.25				2	4	4
Total cases: 36		Initial Saturation					
Soil Type	Thawing Temperature	0.40	0.50	0.60	0.75	0.90	1.00
2	.0				7	8	8
3	.0			7	17	21	22
	.5			1	3	3	5
	1.0					1	1
	2.0				1		
4	.0		9	36	33	36	35
	.5		1	34	23	33	26
	1.0			28	17	30	22
	2.0			22	12	26	17
	3.0			17	10	19	13

<i>Total cases: 36</i>		<b>Initial Saturation</b>					
<b>Soil Type</b>	<b>Inflow rate</b>	0.4	0.5	0.6	0.75	0.9	1
2	1.00				2	2	2
	2.00				2	2	2
	3.00				2	2	2
	4.00				1	2	2
3	.25					1	2
	.50				3	3	3
	1.00			2	4	4	4
	2.00			3	5	6	7
	3.00			1	5	6	6
	4.00			2	4	5	6
4	.25			1	4	15	8
	.50		2	16	10	22	14
	1.00		2	22	12	27	21
	2.00		2	33	22	31	25
	3.00		3	35	26	34	28
	4.00		1	35	28	34	29
5	.25				4	10	11
	.50		1	4	10	16	18
	1.00		3	6	18	23	24
	2.00	1	5	13	25	28	29
	3.00	1	6	17	28	30	30
	4.00		5	15	29	31	32
6	.25			2	5	10	11
	.50		3	4	10	18	19
	1.00	2	4	7	19	24	25
	2.00	3	7	13	25	28	29
	3.00	1	3	4			
7	.25				3	13	14
	.50			2	7	21	21
	1.00		1	3	14	26	26
	2.00		2	6	18	30	30
	3.00			2			

<i>Total cases: 48</i>		Thawing temperature					
Soil Type	Freezing temperature	0	0.5	1	2	3	4
2	-4.00	12					
	-3.00	11					
3	-4.00	19	7	2	1		
	-3.00	19	2				
	-2.00	16	3				
	-1.00	10					
	-0.50	3					
4	-4.00	28	24	21	18	15	15
	-3.00	28	23	20	19	15	14
	-2.00	24	22	20	16	13	12
	-1.00	24	20	17	13	9	7
	-0.50	23	16	12	6	5	4
	-0.25	22	12	7	5	2	
5	-4.00	30	24	20	16	14	12
	-3.00	27	21	20	15	13	11
	-2.00	27	20	17	12	11	10
	-1.00	26	17	13	9	8	6
	-0.50	21	13	8	4	1	
	-0.25	17	8	2			
6	-4.00	24	15	12	9	8	7
	-3.00	23	14	12	8	8	5
	-2.00	21	12	9	7	5	5
	-1.00	18	9	6	4	2	1
	-0.50	14	5	2			
	-0.25	9	2				
7	-4.00	18	12	10	10	8	6
	-3.00	17	12	10	9	6	6
	-2.00	14	10	10	7	4	4
	-1.00	12	8	7	4	2	2
	-0.50	11	4	4	2		
	-0.25	8	2				

<i>Total cases: 48</i>		<b>Inflow rate</b>					
<b>Soil Type</b>	<b>Freezing temperature</b>	0.25	0.5	1	2	3	4
2	-4.00			3	3	3	3
	-3.00			3	3	3	2
3	-4.00	2	3	4	7	6	7
	-3.00	1	3	4	5	5	3
	-2.00		3	3	4	4	5
	-1.00			3	3	3	1
	-.50				2		1
4	-4.00	10	16	20	25	26	24
	-3.00	9	17	19	24	25	25
	-2.00	7	12	17	23	24	24
	-1.00	6	8	13	19	21	23
	-.50	3	6	8	13	18	18
	-.25	2	5	7	9	12	13
5	-4.00	8	16	20	24	25	23
	-3.00	7	13	19	22	24	22
	-2.00	5	9	17	22	22	22
	-1.00	3	6	9	18	21	22
	-.50	2	3	6	9	13	14
	-.25		2	3	6	7	9
6	-4.00	10	17	21	24	3	
	-3.00	8	15	21	24	2	
	-2.00	5	11	18	23	2	
	-1.00	3	6	12	18	1	
	-.50	2	3	6	10		
	-.25		2	3	6		
7	-4.00	10	15	18	20	1	
	-3.00	9	15	16	19	1	
	-2.00	7	9	16	17		
	-1.00	2	7	10	16		
	-.50	2	3	7	9		
	-.25		2	3	5		



<i>Total cases: 48</i>		<b>Inflow rate</b>					
<b>Soil Type</b>	<b>Thawing temperature</b>	0.25	0.5	1	2	3	4
2	.0			6	6	6	5
3	.0	3	9	14	17	13	11
	.5				4	4	4
	1.0					1	1
	2.0						1
4	.0	21	26	25	26	26	25
	.5	10	17	20	22	24	24
	1.0	4	11	18	20	22	22
	2.0	2	6	11	18	20	20
	3.0		2	5	15	18	19
	4.0		2	5	12	16	17
5	.0	14	22	26	29	29	28
	.5	6	11	15	22	25	24
	1.0	4	8	11	17	19	21
	2.0	1	4	9	12	16	14
	3.0	0	3	8	11	12	13
	4.0	0	1	5	10	11	12
6	.0	16	24	29	32	8	
	.5	7	11	16	23		
	1.0	4	8	12	17		
	2.0	1	5	10	12		
	3.0		4	8	11		
	4.0		2	6	10		
7	.0	13	19	22	24	2	
	.5	6	10	14	18		
	1.0	6	8	13	14		
	2.0	4	6	9	13		
	3.0	1	4	6	9		
	4.0		4	6	8		

## Appendix C. Chapter 7

This appendix contains information on the configuration of the numerical groundwater model MODFLOW to simulate the catchment of Gryteland in winter 2019 (Figures A and B). In addition, in this appendix several images are shown of seepage springs as they occurred during snowmelt in Gryteland, winter 2019 (Figure C).

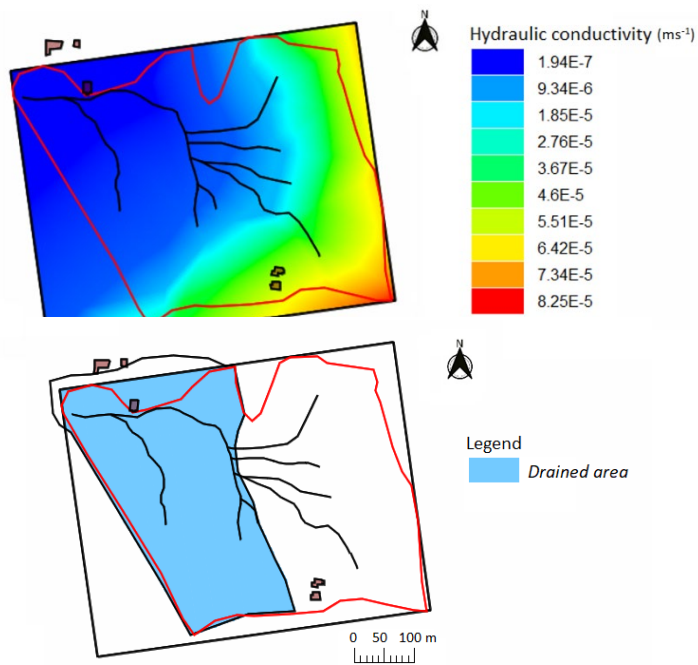


Figure A. Spatial distribution of hydraulic conductivity in the model simulations (upper) and the drained area (lower).

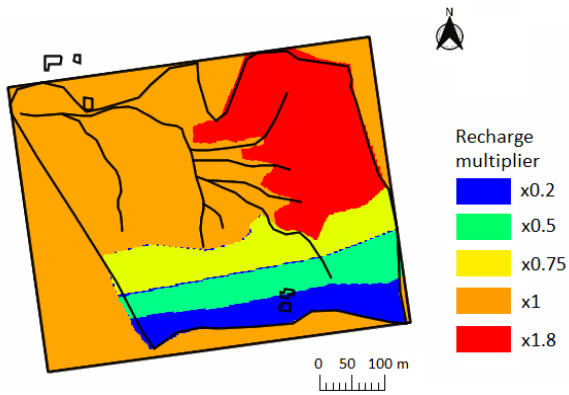


Figure B. Spatial distribution of recharge employed in the simulations by multiplying the background recharge value with a number between 0.2 and 1.8.



Figure C. Photographs of several groundwater springs in the Gryteland catchment, during or right after snowmelt in winter 2019.

## Appendix D. CryoFlow-1D manual

### **Manual to the calculations, equations, and setup of the model.**

Manual version: 1.3, August 2023.

Model version: CryoFlow-1D v2.1, December 2022.

#### **1. Introduction**

The CryoFlow model simulates water and heat transport in unsaturated porous media with phase change for a one-dimensional column. Key processes specific to freezing of soil are included: freezing point depression, permeability reduction and cryosuction. An atmospheric module can be incorporated to simulate heat exchange between the soil and the atmosphere. Frost heave, i.e., soil structure change upon pore ice growth, is not incorporated. Applications of the model could include theoretical study of freeze/thaw problems in the unsaturated zone, the testing of governing equations against experimental data, study of the practical performance of constructed systems such as landfill insulation covers and vegetated infiltration swales in cold climates, and education on unsaturated freezing phenomena. It is not suited for geotechnical problems related to frost heave.

Freezing of soil can induce flood hazard by reducing the soil's infiltration capacity. From a broader research perspective, the main goal of the model is therefore to aid in improving flood hazard forecasting during frozen soil conditions. More accurate predictions of soil infiltrability in cases of critically high water input, such as with snowmelt over potentially frozen soil, would be paramount. Secondary goals include improved prediction of contaminant pathways, groundwater recharge, and frost vulnerability of (constructed) porous media in cold climates. It is hoped that the modelling code provided will also aid multidimensional catchment-scale modellers with incorporating freezing routines.

The model was initially created as a macro-enabled Excel document with VBA code – it might be released later as a Python program. The VBA-based model requires only basic knowledge of Excel to be operated, but expert understanding of unsaturated zone behaviour is recommended to interpret

the results. Currently, there is a user-friendly input form which removes interaction by the user with the Excel sheet itself. The model configuration is setup in the user form, after which the simulation will run.

This document will provide the underlying equations used in the model, the required input variables, the provided output variables, the basic part of the implemented VBA code. Validation test cases are available in the thesis chapters and in earlier published articles. An overview of different model variants is also given in this document.

#### *A note on Excel and VBA*

Excel with VBA sometimes has a diminutive status as a modelling tool in physical sciences compared to e.g., Python, R and Fortran. This status is however deemed unfounded by the author since Excel with VBA as a sheet-based code can provide the exact same results compared to array-based codes. Essentially, different modelling tools have different benefits and disadvantages at the level of personal preference and user friendliness. Nevertheless, certain limitations are present with Excel and VBA, for example regarding the implementation of complex numerical methods. Possible benefits of using Excel with VBA in modelling are not insignificant however:

- Sheet-based modelling allows for direct visual access to all equations, connections between variables, and parameter and variable values. This aids in error-finding and promotes transparency. Essentially, nothing is “hidden” behind complex code.
- Running the model with in-situ visual updating of all variables is easily implemented, hence enabling the user to “see” the simulation in real-time (although this increases processing time greatly). Live simulation could be very useful for error-finding but also as an educational tool.
- Excel is a widely used program in various disciplines and work fields. It is therefore more easily understood by a greater number of users as opposed to codes such as Python and R which require expertise of coding language. In addition, the accessibility of an Excel model might benefit sharing and easy adaptation of basic functions by

other users. Adjusting an equation simply entails changing the Excel formula in certain cells.

A disadvantage that contradicts the accessibility of an Excel-based model is that with increasing complexity, it becomes increasingly time-consuming for a user to uncover mathematical links between cells.

## 2. Equations and calculations

This section provides all the equations used in the model to calculate water transport, heat transport and phase change in porous media. Variants of the model are described at the end of the section.

### Matric pressure

The van Genuchten model is used to relate water content to matric pressure ( $m$ ). An empirical function is used to further reduce matric pressure based on ice content of the soil (cryosuction). This gives the following soil water retention curve (van Genuchten, 1980):

$$\psi_m = \frac{1}{a} \left[ \left( \frac{\theta_s - \theta_r}{\theta_w - \theta_r} \right)^{\frac{n}{n-1}} - 1 \right]^{\frac{1}{n}} (1 + \Phi_i \theta_i)^2 \quad [A]$$

Where  $\psi_m$  (Pa) is the total matric pressure of the soil (including the effect of cryosuction),  $a$  ( $\text{Pa}^{-1}$ ) and  $n$  (-) are model parameters,  $\theta_w$  is the total water content (including ice and liquid water) ( $\text{m}^3\text{m}^{-3}$ ),  $\theta_r$  is the residual total water content ( $\text{m}^3\text{m}^{-3}$ ),  $\theta_s$  is the saturated total water content ( $\text{m}^3\text{m}^{-3}$ ),  $\Phi_i$  (-) is an empirical factor that represents the effect of ice on matric pressure (standard value = 1.8).

### Permeability

Relative permeability is a factor between 0 and 1 that indicates decreasing permeability with decreasing liquid water content. Whether the reduction in liquid water content is due to water drainage or phase change to solid, the resulting drop in permeability is considered similar based on the analogy between freezing and drying. Relative permeability is calculated with the Mualem-van Genuchten approach (Mualem, 1976; van Genuchten, 1980):

$$k_r = \left( \frac{\theta_s - \theta_r}{\theta_u - \theta_r} \right)^{0.5} \left\{ 1 - \left[ 1 - \left( \frac{\theta_s - \theta_r}{\theta_u - \theta_r} \right)^{\left( \frac{n-1}{n} \right)} \right]^{\left( \frac{n-1}{n} \right)} \right\}^2 \quad [\text{B}]$$

Where  $k_r$  is the relative permeability (-) and  $\theta_u$  is the unfrozen (liquid) water content ( $\text{m}^3\text{m}^{-3}$ ).

Subsequently, to obtain the current hydraulic permeability at a certain liquid water content, the following formula is applied:

$$k = k_s k_r \quad [\text{C}]$$

Where  $k$  is the permeability of the soil ( $\text{m}^2$ ) and  $k_s$  is the saturated permeability ( $\text{m}^2$ ).

### Water transport

The transport of fluid is governed by a 1-dimensional form of the Richards Equation:

$$\frac{\partial \theta_w}{\partial t} = \frac{\partial}{\partial z} \left[ \frac{k}{\mu} \left( \frac{\partial \psi_m}{\partial z} + \rho_w g \right) \right] \quad [\text{D}]$$

Where  $z$  is the elevation (m),  $\psi_m$  is the matric pressure (Pa),  $\mu$  is the fluid viscosity ( $\text{kgm}^{-1}\text{s}^{-1}$ ),  $\rho_w$  is the fluid density ( $\text{kgm}^{-3}$ ),  $g$  is the gravitational acceleration ( $\text{ms}^{-2}$ ) and  $t$  is discretized time (s). This universal version of the Richards Equation (Richards, 1931) allows for simulation of different planetary gravities and different fluid properties.

### Thermal conduction

Thermal conduction is based on the following equation (Giancoli, 2010):

$$\frac{dQ_c}{dt} = c \frac{dT}{dz} \quad [\text{E}]$$

Where  $Q_c$  is the amount of heat conducted (J),  $c$  is the thermal conductivity of the soil, including water, ice, air and soil thermal conductivities ( $\text{Wm}^{-1}\text{K}^{-1}$ ),  $T$  is the temperature (K) and  $z$  is the soil depth (m).

### Advection

The amount of heat transported through advection is calculated with the following equation:

$$\frac{dQ_a}{dt} = \theta_g T_d \rho_w S_w V \quad [F]$$

Where  $Q_a$  is the amount of heat advected (J),  $\theta_g$  is the volumetric water content gained at a discretized soil unit ( $\text{m}^3\text{m}^{-3}$ ) based on Eq. D ( $\text{Max}(\theta_g = \frac{\partial \theta_w}{\partial t} \partial t, 0)$ ),  $T_d$  is the difference in temperature (K) between two discretized soil units that exchanged water,  $S_w$  is the specific heat of water ( $\text{Jkg}^{-1}\text{K}^{-1}$ ) and  $V$  is the discretized soil volume ( $\text{m}^3$ ). Note: *Max* returns the maximum value of a series of numbers separated by a “,”.

### Total energy change

The total change in energy of a certain cell is calculated the following way:

$$\frac{dQ_t}{dt} = \frac{dQ_c}{dt} + \frac{dQ_a}{dt} \quad [G]$$

Where  $Q_t$  is the total energy change (J) gained or lost at a discretized soil unit (cell).

### Soil temperature change

The change in temperature of a cell is calculated with the following equation, which includes conduction, advection and latent heat flux:

$$\frac{dT}{dt} = \frac{dQ_t + d\theta_i L_f \rho_w V}{S_t} \quad [H]$$

Where  $\theta_i$  is the volumetric ice content,  $L_f$  is the latent heat of fusion of the liquid-solid phase change ( $\text{Jkg}^{-1}$ ) and  $S_t$  is the total specific heat of the discretized soil volume.

The  $d\theta_i L_f \rho_w V$  term is the latent heat flux. An increase in ice content results in an increase in soil temperature through release of latent heat, and vice versa with a decrease in ice content.

### Specific heat



The specific heat of the soil is calculated as the sum of the specific heat of all soil constituents:

$$S_t = [S_w \theta_u \rho_w + S_i \theta_i \rho_i + S_a (\theta_s - \theta_w) \rho_a + S_g (1 - \theta_s) \rho_g] V \quad [1]$$

Where  $S_w$  is the specific heat of water ( $\text{Jkg}^{-1}\text{K}^{-1}$ ),  $S_i$  is the specific heat of ice ( $\text{Jkg}^{-1}\text{K}^{-1}$ ),  $S_a$  is the specific heat of air,  $S_g$  is the specific heat of soil grains ( $\text{Jkg}^{-1}\text{K}^{-1}$ ),  $\rho_i$  is the density of ice ( $\text{kgm}^{-3}$ ),  $\rho_a$  is the density of air ( $\text{kgm}^{-3}$ ) and  $\rho_g$  is the density of soil grains ( $\text{kgm}^{-3}$ ).

### Thermal conductivity

In reality, thermal conductivity of unsaturated soil, especially frozen unsaturated soil, is highly complex and time-variant. To avoid over-parametrizing the model, complicated thermal conductivity equations with several empirical constants are not used. Instead, the thermal conductivity of the soil is calculated as the geometric mean of the thermal conductivities of soil constituents:

$$c = c_w^{\theta_u} c_i^{\theta_i} c_a^{(\theta_s - \theta_w)} c_g^{(1 - \theta_s)} \quad [J]$$

Where  $c_w$  is the thermal conductivity of water ( $\text{Wm}^{-1}\text{K}^{-1}$ ),  $c_i$  is the thermal conductivity of ice ( $\text{Wm}^{-1}\text{K}^{-1}$ ),  $c_a$  is the thermal conductivity of air ( $\text{Wm}^{-1}\text{K}^{-1}$ ) and  $c_g$  is the thermal conductivity of soil grains ( $\text{Wm}^{-1}\text{K}^{-1}$ ).

In practice, the thermal conductivity of the soil grains can be used as a factor for calibration, especially since it is often of unknown magnitude. Although far from ideal, this calibration approach yielded adequate results in our tests.

### Soil freezing routine

The relationship between liquid water content and temperature in the soil is given by the Soil Freezing Curve (SFC). It derives from the relationship between surface tension and freezing point depression, which is linked to capillary radius and interfacial energies at the liquid-air and liquid-solid boundaries. The resulting physical relationships can mathematically be found in either the Clausius-Clapeyron relation or the Kelvin equation, both

of which render the same implementation of the van Genuchten model to determine liquid water content based on capillary action:

$$\theta_u = \theta_r + (\theta_s - \theta_r) \left[ 1 + \left( -a \frac{L_f T \rho_w}{T_s} \right)^n \right]^{-\left(1 - \frac{1}{n}\right)} \quad [\text{K}]$$

Where  $T$  is the current soil temperature (K),  $T_s$  is the standard solid-liquid phase change temperature when matric pressure is absent (i.e., only atmospheric pressure) (K) (default value 273.15K).

The equation is not directly incorporated into the model. Instead, phase change is calculated via different routines in which it is integrated with the latent heat flux (described below). These routines allow for more efficient calculation than would otherwise be the case with directly applying the above equation.

#### *Fast+ routine*

The Fast+ routine is the simplest but most imprecise approach (Figure 1), yet it is reliable in providing a final solution to a frozen soil situation (tested with 1-second timesteps, 1 cm spatial discretization, extreme temperature boundary conditions, sandy loam soil type and minimum of 1 day of simulated time).

First, the current solid-liquid phase change temperature of water is calculated based on the matric pressure on the liquid water:

$$T_p = -\frac{T_s}{L_f \rho_w} \psi_u (\theta_u + d) + T_s \quad [\text{L}]$$

Where  $T_p$  is the current solid-liquid phase change temperature (C),  $\psi_u$  is the matric pressure (Pa) on the liquid water calculated with Eq. A but with  $\theta_i = 0$  and  $\theta_w = \theta_u$  and  $d$  is the soil water deficit content.

The soil water deficit equals the amount of liquid water that drained from a soil volume while it contained ice. Without the concept of a soil water deficit, at steady soil temperature, ice would otherwise melt if liquid water content dropped. This is a consequence of the lowering of the solid-liquid phase

change temperature point of water with lower liquid water content. The soil water deficit is stored as a memory variable and keeps the ice frozen upon desaturation. An influx of liquid water reduces the soil water deficit until zero. The soil water deficit is described with the following formula:

$$d = \text{Max} \left[ d_{old} + \text{if}(\theta_i > 0 \text{ and } \frac{\partial \theta_u}{\partial t} < 0, \frac{-\partial \theta_u}{\partial t}) - \text{Max} \left( \frac{\partial \theta_u}{\partial t}, 0 \right), 0 \right] \text{ [M]}$$

Where  $d_{old}$  is the soil water deficit at the previous timestep. The If and Max functions ensure that the soil water deficit never becomes less than zero, only decreases with positive liquid water flux (melt or flow) and only increases with negative positive water flux (flow) if ice is present.

The ice content of the soil is determined with the following formulas and statements:

$$\text{If } T < T_p: \frac{d\theta_i}{dt} = -\frac{dQ_t}{L_f \rho_w V} + i; \text{ else: } \frac{d\theta_i}{dt} = \frac{dQ_t}{L_f \rho_w V} + i; \text{ with: } \theta_i \geq 0 \text{ and } \theta_i \leq (\theta_w - \theta_r)$$

$$\text{If } \theta_i \text{ and } \frac{\partial \theta_w}{\partial t} > 0: i = \frac{\partial \theta_w}{\partial t}; \text{ else: } i = 0 \quad \text{[N]}$$

Where  $i$  is the volumetric ice content gained due to positive water flux. The change in volumetric ice content ( $d\theta_i$ ) is restricted: ice content can never decrease below zero, and it can never increase above the current total water content minus the residual water content. The second statement ensures that if water flows to a soil volume where there is already ice, it immediately freezes, because any increase in water content is at a pressure that results in a freezing point above the current temperature.

### *Fast routine*

With the fast routine, results in a time plot show a more stable graph, i.e., diminished oscillation (Figure 1). A change is made to the amount of energy available for phase change, otherwise all above equations are true for the fast routine.

First, the current soil temperature is determined if no phase change would occur:

$$T_n = T_{old} + \frac{dQ_t}{S_t} \quad [O]$$

Where  $T_n$  is the current soil temperature when phase change is excluded, and  $T_{old}$  is the soil temperature at the previous timestep.

Subsequently, the amount of energy available for phase change is determined:

$$dQ_* = (T_n - T_p)S_t \quad [P]$$

Where  $Q_*$  is the energy (J) available for phase change.

Finally, in Eq. G,  $dQ_t$  is replaced by  $dQ_*$ . Therefore, the amount of energy that was required to reach the solid-liquid phase temperature point is not used for phase change, only excess energy is. Therefore, the result is more precise. It renders the following equation as a replacement for the first half of Eq. N:

$$\text{If } dQ_* > 0: \frac{d\theta_i}{dt} = \frac{dQ_*}{L_f \rho_w V} + i; \quad \text{else: } \frac{d\theta_i}{dt} = -\frac{dQ_*}{L_f \rho_w V} + i; \quad \text{with: } \theta_i \geq 0 \text{ and } \theta_i \leq (\theta_w - \theta_r) \quad [Q]$$

### *Slow routine*

The relatively slower routine adds a few more details to the latent heat flux calculation. While liquid water is turning to ice, the freezing temperature point is dropping. If the freezing temperature is not dropped during water to ice transformation, at the next timestep, ice formation might temporarily halt until freezing temperature is reached again. This leads to slightly imprecise results in case of substantial ice content changes in a short period of time at the scale of a second, although no actual deviation from the outcome could be observed so far during testing (Figure 1). Hypothetically however, it is more accurate to consider ice formation itself as related to a differential equation.

First, the latent heat per 1 unit of liquid water content phase change is calculated:

$$L_p = \frac{dL_f}{d\theta_p} = L_f \rho_w V \quad [R]$$

where  $L_p$  is the latent heat flux (J) per 1 unit liquid water content of phase change and  $\theta_p$  is the change in liquid water content specifically due to phase change.

In addition, the sensible heat per 1 unit of liquid water content phase change is calculated by combining the derivative of the van Genuchten equation in terms of pressure with the freezing point equation (Eq. L) and the specific heat of the soil:

$$H_p = \frac{dH_s}{d\theta_p} = \frac{1}{amn(a\psi_u)^{n-1}(1+(a\psi_u)^{n-1})^{-m-1} \frac{T_p}{L_f \rho_w} S_t} \quad [S]$$

where  $H_p$  is the sensible heat flux (J) per 1 unit of liquid water content phase change,  $H_s$  is the sensible heat (J) and  $m$  is  $1 - \frac{1}{n}$ .

The part  $\frac{T_p}{L_f \rho_w}$  provides the change in freezing point per 1 unit of pressure (KPa<sup>-1</sup>).

Finally, the ratio ( $j$ ) between sensible heat flux and latent heat flux per 1 unit of phase change is determined:

$$j = \frac{L_p}{H_p} \quad [T]$$

This ratio is used to more accurately determine the energy available for phase change when freezing temperature point would simultaneously change. The following equation therefore replaces Eq. Q:

$$\text{If } dQ_* > 0: \frac{d\theta_i}{dt} = \frac{j dQ_*}{L_f \rho_w V} + i; \text{ else: } \frac{d\theta_i}{dt} = -\frac{j dQ_*}{L_f \rho_w V} + i; \text{ with: } \theta_i \geq 0 \text{ and } \theta_i \leq (\theta_w - \theta_r) \quad [U]$$

Top boundary

At the top boundary of the model, a fixed boundary temperature can be set as well as a water input rate along with the input water temperature. The top temperature boundary is regarded as exchanging energy with the soil based on the thermal conduction equation. Alternatively, the atmospheric module can be used to simulate energy exchange between the soil and atmosphere (later described).

### Bottom boundary

Regarding the water transport, at the bottom boundary there are two options in the model: a no-flux boundary and free gravitational drainage. The temperature boundary can either be set to a no-flux boundary or a fixed temperature similar to the top boundary.

### Atmospheric module

Instead of the original surface temperature boundary of the model, a more realistic soil-atmosphere energy exchange boundary can be employed. All equations are based on Rango and DeWalle (2008). Sensible heat convection is simulated the following way:

$$Q_a = \rho_a H_a C_h u_a (T_a - T_s) \quad [V]$$

where  $Q_a$  is the energy exchange between the atmosphere and soil (J),  $\rho_a$  is the density of air ( $\text{kgm}^{-3}$ ),  $H_a$  is the specific heat of air ( $\text{Jkg}^{-1}\text{K}^{-1}$ ),  $C_h$  is the bulk transfer coefficient for sensible heat,  $u_a$  is the windspeed at height  $z_a$  ( $\text{ms}^{-1}$ ),  $T_a$  is the air temperature at height  $z_a$  ( $^{\circ}\text{C}$ ) and  $T_s$  is the soil surface temperature ( $^{\circ}\text{C}$ ).

$$R = [gT_m^{-1}]z_a(T_a - T_s)/(u_a^2) \quad [W]$$

Positive values indicate stable atmosphere, negative values an unstable atmosphere.

Then:

$$\begin{aligned} \text{If } R > 0: C_h &= (1 - 5R)^2 k^2 \left[ \ln \left( \frac{z_a}{z_0} \right) \right]^{-2}; \\ \text{else: } C_h &= (1 - 16R)^{0.75} k^2 \left[ \ln \left( \frac{z_a}{z_0} \right) \right]^{-2} \end{aligned} \quad [X]$$

Where  $k$  is von Karmin's constant (0.4) and  $z_0$  is the aerodynamic roughness of the soil surface (m).

Radiative transfer included in the atmospheric module is under development. The following equation will be added for shortwave radiation:

$$Q_s = K\alpha \quad [Y]$$

Where  $Q_s$  is the amount of short-wave solar radiation absorbed by the soil,  $K$  is the amount of solar shortwave radiation (J) (wavelengths = 0.4–2  $\mu\text{m}$ ) and  $\alpha$  is the albedo of the soil. A horizontal surface is assumed.

### 2D overland flow variant

Flow velocity on top of a sloping surface is calculated using Manning's Equation (Manning, 1891):

$$v = \frac{1}{n} h^{\frac{5}{3}} s^{0.5} \quad [Z]$$

Where  $v$  is the flow velocity,  $n$  is Manning's roughness coefficient,  $h$  is the water height, and  $s$  is the slope (unitless, i.e., m/m).

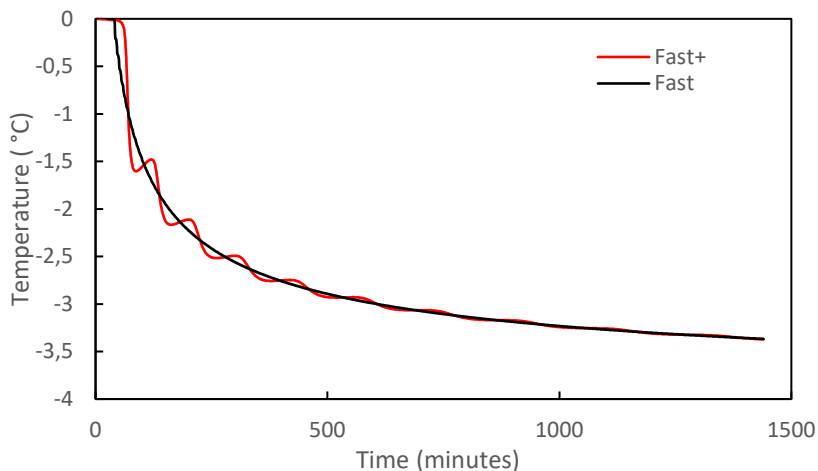


Figure 1. Comparison of results with two different freezing routines used (Fast+ and Fast), while parameter configuration, boundary conditions and initial conditions are similar.

#### 4. Input parameters and variables

The model requires the following list of base parameters. Standard values are shown, but these can be adjusted.

Table 2. Default physical constants and parameter values in the model.

Parameter		Value	Units
Cryosuction	$\Phi_i$	1.8	-
Thermal conductivity (water)	$c_w$	0.6	$Wm^{-1}K^{-1}$
Thermal conductivity (ice)	$c_i$	2.22	$Wm^{-1}K^{-1}$
Thermal conductivity (air)	$c_a$	0.024	$Wm^{-1}K^{-1}$
Specific heat (water)	$H_w$	4182	$Jkg^{-1}K^{-1}$
Specific heat (ice)	$H_i$	2108	$Jkg^{-1}K^{-1}$
Specific heat (soil particles)	$H_s$	840	$Jkg^{-1}K^{-1}$
Specific heat (air)	$H_a$	1003	$Jkg^{-1}K^{-1}$
Latent heat of fusion (water)	$L_f$	334000	$Jkg^{-1}$
Density (water)	$\rho_w$	998	$kgm^{-3}$
Density (ice)	$\rho_i$	916	$kgm^{-3}$
Density (soil particles)	$\rho_s$	2648	$kgm^{-3}$
Density (air)	$\rho_a$	1.2754	$kgm^{-3}$
Gravitational acceleration	$g$	9.807	$ms^{-2}$
Liquidus	$T_p$	273.15	K
Viscosity (water)	$\mu$	1.002e-04	$kgms^{-1}$
Stefan Boltzman constant (atmospheric module)		5.67e-08	$Wm^{-2}K$
Von Karmin constant (atmospheric module)	$k$	0.4	-

The following variables and parameters must be defined by the user:

Parameter	Units
Soil permeability	$m^2$
Soil porosity	-
Soil residual water content	-
van Genuchten SWRC constant, a	$m^{-1}$



van Genuchten SWRC constant, n	-
Initial total water content	-
Initial soil temperature	°C
Temperature boundary upper	°C
Temperature boundary lower	°C
Water flux boundary upper	mmhr <sup>-1</sup>
Water flux boundary lower	-
Water input temperature	°C
Air temperature	°C
Windspeed	ms <sup>-1</sup>
Cloud cover	-
Solar radiation	Wm <sup>-2</sup>
Albedo	-
Aerodynamic roughness	m
Manning's coefficient	-

## 5. Output variables

The model will provide the state of the soil at the end of the simulation. It can also record output variables at pre-set time intervals during the simulation to construct timeplots.

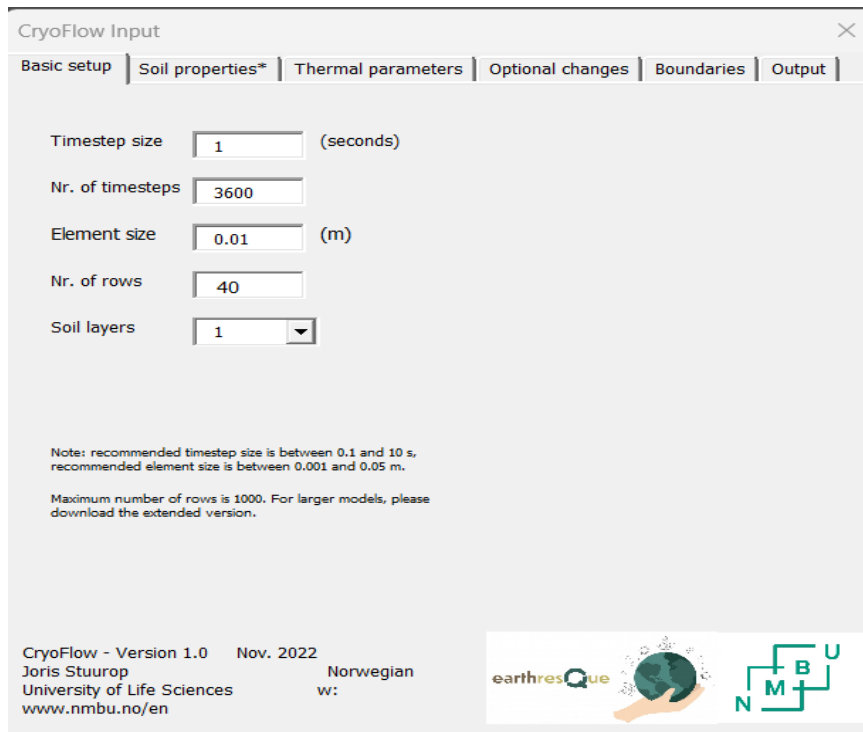
The following are considered to be the output variables for each discretized soil depth:

- Soil temperature
- Total water content
- Liquid water content
- Ice content
- Matric pressure
- Relative permeability

## 6. How to use the model

The program opens with a user form in which the model setup can be configured. For basic use, the user form suffices. For more advanced use,

changes need to be made directly in the Excel sheet. Here, basic use will be explained.



The screenshot shows the 'CryoFlow Input' dialog box with the following settings:

- Timestep size: 1 (seconds)
- Nr. of timesteps: 3600
- Element size: 0.01 (m)
- Nr. of rows: 40
- Soil layers: 1


Note: recommended timestep size is between 0.1 and 10 s, recommended element size is between 0.001 and 0.05 m.

Maximum number of rows is 1000. For larger models, please download the extended version.

CryoFlow - Version 1.0 Nov. 2022  
Joris Stuurup  
University of Life Sciences  
www.nmbu.no/en

Norwegian  
w:

earthresQue



In the first window, as shown above, the timestep size and number of timesteps can be set. Note: simulated time will be timestep size \* number of timesteps.

Furthermore, the element size can be set and the nr. of rows. Note: the total vertical extent of the model will be the element size \* nr. of rows.

Also, the number of soil layers can be configured. Every soil layer will have its own set of hydraulic and thermal properties.

CryoFlow Input

Basic setup | **Soil properties\*** | Thermal parameters | Optional changes | Boundaries | Output

Ks  m/s Preset soil type

a  1/m (van Genuchten)

n  (van Genuchten)

ResidualWC  Solid particle thermal conductivity  W/mK

SaturatedWC  Solid particle density  kg/m<sup>3</sup>

Initial soil temperature  °C

Initial soil total water content

Manual setup of initial conditions

\*If multiple soil layers selected, these properties are for layer 1 only. A new pop-up will appear to enter properties for other layers.

In the second tab, the hydraulic soil properties of the First layer can be set (for other layers, a pop-up will show later). Ks is the saturated hydraulic conductivity, a and n are van Genuchten soil water retention parameters. WC stands for water content. Also, the thermal conductivity and particle density of individual solid grains can be configured. Standard values are pre-filled in. A preset soil type can be chosen which will configure the hydraulic properties. Also, the initial temperature and total water content for the vertical soil profile can be given (note: all discretized cells will receive this value). If more complex initial conditions are needed, it is recommended to simulate a pre-period before the actual simulation. Alternatively, the initial

conditions can be manually changed within the Excel sheet (check box option).

The image shows a screenshot of the 'CryoFlow Input' dialog box, specifically the 'Thermal parameters' tab. The dialog has a title bar with a close button (X) and a tabbed interface with the following tabs: 'Basic setup', 'Soil properties\*', 'Thermal parameters', 'Optional changes', 'Boundaries', and 'Output'. The 'Thermal parameters' tab is active and contains the following parameters, each with a text input field and a unit label:

Parameter	Value	Unit
Thermal conductivity fluid	0.6	W/mK
Thermal conductivity ice	2.22	W/mK
Thermal conductivity air	0.024	W/mK
Specific heat soil particle	840	J/kgK
Specific heat fluid	4182	J/kgK
Specific heat ice	2108	J/kgK
Specific heat air	1003	J/kgK
Latent heat of fusion	334000	J/kg
Standard freezing point	273.15	K

In the third tab, the basic thermal parameters of the model can be configured. It is recommended to leave the values as they are pre-filled in (standard values for water, etc.). Changes can of course be made if needed. The standard freezing point and latent heat of fusion refer to the fluid that is being simulated.

CryoFlow Input

Basic setup | Soil properties\* | Thermal parameters | Optional changes | Boundaries | Output

Planet (gravity)

Fluid density  kg/m<sup>3</sup>

Fluid viscosity  kg/ms

Ice density  kg/m<sup>3</sup> Freezing routine\*\*

Air density  kg/m<sup>3</sup> Add landfill waste layer\*\*\*

Cryosuction (Ck)\*   Enhance flow stability\*\*\*\*

\*The Ck value was determined after experimental testing (Stuuroop et al., 2021). Not recommended to change.

\*\*Read the manual before changing.

\*\*\*A new pop-up will appear to enter details for the landfill waste layer; make sure the waste layer is not included in the nr. of rows (under basic setup). The bottom temperature boundary will be replaced by the waste layer. It serves only as a sink or source for heat.

\*\*\*\*Slight runtime increase for improved flow stability; recommended with high hydraulic conductivity or with very fine spatial discretization.

In the fourth window, some optional elements can be configured. For instance, gravity and fluid basic properties can be changed. The Cryosuction parameter should be kept at 1.8, unless the parameter itself is the subject of study. Regarding the freezing routines, these represent different calculation methods, which are described below. In most cases, the Fast freezing routine is recommended, but trial-and-error can be performed to ascertain the best calculation method if results are not optimal. Flow stability can be enhanced for a slight runtime increase, relevant for very coarse soils or with very fine spatial discretization (ca. 1 mm). A landfill waste layer can be included for the specific purpose of landfill barrier modelling. The landfill will simply act as a

source or sink of heat at the bottom of the model; a new pop-up later will have the form to enter the properties of the waste layer.

The image shows a software dialog box titled "CryoFlow Input" with a close button (X) in the top right corner. The dialog has six tabs: "Basic setup", "Soil properties\*", "Thermal parameters", "Optional changes", "Boundaries", and "Output". The "Boundaries" tab is currently selected. It contains five rows of configuration options:

- Upper temperature boundary:** A dropdown menu set to "Fixed temperature" and a text input field containing the value "5", followed by the unit "°C".
- Lower temperature boundary:** A dropdown menu set to "Fixed temperature" and a text input field containing the value "4", followed by the unit "°C".
- Water flux upper boundary:** A dropdown menu set to "Fixed input" and a text input field containing the value "3.2", followed by the unit "mm/hr".
- Water input temperature:** A text input field containing the value "1", followed by the unit "°C".
- Water flux lower boundary:** A dropdown menu set to "NoFlux".

At the bottom of the dialog, there is a checkbox labeled "Time-variant manual input (upper boundary)" which is currently unchecked.

The fifth tab enables configuration of all the boundary conditions in the model (time invariant). The fixed temperature and atmospheric temperature boundaries are described more under the section Equations and calculations. If only a top boundary temperature is required, the Fixed temperature boundary should be chosen. If more realistic atmospheric energy exchange is supposed to be simulated, 'atmospheric' should be chosen. A later pop-up will provide configuration of variables such as windspeed, air temperature and solar radiation. Snowpack simulation is currently not possible.

Water flux represents the water input at the top boundary of the soil column. At the bottom of the model, water can either not drain (impermeable barrier, 'no flux' option), drain freely due to gravity, or leave via a drainpipe (water is removed that would oversaturate the lowest cell, i.e., water is only removed if the bottom cell is saturated). The model output will show how much water drained out.

If time-invariant boundary conditions are desired, the corresponding option should be ticked. Later, an Excel-sheet will be enabled in which all the time-variant data can be entered.

CryoFlow Input

Basic setup | Soil properties\* | Thermal parameters | Optional changes | Boundaries | Output

Sensor output every  timesteps

Sensor 1 depth  cm

Sensor 2 depth  cm

Sensor 3 depth  cm

Sensor 4 depth  cm

Sensor 5 depth  cm

Sensor 6 depth  cm

Produce plots

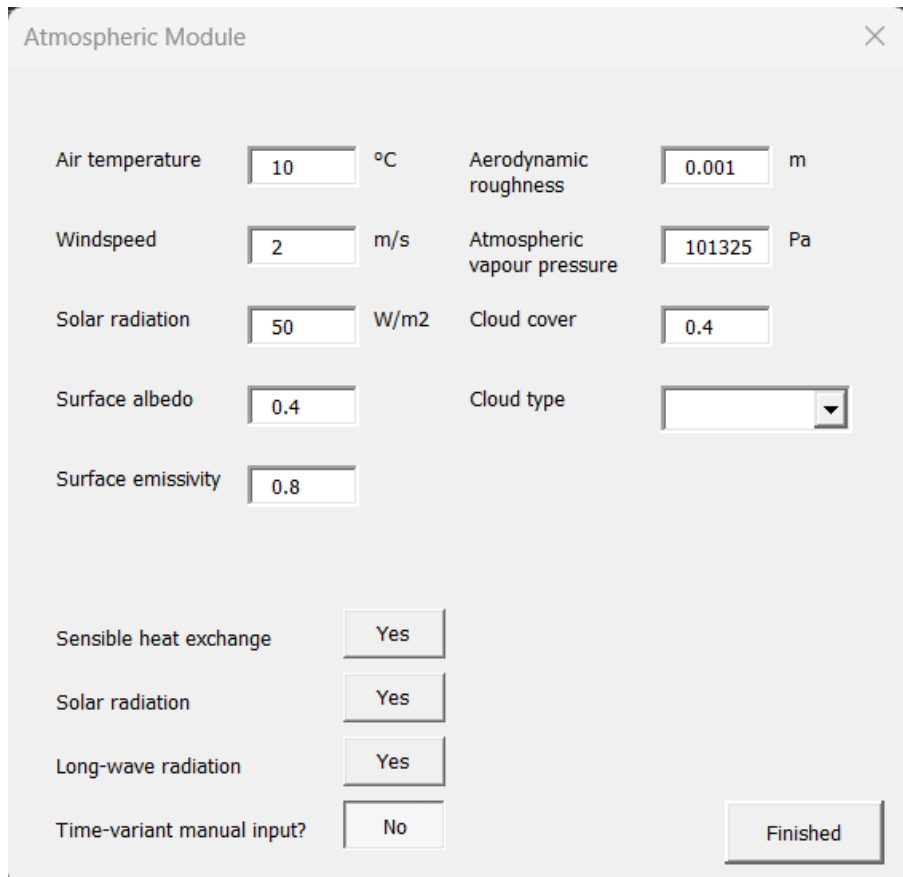
Note: each sensor records the temperature, unfrozen water content, total water content and ice content.

This takes several seconds

In the final tab, the output can be configured, such as output frequency, and at which soil depths (in real length units). These sensors can also be turned on or off. If produce plots is checked, graphs will automatically be made at the end of the simulation. Note: a sensor can only be on if the overlying

sensor is also on. Now, if Generate Model is clicked, the simulation will run, unless new pop-up windows were required for further configuration of the model. These additional pop-up windows will be described further below.

### Optional Pop-ups after initial setup



The screenshot shows a window titled "Atmospheric Module" with a close button (X) in the top right corner. The window contains several input fields and checkboxes for configuring atmospheric parameters. The parameters and their values are as follows:

Parameter	Value	Unit
Air temperature	10	°C
Windspeed	2	m/s
Solar radiation	50	W/m <sup>2</sup>
Surface albedo	0.4	
Surface emissivity	0.8	
Aerodynamic roughness	0.001	m
Atmospheric vapour pressure	101325	Pa
Cloud cover	0.4	
Cloud type		

Below the input fields, there are four checkboxes with buttons:

- Sensible heat exchange: Yes
- Solar radiation: Yes
- Long-wave radiation: Yes
- Time-variant manual input?: No

A "Finished" button is located in the bottom right corner of the window.

In the atmospheric module, the sensible heat exchange, solar radiation, and longwave radiation can be turned off or on. For sensible heat exchange simulation, the air temperature, windspeed and aerodynamic roughness length have to be configured. For solar radiation, the solar radiation amount, surface albedo and surface emissivity need to be configured. For long-wave radiation simulation, the atmospheric vapour pressure, fractional cloud cover, and cloud type need to be set up. If these data should be time-variant,



the corresponding box should be set to “Yes”. In that case, the data can later be entered in a special Excel sheet.

Soil properties - additional layers

Layer2 | Layer3 | Layer4 | Thickness

Ks  m/s Preset soil type

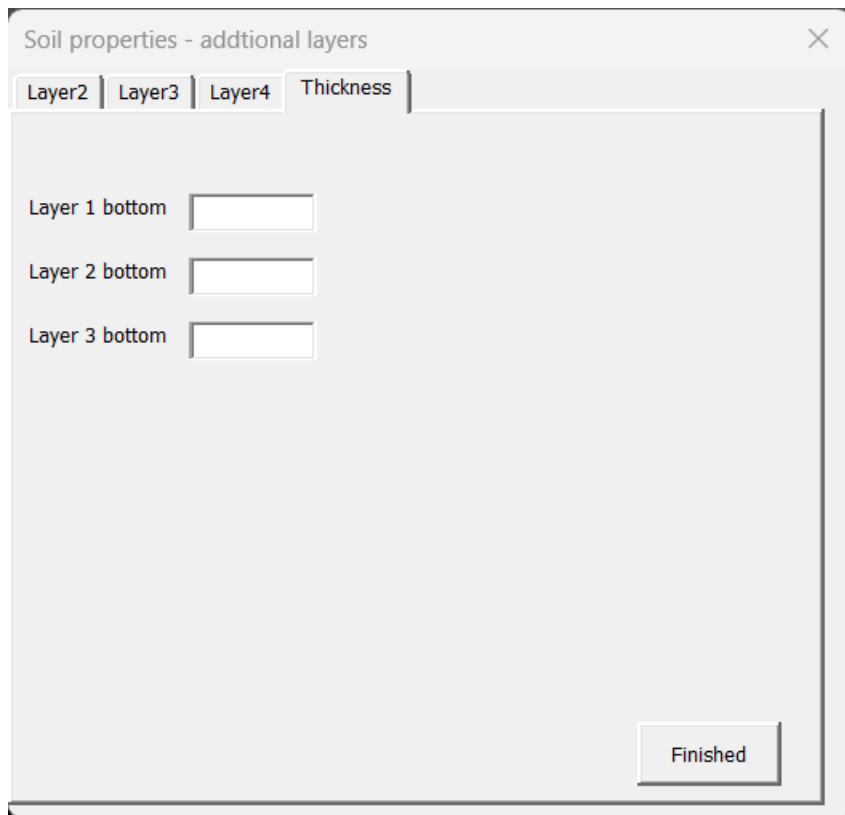
a  1/m (van Genuchten)

n  (van Genuchten)

ResidualWC  Solid particle thermal conductivity  W/mK

SaturatedWC  Solid particle density  kg/m<sup>3</sup>

In the soil properties – additional layers module, the hydraulic and thermal properties of the remaining soil layers can be configured.



Under the tab Thickness, note that the layer bottoms configure the vertical extent of all the layers. These should be given in cm (not a certain row number).

## 7. References

DeWalle, D. R., & Rango, A. (2008). **Principles of snow hydrology**. Cambridge: Cambridge University Press.

van Genuchten, M. (1980). **A closed-form equation for predicting the hydraulic conductivity of unsaturated soils**. *Soil Science Society of America Journal*, 44(5): 892-898.  
<http://dx.doi.org/10.2136/sssaj1980.03615995004400050002x>

Giancoli, D.C. (2010). **Physics**. Addison-Wesley, London, United Kingdom; 6th edition.

- Manning, R. (1891). **On the flow of water in open channels and pipes.** Transactions of the Institution of Civil Engineers of Ireland. 20: 161–207.
- Mualem, Y. (1976). **A new model predicting the hydraulic conductivity of unsaturated porous media.** *Water Resources Research*, **12**: 513-522.
- Richards, L.A. (1931). **Capillary conduction of liquids through porous mediums.** *Physics*, 1(5): 318-333. <https://doi.org/10.1063/1.1745010>

ISBN: 978-82-575-2104-2

ISSN: 1894-6402



Norwegian University  
of Life Sciences

Postboks 5003  
NO-1432 Ås, Norway  
+47 67 23 00 00  
[www.nmbu.no](http://www.nmbu.no)